AD-A053 635 PURDUE UNIV LAFAYETTE IND COMBUSTION LAB F/G 20/2
FLAME EFFICIENCY, STABILIZATION AND PERFORMANCE IN PREVAPORIZIN--ETC(U)
DEC 77 S L PLEE, D A SCHMIDT, A M MELLOR AFOSR-76-2936
UNCLASSIFIED PURDU-CL-77-07 AFOSR-TR-78-0736 NL

1 OF 3
ADA
053635

SECURITY CLASSIFICATION OF THIS PAGE (When Data Entered)

REPORT DOCUMENTATION PAGE

READ INSTRUCTIONS BEFORE COMPLETING FORM

1. REPORT NUMBER: AFOSR-TR-78-0736	2. GOVT ACCESSION NO.
3. RECIPIENT'S CATALOG NUMBER	
4. TITLE (and Subtitle): FLAME EFFICIENCY, STABILIZATION AND PERFORMANCE IN PREVAPORIZING/PREMIXING COMBUSTORS	5. TYPE OF REPORT & PERIOD COVERED: FINAL rept. 1 Sep 75 - 30 Nov 77
	6. PERFORMING ORG. REPORT NUMBER: PURDU-CL-77-07
7. AUTHOR(s): S. L. PLEE, D. A. SCHMIDT, A. M. MELLOR	8. CONTRACT OR GRANT NUMBER(s): AFOSR-76-2936
9. PERFORMING ORGANIZATION NAME AND ADDRESS: PURDUE UNIVERSITY, COMBUSTION LAB, MECHANICAL ENGINEERING, WEST LAFAYETTE, INDIANA 47906	10. PROGRAM ELEMENT, PROJECT, TASK AREA & WORK UNIT NUMBERS: 2308A2, 61102F
11. CONTROLLING OFFICE NAME AND ADDRESS: AIR FORCE OFFICE OF SCIENTIFIC RESEARCH/NA, BLDG 410, BOLLING AIR FORCE BASE, D C 20332	12. REPORT DATE: Dec 77
	13. NUMBER OF PAGES: xiii + 200 (214 pp.)
14. MONITORING AGENCY NAME & ADDRESS (if different from Controlling Office): 61102F 2308A2	15. SECURITY CLASS. (of this report): UNCLASSIFIED
	15a. DECLASSIFICATION/DOWNGRADING SCHEDULE

16. DISTRIBUTION STATEMENT (of this Report)

Approved for public release; distribution unlimited.

17. DISTRIBUTION STATEMENT (of the abstract entered in Block 20, if different from Report)

18. SUPPLEMENTARY NOTES

19. KEY WORDS (Continue on reverse side if necessary and identify by block number)

PREVAPORIZING/PREMIXING COMBUSTORS
COMBUSTION EFFICIENCY
FLAME STABILIZATION
FLASHBACK
LEAN BLOWOFF

20. ABSTRACT (Continue on reverse side if necessary and identify by block number)

Problems of combustion efficiency, incomplete prevaporization and flame stabilization (blowoff and/or flashback) associated with advanced prevaporizing/premixing turbojet combustors, afterburners and ramjet combustors are examined experimentally using a simplified axisymmetric burner. In addition to variations in combustor pressure, inlet temperature, equivalence ratio and air velocity typical of modern combustors, geometry and heterogeneous effects are also considered. Both flame stabilization and combustion efficiency data are examined using conventional and characteristic time correlations. Characteristic times, which have already been used to correla[illegible] and predict gaseous

emissions in conventional combustors are quantified here for blowoff. The model is based on the flame stabilization theory of Zukoski and Marble and includes inlet, geometry and heterogeneous effects simultaneously, unlike traditional loading parameters. Combustion efficiency data obtained for this study are not yet included in the correlation. Detailed internal species concentration, temperature and velocity measurements are planned to help identify proper scaling parameters for the combustion efficiency model. Flame flashback into the fuel preparation tube has not been observed for any of our operating conditions. This study shows that flow disturbances rather than combustor inlet conditions are responsible for the "flashback" reported in non-catalytic combustors.

FLAME EFFICIENCY, STABILIZATION AND PERFORMANCE IN PREVAPORIZING/PREMIXING COMBUSTORS

Air Force Office of Scientific Research

Grant No. AFOSR 76-2936 - Final Report

by

S. L. Plee, D. A. Schmidt and A. M. Mellor

Report No. PURDU-CL-77-07

The Combustion Laboratory
School of Mechanical Engineering
Purdue University
West Lafayette, Indiana

December 1977

ACKNOWLEDGEMENTS

The authors gratefully recognize T. Miller and J. Hersh for their valuable assistance in the maintenance and operation of the experimental facility. Additional aid with the experimental portion of this program was provided by W. Dodds, J. Peters, J. Stefucza, R. Washam and B. Wyatt. The authors are particularly grateful to D. Ramsey for his unlimited assistance in the data reduction and analysis.

The authors also appreciate the valuable discussions with Dr. M. B. Colket currently with United Technologies Research Center, as well as with Profs. A. H. Lefebvre and C. Ferguson of Purdue University.

Thanks are also extended to Dr. B. T. Wolfson of the Air Force Office of Scientific Research who served as a most helpful contract monitor. Research sponsored by the Air Force Office of Scientific Research, Air Force Systems Command, USAF, under Grant No. AFOSR-76-2936.

TABLE OF CONTENTS

LIST OF TABLES

LIST OF FIGURES

ABSTRACT

Problems of combustion efficiency, incomplete prevaporization and flame stabilization (blowoff and/or flashback) associated with advanced prevaporizing/premixing turbojet combustors, afterburners and ramjet combustors are examined experimentally using a simplified axisymmetric burner. This flameholder configuration retains the same fundamental combustion processes of prevaporizing/premixing combustors while eliminating some of the complexity of the practical hardware. In addition to variations in combustor pressure, inlet temperature, equivalence ratio and air velocity typical of modern combustors, geometry and heterogeneous effects are also considered.

Both flame stabilization and combustion efficiency data are examined using conventional (Lefebvre, 1966) and characteristic time (Mellor, 1976) correlations. Characteristic times, which have already been used to correlate and predict gaseous emissions in conventional combustors, are quantified here for blowoff. The model is based on the flame stabilization theory of Zukoski and Marble (1956) and includes inlet, geometry and heterogeneous effects simultaneously, unlike traditional loading parameters. Combustion efficiency data obtained for this study are not yet included in the correlation. Detailed internal species concentration, temperature and velocity measurements are planned to help identify proper scaling parameters for the combustion efficiency model.

Flame flashback into the fuel preparation tube has not been observed for any of our operating conditions. These results are consistent with a recent literature review (Plee and Mellor, 1977) which has identified important mechanisms of upstream flame propagation. This study shows that flow disturbances rather than combustor inlet conditions are responsible for the "flashback" reported in non-catalytic combustors.

I. INTRODUCTION AND SUMMARY

Gas turbine combustion systems currently provide the major source of propulsion for both military and commercial aircraft. In addition, continuous flow combustors are used in ramjets and are becoming increasingly important as a secondary energy source in stationary power plant applications. In the latter case, they provide an effective method for satisfying peak load requirements. These combustors, many of which were originally developed for aircraft applications, are designed to maximize the amount of energy release per unit volume. Fig. 1-1 illustrates schematically a typical gas turbine combustor consisting of three zones, primary combustion, secondary combustion and dilution, which are usually established by discrete air addition through the liner wall.

The primary zone normally extends from the injector to the first set of air addition holes. This region is characterized by fuel vaporization and recirculating air flow as well as the most intense combustion. Flame stabilization is accomplished by swirling the inlet flow, air penetration jet impingement and sudden expansion of the combustor liner. The creation of hot recirculating flow regions provides heat and free radicals to the shear layer and serves as a continuous ignition source; the shear layer is a region of extremely high turbulence located between the low velocity central recirculation zone and the high velocity inlet air stream. Liquid fuel injected into the shear layer rapidly vaporizes and reacts with the incoming air forming a hollow shear layer flame zone which surrounds the central recirculation zone and eventually closes to the centerline (Mellor et al., 1972; Tuttle et al., 1973). Tuttle et al. (1973) and Shisler et al. (1974) have probed these flames and found that the hollow shear layer flame resembles a turbulent diffusion flame. Because of the very nature of this type of flame and the fact that very little air is added in the primary zone, both local and overall equivalence ratios are high providing relatively wide ignition and blowoff limits.

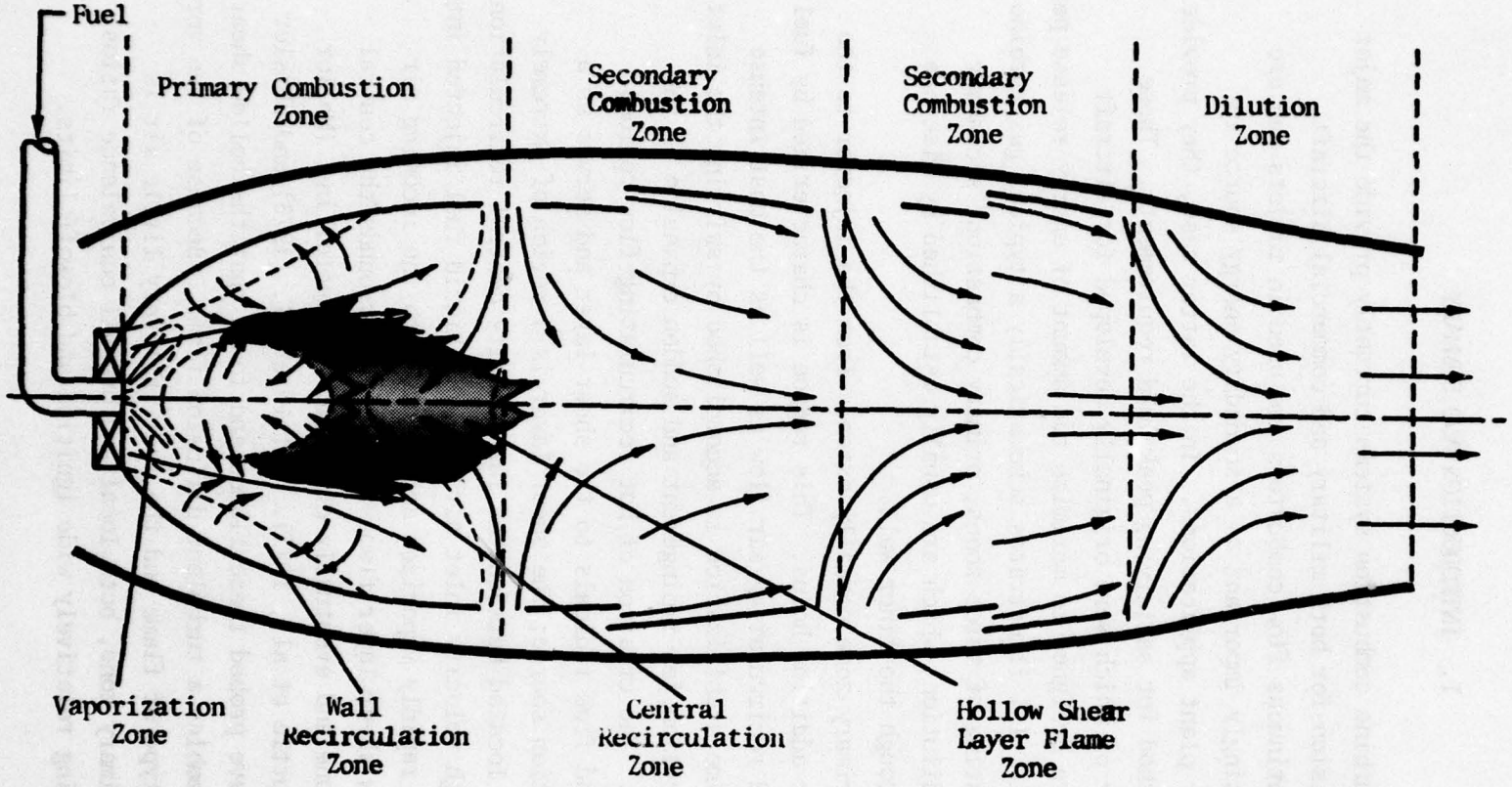

Figure 1-1. Typical gas turbine combustor flow schematic.

CL-648

The combustion process continues to completion in the secondary zone. Here additional air is provided to further oxidize the remaining carbon monoxide and unburned hydrocarbons. Finally, the products of combustion are further cooled in the dilution zone. It is the purpose of this section to lower the exhaust gases to an acceptable temperature for the turbine inlet. Thus, the overall combustor operates quite fuel lean; however, locally high equivalence ratios and temperatures are present in the primary zone. Typical combustion efficiencies for this type of burner are in excess of 99% at full power.

Although local stoichiometric regions provide excellent ignition and blowoff characteristics, they are also the primary source of NO_x since extremely high temperatures are present. Mellor (1976) and Verkamp et al. (1974) have compared the emission levels from conventional combustors with the proposed aircraft emission goals of the future (EPA, 1973; Blazowski and Henderson, 1974) and concluded that major burner modifications are required to meet these new standards. The problem is illustrated in Fig. 1-2 for the EPA class T-2 regulations. Conventional combustors do not appear capable of meeting both the NO_x and CO emission levels simultaneously over their entire operating range; instead, CO quenched by the cold incoming air and NO_x formed in high temperature regions of the flow are problems at idle and maximum power, respectively. Minor burner modifications to conventional combustors only allow movement within the shaded region rather than in a direction toward the origin (Mellor, 1976; Verkamp et al., 1974).

In an effort to simultaneously reduce NO_x and CO levels, advanced combustor concepts involving fuel prevaporization and premixing are currently being considered for aircraft (Roffe and Ferri, 1975 and 1976; Roberts, P. et al., 1976; Niedzwiecki, 1975; Fear, 1976; Roberts, R. et al., 1975 and 1976; Mosier and Roberts, 1974; Bahr, 1975; Gleason et al., 1976; Roffe, 1976), automotive (Spadaccini and Szetela, 1975; Azelborn et al., 1973), ramjet (Stull et al., 1974) and catalytic (Anderson et al., 1975; Blazowski and Bresowar, 1974; Blazowski and

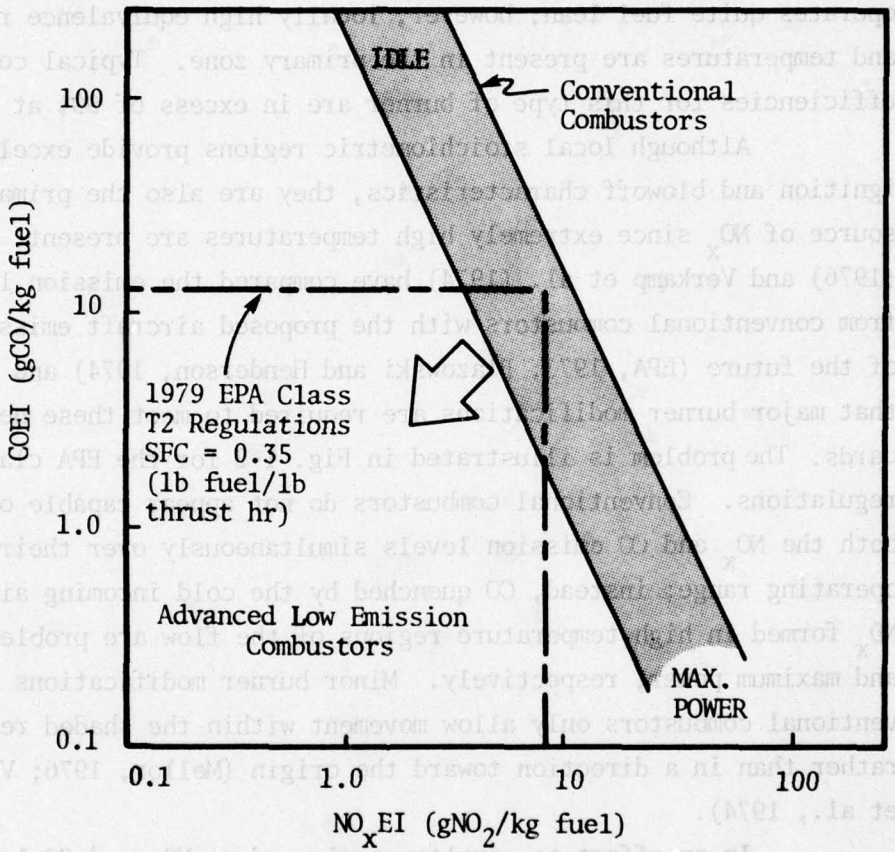

Figure 1-2. Relationship between advanced low emission combustors and conventional combustors vs. 1979 EPA regulations (revised from Verkamp et al., 1974).

Walsh, 1975; Wampler et al., 1976) propulsion systems. Here the combustor of Fig. 1-1 is modified to include a fuel preparation tube located upstream of the primary combustion zone. The sole purpose of the mixing tube is to completely prevaporize the liquid fuel and mix the resulting fuel vapor with air prior to combustion. This not only reduces thermal NO_x substantially (Mellor, 1976; Verkamp et al., 1974) but also leads to reduced smoke and radiation levels as well as improved turbine inlet temperatures (Verkamp et al., 1974) because regions of near stoichiometric equivalence ratio and temperature normally present in conventional combustors are eliminated.

Unfortunately, the absence of high local fuel concentrations and temperatures in the primary combustion zone severely narrows the flame stabilization limits (Verkamp et al., 1974; Roberts, P. et al., 1976; Niedzwiecki, 1975; Roberts, R. et al., 1975 and 1976; Roffe and Ferri, 1976; Anderson, 1975) causing blowoff, ignition and altitude relight problems over the range of normal combustor operating conditions. Furthermore, since the fuel is introduced upstream of the flameholder, flame propagation and autoignition have been observed in the fuel preparation tube (Roffe and Ferri, 1975; Roberts, P. et al., 1976; Niedzwiecki, 1975; Bahr, 1975; Gleason et al., 1976; Roffe, 1976; Anderson et al., 1975; Blazowski and Bresowar, 1974; Blazowski and Walsh, 1975; Wampler et al., 1976; Marek and Papathakos, 1976; Anderson, 1975 and 1976; Craig, 1976; Clayton, 1976; Marek et al., 1977). Problems of incomplete prevaporization and premixing also limit the effectiveness of these combustors. Several investigators (Mellor, 1976; Roffe and Ferri, 1975 and 1976; Roberts, P. et al., 1976; Roberts, R. et al., 1975 and 1976; Mosier and Roberts, 1974; Azelborn et al., 1973; Blazowski and Bresowar, 1974; Altenkirch and Mellor, 1974; Marek and Papathakos, 1976; Tacina, 1976) have found it extremely difficult to prevaporize and premix typical hydrocarbon fuels in a period of milliseconds.

The present study examines problems of blowoff, flashback, incomplete prevaporization and combustion efficiency associated with prevaporizing/premixing combustors using a simplified axisymmetric flameholder configuration (Chapter III). This combustor represents a

compromise between the disc configuration studied by Tuttle et al. (1975, 1976, 1977), the dump ramjet combustor, and the prevaporizing/premixing tube in a turbojet. A fuel preparation tube attached to the front of a disc permits at least partial vaporization of the liquid fuel (injected at the upstream end on the centerline of the tube) prior to combustion. The disc, mounted at the end of the fuel preparation tube, stabilizes the flame by means of a bluff body recirculation zone which is essentially identical to the flame stabilization employed in ramjet and turbojet afterburners. Data obtained include variations in combustor pressure, inlet temperature, velocity, geometry and equivalence ratio. In addition, the degree of prevaporization is also examined by varying injector size and fuel type.

Chapter II introduces the modeling approach, which will be used for the combustion efficiency and flame stabilization data, and shows examples of previous correlations. The model proposed by Mellor (1976) separates the combustion process into heterogeneous, fluid mechanic and chemical effects each of which are characterized by an appropriate time scale and easily computed from combustor inlet conditions. Although these characteristic times are order of magnitude estimates, they can be used to identify the important physical processes occurring in a particular region of the flow field. Tuttle et al. (1977) developed linear correlations for NO_x and CO emissions using a simple disc configuration. Recently, Mellor (1977a,b) and Hammond (1977) have been able to extend these emission models to practical gas turbine combustors. In addition to correlation of existing experimental data, the characteristic time approach has been used to optimize burner design (Mellor, 1977a) and predict quite accurately resulting NO_x and CO emission levels (Hammond, 1977). However the model does not yet consider lean blowoff which was observed under low power conditions (Hammond, 1977) or problems associated with prevaporizing/premixing combustors.

Limited pressure, temperature and velocity measurements were performed (Chapter IV) in the immediate vicinity of the fuel preparation tube to help characterize the flow field for the combustion efficiency

(Chapter V) and flame stabilization (Chapter VI) correlations. In this study, characteristic times for lean blowoff are quantified for the AFOSR configuration as well as data obtained by Ballal and Lefebvre (1977) using a baffle flameholder. Following Zukoski and Marble (1956), the characteristic time model compares a fluid mechanic time which is a function of geometry and velocity, to a fuel ignition delay time. Both times are evaluated in the shear layer region between the recirculation zone established by the disc and the main stream. The result is a linear correlation with a y-intercept near zero as the theory predicts. Analysis of the fluid mechanic time also predicts an optimum flameholder size for stability at a given power setting which is solely a function of housing diameter. In addition, the fluid mechanic time for lean blowoff is identical to the one obtained by Tuttle et al. (1977) for minimum CO emissions; however, chemical times are different. Incomplete vaporization is also included in the model through a heterogeneous droplet evaporation time.

Flame flashback into the fuel preparation tube is also considered in Chapter VI. Plee and Mellor (1977) have reviewed the literature and found that classical flashback has not been observed in non-catalytic combustors burning hydrocarbon fuels. Instead, autoignition of the air stream, flame propagation through reversed flow fields and preignition of the fuel/air mixture in separated flow regions of the mixing tube are responsible for the reported phenomena. Therefore, in non-catalytic combustors, classical flashback can be avoided by eliminating all possible flow disturbances. Only catalytic combustors operating at very low reference velocities appear capable of experiencing classical flashback.

Combustion efficiency measurements have not been completely correlated to date using the characteristic time model (Chapter V). Therefore, detailed internal measurements are planned in the future (Chapter VII) to help characterize regions of combustion inefficiency. These measurements include local species concentration and temperature, as well as velocity magnitude and direction via LDV.

II. CHARACTERISTIC TIME MODEL FOR SPRAY COMBUSTION

Modeling of liquid fueled combustors is an extremely complicated problem involving two phase turbulent flow with chemical reaction. Fluid mechanics, homogeneous kinetics, fuel properties and fuel spray characteristics are all important parameters which control the combustion process. Since simultaneous mathematical modeling of the fluid mechanic, chemical and heterogeneous effects represents a formidable task at the present time, a characteristic time model has been developed as a convenient tool for correlating and predicting continuous combustor* behavior.

Other phenomenological models for high intensity gas turbine combustors exist. However, the characteristic time model appears capable of including effects of changes in not only inlet conditions, but also combustor geometry on gaseous emissions, and thus due to space limitations will receive primary attention here. The interested reader is referred to recent reviews by Odgers (1975) and Hammond and Mellor (1970) for description of other such models. A complete model would also predict smoke emissions, local heat flux to the wall, lean blowoff limit, combustor exhaust plane temperature profile (pattern factor) and so on.

The characteristic time model separates spray combustion into three subprocesses which include 1) vaporization of the liquid fuel droplets, 2) mixing of the fuel vapor with air, and 3) combustion of the resulting fuel/air mixture. Each of these subprocesses must occur before combustion is complete. According to Mellor (1976), these subprocesses can be represented by characteristic times (Table 2-1) which control emissions, performance and flame stabilization.

*E.g., as in turbojets and ramjets.

A. Characteristic Times

The first time (τ_{eb}) listed in Table 2-1 is the fuel droplet lifetime which determines the heterogeneous properties of the combustion process. This time is a function of nozzle characteristics, fuel properties, fuel flow rate and ambient combustor conditions. For a properly designed injector and combustor, τ_{eb} should be negligible (Mellor, 1977a,b).

The second and third characteristic times refer to fluid mechanic mixing processes occurring in the flow field. τ_{fi} represents the mixing process in the region of the fuel injector which is expected to be important in combustors utilizing air blast and air assist nozzles to decrease smoke emissions. Only gaseous emissions are of concern in the present work (but see Dodds et al., 1976); therefore, τ_{fi} will be omitted from further discussion.

Table 2-1. Characteristic Times for Combustion and Pollutant Formation in Two-phase Turbulent Flow (from Mellor, 1976)

Time	Symbol	Physical or Chemical Processes
Fuel droplet lifetime	τ_{eb}	Droplet evaporation and/or combustion
Eddy dissipation time for injected fluid	τ_{fi}	Small scale turbulent mixing near the fuel injector in the recirculation zone
Eddy dissipation time in the shear layer	$\tau_{s\ell}$	Large scale turbulent mixing between fresh air and the recirculating burned gas-fuel mixture
Fuel ignition delay and burning time	τ_{hc}	Homogeneous combustion of the fuel to CO_2
NO formation time	τ_{no}	Homogeneous kinetics for NO formation

$\tau_{s\ell}$ characterizes the turbulent mixing process in the shear layer between the fresh incoming air and the recirculated burned

gas-fuel mixture. For premixed/prevaporized combustors, this mixing time in the shear layer would refer to the turbulent heat transfer between the incoming mixture and the hot burned gases which hold the flame.

The last two times, τ_{hc} and τ_{no}, listed in Table 2-1 represent homogeneous kinetic times for the combustion of the fuel and NO formation. These processes occur after the fuel and oxidizer have been mixed on a molecular level and are functions of the local equivalence ratio, temperature and combustor pressure. τ_{hc} may be used to characterize CO and HC oxidation (combustion efficiency) or HC ignition delay time (blowoff and flashback). Examples of previous work utilizing the characteristic time model follow.

B. Applications of the Model--Disc-in-Duct Burner

Under EPA sponsorship Tuttle et al. (1976) have extensively studied exhaust pollutant emissions for the configuration shown in Fig. 2-1, an axisymmetric disc-in-duct burner with liquid fuel injection via a hollow cone spray nozzle mounted at the center of the disc. Inlet air temperature, pressure, air and fuel flow rates, fuel and nozzle type and disc geometry (diameter and in some cases teeth on the outer circumference) all were varied. Gas sampling and temperature measurements were also made at various points inside the combustor and used to develop the flow model shown in Fig. 2-2. Note that the region of HC and CO quenching is separate from the region of NO formation.

The correlations are developed from the characteristic times as follows, assuming for the moment that the droplet evaporation time τ_{eb} is negligible compared to the shear layer mixing time $\tau_{s\ell}$: for a near-stoichiometric eddy capable of forming NO, just downstream of the recirculation zone shown in Fig. 2-2

$$\left.\frac{d[NO]}{dt}\right|_{eddy} = 2k_1[O][N_2] \qquad 2\text{-}1$$

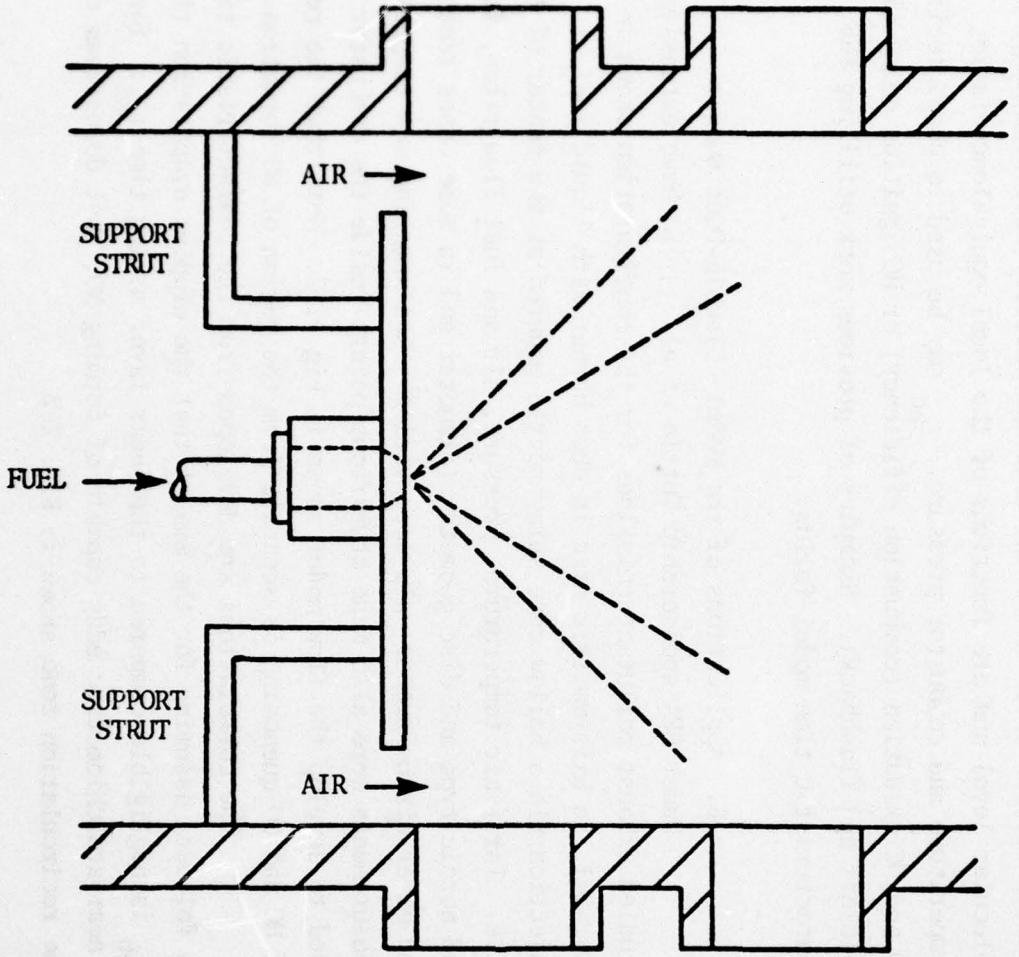

Figure 2-1. Schematic of disc mounting arrangement (Tuttle et al., 1976).

CL-726

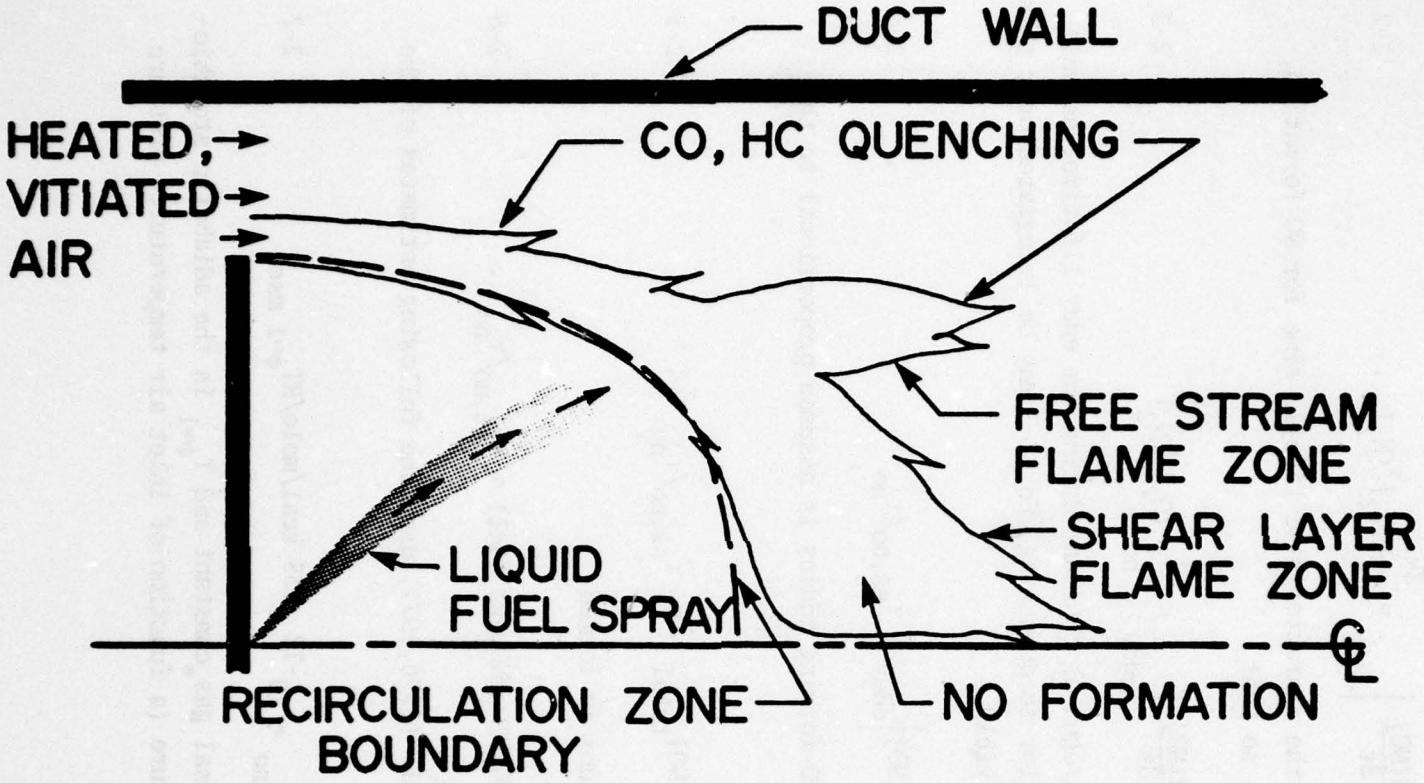

Figure 2-2. Burner and flame schematic (Tuttle et al., 1976).

where the Zeldovich mechanism is assumed to apply and where k_1 refers to $O + N_2 \rightarrow NO + N$. Invoking $O \rightleftarrows \frac{1}{2}O_2$ equilibrium with equilibrium constant K

$$\left.\frac{d[NO]}{dt}\right|_{eddy} = \frac{2k_1}{K}[O_2]^{\frac{1}{2}}[N_2] \quad . \tag{2-2}$$

τ_{no} by definition is the characteristic kinetic time for NO formation, proportional to K/k_1, so that

$$\left.\frac{d[NO]}{dt}\right|_{eddy} \sim \frac{1}{\tau_{no}}\,[O_2]^{\frac{1}{2}}[N_2] \quad . \tag{2-3}$$

Taking oxygen and nitrogen as constant during the eddy lifetime, as well as its temperature prior to quenching, Eq. 2-3 may be integrated over this lifetime, $\tau_{s\ell,no}$, to yield

$$[NO]\Big|_{eddy} \sim \tau_{s\ell,no}/\tau_{no} \quad . \tag{2-4}$$

The total number of NO-forming eddies is assumed proportional to the total fuel flow $\dot{m}_f$

$$[NO]_{total} \sim \dot{m}_f\, \tau_{s\ell,no}/\tau_{no} \quad . \tag{2-5}$$

Thus the emissions index is formed

$$NO_x EI\ (g\,NO_2/kg\ fuel) \sim \tau_{s\ell,no}/\tau_{no} \quad . \tag{2-6}$$

Tuttle et al. (1976,1977) used the following estimates of the characteristic times

$$\tau_{no} = 10^{-12}\, e^{135\ kcal/mole/RT_{\phi=1}}\ msec \tag{2-7}$$

where R is the universal gas constant and $T_{\phi=1}$ is the adiabatic stoichiometric flame temperature (a function of inlet air temperature, pressure and fuel type).

$$\tau_{s\ell,no} = d/V_{bg} \qquad 2\text{-}8$$

where d is disc diameter and V_{bg} is an estimated velocity downstream of the recirculation zone in Fig. 2-2. Their correlation is shown in Fig. 2-3 for liquid propane injection (negligible heterogeneous effects); r, the correlation coefficient, is a measure of the goodness of the least squares fit shown in the figure and equals one in the ideal case; σ is the standard deviation.

As droplet evaporation times were increased (Jet A fuel), NO_xEI decreased, most likely since fuel drops were thrown into the relatively cold free stream flame zone in Fig. 2-2. Tuttle et al. (1977) thus chose to correlate the results in terms of

$$NO_xEI \sim \tau_{s\ell,no}/(\tau_{no} + a\tau_{eb}) \qquad 2\text{-}9$$

with a determined empirically. The combined correlation for the two fuels is shown in Fig. 2-4.

Droplet evaporation times, τ_{eb}, were estimated as follows: the basic physical relation which governs either droplet evaporation or combustion is the "d^2 law" of Godsave (1953)

$$d_f^2 = d_o^2 - \beta_c t \qquad 2\text{-}10$$

where d_f = instantaneous fuel droplet diameter
d_o = initial droplet diameter
β_c = evaporation or combustion coefficient in the combustion region
t = time.

By allowing d_f to become zero, the characteristic time for droplet evaporation or combustion derived from Eq. 2-10 is

$$\tau_{eb} = \frac{d_o^2}{\beta_c} \quad . \qquad 2\text{-}11$$

d_o is a function of the fuel injector type, fuel properties and fuel flow rate while β_c is a function of fuel properties and ambient combustor

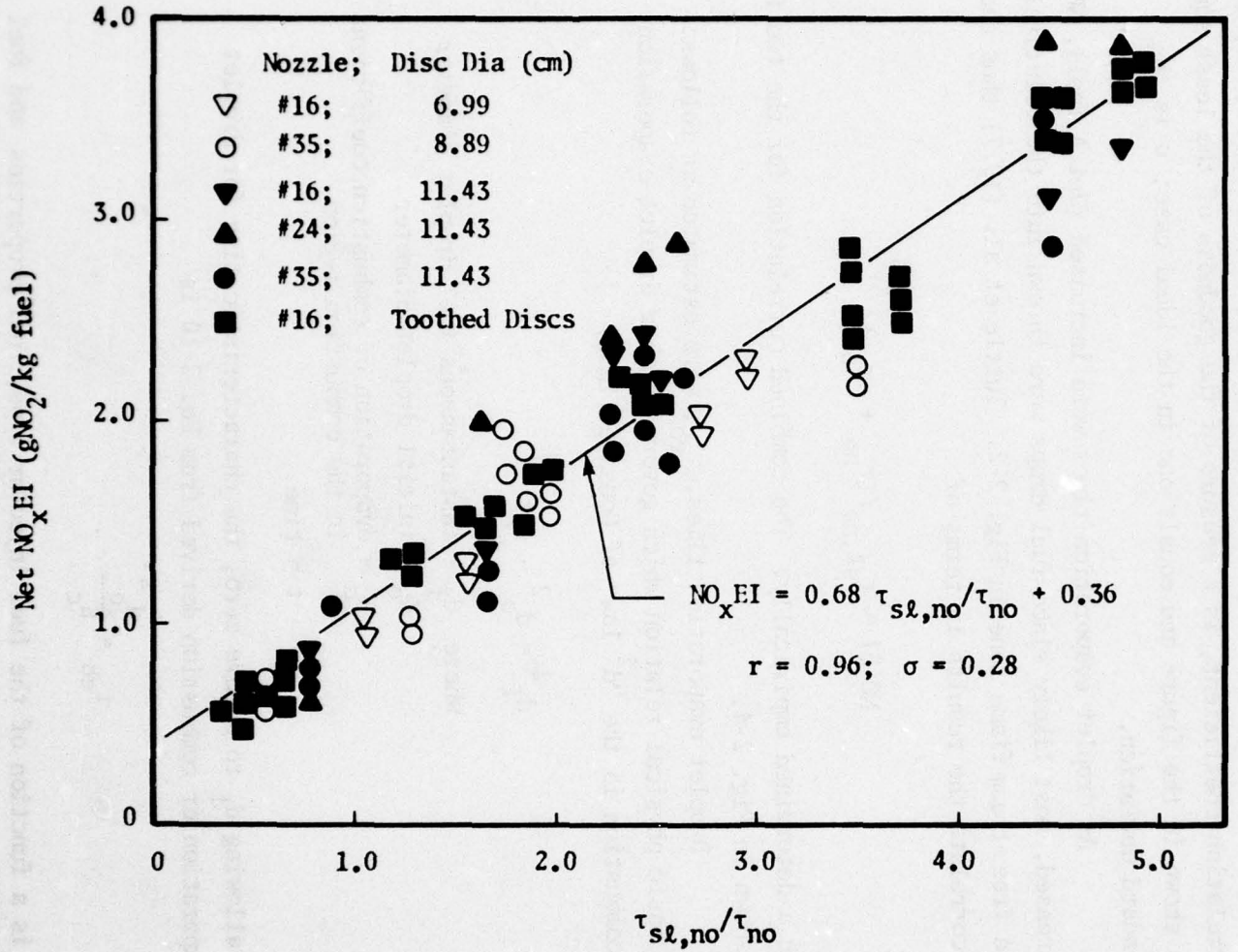

Figure 2-3. NO_xEI versus $\tau_{s\ell,no}/\tau_{no}$ (propane fuel) (Tuttle et al., 1976).

CL-659

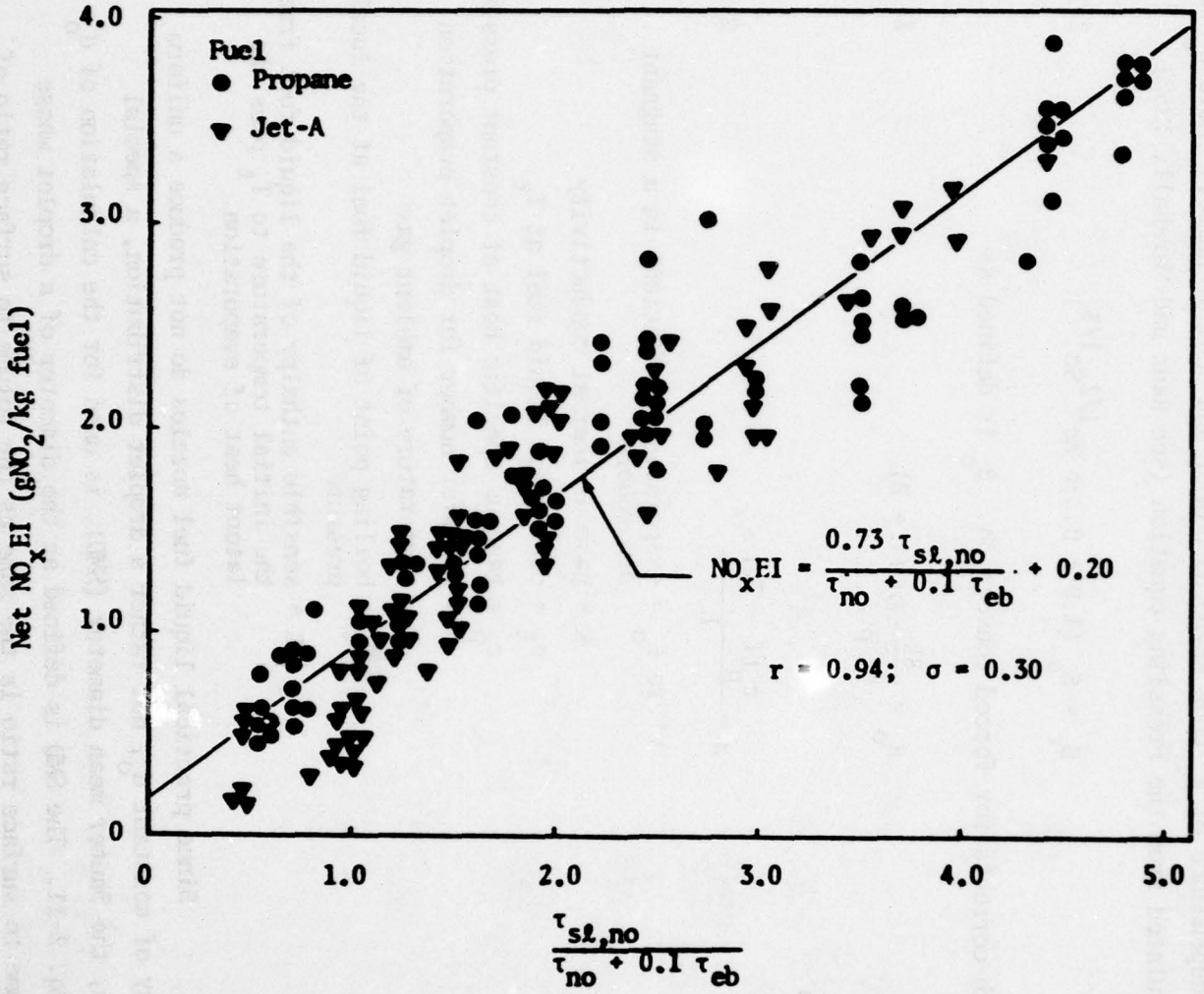

Figure 2-4. Correlation of all disc burner NO_xEI data (Tuttle et al., 1976).

CL-686

conditions. For a convective atmosphere, β_c is also related to the Reynolds number (based on mean droplet size and droplet relative velocity) and the Schmidt number.

Mellor (1972) has summarized several empirical relationships for the dependence of β_c upon Reynolds number and Schmidt number. Here β_c was calculated from the Frössling equation (see Ranz and Marshall, 1952)

$$\beta_c = \beta_o \, (1.0 + 0.276 \, Re^{1/2} Sc^{1/3}) \qquad 2\text{-}12$$

which corrects for forced convection. β_o is defined as

$$\beta_o = \frac{8k}{\rho_\ell c_p} \ell n \, (1 + B) \qquad 2\text{-}13$$

with

$$B = \frac{c_p (T - T_\ell)}{L} \qquad 2\text{-}14$$

where β_o = evaporation coefficient in a stagnant atmosphere

k = gaseous thermal conductivity

ρ_ℓ = density of liquid fuel at T_ℓ

c_p = gaseous specific heat at constant pressure

B = transfer number for droplet evaporation

T = temperature of ambient gas

T_ℓ = boiling point of liquid fuel at the local pressure

L = sensible enthalpy of the liquid fuel from the initial temperature to T_ℓ plus the latent heat of evaporation.

Since practical liquid fuel nozzles do not produce a uniform spray of constant d_o, but rather a droplet distribution, a special mean, the Sauter mean diameter (SMD), is used for the calculation of d_o in Eq. 2-11. The SMD is defined as the diameter of a droplet whose volume to surface ratio is the same as the volume to surface ratio of the entire spray. Thus, the SMD is a measure of the degree of atomization and can be computed via empirical relations which are summarized in Tuttle et al. (1975). For the simplex pressure atomizing nozzles in that study,

the empirical equation of Hunter et al. (1974) shown below was used to calculate the initial droplet diameter

$$SMD = \frac{90.5\nu^{.3}\,\rho^{.205}\,Q^{.205}}{\Delta P^{.354}} \qquad 2\text{-}15$$

where SMD = Sauter mean diameter, micron
ν = viscosity, centistoke
ρ = density, gm/cm^3
Q = volumetric flow rate, lit/hr
ΔP = nozzle differential pressure, atm.

CO emissions, which contribute to combustion inefficiency, were correlated in a similar fashion. For lean eddies in which CO (and HC) oxidation is quenched (near the disc edge)

$$\frac{d[CO]}{dt} = -k_2[CO][OH] \qquad 2\text{-}16$$

where k_2 refers to $CO + OH \rightarrow CO_2 + H$. Again, the characteristic time for CO oxidation is taken as

$$\tau_{co} \sim 1/k_2 \qquad 2\text{-}17$$

but was obtained empirically from the data of Tuttle et al. (1977) in terms of inlet air temperature T_{in}

$$\tau_{co} = e^{2200\ \text{cal/mole}/RT_{in}}\ \text{msec} \quad . \qquad 2\text{-}18$$

Arbitrarily assuming [OH] constant during the oxidation process yields from Eq. 2-16

$$\frac{d[CO]}{[CO]} \sim -\frac{dt}{\tau_{co}} \quad . \qquad 2\text{-}19$$

Integrating over the eddy lifetime at the outer edge of the shear layer ($\tau_{s\ell,co}$)

$$\ell n \frac{[CO]}{[CO]_i} \sim -\tau_{s\ell,co}/\tau_{co} \qquad 2\text{-}20$$

$$[CO]/[CO]_i = e^{-\tau s\ell,co/\tau co} \qquad 2\text{-}21$$

where $[CO]_i$ is the initial CO concentration within the eddy, taken proportional to fuel flow rate so that

$$[CO]/[CO]_i \sim COEI \text{ (g CO/kg fuel)} \quad . \qquad 2\text{-}22$$

Tuttle et al. (1976) expanded the exponential into an equivalent power series in $\tau_{co}/\tau_{s\ell,co}$ and found that a two term approximation was adequate

$$COEI \sim b + c\ \tau_{co}/\tau_{s\ell,co} \qquad 2\text{-}23$$

where for the parameter ranges of interest

$$b << c\ \tau_{co}/\tau_{s\ell,co}$$

and hence

$$COEI \text{ (g CO/kg fuel)} \sim \tau_{co}/\tau_{s\ell,co} \quad . \qquad 2\text{-}24$$

The mixing time in the CO quenching region of the flow (Fig. 2-2) is taken as disc diameter* divided by cold air velocity in the annulus surrounding the disc, V_a

$$\tau_{s\ell,co} = d/V_a \quad . \qquad 2\text{-}25$$

Corresponding results for C_3H_8 fuel are shown in Fig. 2-5.

When Jet A was burned in the disc-in-duct configuration, combustion inefficiency increased due to the effective increase in droplet lifetime with this heavier fuel and the consequent penetration of droplets

*For discs with teeth a more complicated scale factor was required; see Tuttle et al. (1976).

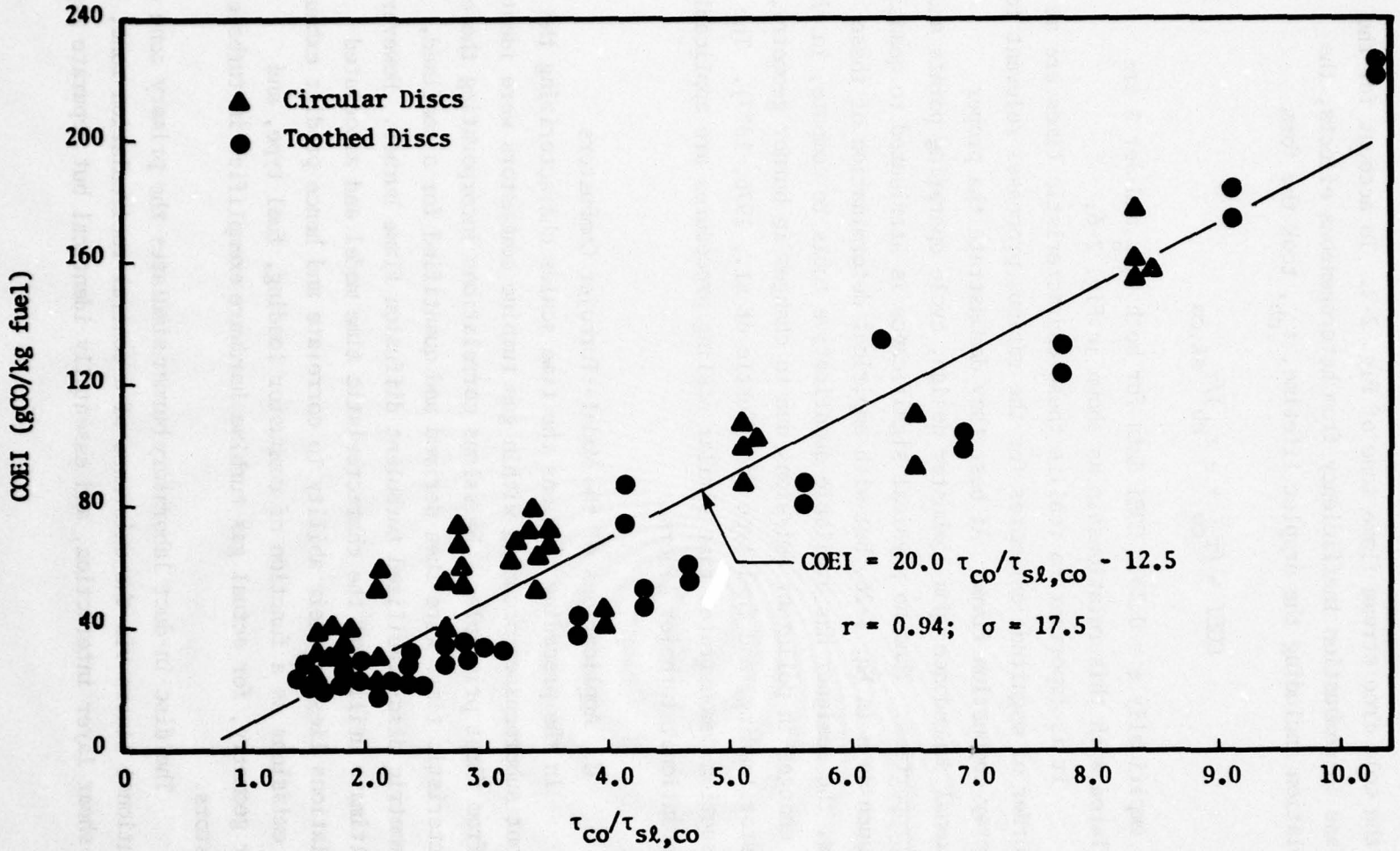

Figure 2-5. **COEI versus $\tau_{co}/\tau_{s\ell,co}$ (propane fuel)** (Tuttle et al., 1976).

CL-663

into the cold free stream flame zone of Fig. 2-2. To account for the increase in combustion inefficiency from heterogeneous effects, the correlation including the droplet lifetime, τ_{eb}, took the form

$$COEI \sim (\tau_{co} + e\,\tau_{eb})/\tau_{s\ell,co} \qquad 2\text{-}26$$

where empirically e = 0.24. COEI data for both C_3H_8 and Jet A are correlated with this relationship as shown in Fig. 2-6.

It is important to realize these characteristic times are at most order of magnitude estimates for the various processes relevant to the spray combustion flame. At best they demonstrate the proper functional dependence upon combustor design, cycle operating points and fuel properties. Thus no physical significance is attributed to quantities such as e in Eq. 2-26, but with empirical determination of these values, the designer has available quantitative tools to compute, in this case, changes in pollutant emissions due to changes in burner geometry, combustor loading, and fuel type (see Tuttle et al., 1976, 1977). The next section demonstrates that similar scaling procedures are applicable to conventional turbojet liners.

C. Applications of the Model--Turbojet Combustors

In the preceding sections the time scales characterizing the dominant subprocesses occuring within gas turbine combustors were identified from first principles. Emissions correlations incorporating these characteristic times were then derived and quantified for a confined, axisymmetric disc-stabilized turbulent diffusion flame burner. However, the ultimate utility of the characteristic time model and associated correlations lies in their ability to correlate and hence predict exhaust plane emissions as a function of combustor loading, fuel type, and burner geometry, for actual gas turbine hardware exemplified in turbojet combustors.

The disc-in-duct laboratory burner simulates the primary zone of conventional liners via the existence of a central recirculation zone, fuel spray-shear layer interaction, and essentally identical but separate regions

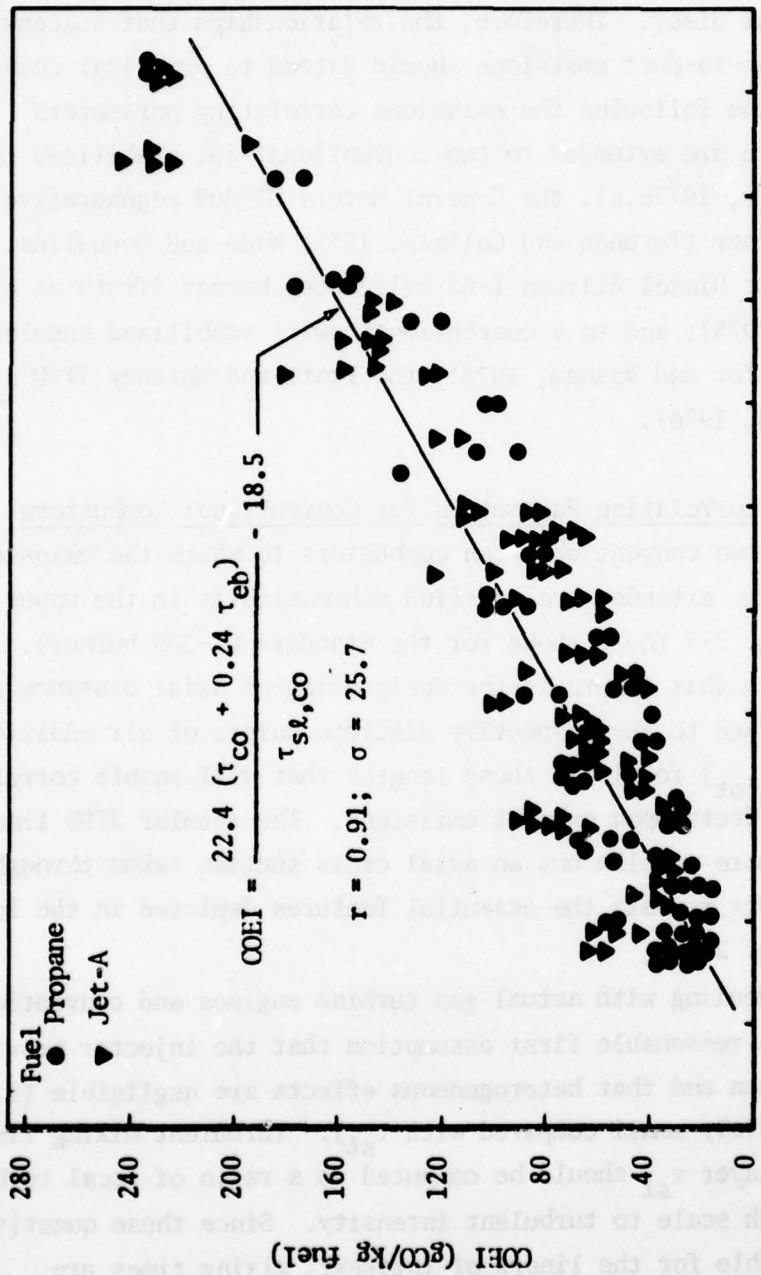

Figure 2-6. Correlation of all disc burner COEI data (Tuttle et al., 1976).

CL-687

of high concentrations of NO and combustion inefficiency (see Fig. 2-2). That is, in a conventional combustor (see for example Mellor, 1976) NO generally forms just downstream of the recirculation zone(s), whereas HC and CO quench as a result of air addition through the liner walls (air addition for the disc-in-duct burner is limited to the annulus surrounding the disc). Therefore, the relationships that successfully correlated disc-in-duct emissions should extend to practical combustors.

In the following the emissions correlating parameters developed above are extended to two conventional jet stabilized can combustors (Mellor, 1977a,b): the General Motors GT-309 regenerative automotive burner (Turunen and Collman, 1965; Wade and Cornelius, 1972) and the Detroit Diesel Allison T-63 helicopter burner (Troth et al., 1973, 1974; Moses, 1975); and to a conventional swirl stabilized annular combustor (Mellor and Washam, 1978), the Pratt and Whitney JT9D aircraft burner (Nelson, 1976).

1. Emissions Correlating Parameters for Conventional Combustors

The two conventional can combustors to which the emissions correlations are extended are typified schematically in the upper portion of Fig. 2-7 (here shown for the standard GT-309 burner). Of significance in this figure is the designation of axial distance from the injector face to the respective discrete points of air addition (i.e., $\ell_{hole,slot}$) for it is these lengths that will enable correlation of geometry effects upon exhaust emissions. The annular JT9D liner is considerably more complex but an axial cross section taken through one of the injectors reveals the essential features depicted in the lower portion of Fig. 2-7.

In dealing with actual gas turbine engines and conventional fuels, it is a reasonable first assumption that the injector provides good atomization and that heterogeneous effects are negligible (i.e., τ_{eb} is effectively small compared with $\tau_{s\ell}$). Turbulent mixing times in the shear layer $\tau_{s\ell}$ should be computed as a ratio of local turbulence integral length scale to turbulent intensity. Since these quantities are not available for the liners of interest, mixing times are evaluated as proportional to the ratio of a significant macrodimension

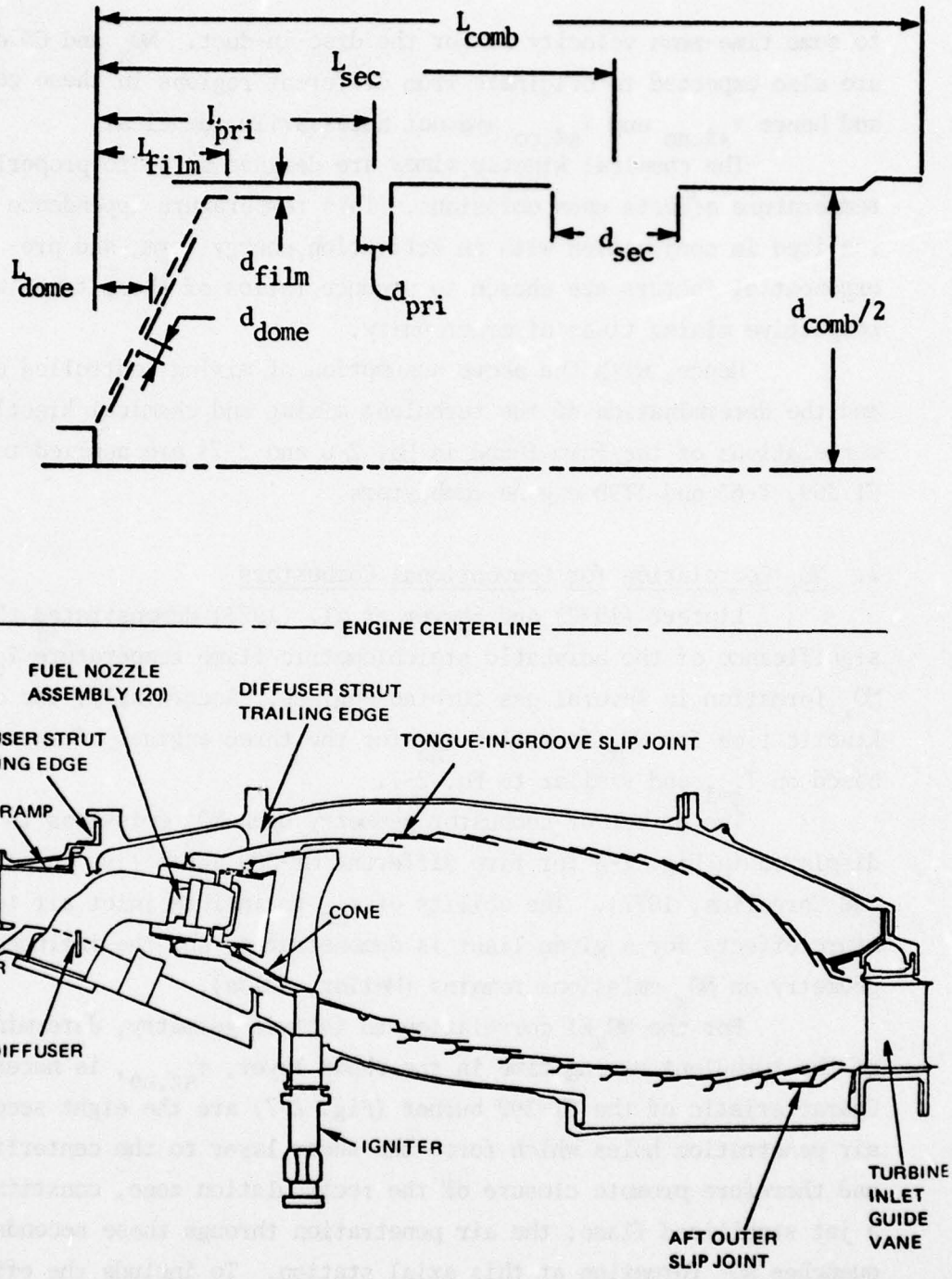

CL-899

Figure 2-7. Schematic of the standard GT-309 can (upper) and JT9D annular (lower) combustors.

to some time-mean velocity as for the disc-in-duct. NO_x and CO emissions are also expected to originate from different regions in these combustors and hence $\tau_{s\ell,no}$ and $\tau_{s\ell,co}$ are not necessarily identical.

The chemical kinetic times are defined so as to properly include temperature effects upon emissions. This temperature dependence is realized in conjunction with an activation energy term, and pre-exponential factors are chosen to produce ratios of these times with respective mixing times of order unity.

Hence, with the above assumption of mixing controlled combustion and the determination of the turbulent mixing and chemical kinetic times, correlations of the form found in Eq. 2-6 and 2-24 are applied to the GT-309, T-63 and JT9D engine combustors.

2. NO_x Correlation for Conventional Combustors

Lipfert (1972) and Sawyer et al. (1973) demonstrated the significance of the adiabatic stoichiometric flame temperature $T_{\phi=1}$ on NO_x formation in several gas turbine engines. Accordingly, the chemical kinetic time for NO_x formation τ_{no} for the three engines of interest is based on $T_{\phi=1}$ and similar to Eq. 2-7.

The effect of combustor geometry upon NO_x emissions is displayed in Fig. 2-8 for five different GT-309 automotive burners (Wade and Cornelius, 1972). The ability of τ_{no} to include inlet air temperature effects for a given liner is demonstrated, but the influence of geometry on NO_x emissions remains (Mellor, 1977a).

For the NO_xEI correlation to include geometry, determination of the turbulent mixing time in the shear layer, $\tau_{s\ell,no}$, is necessary. Characteristic of the GT-309 burner (Fig. 2-7) are the eight secondary air penetration holes which force the shear layer to the centerline and therefore promote closure of the recirculation zone, constituting a jet stabilized flame; the air penetration through these secondary jets quenches NO_x formation at this axial station. To include the effect of burner diameter it was necessary to assume for the NO_x macroscale

$$\ell_{no}^{-1} \equiv \ell_{sec}^{-1} + d_{comb}^{-1} \qquad 2\text{-}27$$

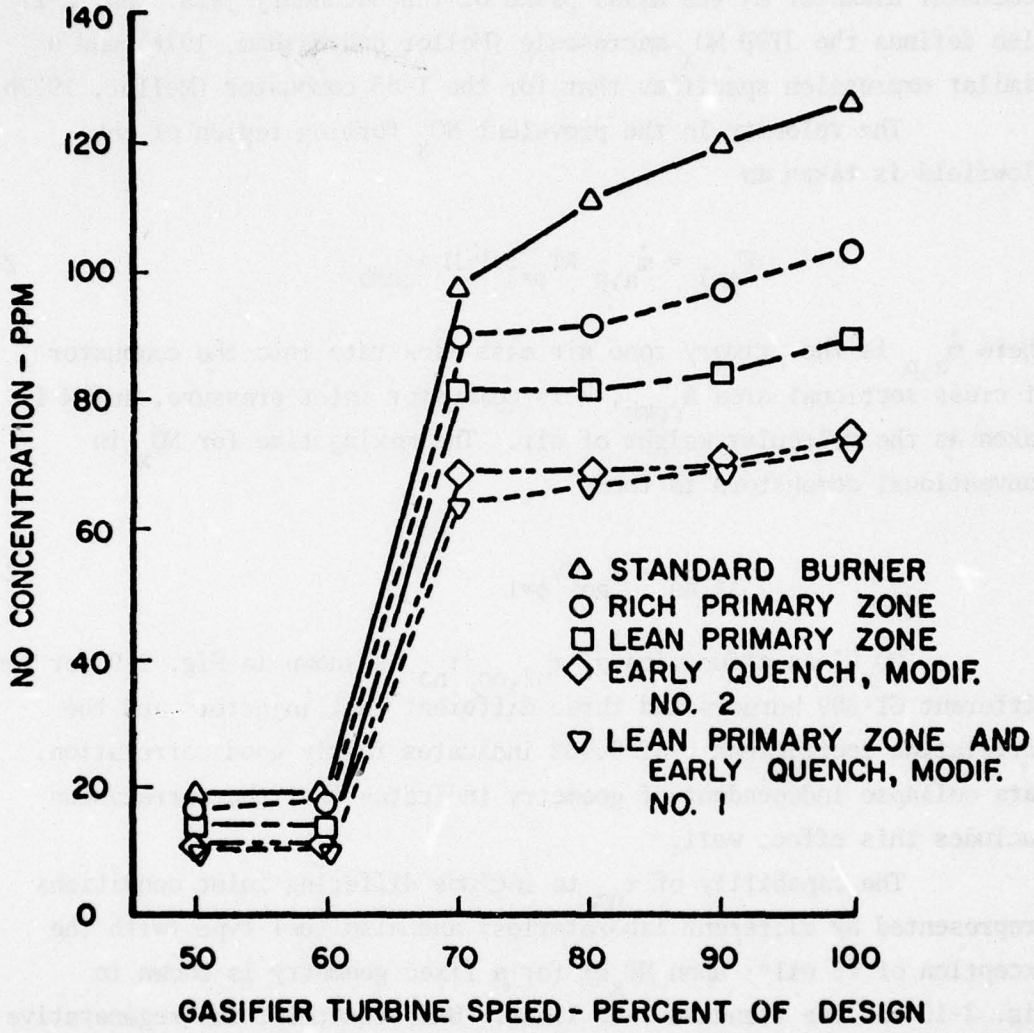

Figure 2-8. NO (ppm) versus percent of design power for five GT-309 burners (from Wade and Cornelius, 1972).

CL-672

where ℓ_{sec} is the axial distance from the point of fuel injection to the centerline of the secondary hole row (see Fig. 2-7) and d_{comb} is combustor diameter at the axial plane of the secondary jets. Eq. 2-27 also defines the JT9D NO_x macroscale (Mellor and Washam, 1978) and a similar expression specifies that for the T-63 combustor (Mellor, 1977b).

The velocity in the prevalent NO_x forming region of the flowfield is taken as

$$V_{\phi=1} = \dot{m}_{a,p} RT_{\phi=1}/P M A_{comb} \qquad 2\text{-}28$$

where $\dot{m}_{a,p}$ is the primary zone air mass flow rate into the combustor of cross sectional area A_{comb}, P is combustor inlet pressure, and M is taken as the molecular weight of air. The mixing time for NO_x in conventional combustors is then

$$\tau_{s\ell,no} = \ell_{no}/V_{\phi=1} \quad . \qquad 2\text{-}29$$

$NO_x EI$ as a function of $\tau_{s\ell,no}/\tau_{no}$ is shown in Fig. 2-9 for ten different GT-309 burners and three different fuel injectors and the correlation coefficient r of 0.932 indicates fairly good correlation. Data collapse independent of geometry indicates that the correlation includes this effect well.

The capability of τ_{no} to include differing inlet conditions (represented by different laboratories) and also fuel type (with the exception of #5 oil*) upon $NO_x EI$ for a fixed geometry is shown in Fig. 2-10 for the standard T-63 liner. Unfortunately, the regenerative cycle was not as effectively correlated. Furthermore, in that nozzle variations also collapsed to the curve (within the scatter) for the T-63 and GT-309 (Fig. 2-9) combustors confirms the initial assumption that for these injectors distributing the listed fuels (DF2 was the only fuel burned in the GT-309), the flame remains mixing controlled (i.e., $\tau_{s\ell,no} >> \tau_{eb}$). Note that the #5 oil is the only fuel of those listed with substantial fuel-bound nitrogen. Geometry effects for

*It is the convention here to flag data that are excluded from the least squares fit.

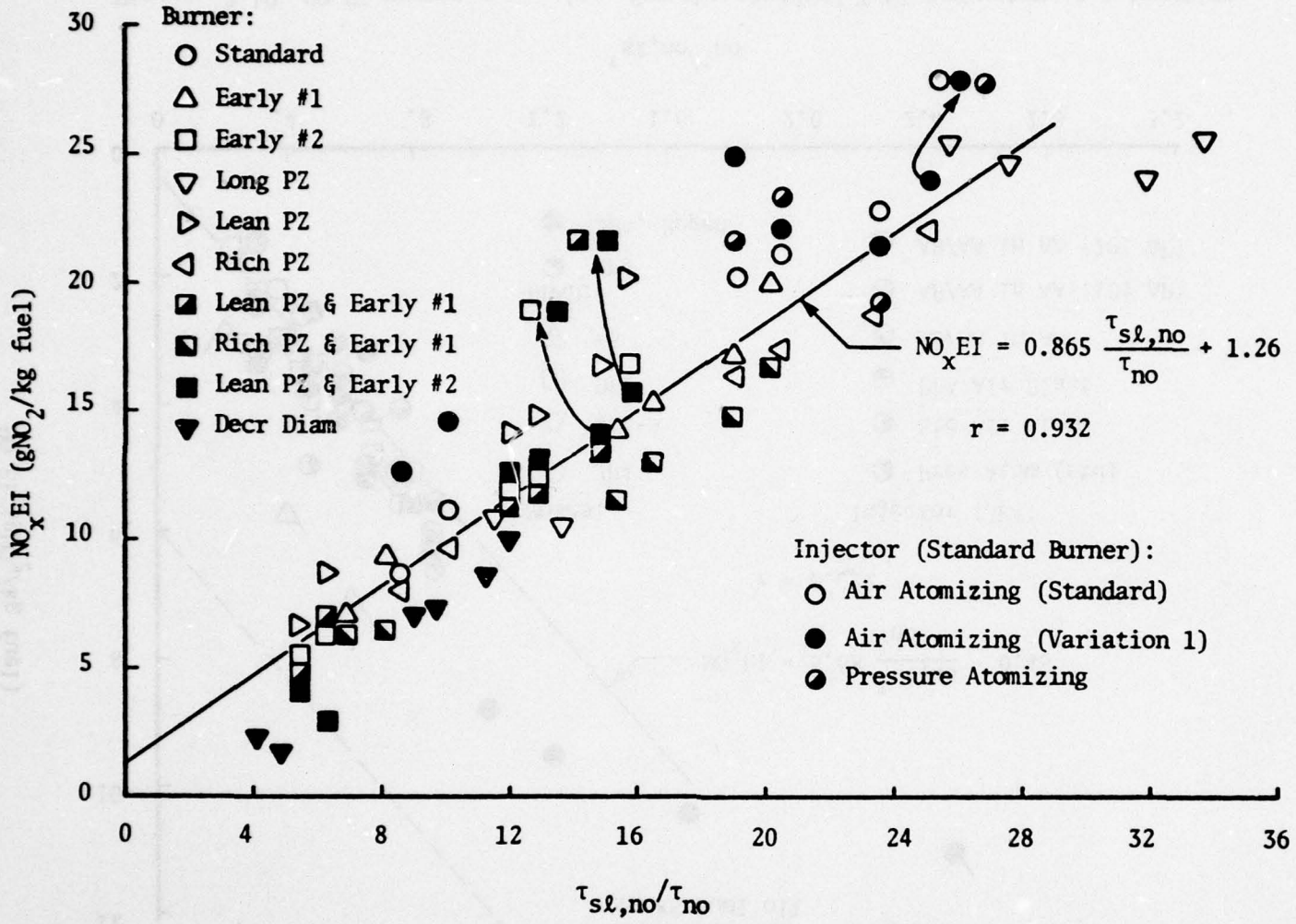

Figure 2-9. $NO_x EI$ versus $\tau_{s\ell,no}/\tau_{no}$ for ten GT-309 burners and three fuel injectors (Mellor, 1977a).

CL-674

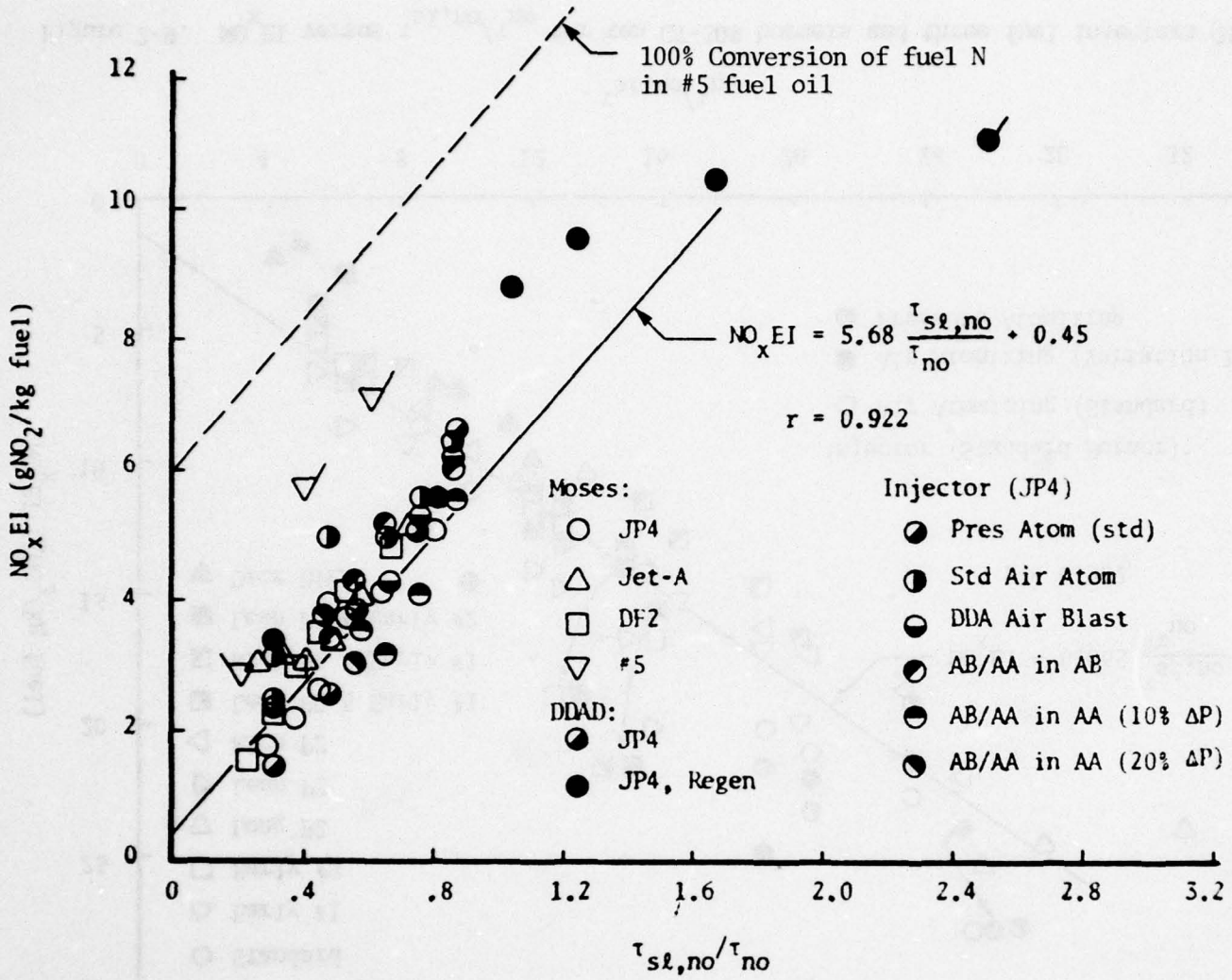

Figure 2-10. NO_xEI versus $\tau_{s\ell,no}/\tau_{no}$ for the standard T-63 combustor as a function of fuel and injector type (modified from Mellor, 1977b).

CL-688

conventional T-63 combustors were correlated with a result similar to that shown in Fig. 2-9 (see Mellor, 1977b). NO_xEI data from the JT9D Mod II combustor geometry also correlated quite well with $\tau_{s\ell,no}/\tau_{no}$. Data supplied indicated that τ_{no} also includes the effect of ambient humidity upon NO_x emissions (Mellor and Washam, 1978).

3. CO Correlation for Conventional Combustors

In a gas turbine combustor it is the discrete addition of cooler inlet air through penetration holes and film cooling slots that quenches the CO oxidation reaction in the outer regions of the spray flame. The aerothermodynamic parameters in this region of the liner flowfield then are incorporated in the CO emissions correlations for engines.

The kinetic time for CO oxidation τ_{co} in liners is a function of the adiabatic burned gas temperature at the overall equivalence ratio, T_b. Results reported for the GT-309 combustor series gave (Mellor, 1977a)

$$\tau_{co} = 10^{-1} \exp (7700 \text{ cal/mole}/RT_b) \text{ msec} \qquad 2\text{-}30$$

whereas those for the T-63 configurations required the mean of inlet air and burned gas temperatures $\bar{T}$ in the CO kinetic time (Mellor, 1977b) such that

$$\tau_{co} = 10^{-3} \exp(10{,}760 \text{ cal/mole}/R\bar{T}) \text{ msec} \quad . \qquad 2\text{-}31$$

Since the burned gas temperature is primarily a function of inlet air temperature, equivalence ratio and fuel type, these effects upon CO emissions are included through τ_{co}. Evidence of this is provided in Fig. 2-11 where COEI data corresponding to different operating conditions and four different fuels for the standard T-63 liner are plotted versus $\tau_{co}/\tau_{s\ell,co}$. With the exception of #2 Diesel fuel and #5 oil (flagged in this figure), data for JP4 and Jet A collapsed to the mixing controlled correlation independent of injection scheme signifying

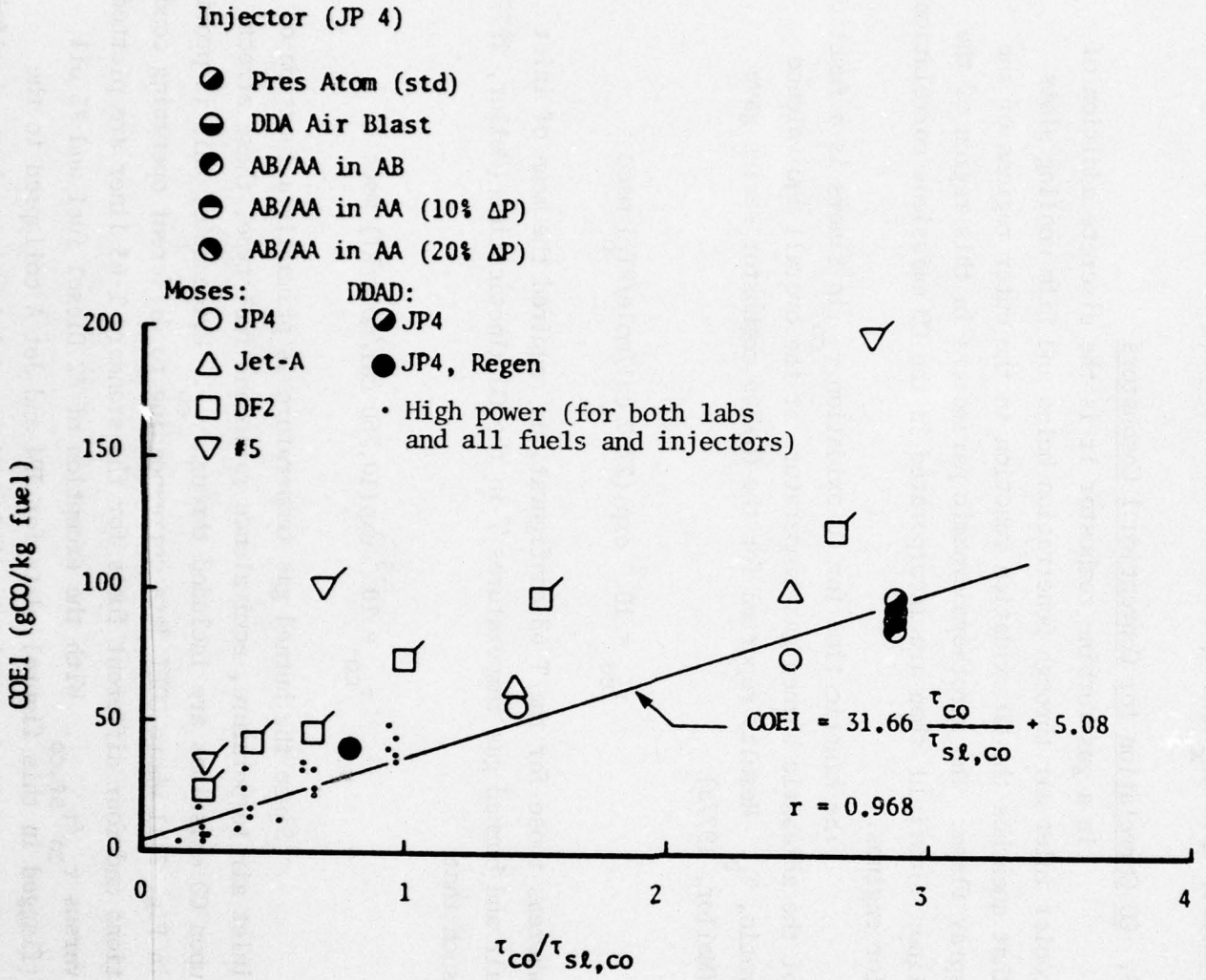

Figure 2-11. COEI vs. $\tau_{co}/\tau_{s\ell,co}$ for standard T-63 combustor as a function of fuel and injector type (from Mellor, 1977b).

CL-682

that heterogeneous effects for these cases are negligible. Different inlet conditions (the two laboratories) as well as both non- and regenerative cycles are also collapsed by the correlation. The increase in combustion inefficiency with #2 Diesel fuel and #5 oil is attributable to the significant droplet effect associated with these relatively heavier fuels (Mellor, 1977b).

Determination of $\tau_{s\ell,co}$ will permit inclusion of geometry effects upon CO emissions. The CO macroscale for liners ℓ_{co} is identical in form to that for NO_xEI given previously, where axial and radial influences are included through

$$\ell_{co}^{-1} \equiv \ell_{quench}^{-1} + d_{comb}^{-1} \quad . \qquad 2\text{-}32$$

However, the CO macroscale exhibits somewhat more complicated behavior than that for NO_x. Specifically, the GT-309 combustor series experienced an axial quench shift for CO with power setting (i.e., ℓ_{quench} decreased with decreasing engine power). For high power (70 to 100% of design) CO quenched in the vicinity of the secondary holes. Hence, for high power, ℓ_{co} was based upon ℓ_{sec}. At low power (50 to 60% of design) CO quenched in either the region of the dome holes, film cooling slot or the primary holes depending upon combustor configuration (geometry). ℓ_{co} for low power conditions, then, was based on ℓ_{dome}, ℓ_{film}, or ℓ_{pri} (Mellor, 1977a). Several T-63 configurations also demonstrated this axial CO quench shift with power.

The turbulent intensity relevant to CO quenching in the GT-309 burners was taken as proportional to the mean air injection velocity through the holes and slots in the liner (Mellor, 1977a)

$$V_{a,holes} = \dot{m}_a RT_{in}/P\,M\,A_{holes} \qquad 2\text{-}33$$

where A_{holes} is the total open area of the particular combustor. In the T-63 series combustors turbulent intensity scaled with combustor reference velocity instead of air injection velocity

$$V_{ref} = \dot{m}_a RT_{in}/P\ M\ A_{comb} \quad . \qquad 2\text{-}34$$

That is, for the T-63 burners, no dependence of COEI on liner open area was found (Mellor, 1977b). Geometry effects upon CO emissions from these two liners are thus included by

$$\tau_{s\ell,co} = \frac{\ell_{co}}{V_{a,holes}\Big]_{GT\text{-}309} \text{ or } V_{ref}\Big]_{T\text{-}63}} \quad . \qquad 2\text{-}35$$

T-63 COEI data are displayed in Fig. 2-12 where (excluding the flagged advanced burner data and by accounting for the CO quench shift) all geometry variations listed are observed to collapse rather well to the curve. GT-309 COEI data also experienced excellent geometry correlation by allowance for the quench shift.

4. Predictions and Validation of the Model

With relatively high statistical levels, NO_x and CO emissions from mixing controlled flames within the GT-309 combustor series have been correlated and hence emissions predictions for this family of geometrically similar burners are possible. Specifically, since these correlations include variations in combustor loading as well as liner geometry, curves particularly relevant to the combustor designer are produced (each at a given power setting) displaying the effect of variations in liner configuration upon exhaust emissions.

Fig. 2-13 is a plot of both NO_xEI and COEI versus the non-dimensionalized geometry parameter ℓ_{sec}/d_{comb} for the 90% power point. The discrete symbols are actual data taken on the listed burners at General Motors. In testing configurational variations on the baseline and decreased diameter burners, two diameters were effectively examined. This graph demonstrates the significant effect of combustor diameter upon high power NO_x: burner diameter can be reduced to achieve a substantial decrease in high power NO_x without appreciable sacrifice in high power CO. Furthermore ℓ_{sec}/d_{comb} can be diminished to approximately 0.3 to effect high power NO_x reduction before incurring a substantial increase in high power CO.

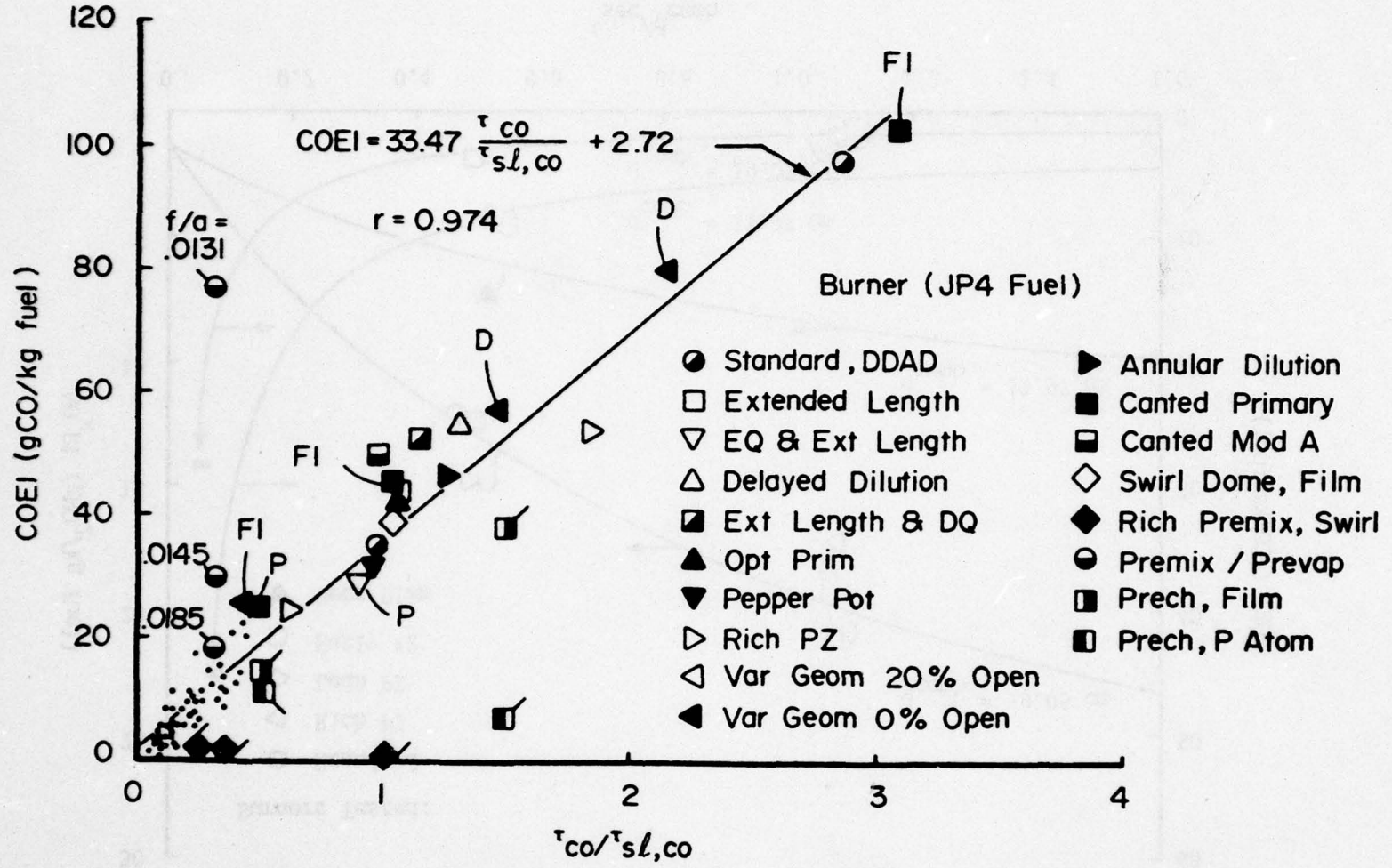

Figure 2-12. COEI versus $\tau_{CO}/\tau_{s\ell,CO}$ for several T-63 burners (Mellor, 1977b).

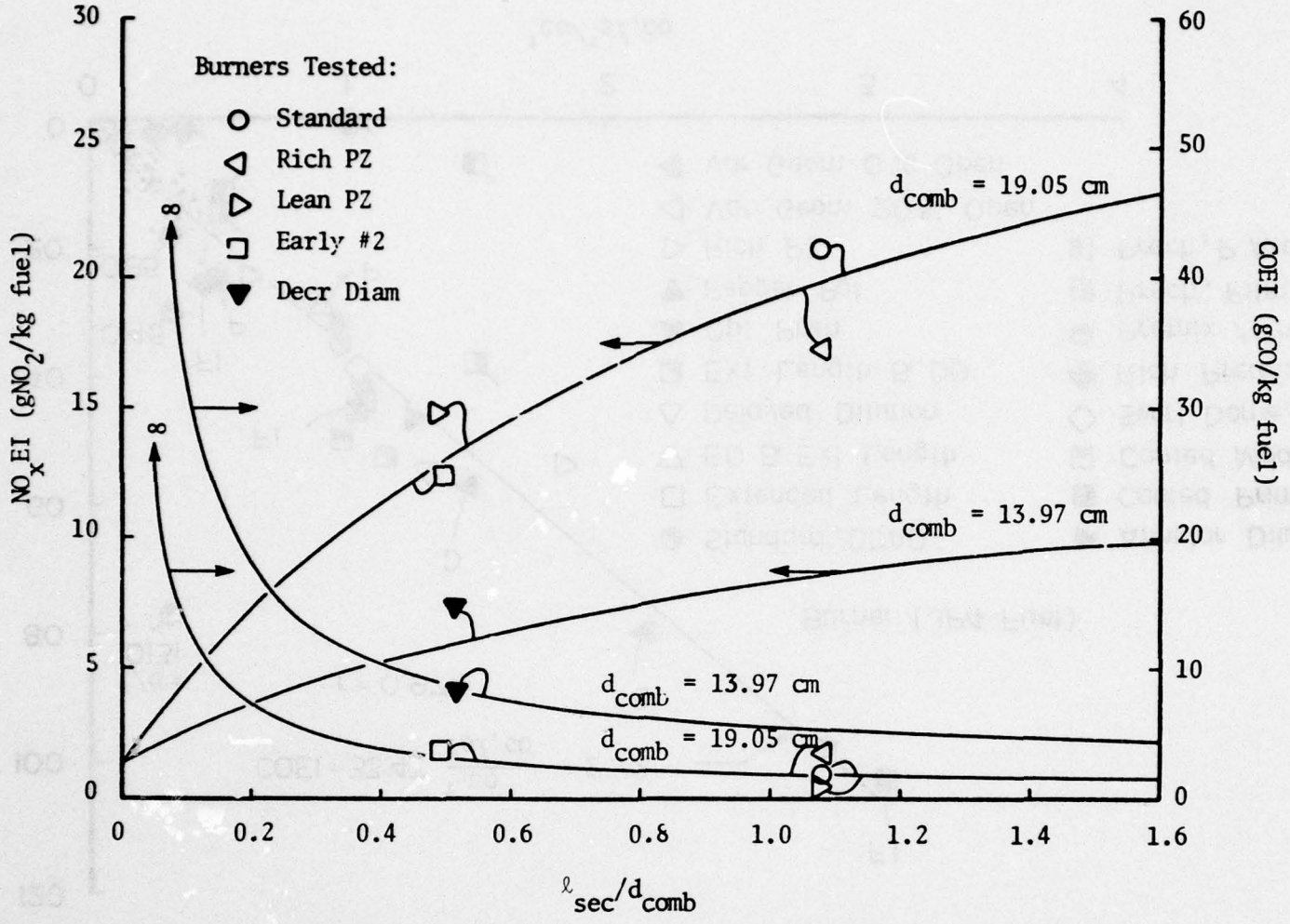

Figure 2-13. Predicted NO_xEI and COEI versus ℓ_{sec}/d_{comb} for combustors of the GT-309 genre at 90% of design power (Mellor, 1977a).

CL-676

Similar graphs for given power points are available from the GT-309 correlations. A plot for 60% power is also examined in Mellor (1977a) and demonstrates the requirement of large combustor diameters and delayed air addition for minimizing low power CO; both trends are opposite to those necessary for reducing high power NO_x. Hence to minimize both NO_x and CO emissions from a given fixed geometry liner will result in a geometry (and therefore emissions) compromise at best. Moreover, these results strongly suggest that the optimal low emissions combustor will require variable geometry.

Results from these plots were then incorporated to design a sample optimum (i.e., low NO_x) GT-309 burner. This sample design was based on the standard GT-309 combustor so that a comparison existed between this optimized design, the known NO_x benefits from the decreased diameter version, and the unaltered standard burner.

The essential feature of the sample optimum is the deletion of the primary hole row to accommodate upstream placement of the secondary jets (to minimize high power NO_x). These relocated secondary holes are enlarged slightly so that standard burner mean air injection velocity is maintained.

The results predicted that the sample optimum design should exhibit only slightly higher NO_x levels over the decreased diameter but without the high levels of CO produced by the latter. These results also suggest that at best a 50% decrease in high power NO_x is expected from conventional (non-prevaporizing/premixing) gas turbine liners (for details of sample optimum design and results consult Mellor, 1977a).

To verify the emissions predictions from the sample optimum burner three GT-309 configurations were tested at General Motors Research Laboratories (Hammond, 1977). These were the standard burner and and two modifications: Mod A, the optimum low NO_x burner designed above and Mod B, essentially Mod A but with four additional secondary jets of the same diameter as those in Mod A provided to examine the predicted effect of mean air injection velocity upon COEI.

Rig test results for these burners are shown first for NO_xEI in Fig. 2-14: the predictions for the low NO_x burners were accurate to within one standard deviation of test results. Hammond (1977) attributes the underpredictions of NO_x at high power for the standard burner to incomplete NO_x quenching by the secondary jets, implying that the axial length scale for these points is effectively greater than ℓ_{sec}.

COEI emissions from these burners are displayed in Fig. 2-15. Agreement between predictions and experimental data is not as good as with NO_x. In general, predictions do not exist within one standard deviation of test data. Above 70% gasifier speed predicted and test points exhibit disparate trends. Upon examination of the actual test trends above 70% power (particularly emphasized in combustors A and B), the data suggest that the axial CO length scale increased continuously with power (i.e., it does not attain an upper limit of ℓ_{sec} at and above 70% power). In fact, according to Hammond (1977), CO quenching occurs at all discrete locations, the position being dictated by power setting.

Also indicated in Fig. 2-15 is the unstable operation experienced by combustors A and B (as would be expected intuitively from the large and early air addition supplied through the secondary jets). Mod B was marginally stable at 60% gasifier speed and blowout occurred for both burners at 50% speed. The characteristic time model correlation did not predict the occurence of blowoff and hence refining the model to include flame stabilization is a major thrust of the research described herein.

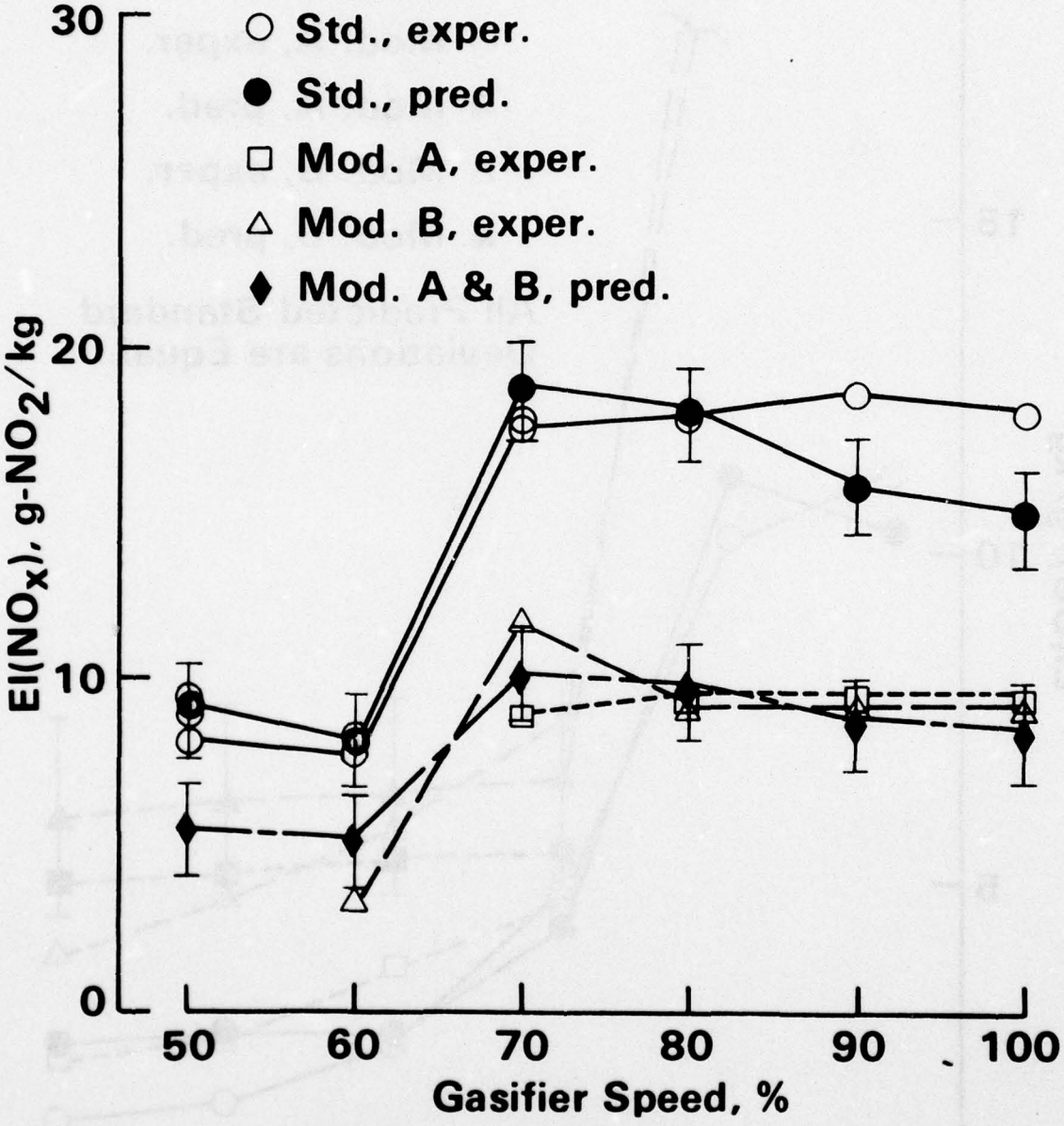

Figure 2-14. Comparison of predicted and experimental EI(NO_x) versus gasifier speed (from Hammond, 1977).

CL-721

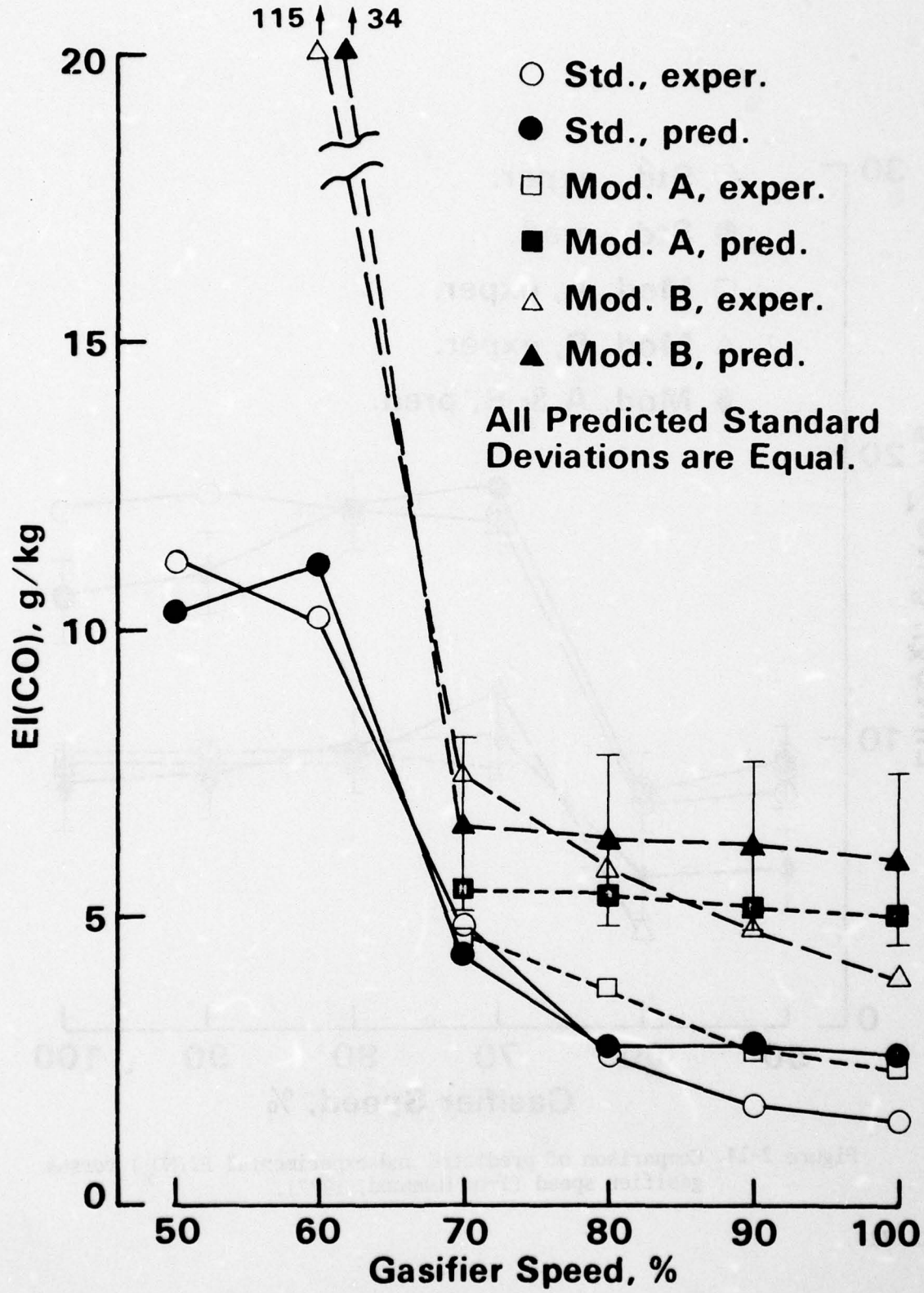

Figure 2-15. Comparison of predicted and experimental EI(CO) versus gasifier speed (from Hammond, 1977).

CL-720

III. DESIGN AND OPERATION OF THE EXPERIMENTAL COMBUSTOR FACILITY

The present combustion facility is equipped for testing conventional gas turbine combustors and simplified laboratory burners such as the tube-and-disc configuration of this study. Instrumentation allows continuous monitoring of all pressures, temperatures and flow rates as well as the important product species concentrations.

Sections A and B of this Chapter review the basic system hardware which has been used extensively for other combustor programs. Details of the facility are found in descriptions by Mellor et al. (1972), Tuttle et al. (1973), Shisler et al. (1974), Tuttle et al. (1975), Dodds et al. (1975) and Tuttle et al. (1976). The remaining four sections concentrate on the design of the Air Force experimental apparatus and the selection of run conditions.

A. Facility Design

Air flow for the burner is supplied by a compressed air blowdown system with a storage volume of approximately 85 m^3. A system pressure of 150 atm permits air flow rates of 3 kg/sec for 40 min; smaller flow rates are generally used, however, which permit operation for correspondingly longer periods of time. The system is capable of flow rates of 4.5 kg/sec. The air flow rate is monitored via a 5.40 cm orifice type flowmeter and regulated by a pneumatically controlled air throttle valve.

A schematic of the experimental apparatus, comprised of two combustors in series, is shown in Fig. 3-1. Commercial grade liquid propane is burned in the slave combustor (a standard Allison T-56 liner with a dual orifice pressure atomizing nozzle) to provide heated vitiated air (of temperatures typical of current air breathing engine operation) to the test combustor. Turbine flowmeters measure the fuel flow to both the preheat and test combustors. A remotely operated back pressure

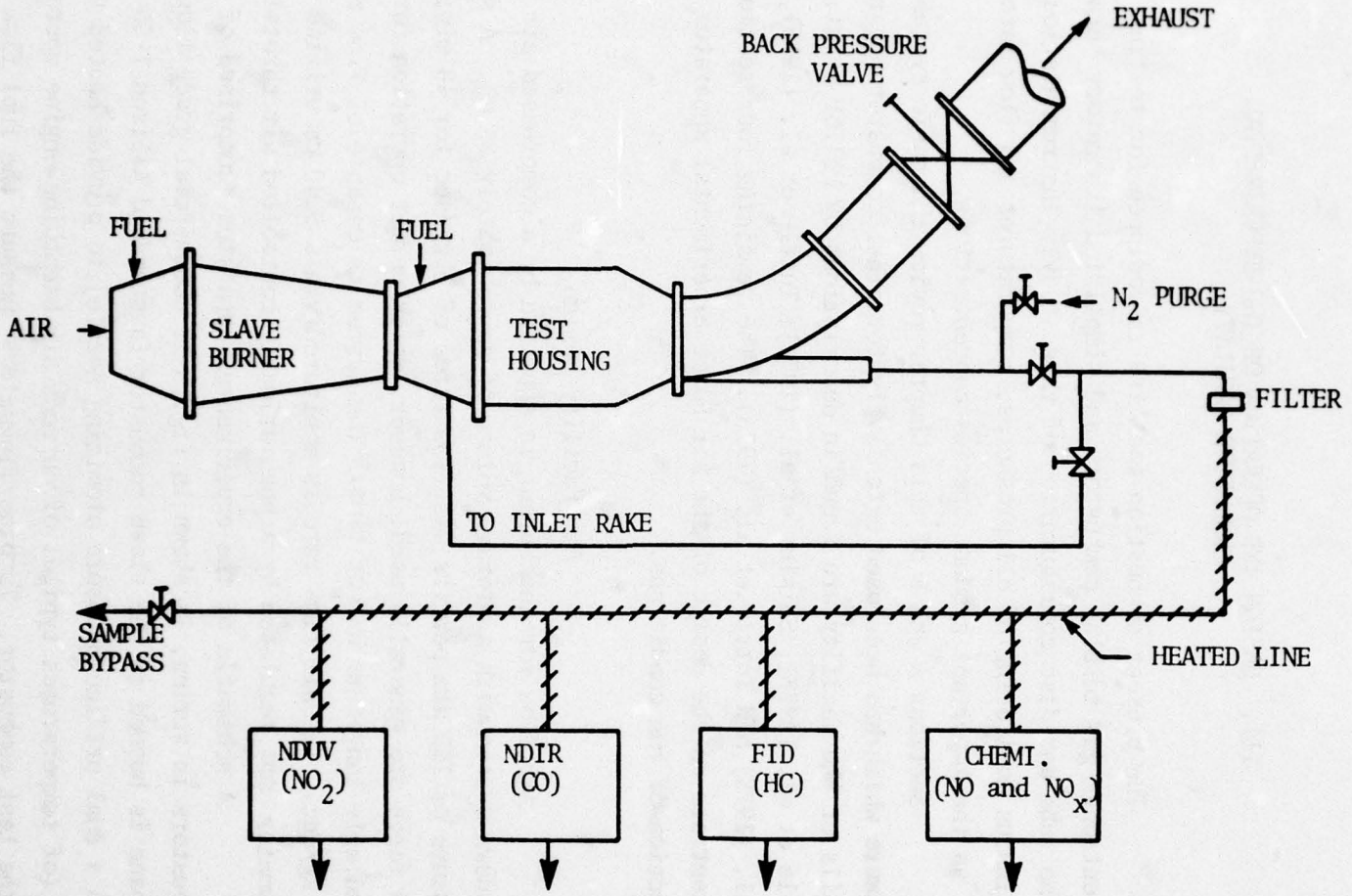

Figure 3-1. Schematic of the experimental apparatus.

CL-653

valve consisting of a movable, conical centerbody controls the pressure in the test section. Before release to the atmosphere, the exhaust flow noise level is reduced by a commercial gas turbine silencer.

The test combustor inlet temperature is monitored with a thermocouple rake mounted across the diffuser section. This rake consists of eight unshielded chromel-alumel thermocouples positioned in a stainless steel support such that they provide an area-averaged temperature. The thermocouple junctions are insulated from the support by ceramic connectors while the thermocouple wires inside the support are protected by an Al_2O_3 ceramic filling. The fuel flow rate to the slave burner controls the test combustor inlet temperature.

Immediately downstream of the temperature rake, gas samples are extracted from the preheat combustor via an uncooled gas sampling rake (cross-shaped) constructed of stainless steel tubing. The rake has a total of sixteen collection holes spaced so as to yield an area-averaged sample.

A water cooled stainless steel rake (described by Shisler et al., 1974) provides area-averaged gas samples from the exit of the test combustor to the gas analysis system. This rake is maintained at 32.2 cm from the injector plane and is inserted through the elbow section. Sampling is accomplished through sixteen sampling holes, four located along each of the four spokes which extend from a central hub.

A water cooled single point stainless steel gas sampling probe (also described by Shisler et al., 1974) may also be inserted in the elbow section. The single point probe is constructed of three concentric stainless steel tubes. Cooling water flows in and out of the two outermost passages while the gas sample flows through the inner passage to the gas analysis system; the collected sample is quenched in the probe by a converging nozzle and the cooling water. The probe tip is offset from the main body so that it sweeps out an arc as it is rotated. The probe can be displaced axially within the test combustor allowing gas sample extraction from any point along the arc at any axial plane. A platinum/platinum-10% rhodium thermocouple mounted on the side of the probe provides an estimate of local gas temperatures.

This system allows direct simulation of run conditions typical of realistic air breathing engines with the exception of the vitiated inlet air. Table 3-1 summarizes the capability of this combustor facility. Note that over the range of operating conditions described in Table 3-1, it is possible to vary pressure, air flow rate, equivalence ratio, inlet temperature and fuel type independently.

Table 3-1. Test Combustor Operating Ranges

Inlet temperature	273-950K
Combustor pressure	slightly > 1 atm-10 atm
Air flow rate	0.5-4.5 kg/sec
Fuel flow rate	0.15-2.1 ℓ/min
Fuel	propane, Jet A or any typical jet or Diesel fuel (fuel preheat temperatures up to 370K)

B. Gas Analysis System

Gas samples are drawn from the preheat and/or test combustor for analysis (see Fig. 3-1). The sample flow proceeds to the instrumentation first through a fiberglass filter for carbon particulate removal (98.7% collection efficiency for 0.05 micron particles) and then through 8 m of stainless steel sample line maintained at 425K (Vaught et al., 1971) by thermostatically controlled heat tapes. Samples are analyzed on a continuous basis for concentrations of carbon monoxide (CO), unburned hydrocarbons (HC), nitric oxide and nitrogen dioxide. CO and HC are monitored with a nondispersive infrared analyzer (Beckman model 315A) and a flame ionization detector (Beckman model 402), respectively. A chemiluminescent NO analyzer (similar to that of Fontijn et al., 1970) equipped with a NO_2 stainless steel converter allows alternate monitoring of NO and total NO_x (NO + NO_2). NO_2 concentrations are measured directly by a nondispersive ultraviolet analyzer (Beckman model 255B).

Each gas analysis instrument produces an output signal as a meter deflection which is observed visually and manually recorded. In addition, a continuous and permanent record of output signals is available from strip chart recorders connected to each instrument (similar records are obtained for temperature monitoring thermocouples).

C. Combustor Design

The test combustor housing shown in Fig. 3-2 is constructed of stainless steel pipe of inner diameter 14.63 cm and wall thickness of 1.1 cm. Five quartz windows (6.35 mm thick, 3.45 cm diameter and 6.35 cm apart) exist on both sides of the housing to allow visual access to the test section. The reducing section is wrapped with a water cooling jacket. High pressure water is injected downstream of all sampling devices at the location of minimum area to protect the combustor facility from high temperature exhaust gases.

The flameholder geometry as positioned within the test section housing is shown schematically in Fig. 3-3. This configuration was selected for the experiments and represents a compromise between the disc-and-duct configuration studied by Tuttle et al. (1976) for EPA (see Chapter II), the dump ramjet burner of Stull et al. (1974) and the prevaporizing/premixing fuel feed tube in a turbojet. Liquid fuel (Jet A or propane) is injected into the center of the tube via a simplex pressure atomizing nozzle. The tube (length typical of a ramjet combustor) provides a region wherein the fuel can be partially prevaporized and premixed before combustion. The disc (mounted in the center of the third window) serves to stabilize the flame by means of a bluff body recirculation zone which is essentially identical to the flame stabilization technique used in ramjet and turbojet afterburners.

To understand the important effect of flameholder geometry upon both combustion efficiency and flame stabilization, five geometry variations of the basic tube-and-disc configuration are utilized. The specific dimensions of these variations are delineated in Table 3-2 where the variables correspond to those depicted in Fig. 3-3.

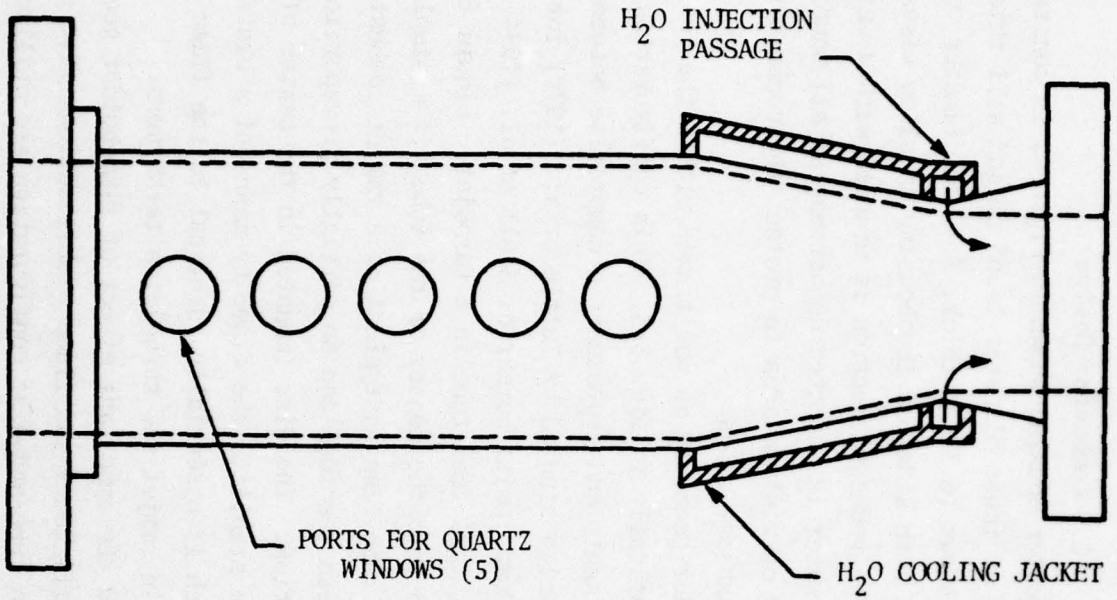

Figure 3-2. Test section housing schematic.

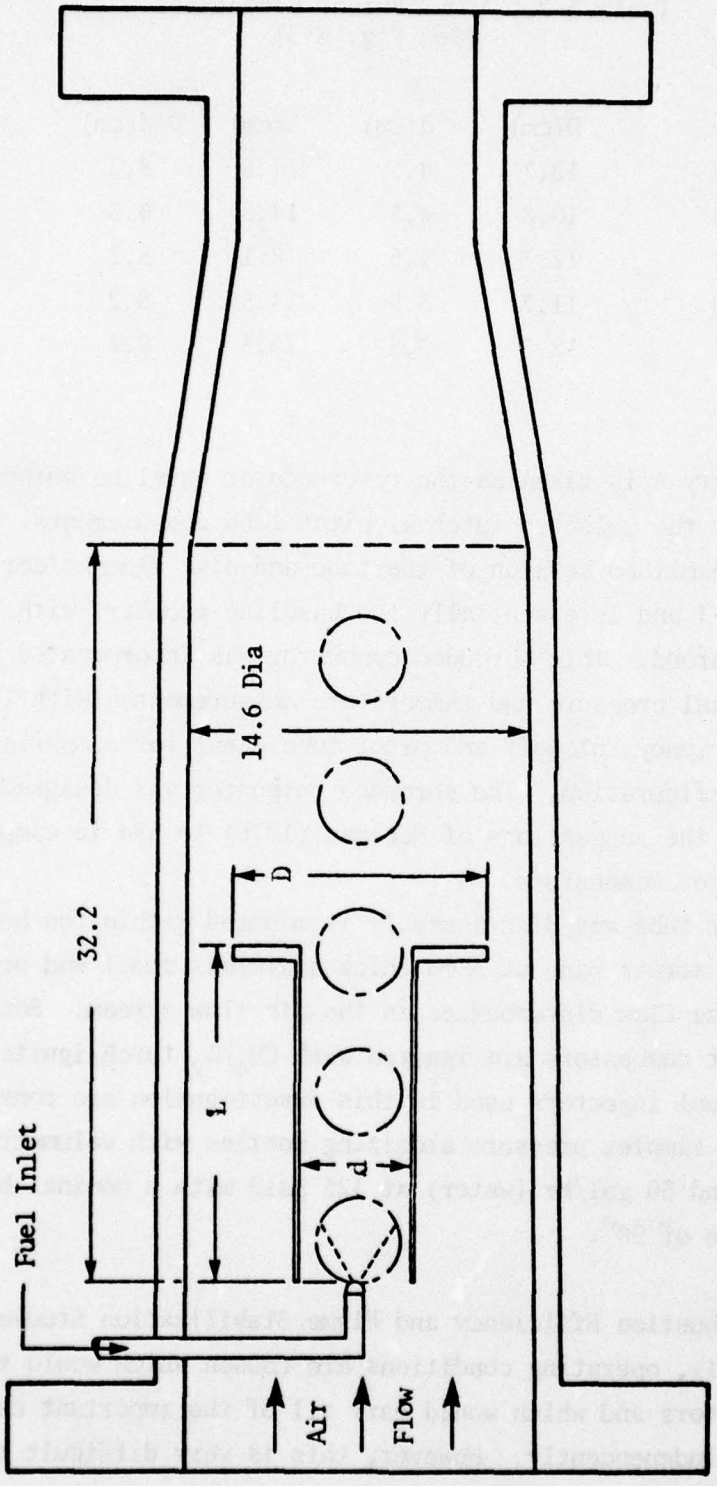

Figure 3-3. AFOSR test section, showing viewpoints relative to the fuel preparation tube.

CL-768

Table 3-2. AFOSR Burner Geometries
(See Fig. 3-3)

	D(cm)	d(cm)	L(cm)	D-d(cm)
A	12.7	4.5	14.5	8.2
B	10.8	4.5	14.5	6.3
C	12.7	4.5	8.1	8.2
D	11.7	3.5	14.5	8.2
E	12.7	3.5	14.5	9.2

Geometry A is taken as the reference or baseline burner and was utilized for the selected internal pitot tube measurements.

A streamlined version of the tube-and-disc flameholder is shown in Fig. 3-4 and is essentially the baseline geometry with the addition of a shroud. This shrouded combustor was incorporated primarily to obtain internal pressure and temperature measurements (with limited combustion efficiency, blowoff and pitot tube data) for comparison with the standard configuration. The shrouded combustor was designed in accordance with the suggestions of Edelman (1976) to aid in computer modeling of ramjet combustors.

Either tube-and-disc assembly is mounted within the housing by thin support struts made of 3 mm thick stainless steel and oriented so as to minimize flow disturbances in the air flow stream. Both the preheat and test combustors are ignited with CH_4/O_2 torch igniters.

The fuel injectors used in this investigation are conventional stainless steel simplex pressure atomizing nozzles with volumetric flow ratings of 16 and 30 gal/hr (water) at 125 psid with a nominal hollow spray cone angle of 90^{o}.

D. Combustion Efficiency and Flame Stabilization Studies

Ideally, operating conditions are chosen which would typify advanced combustors and which would vary all of the important characteristic times independently. However, this is very difficult to do

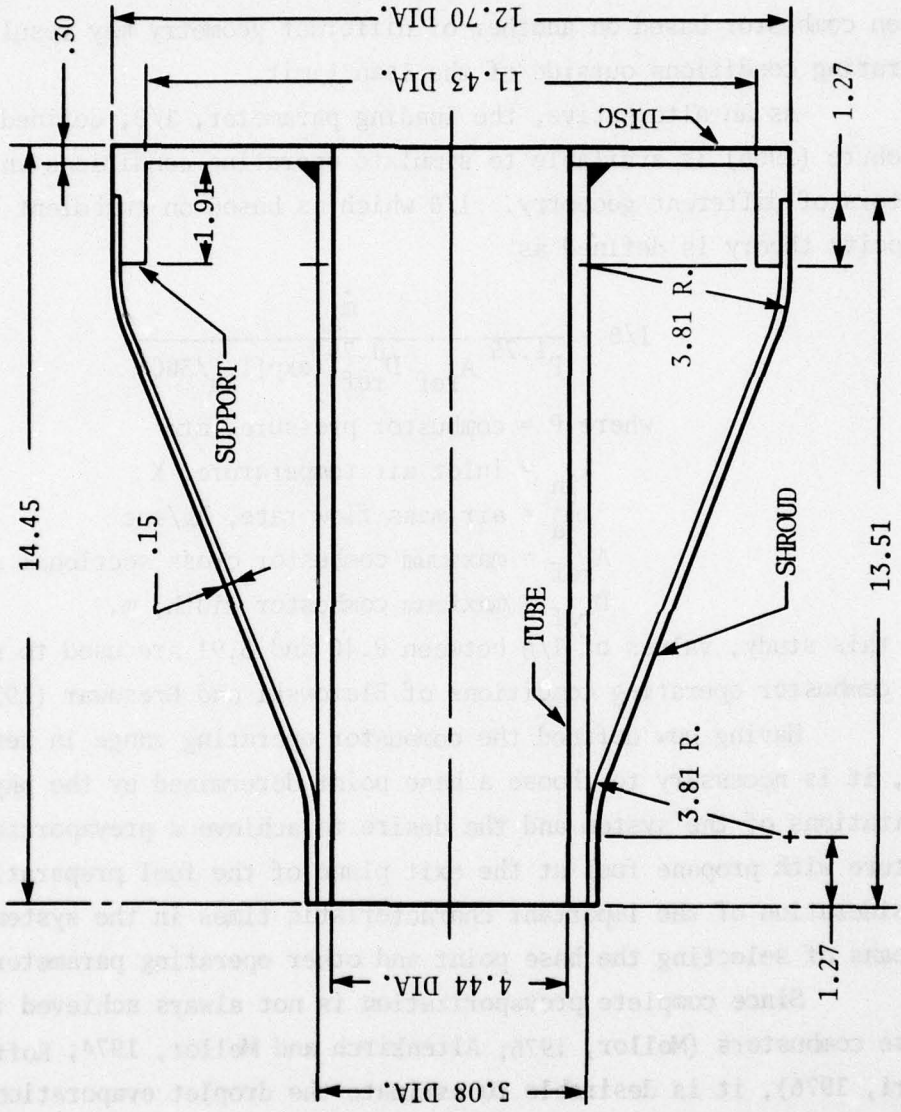

Figure 3-4. Shrouded combustor schematic.

initially because the dependence of combustion efficiency and flame stabilization upon the characteristic times has not been determined for the tube-and-disc burner. Furthermore, exact duplication of pressure, temperature, reference velocity and overall equivalence ratio for a given combustor based on another of different geometry may result in operating conditions outside of the lean limit.

As an alternative, the loading parameter, $1/\theta$, defined by Lefebvre (1966) is available to simulate operating conditions in combustors of different geometry. $1/\theta$ which is based on turbulent burning velocity theory is defined as

$$1/\theta = \frac{\dot{m}_a}{P^{1.75} A_{ref} D_{ref}^{0.75} \exp(T_{in}/300)} \qquad 3\text{-}1$$

where P = combustor pressure, atm

T_{in} = inlet air temperature, K

$\dot{m}_a$ = air mass flow rate, kg/sec

A_{ref} = maximum combustor cross sectional area, m^2

D_{ref} = maximum combustor width, m.

For this study, values of $1/\theta$ between 0.46 and 3.91 are used to simulate the combustor operating conditions of Blazowski and Bresowar (1974).

Having now defined the combustor operating range in terms of $1/\theta$, it is necessary to choose a base point determined by the physical limitations of the system and the desire to achieve a prevaporized mixture with propane fuel at the exit plane of the fuel preparation tube. Consideration of the important characteristic times in the system provides a means of selecting the base point and other operating parameters.

Since complete prevaporization is not always achieved in these combustors (Mellor, 1976; Altenkirch and Mellor, 1974; Roffe and Ferri, 1976), it is desirable to estimate the droplet evaporation time, τ_{eb}, in the fuel preparation tube. To facilitate prevaporization, d_o (Eq. 2-11) is minimized by selecting a low fuel flow, high injection pressure nozzle which will provide enough flow to stabilize the flame (see Eq. 2-15). High inlet air temperatures and low air velocities are

also important. Exact tube velocities to estimate droplet residence time in the tube requires the aid of experimental data (see pitot tube measurements). Hence, combustor operating ranges are chosen which qualitatively meet the conditions described above.

To assist prevaporization, the base point to produce the smallest possible initial droplet diameter is selected as shown in Table 3-3.

Table 3-3. Base Operating Point

Inlet temperature = 800K	Overall equivalence ratio = 0.29
Combustor pressure = 5 atm	Nozzle = 16-90, SMD ≃ 95 μm (Jet A)
Air flow rate = 1 kg/sec	Conventional fuels = Jet A and Propane

From this point, equivalence ratio, pressure and inlet temperature are varied independently to determine the functional dependence of the characteristic times τ_{hc} and $\tau_{s\ell}$ (velocity variations were accomplished by changes in pressure rather than air flow rate). τ_{eb} is varied by selecting a nozzle (30-90) which produces a much larger initial droplet size (∿50 μm larger) and hence changes the prevaporization conditions in the fuel preparation tube.

Exit plane emission data relevant to combustion efficiency were collected with the water cooled, area-averaging rake. Combustion efficiency is then quantified (see Eq. 5-1) for each run point.

Flame stabilization data are obtained in a somewhat different manner. First, the test combustor pressure, inlet temperature, and air and fuel flow rates are adjusted to establish a well stabilized flame. After this condition is maintained for a short time, the fuel flow rate is slowly reduced to approach and ultimately reach the lean blowoff limit or increased in search of flashback. Experimentally, blowoff is the point where the flame becomes visually extinct whereas

flashback is the point at which a thermocouple mounted in the center of the tube near the wall exceeds a temperature of 1200K. If flashback occurs, the fuel flow is automatically terminated and remains so until the fuel supply system is manually restarted.

Table 3-4 summarizes the range of burner conditions used for the combustion efficiency and flame stabilization studies. Selected combustion efficiency and lean blowoff data were also taken with the shrouded combustor under the conditions listed in Table 3-5. Comparison with the unshrouded tube-and-disc geometry is presented in Chapters V and VI. The matrix shown in Fig. 3-5 summarizes the burner operating conditions used in this study as functions of equivalence ratio and $1/\theta$.

E. Pressure, Temperature and Velocity Studies

In addition to the combustion studies discussed in the previous section pressures, temperatures and velocities inside and at the exit of the fuel preparation tube are of interest.

1. Static Pressure and Temperature Measurements

The fluid mechanics of the approach flow in the tube is especially important for the flashback study since classical flashback is a boundary layer phenomenon which may occur near the tube exit. Also, hot and cold flow pressure measurements will show any effects of combustion on the velocity at the disc. To examine these effects, a differential pressure is measured between stations 0 and 8 (Fig. 3-6) in both hot and cold flow. If the pressure drop remains constant for both flows it is assumed that the entrance flow prior to combustion is identical to that in cold flow.

For the remaining measurements, the shrouded tube-and-disc assembly (Fig. 3-4) was instrumented as shown in Fig. 3-6. Of the four static pressure measurements, one (point 1) is an absolute pressure while the other three are differential pressures with point 1 as reference.

Table 3-4. Combustion Efficiency and Flame Stabilization Burner Operating Ranges

$1.0 \leq$ Air Flow Rate ≤ 1.5 kg/sec

Fuels = Jet A, Liquid C_3H_8

$2.3 \leq$ Pressure ≤ 8.0 atm

$600 \leq$ Inlet Air Temperature ≤ 800K

Lean Blowoff Limit $\leq$ Overall Equivalence Ratio ≤ 0.39

Lean Blowoff Limit $\leq$ Tube Equivalence Ratio ≤ 2.80

$12.0 \leq$ Reference Velocity ≤ 75.0 m/sec

$31.0 \leq$ Air Velocity at Tube Exit ≤ 190.0 m/sec

$80 \leq$ Initial Fuel Spray Sauter Mean Diameter* ≤ 160 μm

$0.7 \leq$ Mean Air Residence Time in Tube ≤ 6.1 msec

Table 3-5. Burner Operating Conditions for Combustion Efficiency and Flame Stabilization Using a Shrouded Combustor (Fuel = Jet A; #16-90 Nozzle)

Lefebvre (1966) Loading Parameter $1/\theta\left(\frac{kg}{sec\ atm^{1.75} m^{2.75}}\right)$	Air Flow Rate $\dot{m}_a$ (kg/sec)	Inlet Air Temperature T_{in} (K)	Combustor Pressure P (atm)	Condition
1.55	1.0	800	4	Eff ϕ = 0.29
1.05	1.0	800	5	Eff ϕ = 0.29
.46	1.0	800	8	Eff ϕ = 0.29
1.55	1.0	800	4	b.o.
.46	1.0	800	8	b.o.

*Under all test conditions except perhaps at 8 atm, liquid C_3H_8 is expected to flash vaporize in the fuel preparation tube.

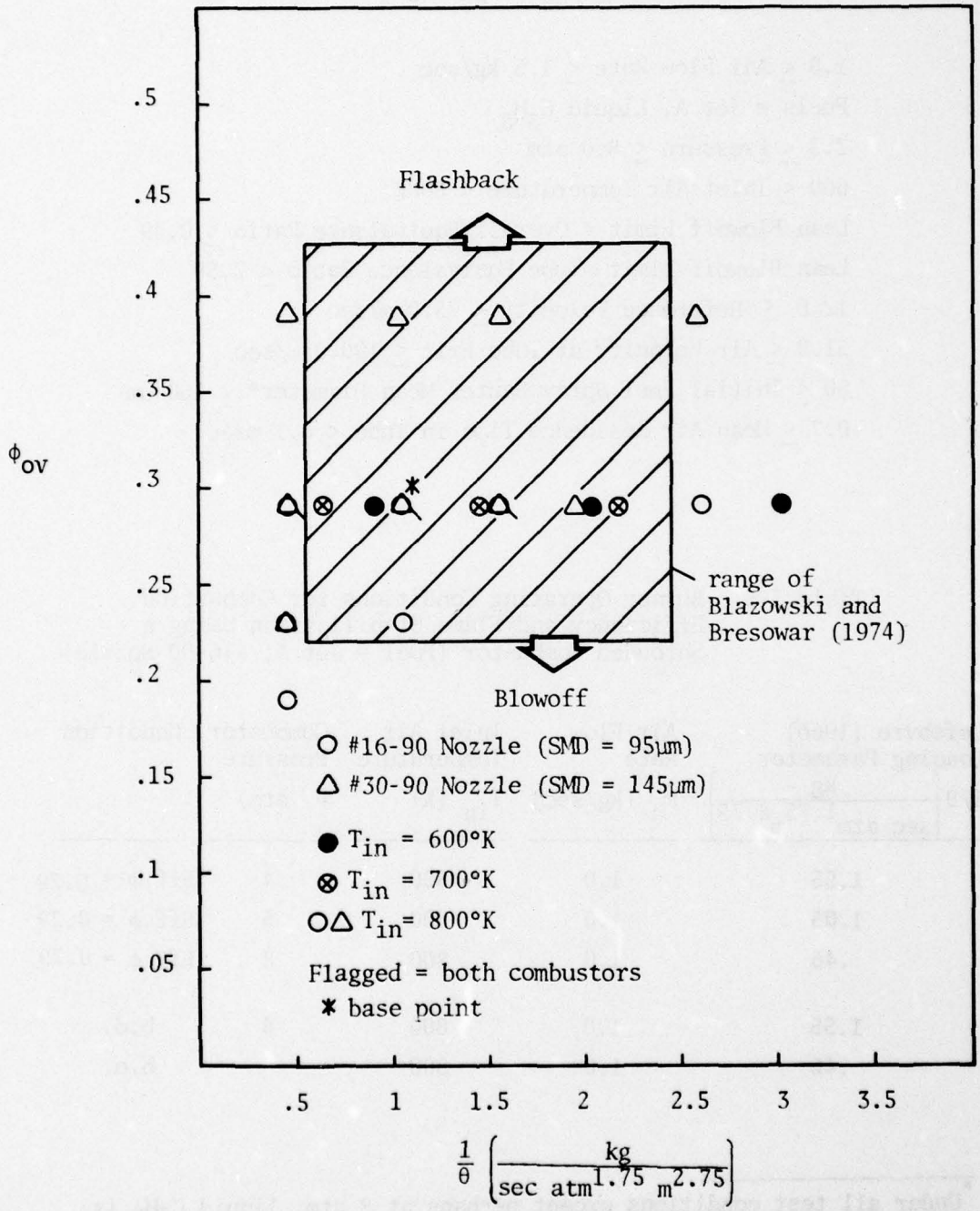

Figure 3-5. Summary of burner operating conditions.

CL-922

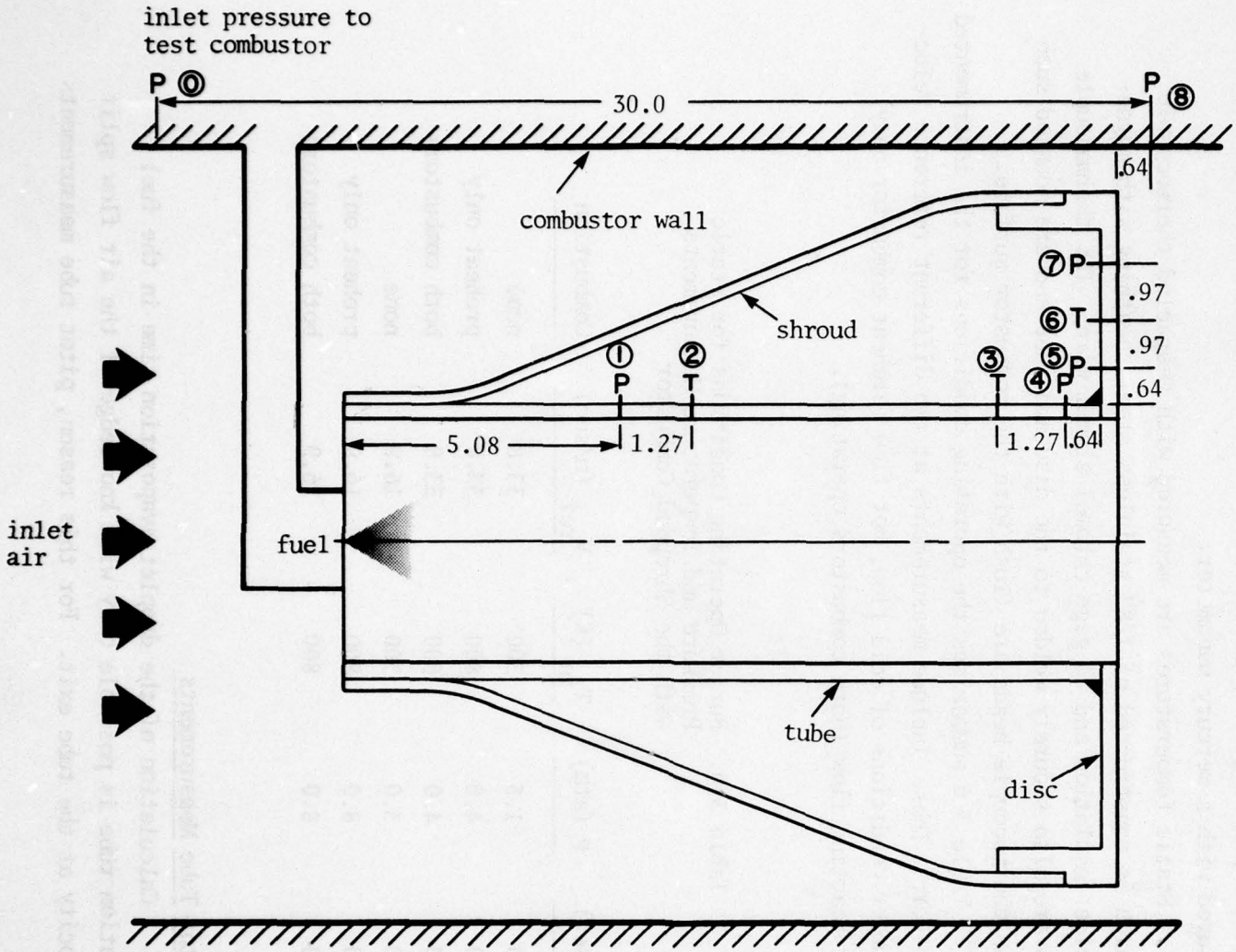

Figure 3-6. Location of static pressure and temperature measurements in shrouded combustor.

Pressure taps are constructed of 1/8" stainless steel tubing and securely welded to the tube and the disc. Model A-10 Sensotec 0-250 psig and ±2 psid pressure transducers monitor the absolute and differential pressures respectively; the combustor differential pressure is measured with a mercury manometer.

Static temperatures are measured with Omegaclad thermocouple wire which is constructed of 1/8" stainless steel sheathing with magnesium oxide insulation and 24 gage chromel-alumel wire. The thermocouple sheaths are also securely welded to the disc and tube and are mounted such that the thermocouple beads are flush with the combustor surface.

Table 3-6 summarizes the operating conditions for the instrumented flameholder. These include measurements at two different reference velocities under conditions of cold flow, hot flow (preheat combustor only) and hot reacting flow (both combustors operating).

Table 3-6. Burner Operating Conditions for Static Pressure and Temperature Measurements with the Shrouded Combustor

$\dot{m}_a$ (kg/sec)	P (atm)	T_{in} (K)	V_{ref} (m/sec)	Combustion
1.0	1.5	300	33.8	none
1.0	4.0	800	33.8	preheat only
1.0	4.0	800	33.8	both combustors
1.0	3.0	300	16.9	none
1.0	8.0	800	16.9	preheat only
1.0	8.0	800	16.9	both combustors

2. Pitot Tube Measurements

Calculation of the droplet evaporation time in the fuel preparation tube is possible only with knowledge of the air flow split or velocity at the tube exit. For this reason, pitot tube measurements

were taken on the baseline tube-and-disc combustor under cold flow conditions at the exit of the tube and in the annular area between the combustor housing and the disc.

The stagnation pressure is measured with the pitot tube as illustrated in Fig. 3-7 (Layne, 1975). The pitot tube is constructed of brass and is mounted in the third window of the test combustor 0.64 cm from the disc and is positioned precisely with the aid of a micrometer. The static pressure is measured with a pressure tap mounted on the combustor wall and in the same axial plane as the stagnation pressure measurement. The static-stagnation differential pressure is monitored in the test cell with a mercury manometer and is directly related to the velocity in the combustor by the Bernoulli equation for steady incompressible flow.

Since the pitot tube is made of brass and is not water cooled, only cold flow measurements were possible. The results of the measurements will determine if these cold flow data are extendable to velocities during combustion. Table 3-7 summarizes the operating conditions for the pitot tube velocity measurements. These measurements were also made with the shrouded combustor under the first condition specified in Table 3-7 (see Figs. 4-1 and 4-2 for the results).

Table 3-7. Burner Operating Conditions for Pitot Tube Studies (No Combustion)

$\dot{m}_a$ (kg/sec)	P (atm)	T_{in} (K)	V_{ref} (m/sec)
1.0	2	300	25.4
1.0	4	300	12.7

F. Single Point Probe Studies

To examine the prevaporizing capability of the fuel preparation tube, the single point gas sampling probe was used to withdraw samples

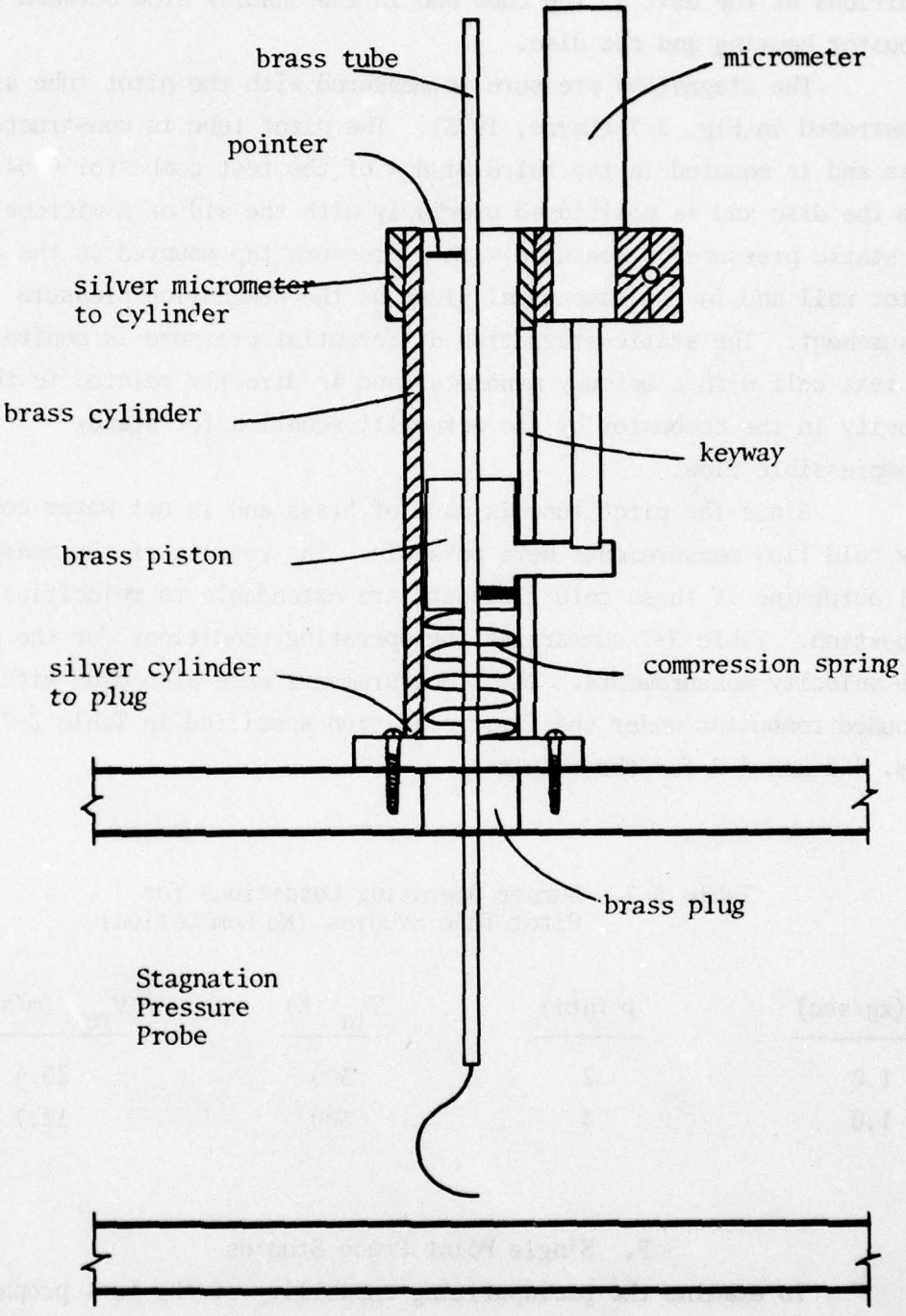

Figure 3-7. Pitot tube schematic (Layne, 1975).

CL-924

from flames corresponding to three different combustor operating conditions using two different nozzles. These operating conditions are listed in Table 3-8 and represent different reference velocities and thus, disparate velocities in the fuel preparation tube.

Table 3-8. Operating Points for Single Point Probe Studies (Fuel = Jet A, ϕ = 0.29)

Nozzle	Lefebvre (1966) Loading Parameter $1/\theta\left(\frac{kg}{sec\ atm^{1.75} m^{2.75}}\right)$	Air Flow Rate $\dot{m}_a$ (kg/sec)	Inlet Air Temperature T_{in} (K)	Combustor Pressure P (atm)
16 and 30-90	.46	1.0	800	8
16 and 30-90	1.05	1.0	800	5
30-90	1.55	1.0	800	4
16-90*	2.57	1.0	800	3

At 1.0 cm downstream of the disc emission concentration data were collected with the probe at two radial positions within the combustor (see Fig. 3-8). These radial positions are the tube centerline and the center of the recirculation zone (i.e., halfway between the inside diameter of the tube and the outside diameter of the disc). Concentrations at the tube centerline are important for examining the condition of the fuel at the tube exit while conditions in the recirculation zone provide information relevant to the blowoff analysis which is a recirculation zone phenomenon (see Tables 4-2 and 4-3). Unfortunately, combustor operating conditions proved too severe for single point temperature measurements in these regions.

*Lean blowoff occurred at this condition with the #30-90 nozzle.

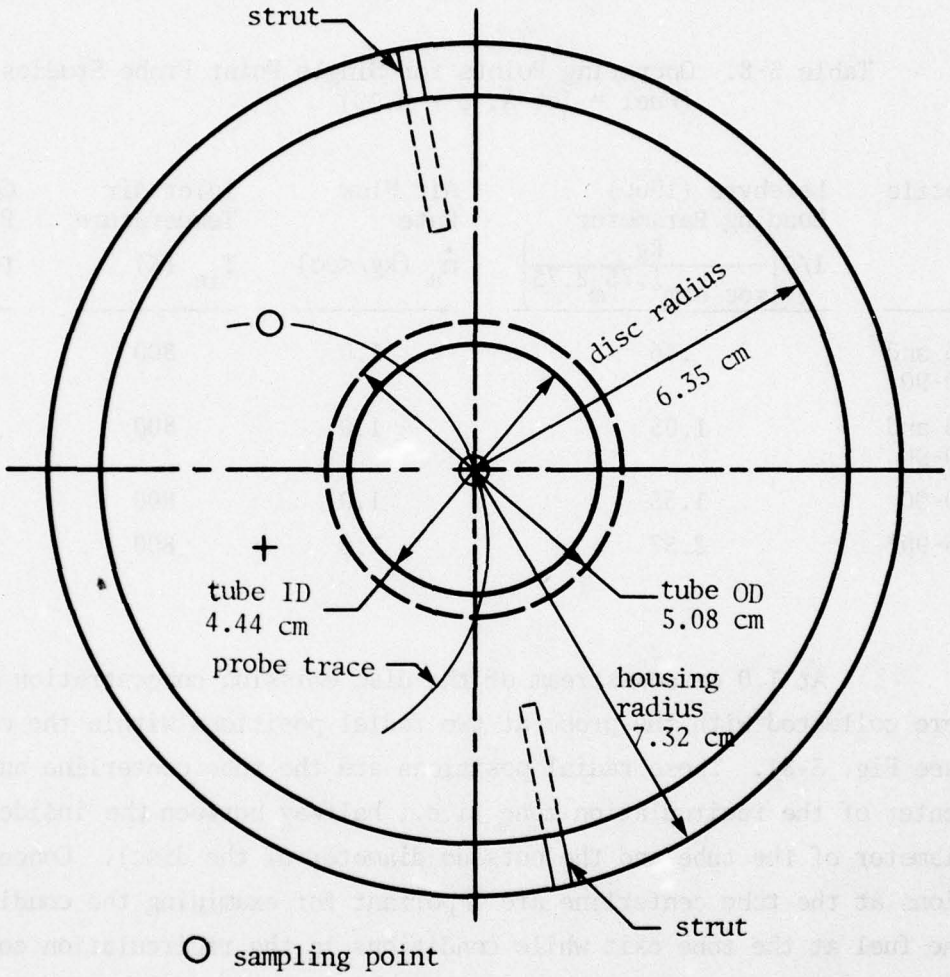

Figure 3-8. View looking upstream of disc, tube and probe trace with sampling points.

Probe misalignment errors are estimated as 0.25 cm (Tuttle et al., 1975) in radial placement. The large length to diameter ratio of the probe encourages some error in the sample tip location from probe flexation during combustor operation. This probe tip oscillation about an equilibrium position is greatest in the region downstream of the disc where main flow streamlines bend toward the duct centerline. Hence, in this region of the flow field, only an average sample over the amplitude of the oscillation is possible.

The variety of experiments mentioned in the preceeding sections are fully discussed in the following three Chapters and provide a guide to the development of the characteristic time model discussed in Chapter II.

IV. FLOW FIELD CHARACTERIZATION

Although the prevaporizing/premixing geometry discussed in the last section represents an extension of the disc-in-duct configuration studied extensively by Tuttle et al. (1976), application of the characteristic time model to this combustor is complicated by the presence of the fuel preparation tube and the requirement that complete fuel vaporization and mixing be achieved prior to combustion. To aid in the development of the characteristic time model for combustion efficiency and flame stabilization, simple flow field measurements were made in the region of the fuel preparation tube. These measurements include static pressures and temperatures along the tube (inside diameter) and disc, velocity profiles in the plane of the disc and species concentrations at the tube exit and in the recirculation zone. Particularly important are the velocity measurements because they provide information regarding the air flow split between the tube and the annulus region as well as the average equivalence ratio at the tube exit. Hopefully these simple experiments will help characterize some of the boundary conditions in the flow field.

A. Static Pressure and Temperature

For the instrumented combustor experiments, static pressures and temperatures were measured in the regions shown in Fig. 3-6 using the shrouded combustor of Fig. 3-4. The purpose of the shroud is to smooth the incoming flow, shield the pressure taps and thermocouples and minimize any flow disturbances caused by these probes. Table 4-1 summarizes the data obtained in cold flow, hot flow (preheat combustor only) and hot reacting flow (both combustors) under typical combustor operating conditions.

Table 4-1

Static Pressure and Temperature Data for Shrouded Combustor
(ϕ_{ov} = .29; fuel = Jet A ; $\dot{m}_a$ = 1.0 kg/sec)

Reference Velocity V_{ref} (m/sec)	*Combustor Pressure P (atm)	Inlet Temperature T_{in} (°K)	Reference Pressure P(1) (atm)	Differential Static Pressure (psid) P(4)	P(5)	P(7)	Static Temperature (°K) T(2)	T(3)	T(6)	Overall Static Differential Pressure Drop (psid) $p_{(0-8)}$	Combustor Operating Condition
33.8	1.5	300	1.68	+.087	-.020	+.020	287	287	287	1.18	cold flow
			1.62	+.067	-.020	+.007	287	287	287	1.23	
33.8	4.0	800	4.11	+.047	-.033	-.013	799	823	807	1.18	hot flow
			4.17	+.053	-.027	-.020	797	802	792	1.22	(preheat only)
33.8	4.0	800	4.17	+.047	-.053	-.046	738	722	1154	1.18	reacting flow
			4.17	+.080	-.053	-.020	729	736	--	1.23	(both combustors)
16.9	3.0	300	3.16	+.007	-.033	-.020	287	287	287	.49	cold flow
			3.04	+.007	-.033	-.013	287	287	287	.55	
16.9	8.0	800	8.36	+.027	-.033	-.007	815	814	807	.39	hot flow
			8.42	+.007	-.040	+.027	816	801	--	.44	(preheat only)
16.9	8.0	800	8.42	+.013	-.040	-.013	673	791	1229	.44	reacting flow
			8.19	+.013	-.067	+.033	676	785	--	.44	(both combustors)

*Pressure monitored with Marsh type pressure gage

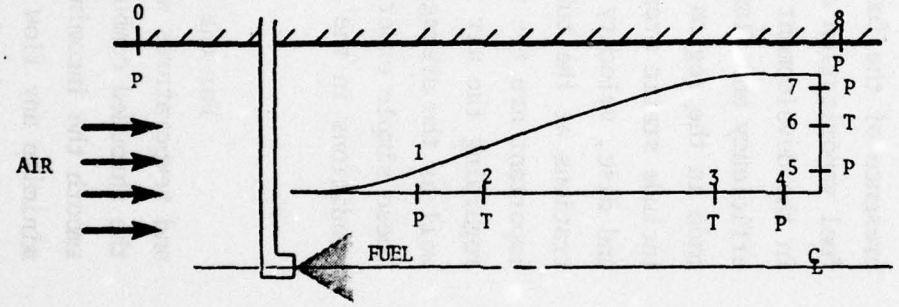

Overall differential pressure measurements (station 0-8) show no variation between cold flow, hot flow (preheat combustor only) and reacting flow (both combustors) at the two reference velocities tested. This implies that turbulence levels and velocity profiles are similar between the reacting and cold flow experiments from the upstream region to the disc. Therefore, cold flow velocity measurements in the plane of the disc can be used to approximate conditions in reacting flow at the same reference velocity.

Other differential pressure measurements are very low (<0.1 psid) and tend to strain the lower range of the pressure transducer. The pressure tap located in the upstream section of the combustor (station 1) measures an absolute pressure which is used as reference for the other readings; the remaining three are differential pressures from this reference point. One result is evident; the pressure at station 4 is distinctly higher than at station 1 for the high reference velocity case. This indicates that some degree of flow separation exists at the exit of the fuel preparation tube. Consequences of flow separation in the mixing tube are discussed in the flashback section of this report.

Thermocouples on the inside of the prevaporizing/premixing tube (station 2 and 3) provide information regarding the fuel vaporization rate at the wall. For the reacting flow results, the temperatures (uncorrected) measured by these thermocouples are substantially lower than the combustor inlet temperature. This temperature decrease may either be caused by the liquid Jet A cooling the air stream as it vaporizes or liquid fuel droplets striking the thermocouple bead and evaporating. If one assumes that all the fuel is vaporized, an inlet temperature decrease of 33K is anticipated from an energy balance. Consequently, the lower temperatures reported in Table 4-1 are probably a result of cooling caused by droplet evaporation on the thermocouple bead. For the low velocity experiments, the temperature at station 3 is very close to the inlet temperature indicating better vaporization near the wall than in the high velocity case.

Finally, the disc thermocouple (station 6) measures the temperature of the gases in the recirculation zone at the disc surface. For the reacting flow experiments, the measured temperature is approximately 80% of the adiabatic flame temperature based on the overall equivalence ratio. It is the recirculation zone that provides heat and active species to the shear layer region which stabilizes the flame. The purpose of the hot recirculation zone will be discussed in more detail in the blowoff section of Chapter VI.

B. Velocity

Results of the overall differential pressure measurements in the previous section show that velocities at the tube exit for reacting flow can be estimated by performing experimental measurements under cold flow conditions. Utilizing the pitot tube of Fig. 3-7 and the operating conditions listed in Table 3-7, velocities in a plane just downstream of the disc were obtained at two different reference velocities. Profiles are shown in Fig. 4-1 and Fig. 4-2 for the low and high reference velocity cases, respectively, using both the simplified (Fig. 4-1 and 4-2) and shrouded (Fig. 4-2) combustor. Note that all velocities are zero near solid boundaries except at the housing wall. This is due to the combustor windows which are recessed in the housing and are in the same plane as the pitot tube. If this distance is taken into account, air flow rates of 1.0 kg/sec are predicted.

In both cases, the velocity at the tube exit can be approximated by the annular velocity V_a (velocity based on the area of the disc). Experimentally determined air flow splits are shown in both figures and compare favorably with the calculated value of $\dot{m}_{a,tube}$ = 0.275 kg/sec. The velocity profile is also symmetric about the combustor centerline; in addition, nozzle and support effects are dissipated in the fuel preparation tube before the flow reaches the tube exit as evidenced by the flat velocity profiles in both Fig. 4-1 and 4-2.

The major effect of the shrouded combustor is to streamline the flow and thus flatten the velocity profile near the outer region of

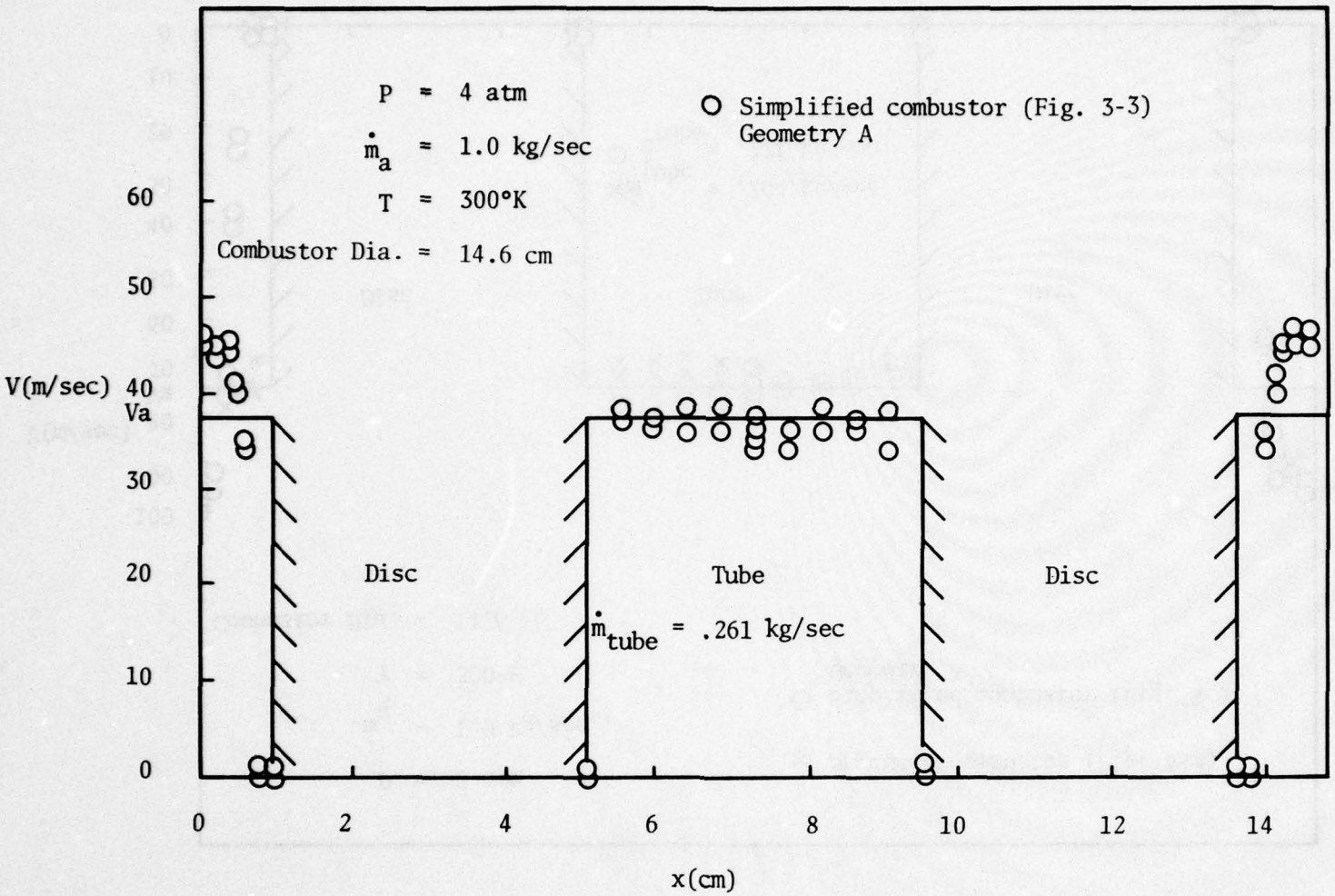

Figure 4-1. Cold flow pitot tube measurements at 4 atm.

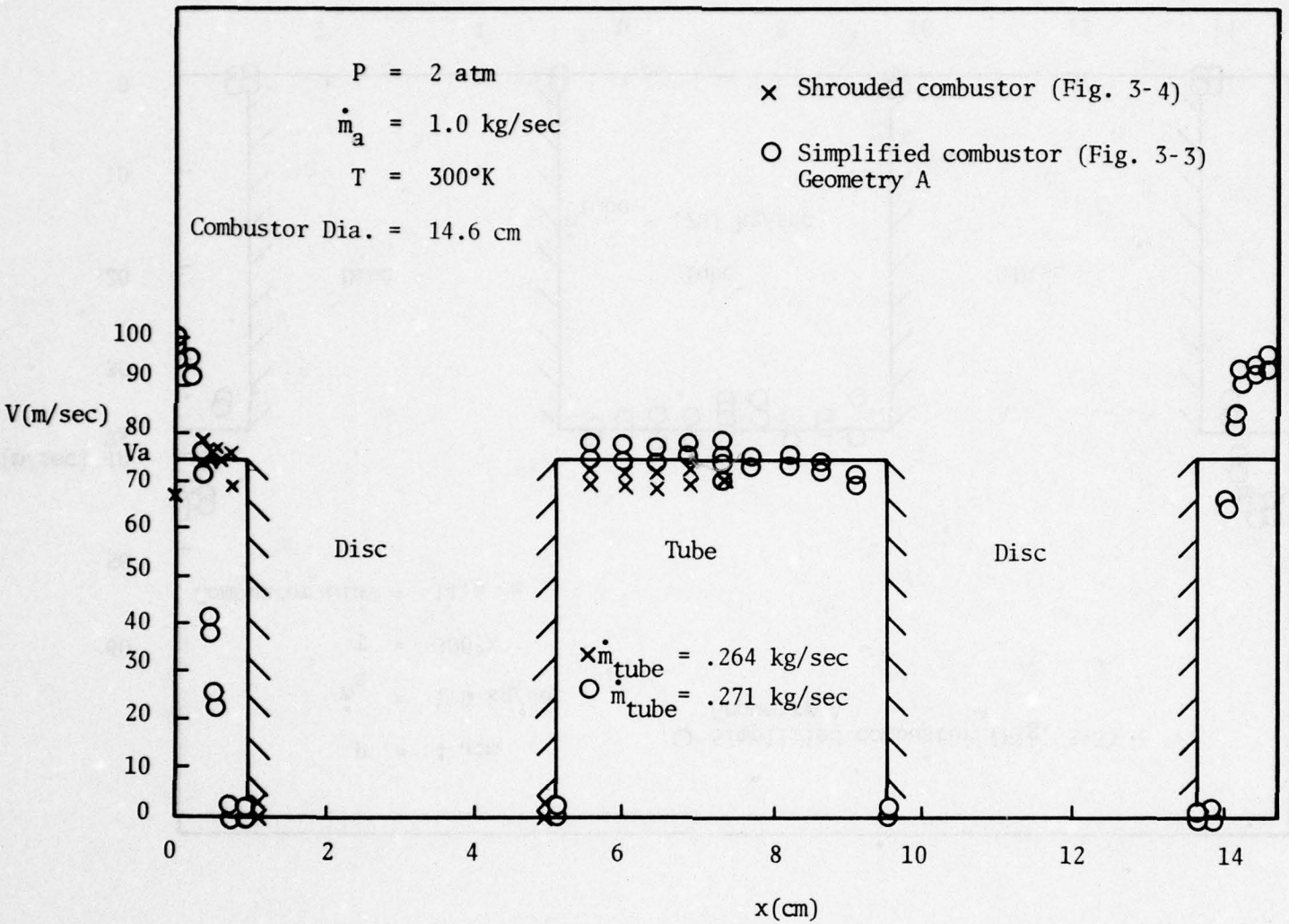

Figure 4-2. Cold flow pitot tube measurements at 2 atm.

the disc (Fig. 4-2). There appears to be only a minimal effect on the velocity at the exit of the prevaporizing/premixing tube.

C. Species Concentrations

The measurement of NO_x internally in a continuous combustor provides a useful tool for the verification of computer modeling techniques. However, in this combustor, high combustion inefficiencies are present causing large amounts of unburned hydrocarbons which distort the NO_x emission results; this effect has been documented in Tuttle et al. (1974). Also, it will become evident later in this chapter that the fuel preparation tube has failed to completely prevaporize the liquid Jet A. For these reasons, detailed probing of the combustor was not performed in this preliminary investigation; rather, single point probe measurements were made at the tube exit (on the centerline) and in the recirculation zone in order to learn more about fuel prevaporization and flame stabilization, respectively.

Internal measurements were obtained under the burner operating conditions of Table 3-8 at two radial points in the combustor using two different nozzles. Table 4-2 summarizes the results for measurements on the tube centerline; NO_x emissions are not tabulated here because of unavoidable HC-NO_x interactions in the sampling system. Table 4-3 presents the results of the data taken on the centerline of the recirculation zone just downstream of the flameholder. In both cases, a high velocity (low P) and low velocity (high P) point were observed along with the base point.

Examination of the results in Table 4-2 show that there is no appreciable nozzle effect on either the unburned hydrocarbon or the CO emissions indexes. Measured HC emissions correspond to an equivalence ratio of 0.15-0.20 at the tube exit. This is very close to the overall equivalence ratio of $\phi_{ov} = 0.29$; however, if the tube equivalence ratio is computed based on the air flow split of Section B, an equivalence ratio of $\phi_t = 1.05$ is obtained which is substantially larger than the measured value. This effect is probably caused by the failure of the fuel preparation tube to completely vaporize the fuel. If liquid drops

Table 4-2. Results of Single Point Probe Measurements on Tube Centerline (0.64 cm from Disc)

($\dot{m}_{air}$ = 1 kg/sec; T_{in} = 800K; ϕ_{ov} = 0.29; Fuel = Jet A; Geometry A)

Combustor Pressure P (atm)	#16-90 Nozzle SMD ∿ 95μm		#30-90 Nozzle SMD ∿ 150μm	
	HCEI	COEI	HCEI	COEI
8	572	14.8	572	21.6
	529	17.0	557	17.0
5	629	7.8	572	7.7
	572	6.5	629	7.7
4	---	----	586	10.0
	---	----	772	9.3
3*	972	19.3	---	----
	858	14.8	---	----

Table 4-3. Results of Single Point Probe Measurements in Centered Recirculation Zone (0.64 cm from disc)

($\dot{m}_{air}$ = 1 kg/sec; T_{in} = 800K; ϕ_{ov} = 0.29; Fuel = Jet A; Geometry A)

Combustor Pressure P (atm)	#16-90 Nozzle SMD ∿ 95μm			#30-90 Nozzle SMD ∿ 150μm		
	NO_xEI	HCEI	COEI	NO_xEI	HCEI	COEI
8	5.4	0.2	1.8	6.8	2.9	4.0
	6.4	1.5	2.4	6.2	0.4	4.0
5	3.5	0.2	6.1	4.3	1.1	8.6
	4.4	0.7	4.5	4.1	0.5	12.4
4	---	---	---	3.8	1.3	16.1
	---	---	---	3.6	0.8	15.7
3*	1.4	15.7	69.2	---	---	----
	2.2	5.6	34.0	---	---	----

*Data cannot be duplicated with the #30 nozzle because it was at the lean blowoff limit.

are present at the tube exit, they (depending on their size) may not be drawn into the sampling probe and measured by the hydrocarbon detector. A non-uniform fuel distribution can also be responsible for the relatively low equivalence ratios observed on the tube centerline. High fuel injection pressures and large droplet evaporation times may force large quantities of fuel to the tube wall and not allow sufficient time for prevaporization and premixing prior to combustion.

Recirculation zone conditions (Table 4-3) show low unburned hydrocarbon and carbon monoxide with relatively high NO_x emission. This implies high temperatures (see Section A) and long mixing times favorable to NO_x formation and CO and HC oxidation. Again, no appreciable fuel injector effect is observed except for a slight increase in CO emissions with increasing droplet SMD.

D. Summary

It has been demonstrated in Section A of this chapter that for high reference velocity flows, a distinct region of flow separation exists within and near the end of the prevaporizing tube. Also, there is a great possibility that fuel droplets are reaching the tube exit (at least near the tube wall) as indicated by static temperature measurements.

However, equally important is the fact that in all cases tested the overall differential pressure drop between the combustor inlet and the disc is the same for cold flow, hot flow (preheat combustor only), and reacting flow (both combustors). This means that velocity measurements at the disc can be made under cold flow conditions and related to a reacting flow environment. Using these results, it was found that the air velocity in the fuel preparation tube can be estimated from the velocity computed on the basis of the disc blockage. This result will prove valuable in the next chapters for estimating not only velocities but local equivalence ratios at the tube exit.

Along the tube centerline in the plane of the disc, unburned hydrocarbon concentrations are high indicating incomplete combustion;

however, HC concentrations are not as high as one would expect if the fuel were completely vaporized and mixed with the air. In the recirculation zone, the opposite is true; low CO and HC emissions as well as high temperatures are present. This is in agreement with Zukoski and Marble (1956) who state that the recirculation zone is a region of hot burned gases providing sufficient thermal energy for ignition.

The following chapters are concerned primarily with input/output experiments rather than detailed single point measurements. Both combustion efficiency and flame stabilization are considered using the geometry of Fig. 3-3. In addition, the degree of prevaporization is varied by injecting two different fuels, Jet A and liquid propane.

V. COMBUSTION EFFICIENCY

A. Quantification of Combustion Efficiency

Combustion efficiency, η_c, is defined as the percentage of available chemical energy released upon combustion of a fuel and oxidizer. One hundred percent combustion efficiency, however, is not attainable due to equilibrium conditions (especially at elevated temperatures); also incomplete combustion through quenching can limit combustion efficiency. This unused chemical energy is a measure of combustion inefficiency, $1-\eta_c$, and manifests itself primarily in concentrations of carbon monoxide (CO) and unburned hydrocarbons (HC). Hence the Air Force equation (Blazowski and Henderson, 1974) readily quantifies combustion inefficiency from practical systems through

$$1-\eta_c = \frac{(EICO)\ Q_{CO} + (EIHC)\ Q_{HC}}{Q_{fuel} \times 10^3} \qquad 5\text{-}1$$

where EIX = emissions index of species X (g X/kg fuel)

Q = respective lower heating value (cal/g)

and HC are measured as CH_4 in the present study.

B. Combustion Efficiency Correlation

Several parameters are available which correlate combustion efficiency from reacting systems. These include percent of maximum rated power (Hammond, 1977), combustor reference velocity (Grobman, 1972), and air loading (Longwell and Weiss, 1955). A traditional correlation for combustion efficiency in gas turbine combustors is the θ parameter (Lefebvre, 1966). This parameter is defined in Eq. 3-1 but reiterated here for convenience

$$\theta = \frac{P^{1.75}\ A_{ref}\ D_{ref}^{0.75}\ \exp(T_{in}/300)}{\dot{m}_a} \qquad 5\text{-}2$$

where P = combustor pressure, atm

T_{in} = inlet air temperature, K

$\dot{m}_a$ = air mass flow rate, kg/sec

A_{ref} = maximum combustor cross sectional area, m^2

D_{ref} = maximum combustor width, m.

The θ parameter is a powerful design tool in that for a given combustor, it will collapse efficiency data onto a single curve for any combination of airflow, inlet temperature and pressure. Unfortunately, the correlation does not account for explicit variations in geometry (for instance a change in the axial location of the secondary air penetration jets in a conventional burner), equivalence ratio, fuel injector or fuel type (Dodds et al., 1975). Correlating deficiencies in the θ parameter do however help identify relative trends, particularly for a combustor exhibiting a radical departure in design from conventional configurations (such as the tube-and-disc burner of this study). Furthermore, the θ parameter can demonstrate when these effects are insignificant.

Combustion efficiency data from the baseline (Geometry A) tube-and-disc flameholder are illustrated as a function of θ in Fig. 5-1. Here data for two simplex pressure atomizing nozzle (SMD) variations utilized in the Jet A experiments are presented at a constant inlet air temperature of 800K, equivalence ratio of 0.29 and air flow rate of 1.0 kg/s (recall from Table 3-3 that these and a combustor inlet pressure of 5.0 atm define the base operating point). It appears from this figure that heterogeneous effects on combustion efficiency are negligible for this geometry, these flow conditions, and this nozzle range except perhaps at low θ where nozzle effects are typically more pronounced. Droplet effects upon efficiency should become more important at the lower inlet air temperatures, lower equivalence ratios, and lower combustor pressures (Lefebvre, 1966).

These results also illustrate the very low combustion efficiencies associated with this type of burner especially at high reference velocities (low θ). Dodds et al. (1975) measured combustion efficiencies from the disc-in-duct burner discussed in Chapter II in the same manner and found minimum efficiencies of 85 percent at a θ value of 0.10. Thus the location of the fuel injector with respect to the recirculation zone has a dramatic effect upon combustion efficiency, a significant finding relevant to the dump burner. Unfortunately, a high degree of data scatter is typical of

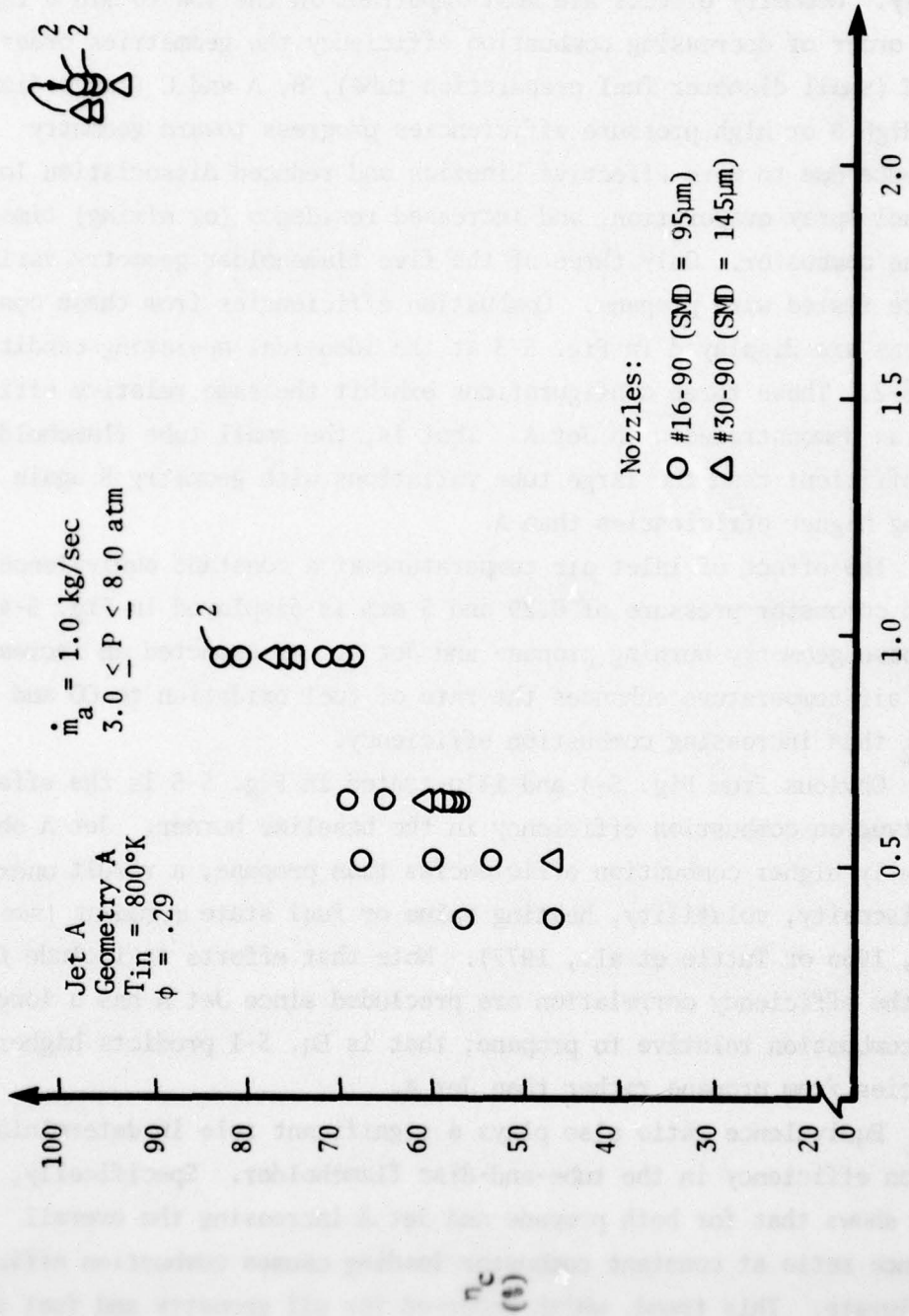

Figure 5-1. Droplet effect on combustion efficiency.

the tube-and-disc configuration for both Jet A and propane (see also Fig. 5-3).

The effect of tube-and-disc flameholder configuration is illustrated in Fig. 5-2 for Jet A and the constant base point conditions enumerated previously. Geometry effects are most important in the low to mid θ regime where in order of decreasing combustion efficiency the geometries order as D or E (small diameter fuel preparation tube), B, A and C (large diameter tube). High θ or high pressure efficiencies progress toward geometry independence due to more effective kinetics and reduced dissociation losses, better fuel spray evaporation, and increased residence (or mixing) times within the combustor. Only three of the five flameholder geometry variations were tested with propane. Combustion efficiencies from these configurations are displayed in Fig. 5-3 at the identical operating conditions of Fig. 5-2. These three configurations exhibit the same relative efficiencies as demonstrated with Jet A. That is, the small tube flameholder is more efficient than the large tube variations with geometry B again exhibiting higher efficiencies than A.

The effect of inlet air temperature at a constant equivalence ratio and combustor pressure of 0.29 and 5 atm is displayed in Fig. 5-4 for the base geometry burning propane and Jet A. As expected an increase in inlet air temperature enhances the rate of fuel oxidation to CO and of CO to CO_2 thus increasing combustion efficiency.

Obvious from Fig. 5-4 and illustrated in Fig. 5-5 is the effect of fuel type on combustion efficiency in the baseline burner. Jet A shows consistently higher combustion efficiencies than propane, a result unexpected from a viscosity, volatility, heating value or fuel state argument (see Lefebvre, 1966 or Tuttle et al., 1977). Note that efforts to include fuel type in the efficiency correlation are precluded since Jet A has a lower heat of combustion relative to propane; that is Eq. 5-1 predicts higher efficiencies from propane rather than Jet A.

Equivalence ratio also plays a significant role in determining combustion efficiency in the tube-and-disc flameholder. Specifically, Fig. 5-6 shows that for both propane and Jet A increasing the overall equivalence ratio at constant combustor loading causes combustion efficiency to deteriorate. This trend, which occurred for all geometry and fuel varia-

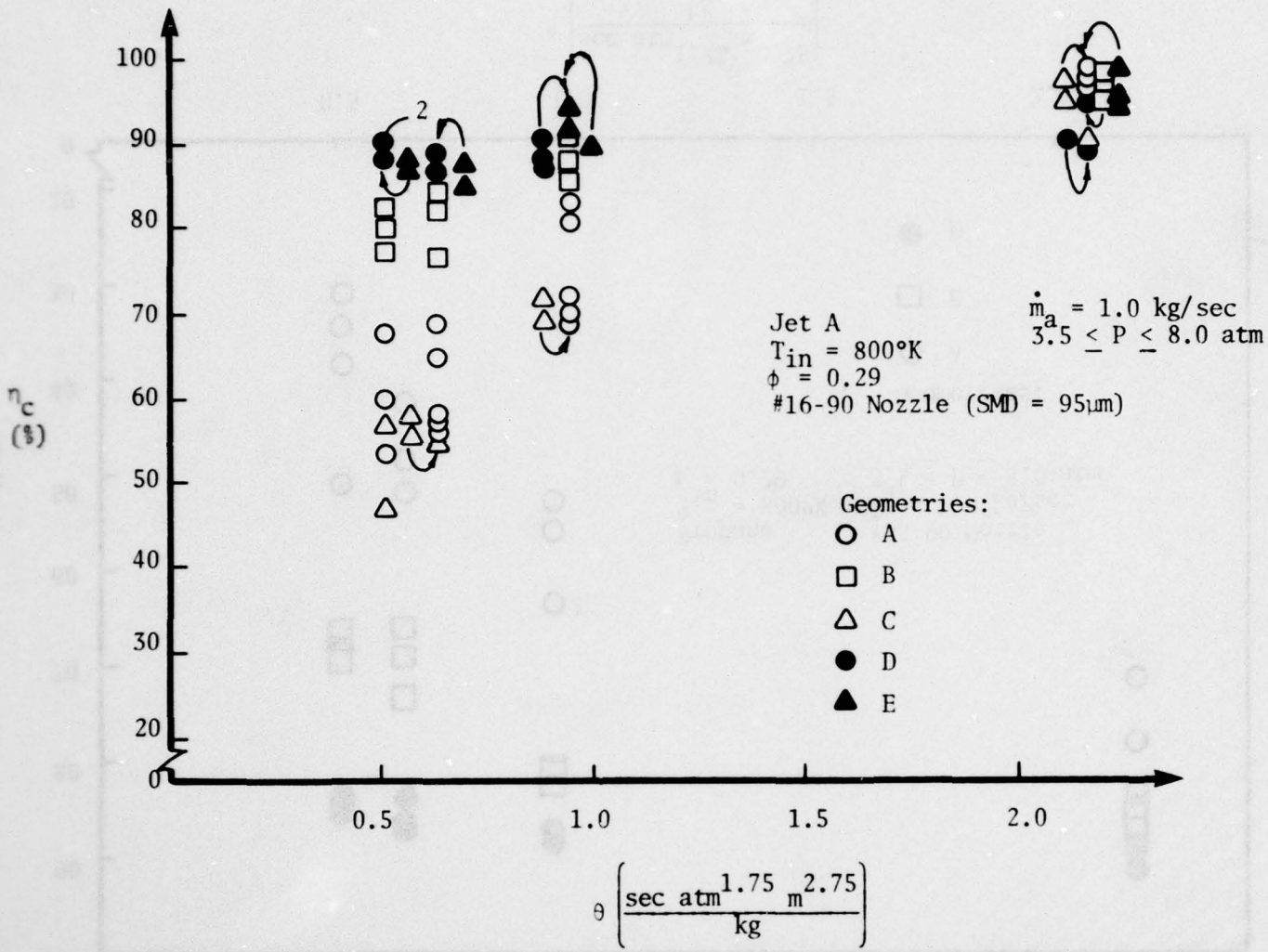

Figure 5-2. Tube-and-disc flameholder geometry effect on combustion efficiency (Jet A).

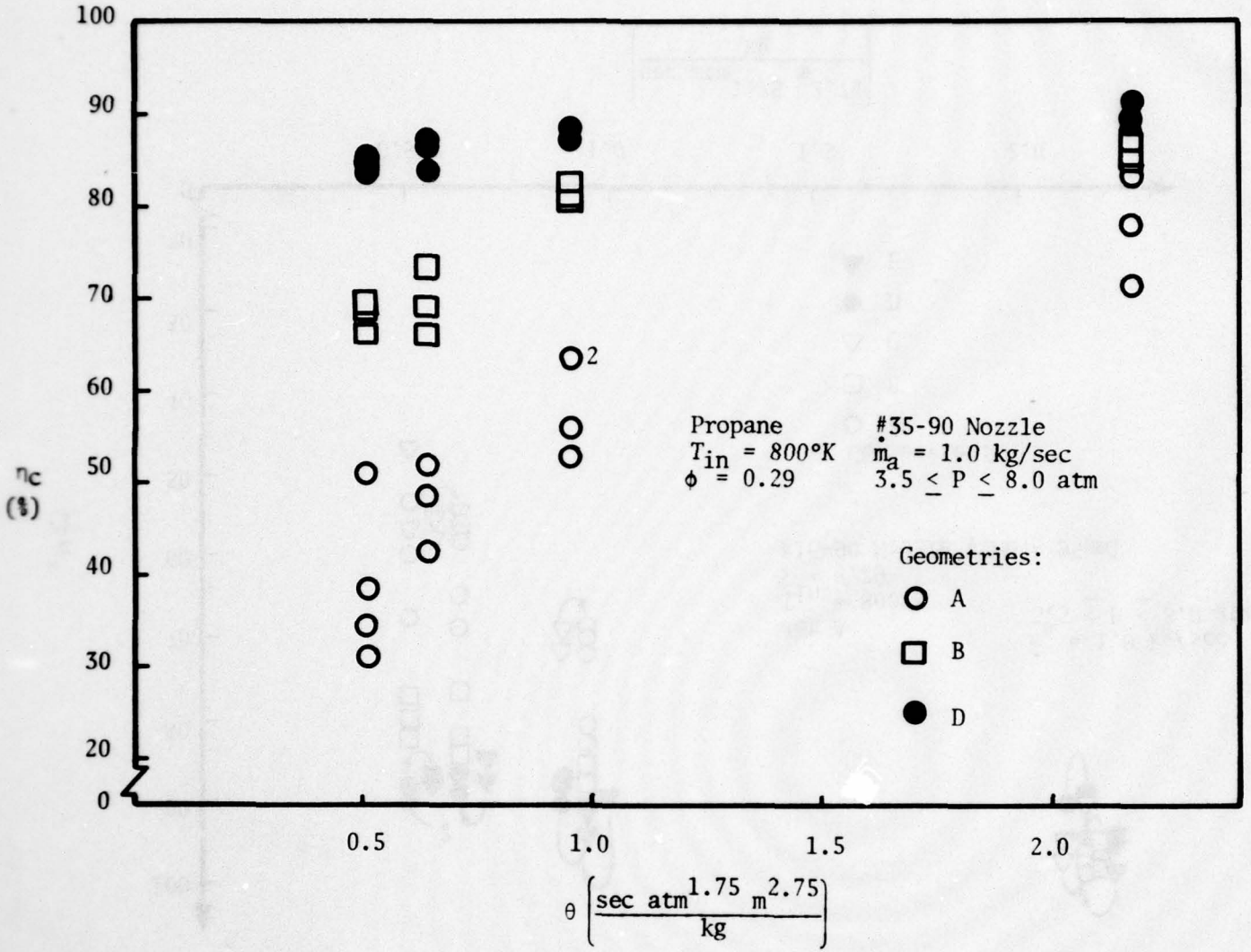

Figure 5-3. Tube-and-disc flameholder geometry effect on combustion efficiency (Propane).

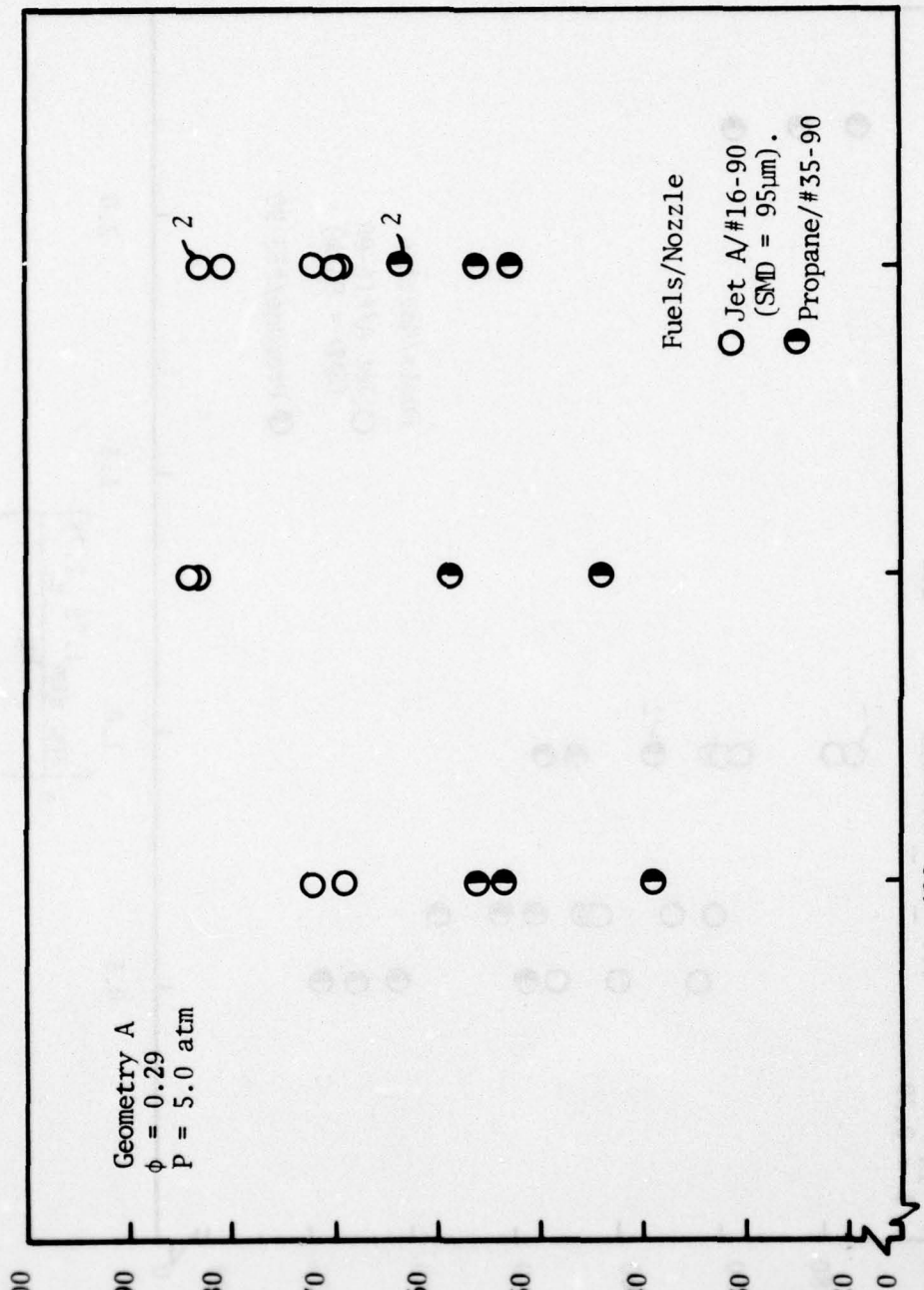

Figure 5-4. The effect of inlet air temperature on combustion efficiency.

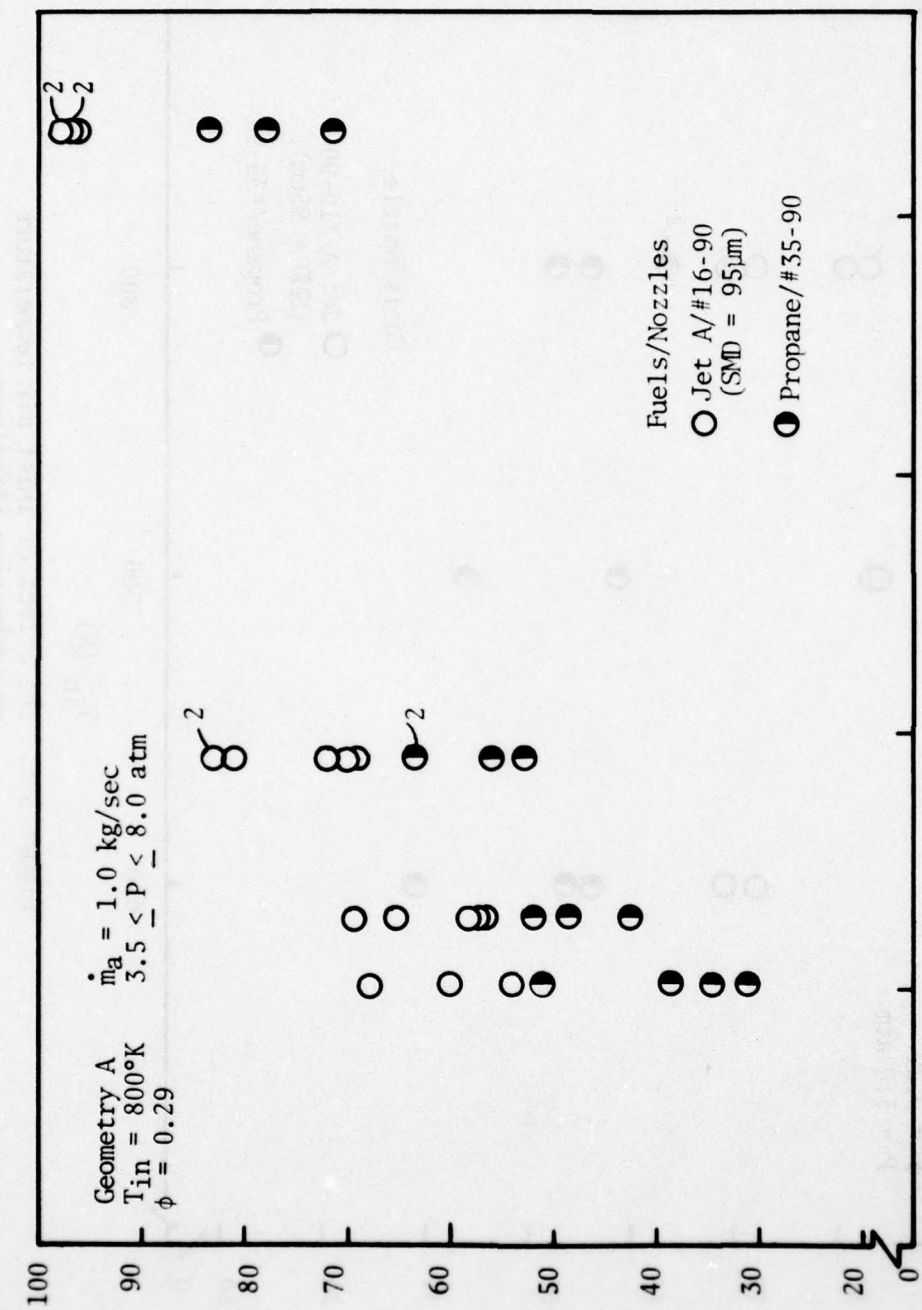

Figure 5-5. The effect of fuel type on combustion efficiency in the tube-and-disc burner.

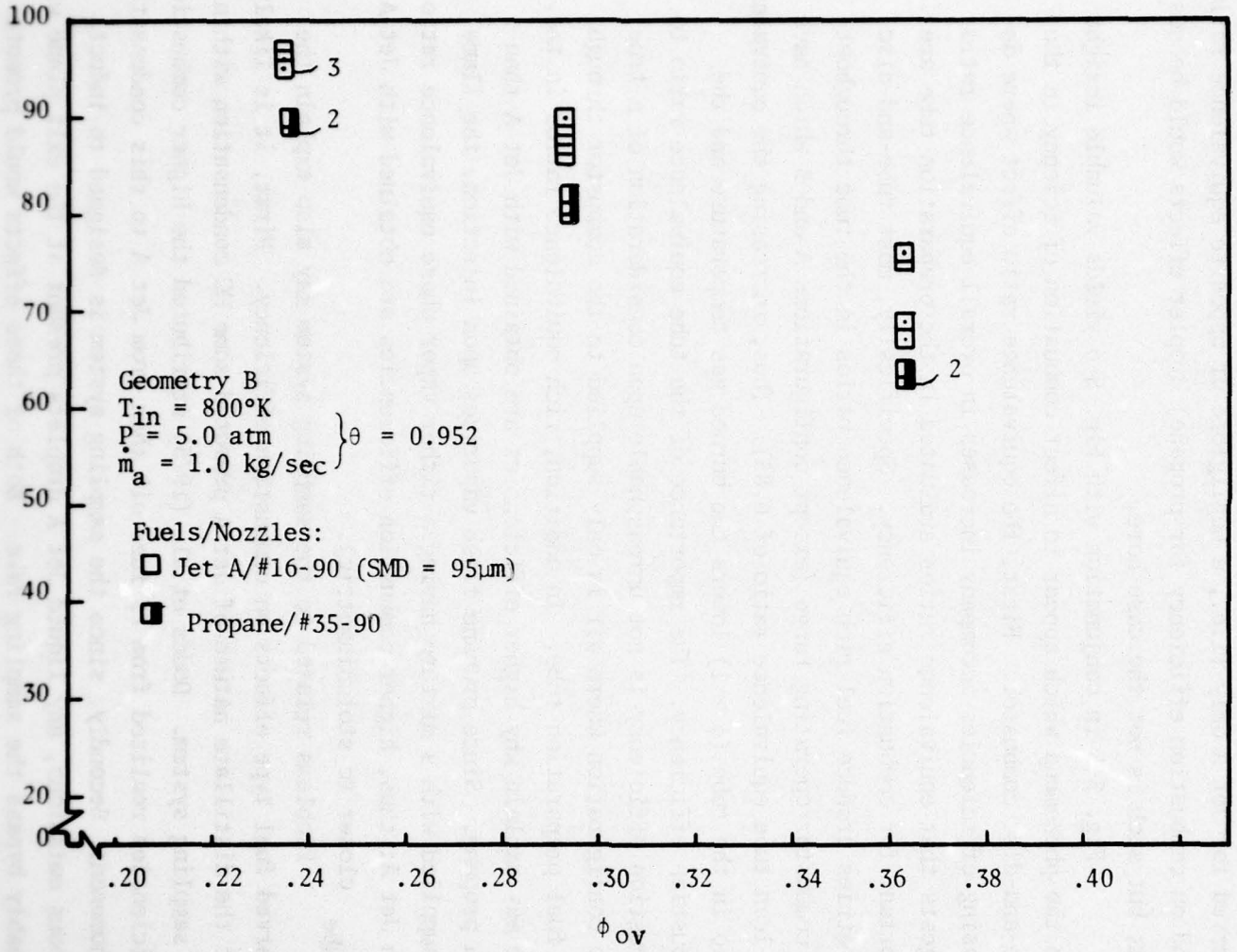

Figure 5-6. The overall equivalence ratio effect on combustion efficiency in the tube-and-disc burner.

tions, is opposite that observed in the disc-in-duct (Tuttle et al., 1977) and conventional (Mellor, 1977b) combustors for essentially the same range in overall equivalence ratio (i.e., $0.1 \leq \phi_{ov} \leq 0.4$). If this effect were observed for Jet A only (i.e., a negligible or opposite equivalence ratio trend on combustion efficiency for propane) droplet effects would be suspect; but such is not the case here.

Fig. 5-5 in conjunction with Fig. 5-6 yields valuable insight into the phenomena which appear to affect combustion efficiency in the tube-and-disc combustor. First, the equivalence ratio effect where decreasing efficiencies accompany increases in overall equivalence ratio suggests that equivalence ratios evaluated in the preparation tube are important for combustion efficiency. Specifically, most tube-and-disc geometries produce fuel rich equivalence ratios in the tube throughout the combustor operating range (except configurations A and B which have one lean tube equivalence ratio of 0.85). Thus, increasing the equivalence ratio in the tube ($\phi > 1$) lowers the burned gas temperature and the combustion efficiency. The importance of the tube equivalence ratio to combustion efficiency is not unreasonable upon consideration of a true dump configuration where air is only supplied to the combustor through the fuel preparation tube. In addition, rich equivalence ratios in the tube may explain why higher efficiencies are obtained with Jet A than with propane. Since propane flash vaporizes upon injection, the flame is supplied with a mixture having a richer vapor phase equivalence ratio than Jet A; thus, higher combustion efficiencies are obtained with Jet A (ϕ_{tube} closer to stoichiometric).

Problems related to the sampling system may also explain the observed fuel type effects on combustion efficiency. First, it is likely that the distillate nature of Jet A promoted some HC condensation within the sampling system. Dodds et al. (1975) attributed the higher combustion efficiencies realized from #5 fuel oil than from Jet A to this condensation phenomenon. Secondly, since the sampling system is designed to induct gaseous emissions, any liquid Jet A droplets present at the exit plane will probably bypass the sampling rake. Both of these effects would promote deceptively higher combustion efficiencies (lower HC readings) with Jet A relative to propane.

The present effort in correlating combustion efficiency in the tube-and-disc flameholder is devoted to extending the characteristic time model (discussed in Chapter II) to this configuration. As noted previously, inclusion of fuel type in these correlations may require more probing experiments based on the relative combustion efficiencies of Jet A and propane. However, it is expected that the characteristic time model will correlate inlet air, equivalence ratio and geometry effects for at least the propane data. In particular, Fig. 5-4 and 5-5 indicate that heterogeneous effects are not significant to combustion efficiency in the tube-and-disc burner within the range of variables incorporated. Therefore, the CO correlation of Tuttle et al. (1977) as expressed in Eq. 2-24 should extend to combustion inefficiency (provided that HC are proportional to CO) giving

$$100-\eta_c \sim \tau_\eta/\tau_{s\ell} \qquad 5\text{-}3$$

where τ_η = chemical kinetic time for fuel and CO oxidation to CO_2 (Arrhenius form)

$\tau_{s\ell}$ = turbulent mixing time in the region of predominant CO and HC quenching (generally a macro length scale divided by a velocity).

Inlet air temperature effects will be included in the characteristic time correlation primarily through the chemical kinetic time for fuel oxidation, τ_η. Inclusion of equivalence ratio is also expected through this kinetic time by utilizing the burned gas temperature based on the total tube equivalence ratio and by accounting for inlet air vitiation. The turbulent mixing time, $\tau_{s\ell}$, should permit inclusion of flameholder geometry effects through proper determination of the length and velocity scales. However, the appropriate characteristic times for combustion efficiency have not yet been determined quantitatively.

Combustion inefficiency was also measured with the shrouded combustor of Fig. 3-4. Results are summarized in Table 5-1 for the burner operating conditions of Table 3-5. In general, the shrouded combustor is slightly more efficient than the simplified combustor. Since the major parameters which influence efficiency (V_{ref}, T_{in}, etc.), have not been changed these results are not unexpected. Therefore, computer modeling

AD-A053 635 PURDUE UNIV LAFAYETTE IND COMBUSTION LAB F/G 20/2
FLAME EFFICIENCY, STABILIZATION AND PERFORMANCE IN PREVAPORIZIN--ETC(U)
DEC 77 S L PLEE, D A SCHMIDT, A M MELLOR AFOSR-76-2936

UNCLASSIFIED PURDU-CL-77-07 AFOSR-TR-78-0736 NL

2 OF 3
ADA
053635

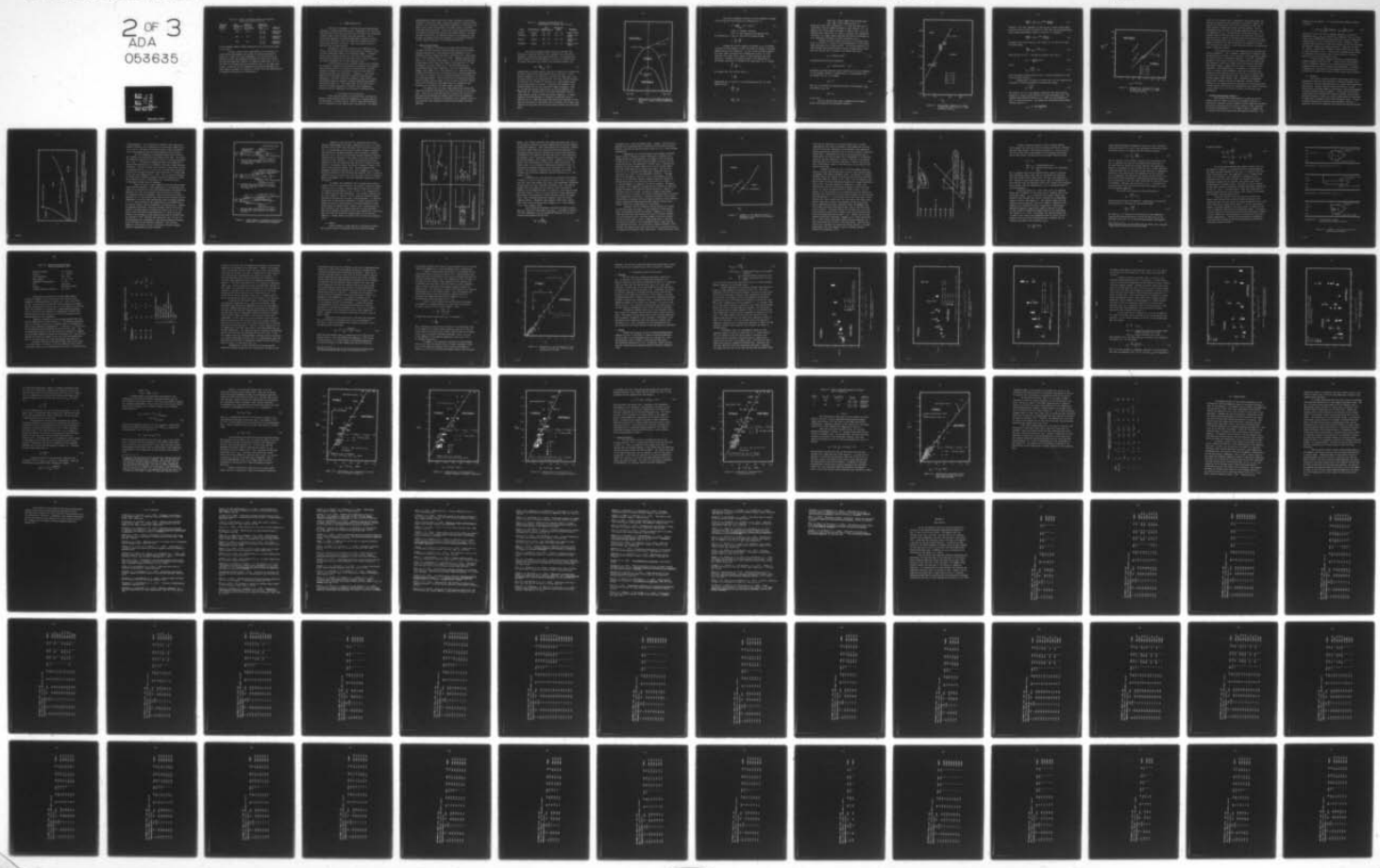

Table 5-1. Effect of Shrouded Combustor on Combustion Inefficiency (ϕ_{OV}=0.29, Jet A)

Combustor Pressure P(atm)	Inlet Temperature T_{in} (K)	Reference Velocity V_{ref} (m/sec)	Combustion Inefficiency 100-η_c	Combustor
8	800	17.0	.02-.03	Simplified
			.02-.06	Shrouded
5	800	27.1	.17-.18	Simplified
			.14-.15	Shrouded
4	800	34.0	.42-.43	Simplified
			.37-.44	Shrouded

for the shrouded combustor should demonstrate only a second order effect of the shroud.

In order to obtain better understanding of the flowfield, detailed internal measurements are proposed for selected tube-and-disc geometries. Single point probe measurements will provide species concentration profiles and temperature estimates and should yield insight into the most significant region(s) of combustion inefficiency, be it in the shear layer encompassing the recirculation zones or some region downstream. In addition, velocity magnitude and direction measurements via laser Doppler velocimetry are expected to further aid in the identification of appropriate characteristic time parameters.

VI. FLAME STABILIZATION

One obvious requirement of advanced prevaporizing/premixing combustors is proper flame stabilization. High approach flow velocities and relatively low fuel flow rates may cause the flame to be extinguished (blowoff) under certain low power operating conditions. This is particularly important in prevaporizing/premixing combustors because locally high equivalence ratios and temperatures normally present in conventional combustors are absent. Thus, lean blowoff as well as ignition limits are much narrower.

Introduction of the fuel upstream of the flameholder also creates a second flame stabilization problem known as flashback, which can cause considerable damage to the combustion chamber. Flashback results from increasing the fuel/air ratio toward stoichiometric (increasing the flame speed) or decreasing the air velocity, allowing the flame to propagate into the fuel preparation tube.

In the following sections, problems associated with flashback and blowoff are examined for both laminar and turbulent flow situations. With the help of existing literature, the characteristic time model discussed in Chapter II is successfully applied to lean blowoff in turbulent bluff body stabilized flames. In addition, a qualitative model has been developed to explain the reported upstream flame propagation. Both these results are extended to flame stabilization data obtained using the simplified prevaporizing/premixing combustor described in Chapter III. The blowoff model for the tube-and-disc combustor correlates variations in pressure, inlet temperature, reference velocity, flameholder size and degree of prevaporization.

A. Derivation of the Correlation

In the previous sections, the characteristic time model was applied to both practical burners and combustors of research interest for the purpose of emission control. However, flame stabilization can also be interpreted via the characteristic time approach. For laminar

premixed gaseous (Bunsen burner type) flames, the model is essentially equivalent to the Peclet number correlation proposed by Putnam and Jensen (1949); it also represents a quantitative application of the Zukoski and Marble (1956) theory for predicting lean blowoff limits in turbulent bluff body stabilized flames. In all cases, flame stabilization involves the competition between fluid mechanic and chemical effects. The model therefore characterizes the combustion process by an appropriate fluid mechanic and chemical time scale evaluated in the particular region of the flow field of importance to the stabilization process.

1. Laminar Premixed Flames

The majority of flashback and blowoff data available in the literature has been obtained in laminar premixed flows for gas-burning appliance applications at room temperature and atmospheric or sub-atmospheric pressure (Putnam and Jensen, 1949; Wohl et al., 1949; Grumer et al., 1953 and 1956; Khitrin et al., 1965). Turbulent approach flows (Wohl et al., 1949; Wohl, 1953; Grumer et al., 1953 and 1956; Boyer and Friebertshauser, 1957; Fine, 1958; Grumer, 1958; Khitrin et al., 1965) and geometry variations (Grumer et al., 1953 and 1956) have also been considered under these conditions. Only a few investigators (Dugger, 1950; Grumer et al., 1956; Khitrin et al., 1965) have reported flashback and blowoff results for approach flows at elevated temperatures (see Table 6-1); however, all are for gaseous premixed systems burning H_2 or pure hydrocarbons. After a brief review of existing correlations, some of the data listed in Table 6-1 will be used to illustrate applications of the characteristic time model and also to demonstrate the equivalence of the model to the Peclet number correlation.

For laminar flow in a tube, flame stabilization involves the competition between fluid mechanics and chemical kinetics in the boundary layer. Early work on flame stabilization in laminar flow consisted of experimentally determining the average velocity at which flashback or blowoff occurred as a function of equivalence ratio. However results of this nature were only valuable for one particular geometry and inlet condition.

Table 6-1. Flashback and Blowoff Data for Heated Reactants (Laminar Flow, P=1 atm)

Limit	Fuel/Oxidizer	Inlet Temperature, K	Equivalence Ratio	Reference
Blowoff	C_3H_8/Air	300 - 620	0.8 - 1.6	Dugger (1950)
Flashback	CH_4/Air	300 - 525	0.6 - 1.4	Grumer et al. (1956)
Blowoff	CH_4/Air	300 - 525	0.6 - 1.4	Grumer et al. (1956)
Flashback	CH_4/O_2	373 - 673	0.3 - 1.6	Khitrin et al. (1965)

The velocity gradient theory of Lewis and von Elbe (see discussion in Lewis and von Elbe, 1961) represents one of the first attempts at correlating flame stabilization data. For flashback, the theory balances the velocity gradient at the wall (g) with the ratio of laminar flame speed (S_L) divided by the quenching distance (d_c),

$$g_{fb} = \left(\frac{du}{dr}\right)_{wall} = \frac{S_L}{d_c} \quad , \qquad 6\text{-}1$$

assuming that the stream velocity curve can be replaced by a straight line having the slope of the stream velocity curve at the wall. If the velocity gradient is less than S_L/d_c, the flame will flash back; if it is greater than S_L/d_c, the flame will blow out of the tube and stabilize on the burner rim. Blowoff is represented in a similar manner except the velocity gradient at the wall is replaced by the gradient at the boundary between the tube flow and outside ambient conditions. When g_{bo} exceeds the critical value of S_L/d_c at the free boundary, the flame blows off. Therefore plots of g versus equivalence ratio (ϕ) should indicate regions of stable and unstable combustion. A typical diagram of velocity gradient as a function of equivalence ratio is shown in Fig. 6-1. Note that in air the blowoff curve continues to rise after the stoichiometric equivalence ratio is reached; this is due to the diffusion of oxygen into the rich mixture which increases the local flame speed.

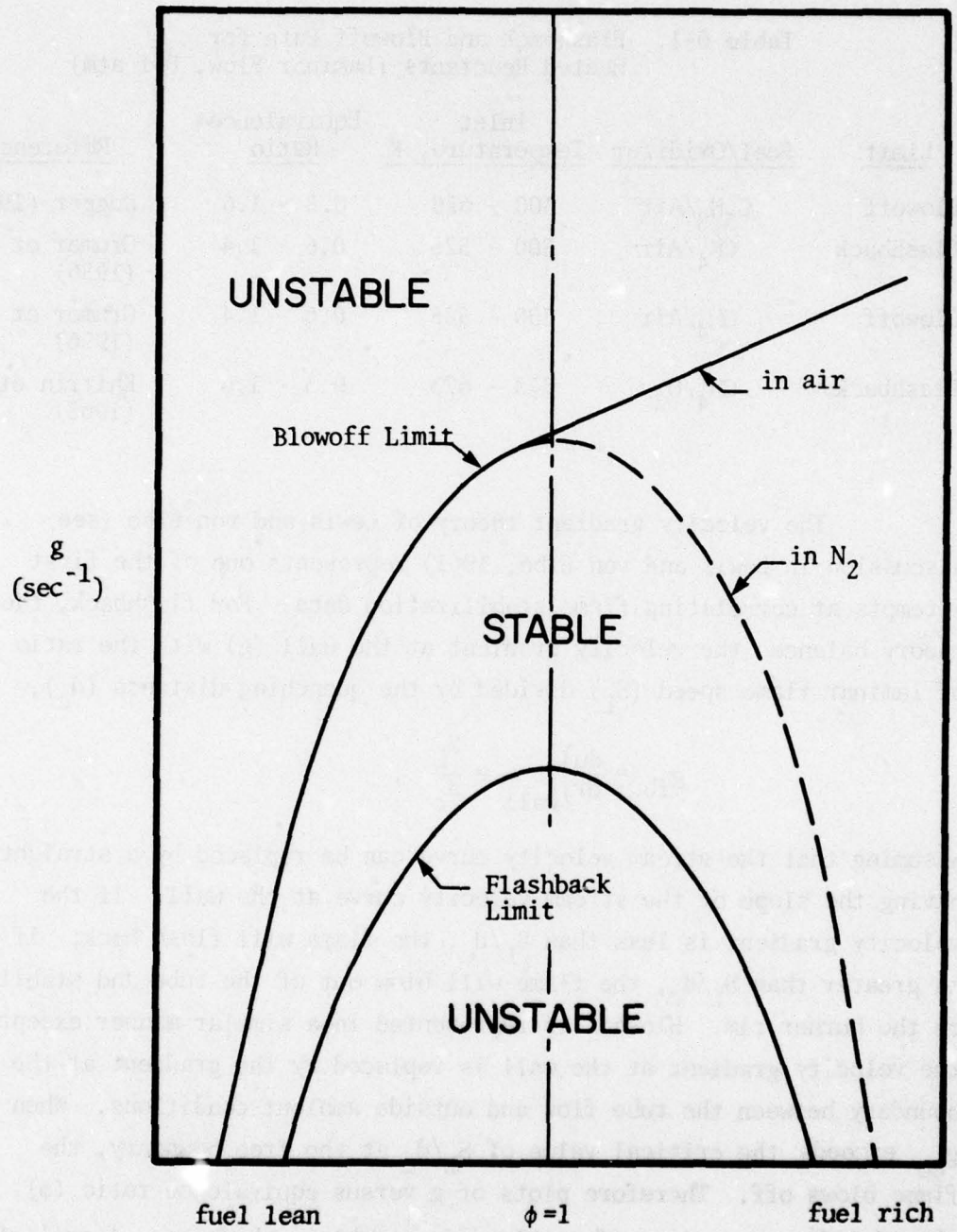

Figure 6-1. Representation of flashback and blowoff limits for a laminar premixed hydrocarbon flame.

The velocity gradient at the wall is easily computed in laminar flow by using the friction factor (f) defined by Eq. 6-2,

$$f = 8\nu \left.\frac{du}{dr}\right|_{wall} \bar{u}^{-2} = 8\nu g\, \bar{u}^{-2} \quad , \qquad 6\text{-}2$$

where ν = kinematic viscosity

and $\bar{u}$ = mean velocity of the approach flow.

By combining Eq. 6-1 and 6-2, the velocity gradient becomes

$$g = \frac{S_L}{d_c} = \frac{f\bar{u}^2}{8\nu} \quad . \qquad 6\text{-}3$$

Although the velocity gradient correlation (g vs. ϕ) includes variations in tube diameter, it fails to account for changes in pressure, temperature and inlet composition. In 1949, Putnam and Jensen proposed the Peclet number correlation for flashback which results in a more universal curve rather than a family of curves dependent upon inlet conditions. Assuming the quenching distance to be proportional to the thermal diffusivity (α) divided by the flame speed, Eq. 6-3 becomes

$$\frac{S_L^2}{\alpha} \sim \frac{f\bar{u}}{8\nu} = g \quad . \qquad 6\text{-}4$$

For laminar flow, the friction factor is

$$f = \frac{64}{Re} \quad . \qquad 6\text{-}5$$

Substituting Eq. 6-5 into Eq. 6-4 and multiplying by d^2/α (d = tube diameter) gives

$$\frac{S_L^2 d^2}{\alpha^2} \sim \frac{\bar{u}d}{\alpha} \quad . \qquad 6\text{-}6$$

or

$$Pe_{S_L}^2 \sim Pe_{\bar{u}} \qquad 6\text{-}7$$

where Pe_{S_L} = Peclet number based on flame speed
and $Pe_{\bar{u}}$ = Peclet number based on $\bar{u}$.

Putnam and Jensen (1949) and Khitrin et al. (1965) have been able to successfully correlate laminar flashback in tubes using Eq. 6-7. An example of the Peclet number correlation is shown in Fig. 6-2 for the flashback data of Khitrin et al. (1965) at elevated inlet temperatures (see Table 6-1); common symbols represent data points corresponding to inlet temperature variations at a given equivalence ratio.

Although the Peclet number correlation is more general than plots of g versus ϕ, it requires accurate determination of the laminar flame speed which is not always possible. An alternate approach is to view the flame stabilization process in terms of characteristic times. Since the reaction rate is related to the laminar flame speed

$$S_L \sim (\text{reaction rate})^{\frac{1}{2}} \quad , \qquad 6\text{-}8$$

an ignition delay time can be defined as

$$\tau_{hc} \sim (\text{reaction rate})^{-1} \sim S_L^{-2} \quad . \qquad 6\text{-}9$$

Furthermore, assuming that the velocity gradient at the wall (flashback) or free boundary (blowoff) is proportional to a fluid mechanic time for laminar flow, Eq. 6-10 becomes

$$\tau_{fm} \sim g^{-1} \quad . \qquad 6\text{-}10$$

Thus, Eq. 6-4 involves the competition between a fluid mechanic (τ_{fm}) and chemical (τ_{hc}) time

$$\tau_{fm} \sim \tau_{hc} \qquad 6\text{-}11$$

at the limit.

The fuel ignition delay time is computed from the general overall rate expression for hydrocarbon oxidation

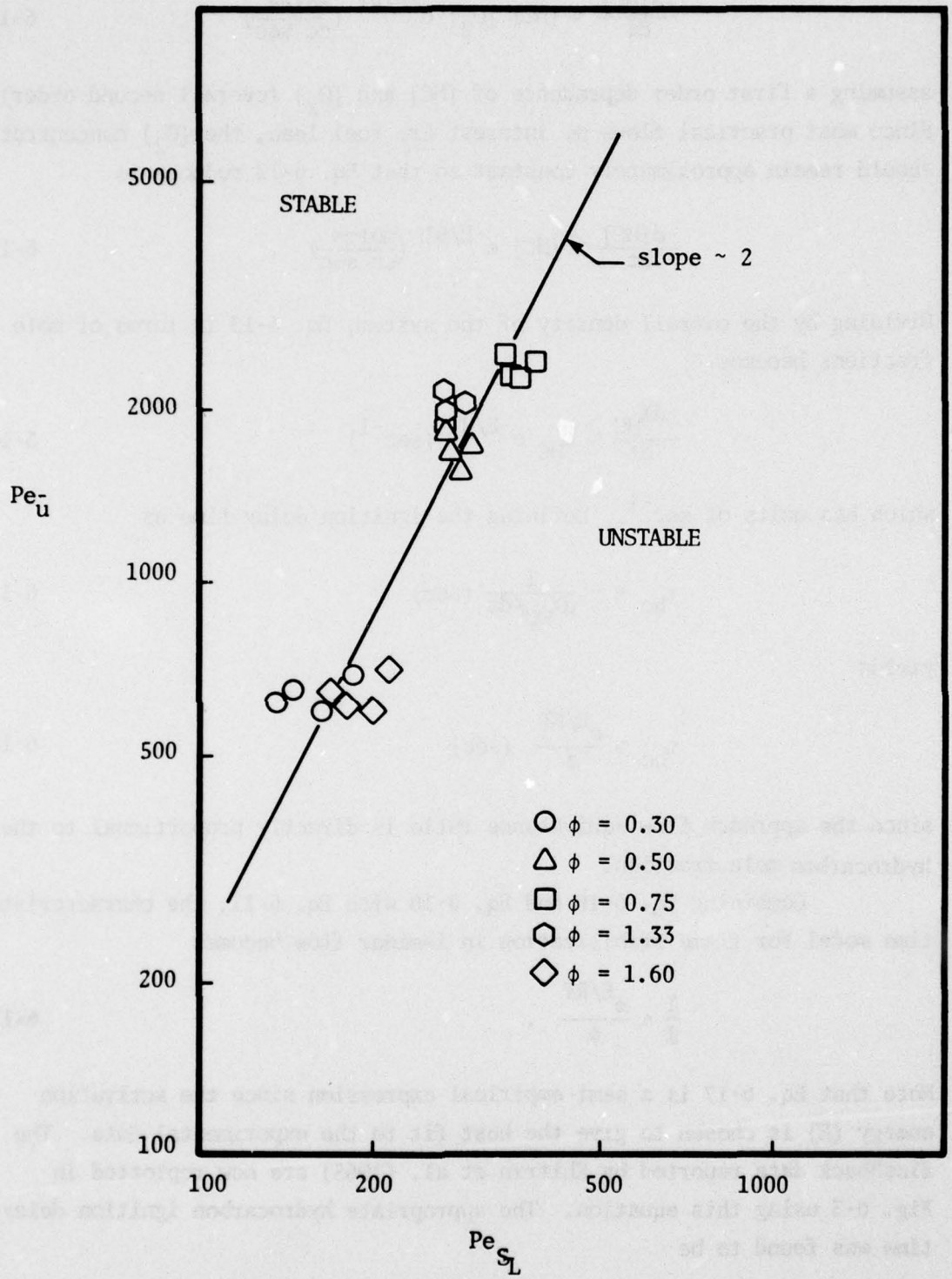

Figure 6-2. Peclet number correlation for CH_4/O_2 flashback data (Khitrin et al., 1965) at various ϕ and T_{in}.

CL-905

$$\frac{-d[HC]}{dt} \sim [HC]\ [O_2]\ e^{-E/RT}\ \left(\frac{\text{moles}}{\text{cc sec}}\right) \qquad 6\text{-}12$$

assuming a first order dependence of [HC] and $[O_2]$ (overall second order). Since most practical flows of interest are fuel lean, the $[O_2]$ concentration should remain approximately constant so that Eq. 6-12 reduces to

$$\frac{-d[HC]}{dt} \sim [HC]\ e^{-E/RT}\ \left(\frac{\text{moles}}{\text{cc sec}}\right) \quad . \qquad 6\text{-}13$$

Dividing by the overall density of the system, Eq. 6-13 in terms of mole fractions becomes

$$\frac{-dX_{HC}}{dt} \sim X_{HC}\ e^{-E/RT}\ (\text{sec}^{-1}) \qquad 6\text{-}14$$

which has units of sec^{-1}. Defining the ignition delay time as

$$\tau_{hc} = -\ \frac{1}{dX_{HC}/dt}\ (\text{sec}) \qquad 6\text{-}15$$

yields

$$\tau_{hc} \sim \frac{e^{E/RT}}{\phi}\ (\text{sec}) \qquad 6\text{-}16$$

since the approach flow equivalence ratio is directly proportional to the hydrocarbon mole fraction.

Combining Eq. 6-16 and Eq. 6-10 with Eq. 6-11, the characteristic time model for flame stabilization in laminar flow becomes

$$\frac{1}{g} \sim \frac{e^{E/RT}}{\phi} \quad . \qquad 6\text{-}17$$

Note that Eq. 6-17 is a semi-empirical expression since the activation energy (E) is chosen to give the best fit to the experimental data. The flashback data reported by Khitrin et al. (1965) are now replotted in Fig. 6-3 using this equation. The appropriate hydrocarbon ignition delay time was found to be

$$\tau_{hc} = 10^{-7}\ \frac{\exp\ (18000/RT)}{\phi} \qquad 6\text{-}18$$

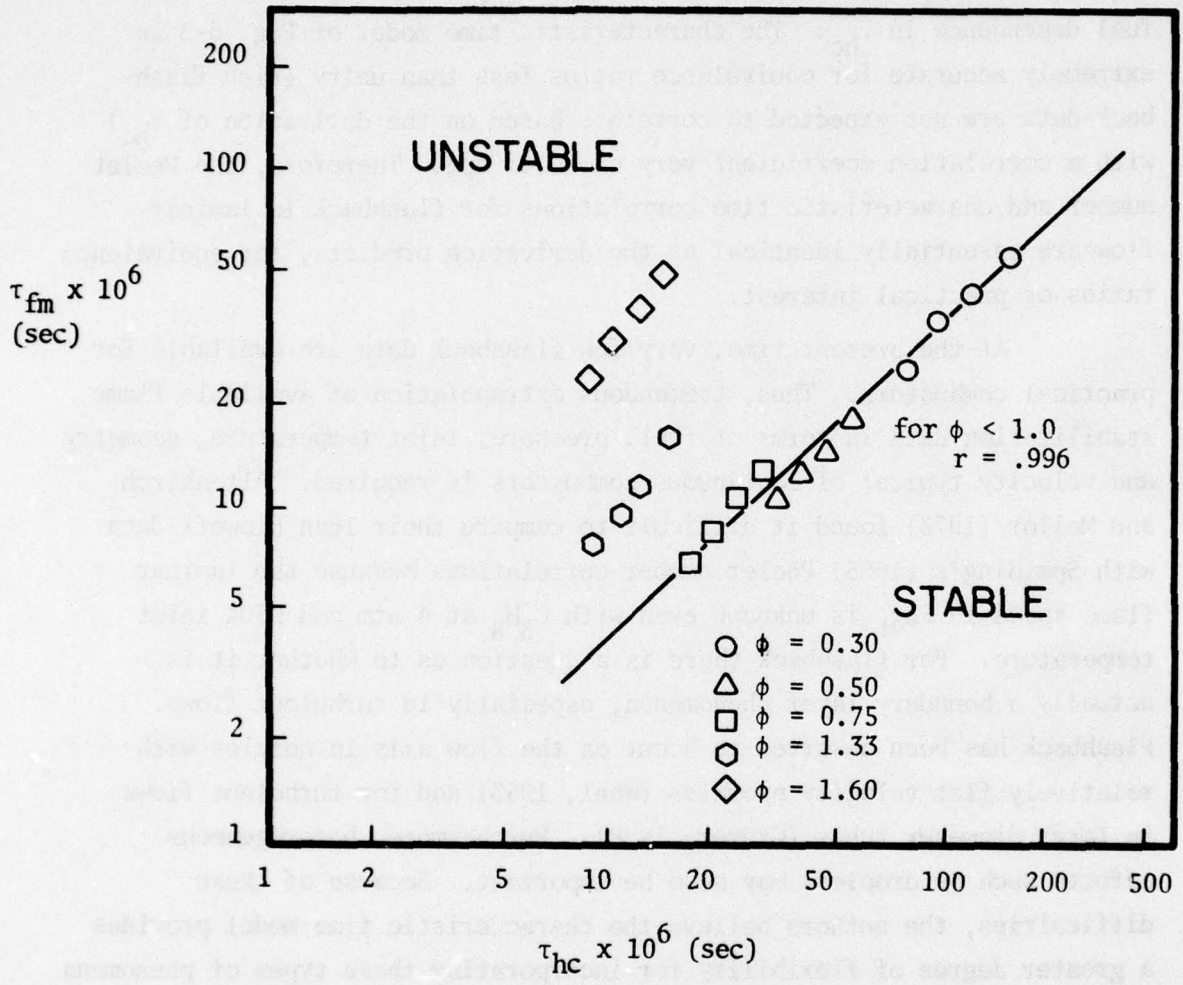

Figure 6-3. Characteristic time model for CH_4/O_2 flashback data (Khitrin et al.,1965) at various ϕ and T_{in}.

(units on E are cal/mole) with T evaluated at the average between the inlet and the adiabatic flame temperature at flashback. However, the apparent activation energy in Eq. 6-18 is substantially lower than values reported in Cooke and Williams (1975) for methane. This is attributed to the selection of an average temperature and first order fuel dependence in τ_{hc}. The characteristic time model of Fig. 6-3 is extremely accurate for equivalence ratios less than unity (rich flashback data are not expected to correlate based on the derivation of τ_{hc}) with a correlation coefficient very close to one. Therefore, the Peclet number and characteristic time correlations for flashback in laminar flow are essentially identical as the derivation predicts, for equivalence ratios of practical interest.

At the present time, very few flashback data are available for practical combustors. Thus, tremendous extrapolation of available flame stabilization data in terms of fuel, pressure, inlet temperature, geometry and velocity typical of continuous combustors is required. Altenkirch and Mellor (1973) found it difficult to compare their lean blowoff data with Spalding's (1955) Peclet number correlations because the laminar flame speed in Pe_{S_L} is unknown even with C_3H_8 at 4 atm and 950K inlet temperature. For flashback there is a question as to whether it is actually a boundary layer phenomenon, especially in turbulent flows. Flashback has been observed to occur on the flow axis in nozzles with relatively flat velocity profiles (Wohl, 1953) and for turbulent flows in large diameter tubes (Grumer, 1958). Furthermore, heterogeneous effects such as droplets may also be important. Because of these difficulties, the authors believe the characteristic time model provides a greater degree of flexibility for incorporating these types of phenomena in flame stabilization correlations for modern air-breathing engine applications.

2. Prevaporizing/Premixing Combustors

Since laminar flame speeds required for both the velocity gradient and Peclet number correlation are extremely difficult to calculate for conditions typical of modern aircraft combustors, we prefer a correlation technique which is directly related to inlet conditions. The inverse theta parameter (θ^{-1}) of Lefebvre (1966) is commonly used to correlate flame stabilization data (and combustion efficiency - see

Chapter V) in gas turbines. θ^{-1}, which represents combustor loading, is given by

$$\frac{1}{\theta} = \frac{\dot{m}_a}{P^{1.75} A_{ref} D_{ref}^{0.75} e^{T_{in}/300}} \quad \left(\frac{kg}{sec\ atm^{1.75}\ m^{2.75}}\right) \qquad 6\text{-}19$$

where $\dot{m}_a$ is the air flow rate, P combustor pressure, T_{in} inlet air temperature and A_{ref} (D_{ref}) combustor area (diameter). Fig. 6-4 illustrates the relationship which exists between the classical flashback and blowoff limits for a fuel lean combustion system. Flashback is most prevalent under conditions of high local equivalence ratio and relatively low combustor loading (low reference velocity). Note that for large θ^{-1} a point is reached where flashback is not possible over any range of local equivalence ratios. Since blowoff is mechanistically similar to flashback, the lean blowoff limit is characterized by relatively high velocities and low equivalence ratios.

In the following, flashback and blowoff in prevaporizing/premixing combustors are discussed. A recent review (Plee and Mellor, 1977) of "flashback" reported in the literature has identified four mechanisms which may lead to upstream flame propagation. In addition, a characteristic time model has been developed for correlating lean blowoff data from bluff body stabilized flames burning gaseous propane.

a. Flashback

For realistic advanced prevaporizing/premixing combustors, no comprehensive study involving flashback is currently available in the literature for practical hydrocarbon fuels at elevated inlet temperatures and pressures. Instead, upstream flame stabilization is usually observed while performing combustion efficiency or emission measurements or during transient combustor operation. A great deal of overlap and inconsistency exists between these reported flashbacks and the stable operating conditions of other investigators which cannot be interpreted by simple inlet or geometry effects (Plee and Mellor, 1977). A recent literature review of this subject by Plee and Mellor (1977) has identified four possible mechanisms which explain the observed upstream

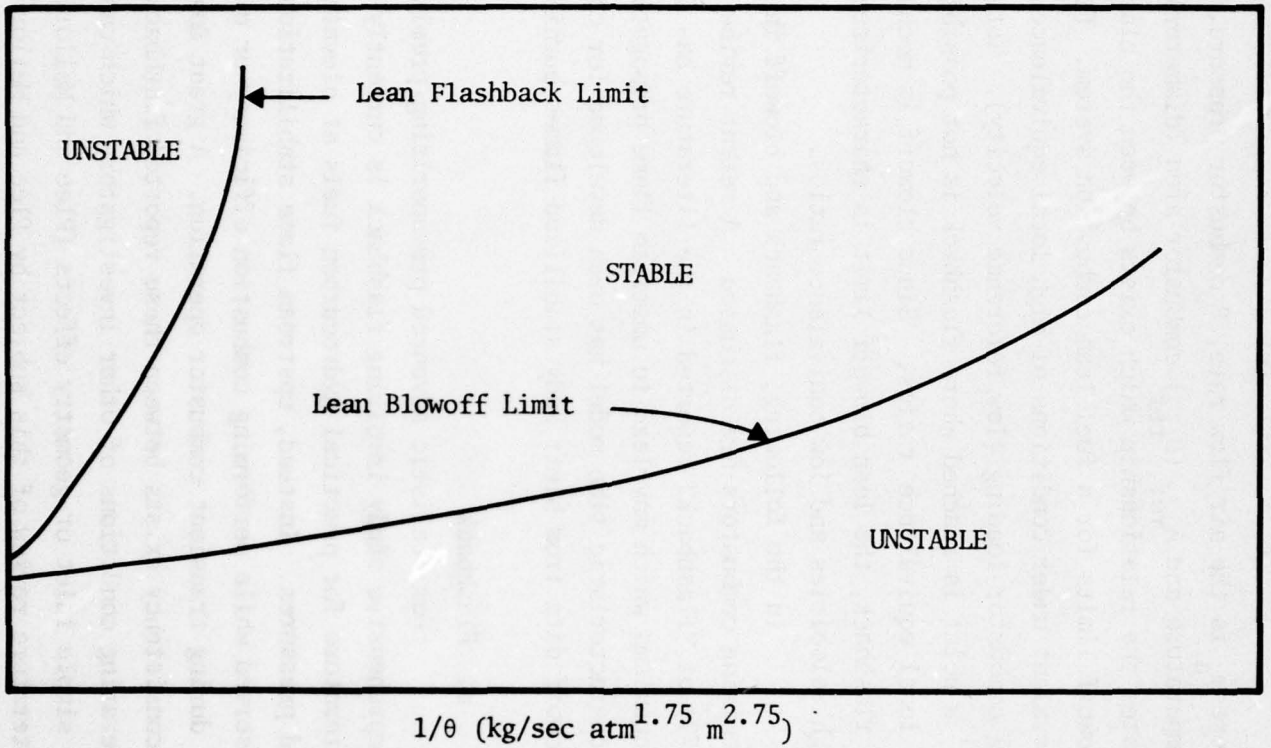

Figure 6-4. Representation of flashback and blowoff limits as a function of ϕ and θ^{-1} for lean prevaporized/premixed combustion systems.

flame propagation. All are functions of combustor inlet temperature, pressure, velocity, local equivalence ratio and overall combustor geometry; however, the latter two are also related to flow disturbances in the fuel preparation tube and even the method of fuel injection.

The first mechanism is autoignition which results from the gas residence time exceeding the fuel ignition delay time. This causes the spontaneous ignition of the fuel/air mixture in the fuel preparation tube. Fig. 6-5 illustrates schematically three other mechanisms of upstream flame propagation for a combustor utilizing a sudden expansion flameholder. Classical flashback (as discussed in the previous section) is represented by Fig. 6-5a. In this case, upstream flame propagation usually occurs through the boundary layer and results in a stable flame at the fuel inlet (Wampler et al., 1976). Thus in classical flashback, the flame actually propagates upstream, while for autoignition, spontaneous combustion occurs. Unfortunately, it is usually difficult to distinguish between these two phenomena.

Figure 6-5b and 6-5c show examples of flow disturbances which induce upstream combustion. Flame stabilization in the separated flow region can be charaterized by the relationship between the characteristic dimension (d) of the flow disturbance and the distance (L) between the disturbance and the flameholder. When these are the same order of magnitude ($d \sim L$), the separated flow region interacts directly with the flameholder recirculation zone enabling the flame to propagate upstream. If $d \ll L$, the recirculation zone established by the disturbance does not interact directly with the flameholder recirculation zone. Instead, the upstream zone provides sufficient residence time for the fuel/air mixture in the wake region to autoignite as shown in Fig. 6-5c. This differs from conventional autoignition which is a result of the gas residence time exceeding the fuel ignition delay time in the mean flow. Plee and Mellor (1977) concluded that mechanisms b and c of Fig. 6-5 and autoignition were responsible for the upstream combustion reported in the literature for non-catalytic combustors. Only catalytic combustors, which operate at very low reference velocities, appear capable of experiencing classical flashback.

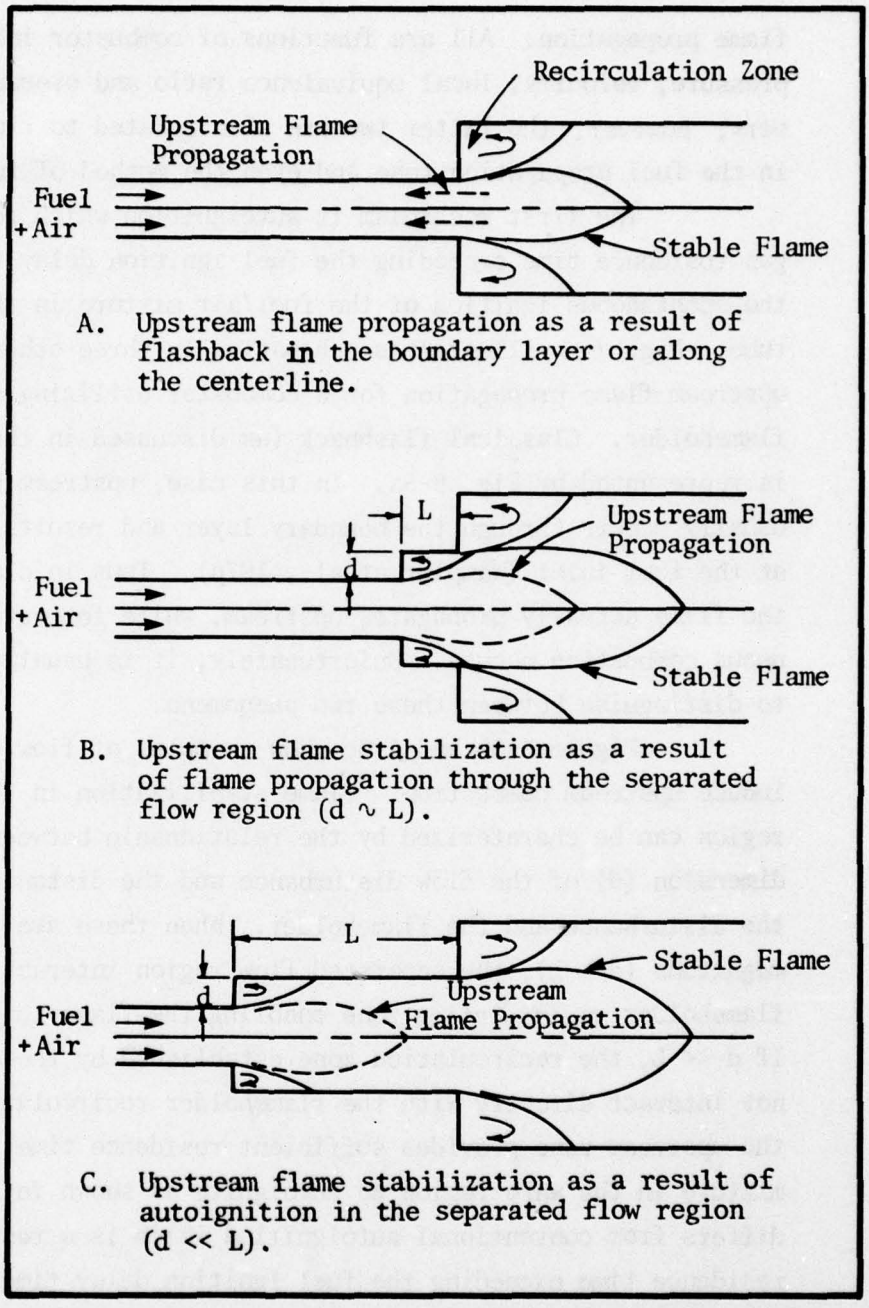

Figure 6-5. Flame schematic illustrating three possible mechanisms of upstream flame propagation.

Examples of other possible flow disturbances which cause upstream flame propagation are shown schematically in Fig. 6-6. Roffe and Ferri (1976), Roffe (1976) and Craig (1976) were able to avoid problems of upstream flame stabilization by using a straight cylindrical fuel preparation tube which eliminated flow disturbances altogether. Roberts, P. et al. (1976) also experienced upstream combustion caused by separated flow at some point in the radial to axial flow transition of a Vortex Air Blast combustor. In fact, flow separation and finally combustion in the fuel preparation tube can even be triggered by small details in the hardware such as the failure to properly connect a slip joint in the mixing tube (Roffe, 1976). Only the upstream flame propagation reported by Anderson et al. (1975), Wampler et al. (1976), Blazowski and Bresowar (1974) and Blazowski and Walsh (1975) in catalytic combustors are in the region where one would expect classical flashback; however, only Wampler et al. (1976) has completely eliminated all flow disturbances.

In summary, Plee and Mellor (1977) concluded that classical flashback has not yet been observed in non-catalytic combustors burning liquid jet fuels or propane. Instead, upstream combustion as a result of autoignition and mechanisms b and c of Fig. 6-5 are responsible for the reported upstream flame propagation. Only catalytic combustors are at a small enough θ^{-1} (see Fig. 6-4) for classical flashback; however, flashback and autoignition are usually indistinguishable. It therefore appears that in non-catalytic combustors a straight cylindrical fuel preparation tube will avoid problems of upstream combustion by eliminating regions of separated flow. However, care is advised since the exact location of the lean flashback limit has not been determined. There may be operating conditions at high inlet temperatures or pressures which are within the classical flashback regime for non-catalytic combustors. Further details are given in the review by Plee and Mellor (1977).

b. Blowoff

Unlike flashback, a large quantity of experimental blowoff data currently exists for turbulent bluff body stabilized flames.

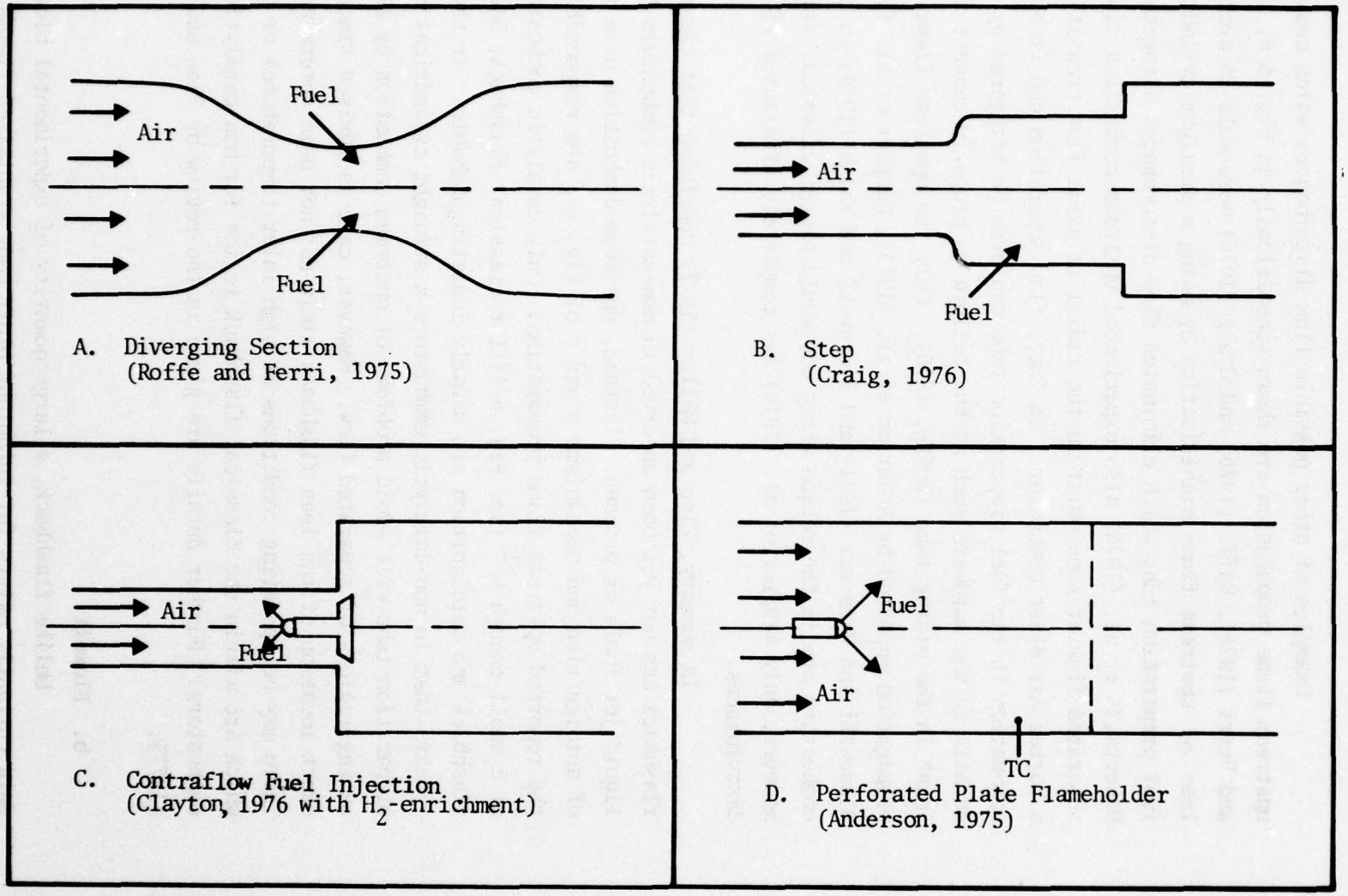

Figure 6-6. Diagram illustrating flow disturbances which cause upstream flame stabilization.

However, early studies considered only simple hydrocarbon fuels such as CH_4 and C_3H_8 at relatively low inlet temperatures and pressures compared to practical combustors. These investigations have shown that in general the blowoff limit widens with increasing pressure and temperature or decreasing reference velocity; maximum flame stabilization occurs near stoichiometric with approach flow equivalence ratio, inlet temperature and reference velocity having the strongest effect (see discussions by Williams and Shipman, 1953; Longwell, 1953). Longwell et al. (1949) report a very weak influence of pressure on flame stabilization. The blowoff limit is also extended by heating the flameholder as well as decreasing the incoming turbulence level (Williams et al., 1949). In addition, the importance of approach flow turbulence on the limit decreases with increasing flameholder dimension (Williams et al., 1949; Longwell, 1953).

Flameholder size, type and shape also influence stabilization. In general, a two-dimensional stabilizer (cylinder across a rectangular duct) has a much wider blowoff limit than a three-dimensional flameholder (circular disc in a duct) (Williams and Shipman, 1953). Williams and Shipman (1953) also report that an increase in the characteristic dimension of the flameholder leads to an increase in the range of stable operation; however, as the size of the stabilizer becomes comparable to the housing or duct dimension, a further increase narrows the blowoff limit. Thus, an optimum flameholder dimension exists for a given combustor housing. Flameholder shape appears to have only a second order effect on the extinction limit (Longwell et al., 1949; Williams et al., 1949; Longwell, 1953).

Early correlation techniques considered the blowoff velocity (V_{bo}) as a function of equivalence ratio (ϕ_{bo}). Variations in pressure (P), inlet temperature (T_{in}) and flameholder dimension (D) were also included using equations of the form

$$\phi_{bo} \sim \frac{V_{bo}}{P^a D^b T_{in}^c} \qquad 6\text{-}20$$

by Longwell et al. (1953) and DeZubay (1950). However, like the velocity gradient versus equivalence ratio correlations of the previous section a universal curve was not possible because values of a, b, c, varied between experimenters.

Spalding and Tall (1954) proposed a Peclet number correlation similar to that of Putnam and Jensen (1949) which is derived by non-dimensionalizing the energy equation. An example of this correlation is shown in Fig. 6-7 where here the Peclet number is based on the free stream velocity past the flameholder at blowoff (V_{bo}), a characteristic dimension (D) and the thermal diffusivity (α) and is plotted against the Peclet number based on the laminar flame speed. The left most curve in Fig. 6-7 represents two-dimensional flameholders while the right most curve refers to three-dimensional stabilizers. The upper part of the axisymmetric curve has a slope of approximately two and relates to the case where turbulent transport properties dominate the stabilization process; the lower part of this curve has a slope of 1.5 and corresponds to a dominance of molecular transport. Variations in pressure, inlet temperature and fuel type are accounted for implicitly through the laminar flame speed and thermal diffusivity. However, as discussed in the last section, calculation of laminar flame speeds required for Pe_{S_L} is difficult for practical hydrocarbon fuels at elevated inlet temperatures and pressures. Altenkirch and Mellor (1973) discuss the difficulty in applying the Peclet number correlation to data obtained using a simplified prevaporizing/premixing combustor burning liquid propane at 950K inlet temperature and 4 atm pressure.

Spalding (1955) has summarized various theories for blowoff of bluff body stabilized flames. In the framework of characteristic times, two different theories have evolved. Longwell et al. (1953) state that bluff body stabilization occurs only if the mass transport to the recirculation zone is not great enough to blow out an equivalent well stirred reactor. Thus, a stable flame exists if the time a fluid particle spends in the recirculation zone is larger than the fuel ignition delay time. The second theory (Zukoski and Marble, 1956) considers the adjacent shear layer rather than the recirculation zone as the region which determines flame stabilization. Zukoski and Marble (1956)

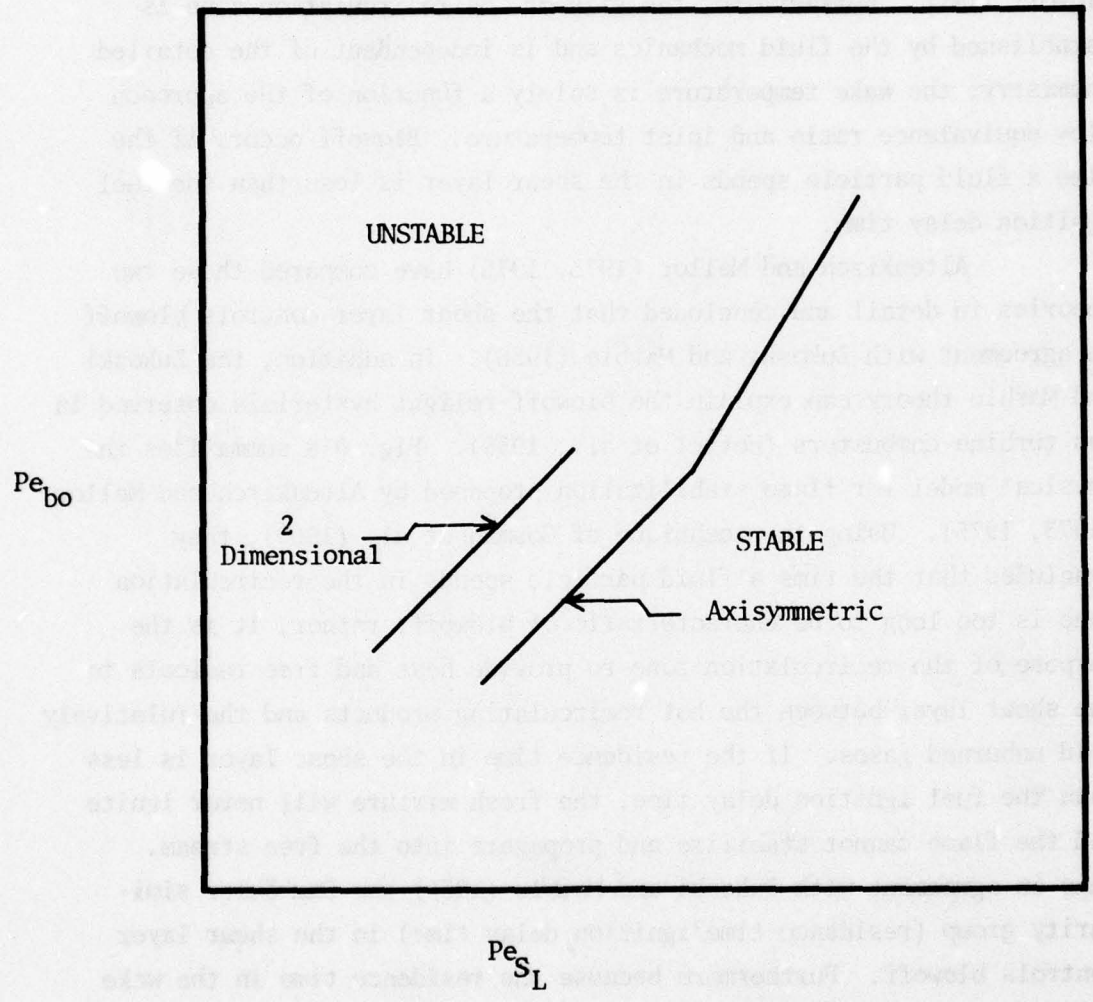

Figure 6-7. Schematic of the stability curve of Spalding and Tall (1954) from Altenkirch and Mellor (1973).

found that the temperature in the recirculation zone is uniform (approximately nine-tenths the adiabatic flame temperature) and that the ratio of the wake temperature to the adiabatic flame temperature remains approximately constant as the air velocity increases toward the blowoff limit. Furthermore, the size of the recirculation zone is established by the fluid mechanics and is independent of the detailed chemistry; the wake temperature is solely a function of the approach flow equivalence ratio and inlet temperature. Blowoff occurs if the time a fluid particle spends in the shear layer is less than the fuel ignition delay time.

Altenkirch and Mellor (1973, 1975) have compared these two theories in detail and concluded that the shear layer controls blowoff in agreement with Zukoski and Marble (1956). In addition, the Zukoski and Marble theory can explain the blowoff-relight hysterisis observed in gas turbine combustors (Hottel et al., 1958). Fig. 6-8 summarizes the physical model for flame stabilization proposed by Altenkirch and Mellor (1973, 1975). Using the technique of Gosman et al. (1969), they concluded that the time a fluid particle spends in the recirculation zone is too long to be characteristic of blowoff; rather, it is the purpose of the recirculation zone to provide heat and free radicals to the shear layer between the hot recirculating products and the relatively cold unburned gases. If the residence time in the shear layer is less than the fuel ignition delay time, the fresh mixture will never ignite and the flame cannot stabilize and propagate into the free stream. Thus in agreement with Zukoski and Marble (1956) the Damköhler similarity group (residence time/ignition delay time) in the shear layer controls blowoff. Furthermore because the residence time in the wake region exceeds the shear layer residence time, the recirculation zone should be extinguished after the shear layer. Indeed, this has been reported in the early literature. Longwell et al. (1949) and Williams et al. (1949) observed that under certain operating conditions the free stream flame blew off prior to the wake region. Since the recirculation zone represents only minor heat release relative to the main stream flame, this final blowout is only of secondary interest (Blazowski and Henderson, 1977).

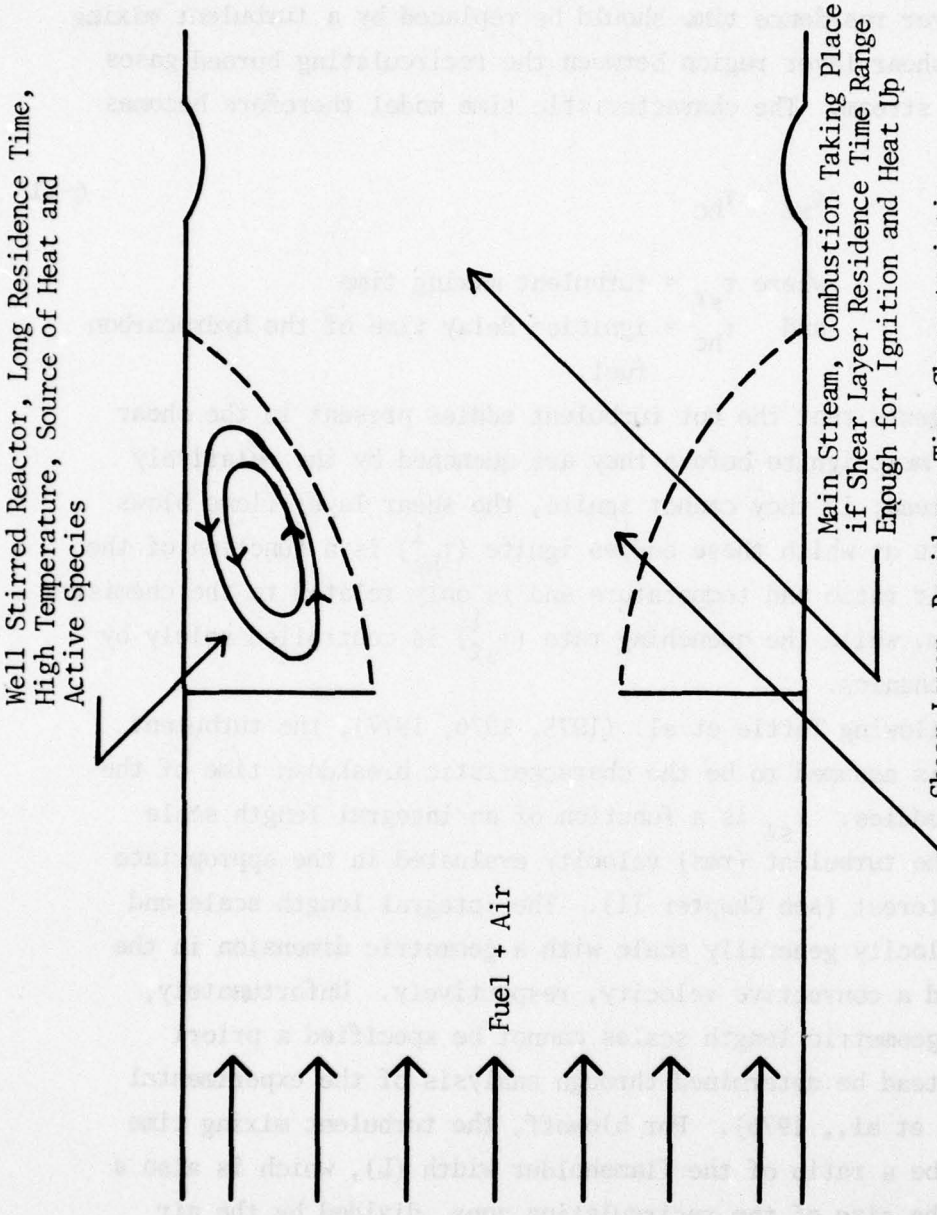

Figure 6-8. Physical Model of Flame Stabilization from Altenkirch and Mellor (1973).

Finally, Altenkirch and Mellor (1975) following Spalding (1971) suggest that since most flows of practical interest are turbulent, the shear layer residence time should be replaced by a turbulent mixing time in the shear layer region between the recirculating burned gases and the free stream. The characteristic time model therefore becomes

$$\tau_{s\ell} = \tau_{hc} \qquad 6\text{-}21$$

where $\tau_{s\ell}$ = turbulent mixing time
and τ_{hc} = ignition delay time of the hydrocarbon fuel.

Eq. 6-21 suggests that the hot turbulent eddies present in the shear layer region must ignite before they are quenched by the relatively cold free stream; if they cannot ignite, the shear layer flame blows off. The rate at which these eddies ignite (τ_{hc}^{-1}) is a function of the local fuel/air ratio and temperature and is only related to the chemistry of the system, while the quenching rate ($\tau_{s\ell}^{-1}$) is controlled solely by the fluid mechanics.

Following Tuttle et al. (1975, 1976, 1977), the turbulent mixing time is assumed to be the characteristic breakdown time of the large scale eddies. $\tau_{s\ell}$ is a function of an integral length scale divided by the turbulent (rms) velocity evaluated in the appropriate region of interest (see Chapter II). The integral length scale and turbulent velocity generally scale with a geometric dimension in the combustor and a convective velocity, respectively. Unfortunately, appropriate geometric length scales cannot be specified a priori but must instead be determined through analysis of the experimental data (Tuttle et al., 1976). For blowoff, the turbulent mixing time is taken to be a ratio of the flameholder width (L), which is also a measure of the size of the recirculation zone, divided by the air velocity at the edge of the stabilizer ($V_{a,T}$),

$$\tau'_{s\ell} \sim \frac{L}{V_{a,T}} \text{ (msec)} \qquad 6\text{-}22$$

(prime denotes temperature dependence in velocity), since according to Zukoski and Marble (1956) this is the region where stabilization occurs. The annulus velocity is computed from the continuity equation,

$$V_{a,T} = \frac{T}{T_{in}} \frac{V_{ref}}{(1-B)} \quad , \qquad 6\text{-}23$$

and is a function of the reference velocity (V_{ref}) and blockage ratio (B). In addition, the velocity is evaluated at the temperature in the shear layer (T) which must be higher than the inlet temperature because it is adjacent to a hot recirculation zone. Zukoski and Marble (1956) have shown that the recirculation zone maintains its temperature regardless of the velocity past the flameholder even up to blowoff. Eq. 6-22 represents the same shear layer mixing time that Tuttle et al. (1977) used for the correlation of carbon monoxide emissions except here the inner part of the shear layer rather than the cold outer region is considered. Therefore, the ratio T/T_{in}* in Eq. 6-23 accounts for the acceleration of the air flow in the shear layer region as a result of the increased temperature.

The ignition delay time for a lean reacting eddy is

$$\tau_{hc} \sim \frac{e^{E/RT}}{\phi} \text{ (sec)} \qquad 6\text{-}16$$

from the previous laminar flow analysis. Combining Eq. 6-22 and 6-16, the characteristic time model for lean blowoff becomes

$$\frac{L}{V_{a,T}} \sim \frac{e^{E/RT}}{\phi} \quad . \qquad 6\text{-}24$$

Now since $V_{a,T}$ is a function of the recirculation zone temperature (approach flow equivalence ratio), we write the ratio T/T_{in} on the right hand side of Eq. 6-24 so that the fluid mechanics and chemistry

*Since velocities here are much higher than for laminar flow, increased compressibility effects must also be included.

are again uncoupled,

$$\frac{L}{V_a} \sim \frac{T}{T_{in}} \frac{e^{E/RT}}{\phi} \qquad 6\text{-}25$$

$$\text{where } \tau_{s\ell} \sim \frac{L}{V_a} \quad , \quad \tau'_{hc} \sim \frac{T}{T_{in}} \frac{e^{E/RT}}{\phi}$$

$$\text{and } V_a = \frac{V_{ref}}{(1-B)} \quad .$$

For the prevaporizing/premixing combustor shown in Fig. 6-8, the appropriate length in $\tau_{s\ell}$ should scale with the housing diameter (D_c) minus the baffle diameter (D) since this is a measure of the size of the recirculation zone. The temperature in τ'_{hc} is assumed proportional to the adiabatic flame temperature at the approach flow equivalence ratio just prior to blowoff (an estimate of the thermal driving force between the recirculation zone and the shear layer) following Zukoski and Marble (1956). The model can also be extended to three other simplified flameholder configurations shown schematically in Fig. 6-9. Each is characterized by a shear layer flame which is ignited through transfer of heat and mass from a central recirculation zone (boundary shown with dashed lines).

Ballal and Lefebvre (1977) have recently obtained lean blowoff data from bluff body stabilized flames operating at inlet temperatures and velocities typical of continuous combustors (Fig. 6-9A); these conditions are summarized in Table 6-2. In this study gaseous propane, introduced upstream of the conical baffle, is mixed with air prior to combustion eliminating any heterogeneous effects. Variations in blowoff equivalence ratio with pressure, inlet temperature, reference velocity, baffle size, housing diameter and blockage ratio have been examined independently. The lean limit was obtained by holding all inlet conditions constant and slowly decreasing the fuel flow until blowoff was observed visually.

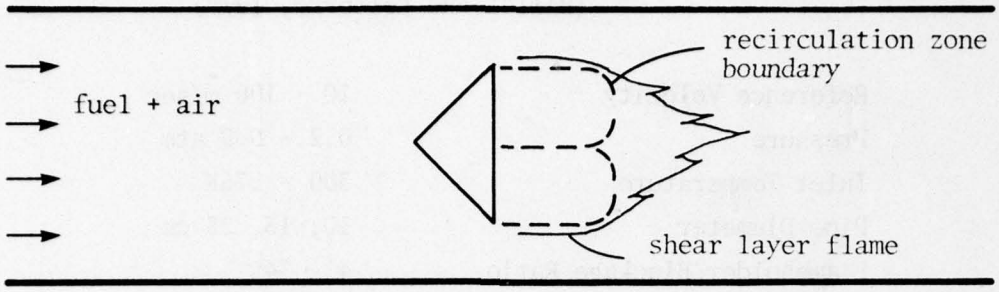

Configuration A Ballal and Lefebvre (1977)

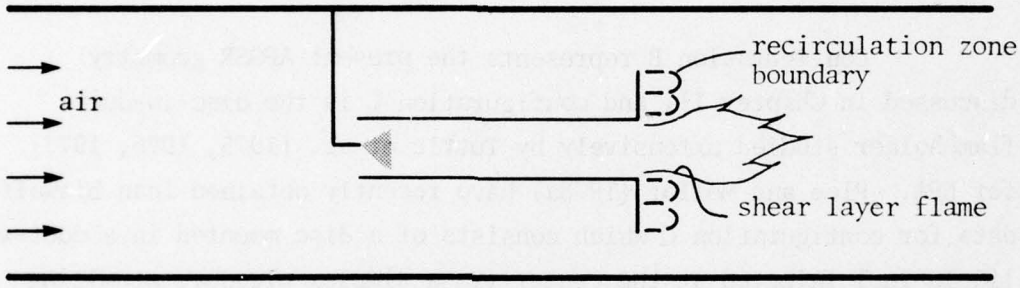

Configuration B AFOSR Combustor (Fig. 3-3)

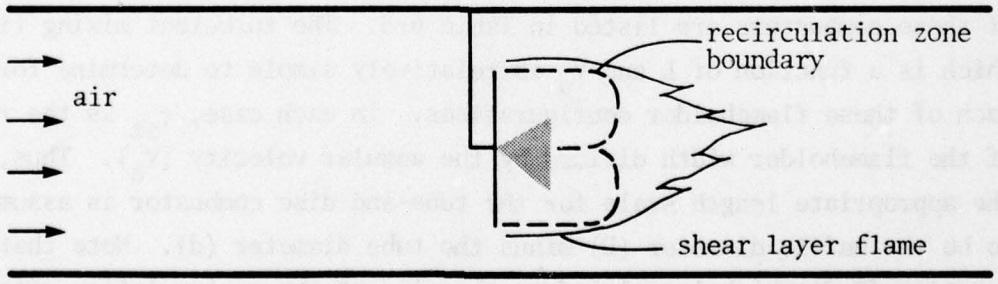

Configuration C Plee and Mellor (1978a)
(negligible heterogeneous effects)

Figure 6-9. Schematic of three simplified bluff body stabilized flames.

Table 6-2. Burner Operating Conditions
(Ballal and Lefebvre, 1977)

Reference Velocity	10 - 100 m/sec
Pressure	0.2 - 0.9 atm
Inlet Temperature	300 - 575K
Pipe Diameter	10, 15, 25 cm
Flameholder Blockage Ratio	4 - 34%
Fuel	C_3H_8 (gas)
Geometry	45° conical baffle
Incoming Turbulence Intensity	up to 15%

Configuration B represents the present AFOSR geometry discussed in Chapter III and configuration C is the disc-in-duct flameholder studied extensively by Tuttle et al. (1975, 1976, 1977) for EPA. Plee and Mellor (1978a) have recently obtained lean blowoff data for configuration C which consists of a disc mounted in a duct with liquid fuel injected at the center via a simplex pressure atomizing nozzle. The disc-in-duct combustor is fundamentally different from these discussed previously because the fuel is not prevaporized and premixed upstream of the flameholder.

Appropriate characteristic time scaling parameters for each of these combustors are listed in Table 6-3. The turbulent mixing time which is a function of L and V_a is relatively simple to determine for each of these flameholder configurations. In each case, $\tau_{s\ell}$ is the ratio of the flameholder width divided by the annular velocity (V_a). Thus, the appropriate length scale for the tube-and-disc combustor is assumed to be the baffle diameter (D) minus the tube diameter (d). Note that the quantity (D-d) which is related to the size of the recirculation zone goes to the proper limit (D) as the tube diameter approaches zero.

Parameters relevant to the ignition delay time are not always as straightforward to evaluate. Since the combustor of Fig. 6-9A is essentially identical to the flameholder shown in Fig. 6-8 except for the

Table 6-3. Parameters for Characteristic Time Model (Eq. 6-25)

Configuration	V	L	ϕ	T
Fig. 6 - 8	V_a	$D_c - D$	ϕ_{ov}	$T_{\phi_{ov}}$
Fig. 6 - 9A	V_a	D	ϕ_{ov}	$T_{\phi_{ov}}$
Fig. 6 - 9B	V_a	D - d	ϕ_t	$(T_{\phi t} + T_{in})/2$
Fig. 6 - 9C	V_a	D	ϕ_{ov}	$T_{\phi=1}$

D_c = combustor housing diameter
D = baffle diameter
d = tube diameter
V_a = annulus velocity
ϕ = equivalence ratio
T_ϕ = adiabatic flame temperature at ϕ
T_{in} = inlet temperature

Subscripts: ov = overall
t = tube

location of the bluff body, the appropriate equivalence ratio and flame temperature are evaluated in the same manner. However, for configuration B, we postulate that the inner shear layer (shear layer beginning at the edge of the tube, Fig. 6-9B) is responsible for flame stabilization since high fuel concentrations are present at this point. Hot recirculating burned gases should also maintain this region at a relatively high temperature based on the temperature measurements of Chapter IV. Therefore, application of Eq. 6-25 requires an appropriate length scale, velocity, equivalence ratio and temperature evaluated in this regime. The equivalence ratio representative of the tube-and-disc combustor is assumed to be ϕ_t which is based on the air flow split through the tube rather than the total air flow rate (ϕ_{ov}). ϕ_t is richer than the overall equivalence ratio and is a better measure of the fuel concentration near the shear layer adjacent to the tube exit.

By analogy with the blowoff model of the previous section, the appropriate temperature for τ_{hc} should be the adiabatic flame temperature (T_{ϕ_t}) based on the equivalence ratio in the fuel preparation tube. However, this does not take into account the influence of the relatively cold inlet air flowing around the outside of the disc. Obviously there exists a fundamental difference between the configurations studied by Ballal and Lefebvre (1977) and the tube-and-disc flameholders. In the latter case, the recirculation zone is not completely surrounded by a hot reacting shear layer; instead, the outer shear layer at the edge of the disc is almost entirely free of fuel and should be relatively unreactive. Therefore, a better representation of the temperature of the inner shear layer is an average between T_{ϕ_t} and the inlet temperature. This simplified analysis allows for the quenching effect of the cold outer recirculation zone (see Fig. 6-9B). If the disc diameter equals the housing diameter, then the entire recirculation zone would be surrounded by either a wall or a reacting shear layer (the dump ramjet combustor) and the appropriate temperature would then be T_{ϕ_t} (equal to $T_{\phi_{ov}}$) as in the case of Fig. 6-8.

Configuration C differs substantially from the previous flameholders studied because the fuel is injected at the center of the

recirculation zone and is not therefore prevaporized or premixed upstream. Tuttle et al. (1976, 1977) successfully treated this configuration as a turbulent diffusion flame for modeling NO_x formation. Their results show that very high fuel/air ratios exist in the recirculation zone due to fuel vaporization and then decrease into the main stream. Maximum reaction rates and very high temperatures characteristic of NO formation are created by the stoichiometric contour present in the shear layer region between the fuel rich recirculation zone and the free stream. These stoichiometric regions also account for the observations that conventional diffusion flame combustors are generally more stable than prevaporizing premixing combustors. Therefore since the maximum reaction rate occurs primarily around the stoichiometric contour, the appropriate flame temperature in τ_{hc} should be evaluated at ϕ=1. The equivalence ratio in τ_{hc} is not evaluated at ϕ=1.0 however since all of the eddies are not at stoichiometric. Instead, the percent of stoichiometric eddies controlling flame stabilization should be proportional to the overall equivalence ratio. Thus as ϕ_{ov} increases, the ignition delay time becomes smaller and the flame becomes more stable. Examples of this particular correlation are shown in Plee and Mellor (1978b).

Application of the characteristic time model and evaluation of τ_{hc} for blowoff are demonstrated first with the flameholder of Fig. 6-9A. Using the experimental data of Ballal and Lefebvre (1977), the ignition delay time becomes

$$\tau'_{hc} = 10^{-4} \frac{T}{T_{in}} \frac{e^{21000/RT}}{\phi} \text{ (msec)} \qquad 6\text{-}26$$

where the prime indicates that τ'_{hc} contains the ratio T/T^*_{in} from the annulus velocity. Note that both the pre-exponential (10^{-4}) and the activation energy (E = 21,000 cal/mole) are determined empirically. An activation energy of 21,000 cal/mole gives the best correlation

---

* Failure to include the ratio T/T_{in} from the velocity term decreases the correlation coefficient in Fig. 6-10 from 0.98 to 0.93.

and compares favorably with values of 24,600 cal/mole and 24,200 cal/mole reported by Engleman et al. (1973) and Edelman (1977), respectively.

Figure 6-10 illustrates the characteristic time model for the lean blowoff data of Ballal and Lefebvre (1977). Here the shear layer mixing time and the fuel ignition delay time are evaluated using Eq. 6-25 with τ'_{hc} evaluated from Eq. 6-26. The temperature in Eq. 6-25 and 6-26 is taken to be the adiabatic flame temperature at the approach flow equivalence ratio just prior to blowoff (Table 6-3) and is computed using a version of the equilibrium computer program of Gordon and McBride (1971). The correlation is shown to be linear with a y-intercept approximately zero as the theory predicts. Thus, one approaches the lean blowoff limit by either increasing the annular velocity or decreasing the flameholder characteristic dimension ($\downarrow\tau_{s\ell}$), or decreasing the overall equivalence ratio ($\uparrow\tau'_{hc}$).

Analysis of the turbulent mixing time predicts an optimum disc diameter for maximum stability at a given power setting which is solely a function of the housing diameter. Since

$$\tau_{s\ell} = \frac{D}{V_a} = \frac{D(D_c^2 - D^2)}{V_{ref} D_c^2} \quad , \qquad 6\text{-}27$$

maximum flame stabilization exists ($\tau_{s\ell}$ is a maximum) at

$$D = \frac{D_c}{\sqrt{3}} \quad . \qquad 6\text{-}28$$

Thus, increasing the characteristic dimension of the flameholder leads to an increase in the range of stable operation; however, as the size of the stabilizer exceeds $D_c/\sqrt{3}$, a further increase narrows the blowoff limit ($\downarrow\tau_{s\ell}$) as reported by Williams and Shipman (1953). Eq. 6-28 is also identical to the equation obtained by Tuttle et al. (1977) for minimum CO emissions.

In summary, a characteristic time model has been developed based on the flame stabilization theory of Zukoski and Marble (1956). $\tau_{s\ell}$ for lean blowoff is identical to the mixing time obtained by Tuttle et al. (1977) for CO emissions; however, kinetic times are quite

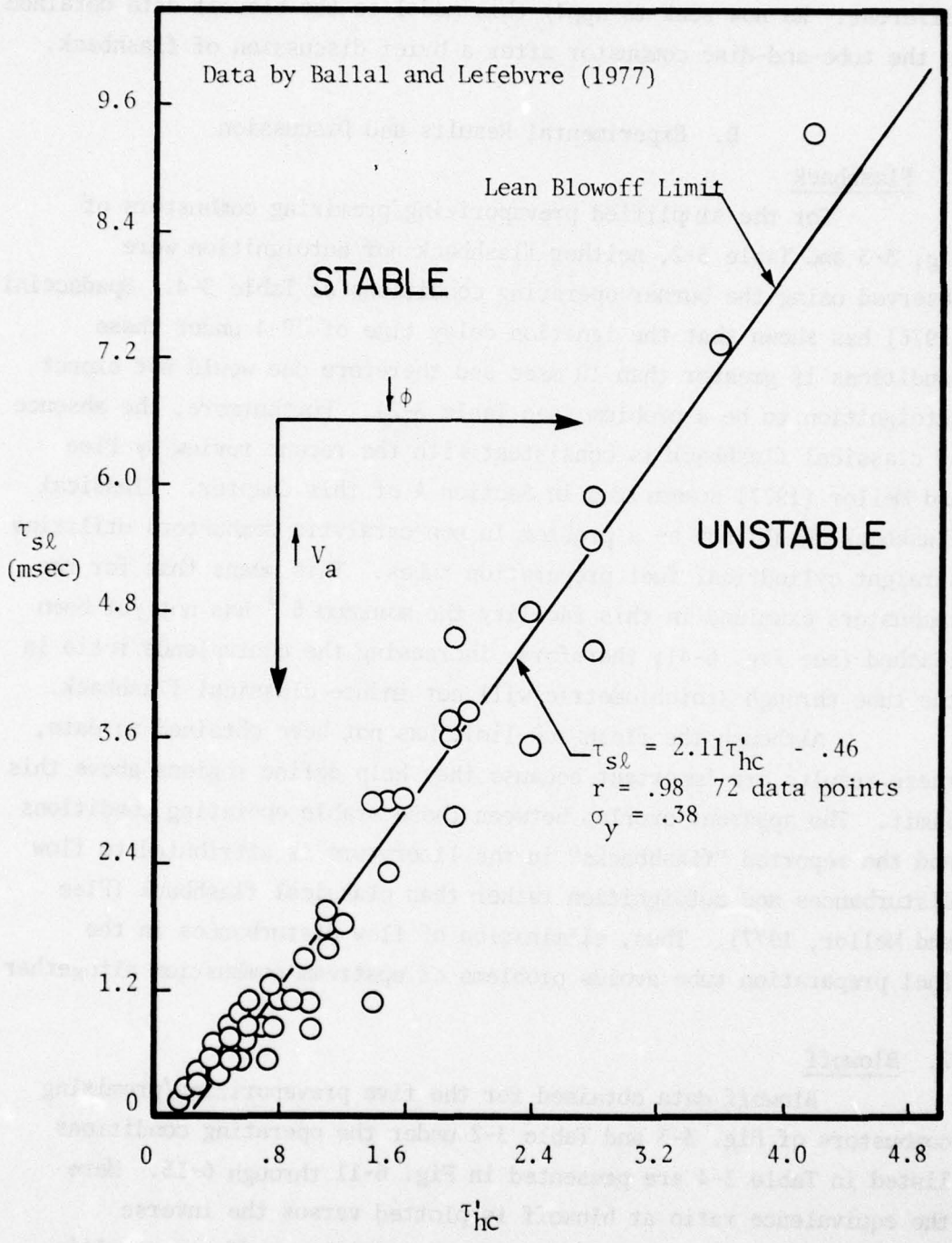

Figure 6-10. Characteristic time correlation for lean blowoff in a bluff body stabilized flame burning gaseous propane.

different. We now seek to apply this model to the blowoff data obtained on the tube-and-disc combustor after a brief discussion of flashback.

B. Experimental Results and Discussion

1. Flashback

For the simplified prevaporizing/premixing combustors of Fig. 3-3 and Table 3-2, neither flashback nor autoignition were observed using the burner operating conditions of Table 3-4. Spadaccini (1976) has shown that the ignition delay time of JP-4 under these conditions is greater than 10 msec and therefore one would not expect autoignition to be a problem (see Table 3-2). Furthermore, the absence of classical flashback is consistent with the recent review by Plee and Mellor (1977) summarized in Section A of this Chapter. Classical flashback should not be a problem in non-catalytic combustors utilizing straight cylindrical fuel preparation tubes. This means that for the combustors examined in this facility the minimum θ^{-1} has not yet been reached (see Fig. 6-4); therefore, increasing the equivalence ratio in the tube through stoichiometric will not induce classical flashback.

Although the flashback limit has not been obtained to date, these results are important because they help define regions above this limit. The apparent overlap between these stable operating conditions and the reported "flashbacks" in the literature is attributed to flow disturbances and autoignition rather than classical flashback (Plee and Mellor, 1977). Thus, elimination of flow disturbances in the fuel preparation tube avoids problems of upstream combustion altogether.

2. Blowoff

Blowoff data obtained for the five prevaporizing/premixing combustors of Fig. 3-3 and Table 3-2 under the operating conditions listed in Table 3-4 are presented in Fig. 6-11 through 6-15. Here the equivalence ratio at blowoff is plotted versus the inverse theta parameter defined by Eq. 6-19. In addition, effects of vitiation are included using an equation defined by Altenkirch and Mellor (1975)

$$\phi_{bo,vit} = \frac{\phi_{bo}}{1 - \phi_h} \qquad 6\text{-}29$$

where $\phi_{bo,vit}$ = blowoff equivalence ratio including vitiation

ϕ_{bo} = apparent blowoff equivalence ratio

and ϕ_h = overall equivalence ratio in slave burner.

Eq. 6-29 corrects the blowoff equivalence ratio for vitiation assuming complete combustion in the preheat burner.

Blowoff equivalence ratios obtained burning liquid propane in geometry A (base geometry) are presented in Fig. 6-11. This plot illustrates that the inverse theta parameter correlates the data reasonably well for varitaions in pressure, inlet temperature and velocity. A similar plot is available for the same flameholder configuration burning Jet A (Fig. 6-12) except here variations in initial fuel spray SMD are also included and are not collapsed by θ^{-1}. An increase in the size of the injector leads to a reduction in the stable operating range because the initial fuel spray SMD also increases. The propane and Jet A blowoff data are plotted together in Fig. 6-13 at one particular inlet temperature to further show the importance of atomization on the limit. For liquid propane, the fuel drops are expected to flash vaporize upon injection under the burner inlet conditions of Table 3-4 (SMD $\sim$ 0 at tube exit). Jet A on the other hand is not expected to completely vaporize prior to combustion as discussed in Chapter IV, and therefore, increased fuel volatility also influences the degree of prevaporization.

According to Fig. 6-13, heterogeneous effects are only important relative to blowoff at large values of θ^{-1} (high velocity). This is attributed to the fact that at high air velocities, less residence time is available in the mixing tube for vaporization, while at low velocities, the residence time is sufficient such that vaporization does not influence the blowoff limit. Therefore, the more fuel vaporized in the fuel preparation tube prior to ignition, the higher the local fuel to air ratio and the wider the blowoff limit.

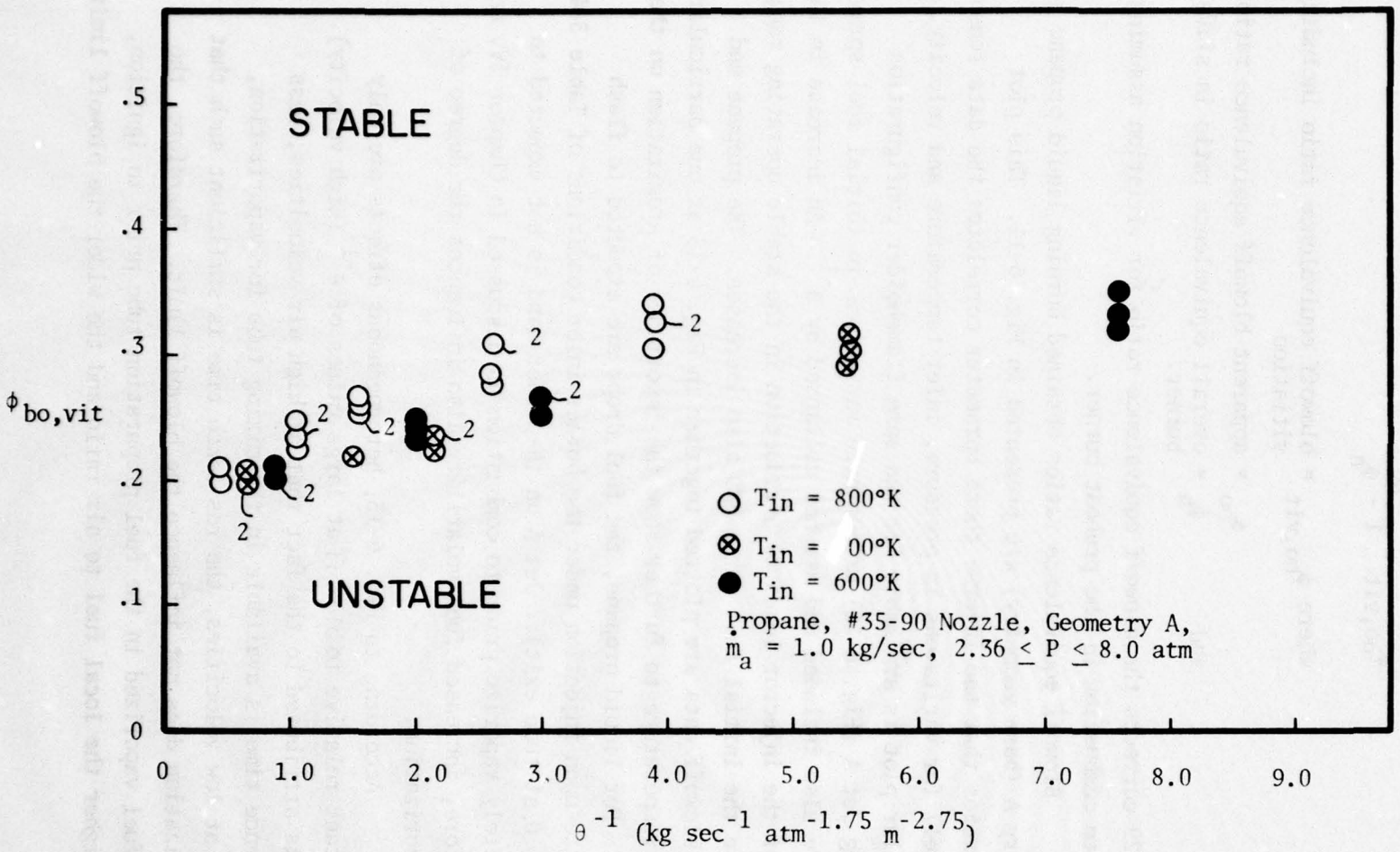

Figure 6-11. Blowoff equivalence ratio versus θ^{-1} (Propane, Geometry A).

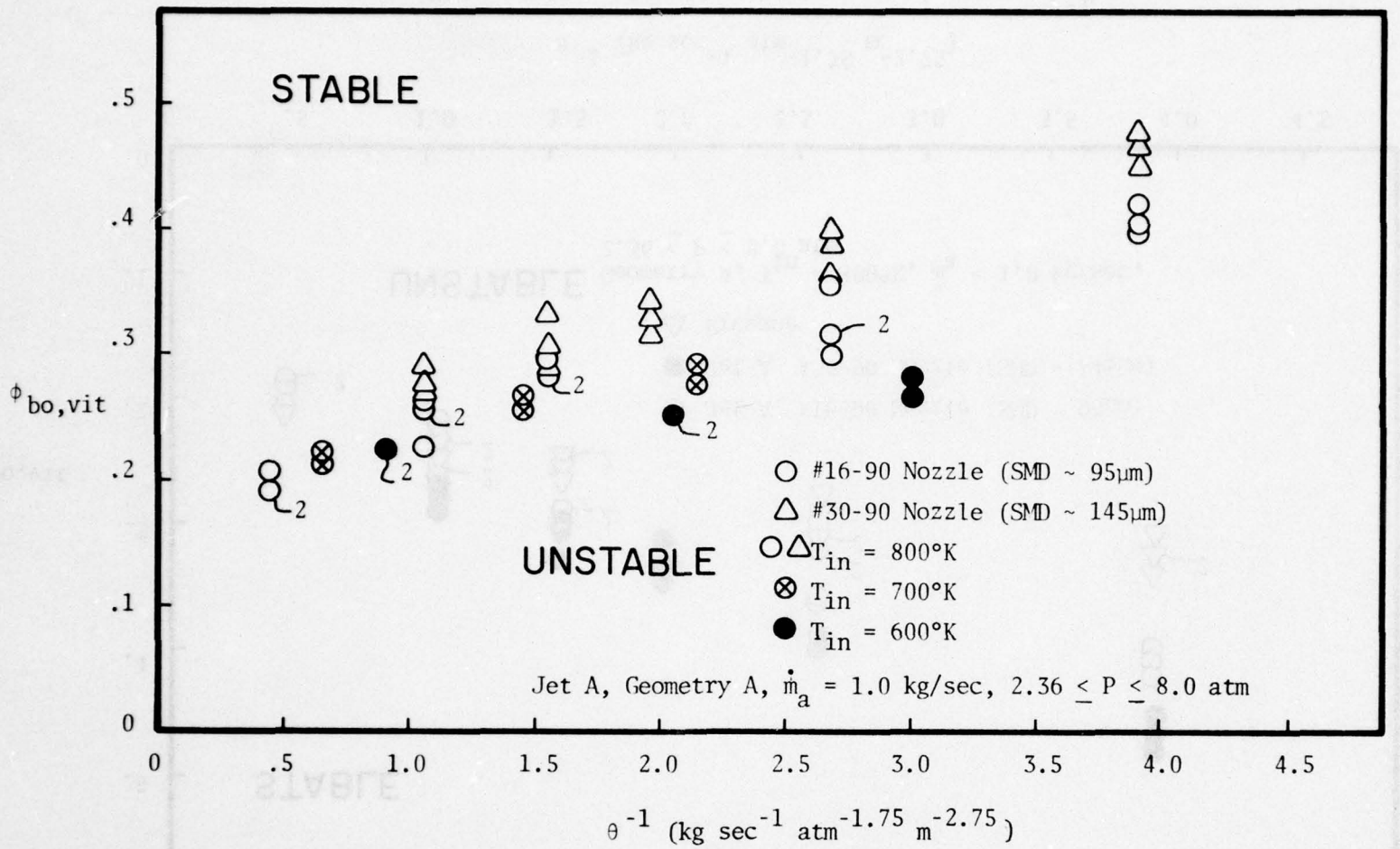

Figure 6-12. Blowoff equivalence ratio versus θ^{-1} (Jet A, Geometry A).

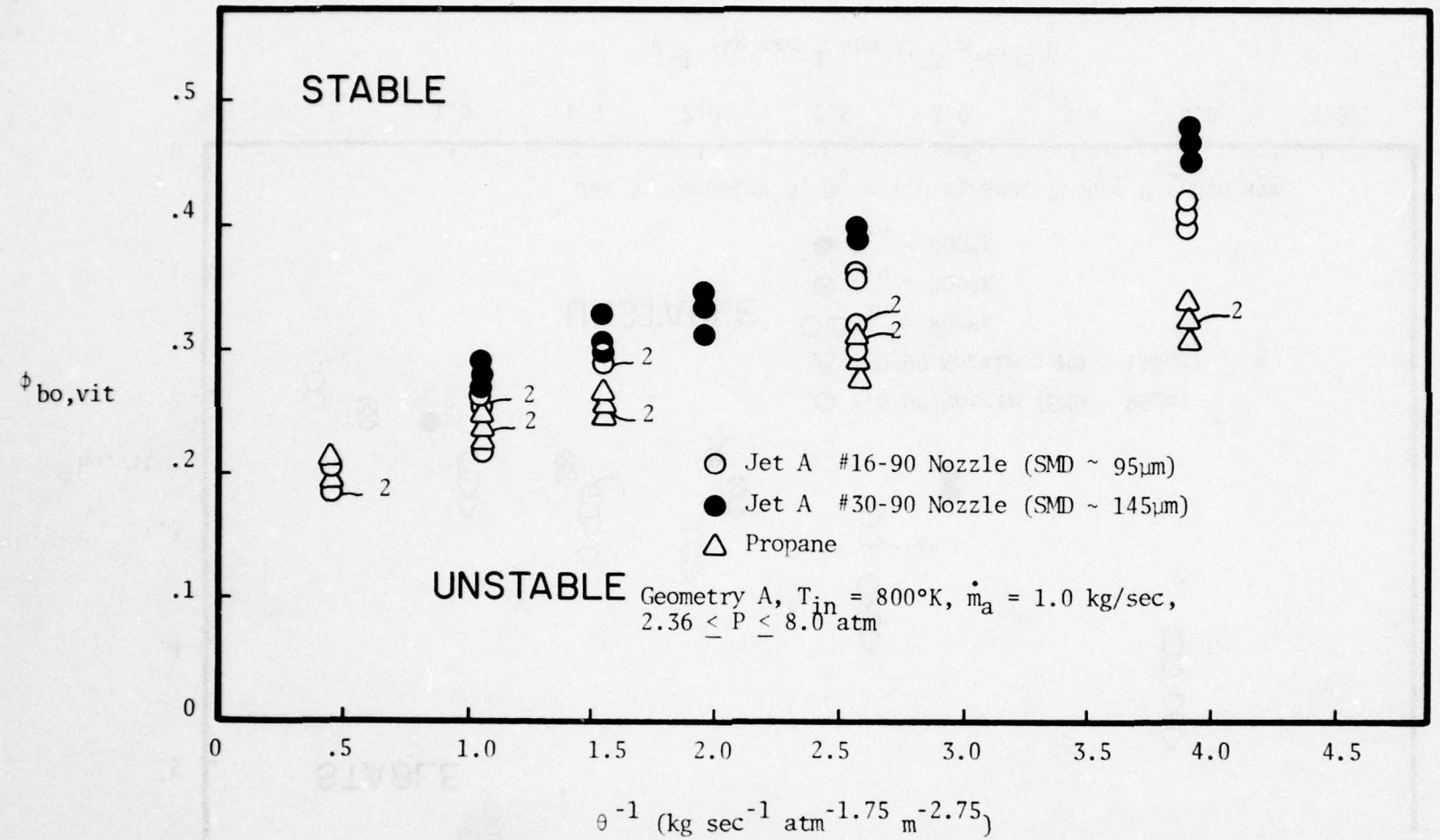

Figure 6-13. Blowoff equivalence ratio versus θ^{-1} (Propane and Jet A, Geometry A).

In summary, both changes in fuel type and injector size can have an adverse effect on the blowoff limit if the initial fuel spray SMD increases.

Geometry variations are shown in Fig. 6-14 and 6-15 for combustors burning propane and Jet A, respectively. In both figures, injector size and inlet temperature are held constant in order to better illustrate geometry changes. Although the inverse theta parameter also does not correlate geometry effects, it does illustrate certain trends. First of all, the small tube flameholders (geometries D and E) are more stable than the 4.4 cm diameter tube configurations (geometries A, B and C) for both fuels. Also, decreasing the disc diameter for a given mixing tube diameter enhances flame stabilization (geometry B versus geometries A and C; geometry D versus geometry E). Another interesting result is that for combustors burning Jet A the shorter tube (geometry C) has the same apparent limit as the base geometry. This can be explained from examination of the characteristic droplet evaporation time introduced in Chapter II.

For the tube-and-disc combustor, Eq. 2-11 must be modified to account for prevaporization occurring in the fuel preparation tube. Using Eq. 2-10, the droplet diameter at the exit of the prevaporizing tube (d_e) becomes

$$d_e^2 = d_o^2 - \beta_t \tau_{res} \qquad 6\text{-}30$$

where β_t = evaporation coefficient evaluated under ambient conditions in the tube

and τ_{res} = droplet residence time in tube.

Since droplet sizes of d_e rather than d_o are exposed to the combustion environment, Eq. 2-11 now becomes

$$\tau_{eb} = \frac{d_o^2 - \beta_t \tau_{res}}{\beta_c} \quad . \qquad 6\text{-}31$$

Thus if the fuel (propane) is completely vaporized in the fuel preparation tube, the numerator of Eq. 6-31 is zero and τ_{eb} can be neglected in

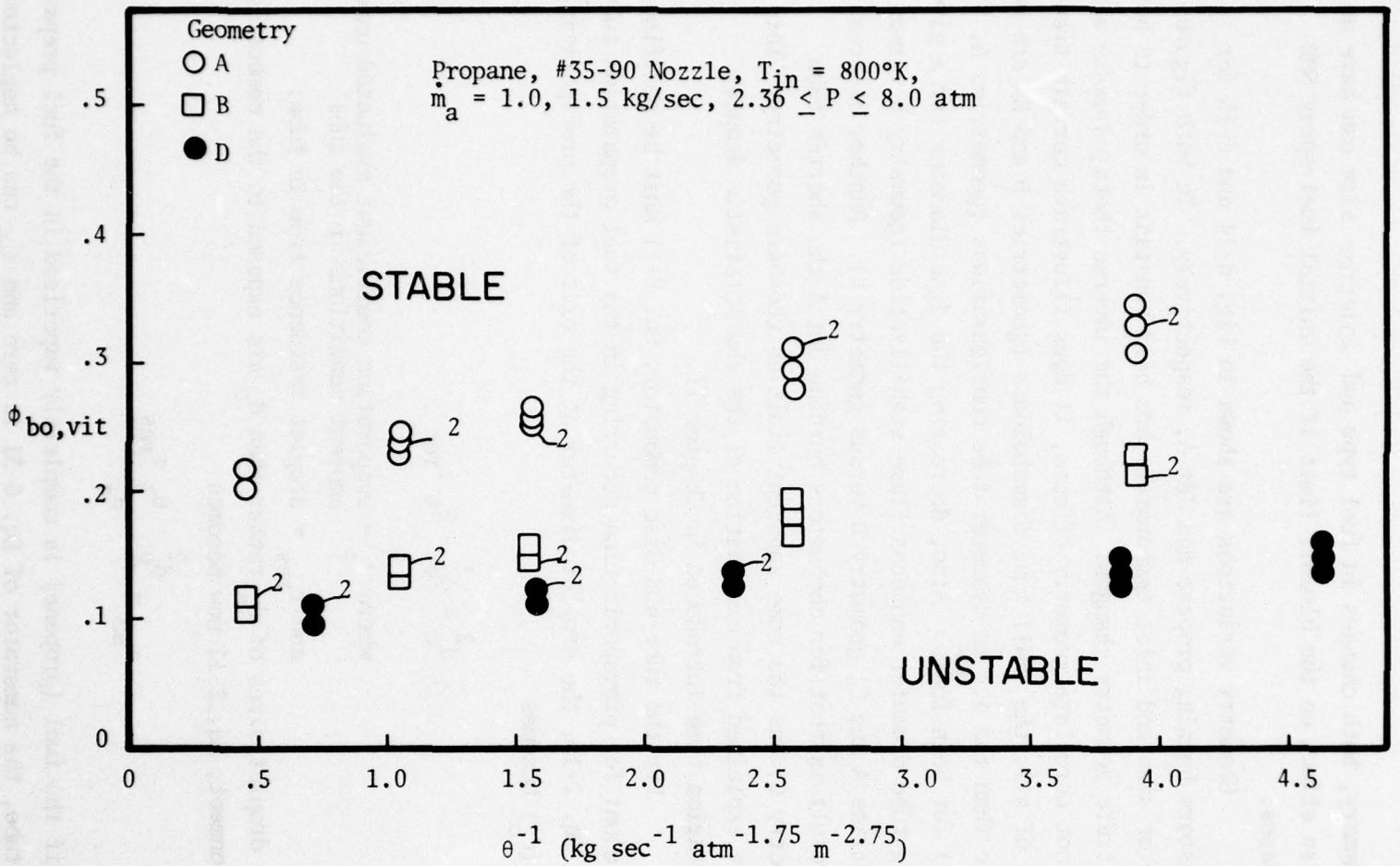

Figure 6-14. Blowoff equivalence ratio versus θ^{-1} (Propane, all geometry variations).

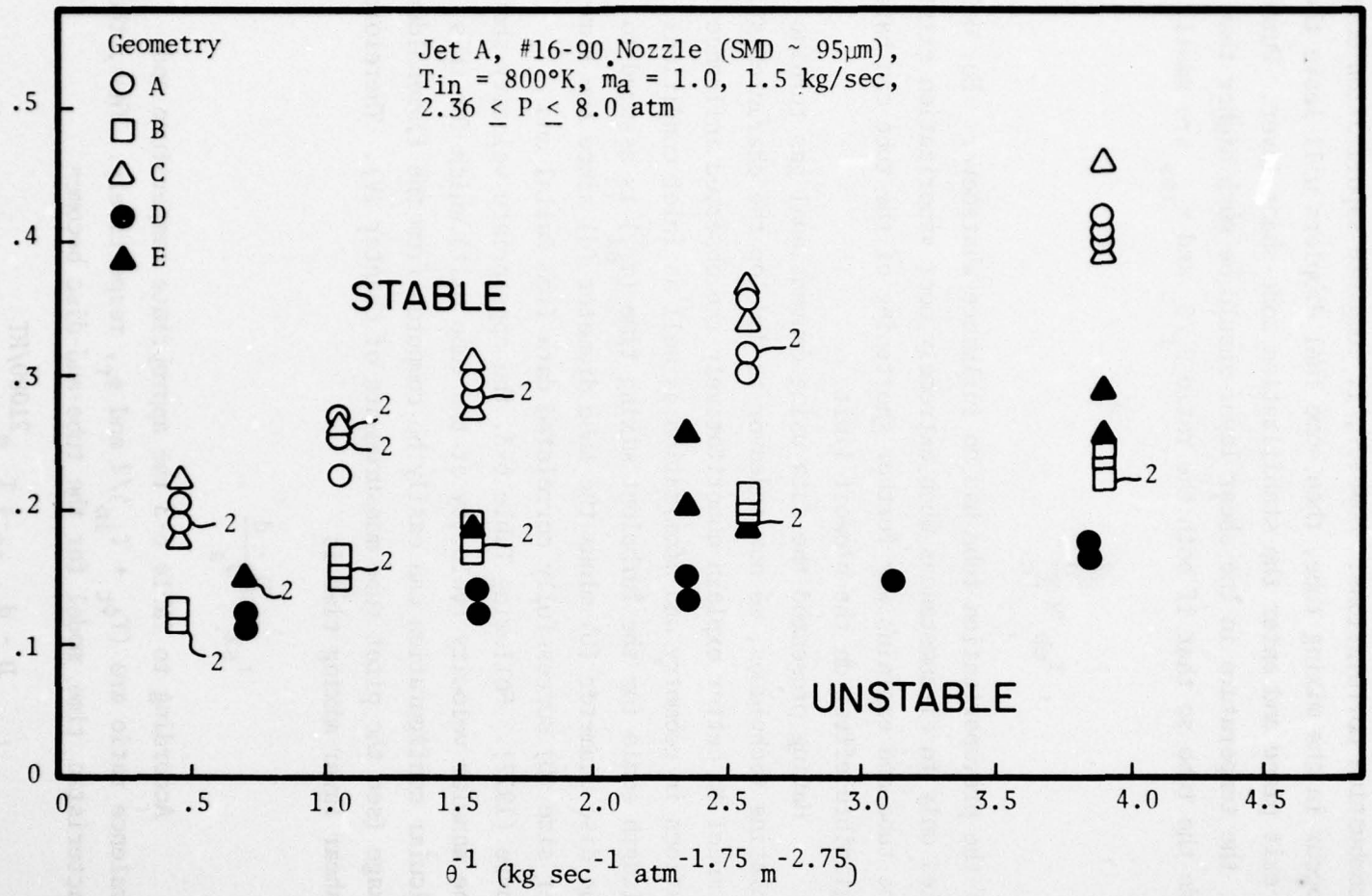

Figure 6-15. Blowoff equivalence ratio versus θ^{-1} (Jet A, all geometry variations).

the combustion correlations. However, if complete vaporization does not occur in the mixing tube, then some fuel droplets will leave the tube exit plane and enter the stabilization zone shear layer. Furthermore, the temperature in the shear layer should be much higher than inside the tube so that if both the ratio β_t/β_c and τ_{res} are small, then

$$\tau_{eb} \sim \frac{d_o^2}{\beta_c} \qquad 6\text{-}32$$

as if the prevaporization tube had no influence whatsoever. Eq. 6-32 applies only to circumstances when extremely poor vaporization exists in the tube and explains why further shortening of the tube can have a negligible effect on the blowoff limit.

Having presented the data using conventional gas turbine correlating techniques, we now endeavor to develop the characteristic time model to better explain quantitatively the observed influence of variations in geometry and atomization as well as inlet conditions. The length scale for the turbulent mixing time ($\tau_{s\ell}$) is assumed to be the disc diameter (D) minus the tube diameter (d) since the flameholder size (D) successfully correlated data from Ballal and Lefebvre (1977). Following Table 6-3, the appropriate velocity should be the annular velocity (velocity at the tube exit) which for this particular configuration can easily be computed from the flameholder blockage (see the pitot tube measurements of Chapter IV). Therefore, the shear layer mixing time is

$$\tau_{s\ell} = \frac{D - d}{V_a} \quad . \qquad 6\text{-}33$$

According to Table 6-3 the appropriate temperature and equivalence ratio are $(T_{\phi_t} + T_{in})/2$ and ϕ_t, respectively. Thus, the characteristic time model for the tube-and-disc becomes

$$\frac{D - d}{V_a} \sim 10^{-4} \frac{T}{T_{in}} \frac{e^{21000/RT}}{\phi} \qquad 6\text{-}34$$

where $\phi = \phi_t$

and $T = (T^*_{\phi_t} + T_{in})/2$.

Vitiation effects are omitted when calculating the tube equivalence ratio because the original derivation contains X_{HC}, the mole fraction of fuel, rather than ϕ. The value of X_{HC} remains unchanged with vitiation (same number of moles of fuel are present; only the composition of the air changes) and is related to either of the following proportionalities:

$$X_{HC} \sim \text{fuel/air} \sim (f/a)_s \, \phi \Big]_{\text{apparent}}$$
$$\sim (f/a)_s \, \phi \Big]_{\text{vitiated}} \quad . \qquad 6\text{-}35$$

Since the stoichiometric fuel/air ratio for $\phi_{apparent}$ is approximately constant with typical hydrocarbon fuels while $f/a)_{s,vit}$ changes with inlet temperature, Eq. 6-35 simplifies to

$$X_{HC} \sim \phi_{app} \sim \phi_{actual} \; f(T_{in}) \quad . \qquad 6\text{-}36$$

Both are valid and equivalent but obviously $X_{HC} \sim \phi_{app}$ is much simpler to use. Vitiation effects must however, be included in flame temperature calculations since the presence of water vapor and carbon dioxide in the approach flow decreases the near stoichiometric flame temperature substantially at inlet temperatures of 800K (Blazowski and Henderson, 1977).

---

*In general, tube equivalence ratios are fuel lean; however, under some circumstances, ϕ_t exceeds unity at blowoff. Thus, the stabilization curve will have the same shape as the laminar flow blowoff curve in air (see Fig. 6-1) due to mixing of the O_2 rich outer flow with the fuel rich mixture from the tube. This form is further evidenced by the ability to obtain combustion efficiency data at tube equivalence ratios in excess of 2.0 (Table 3-4). When blowoff occurs at ϕ_t greater than one, the stoichiometric flame temperature replaces T_{ϕ_t} in Eq. 6-34 to account for the mixing of oxygen and subsequent reduction in τ_{hc}.

However, it has also been observed (Fig. 6-13) that atomization influences flame stabilization. Given the same mixing time as the purely homogeneous sustem, the heterogeneous combustion process must both evaporate the fuel and ignite the fuel vapor in the same time span. Moses (1975) has also reported that poor atomization has a detrimental effect on blowoff. Thus, droplets represent a perturbation on the flame stabilization process which narrow the limit. To account for heterogeneous effects, Eq. 6-24 is modified to

$$\tau'_{s\ell} \sim \tau_{hc} + a\tau_{eb} \qquad 6\text{-}37$$

where τ_{eb} is computed from the "d^2 law" discussed in Chapter II and evaluated under conditions in the shear layer. The parameter "a" in Eq. 6-37 is chosen empirically to give the best fit to the experimental data. Finally, moving the ratio T/T_{in} to the right hand side as before yields

$$\tau_{s\ell} \sim \tau'_{hc} + a\tau'_{eb} \quad . \qquad 6\text{-}38$$

The experimental data obtained for the base geometry burning both C_3H_8 and Jet A are shown in Fig. 6-16 using the model of Eq. 6-38. The correlation includes variations in pressure, inlet temperature, velocity, fuel type and injector size. It can be seen that one approaches the blowoff limit by increasing the velocity ($\downarrow \tau_{s\ell}$), increasing the initial droplet size ($\uparrow \tau'_{eb}$) and decreasing the tube equivalence ratio ($\uparrow \tau'_{hc}$). The model also predicts that droplet effects will become important at high velocities (small $\tau_{s\ell}$) since at this point τ'_{hc} and τ'_{eb} are the same order of magnitude. This is verified experimentally in Fig. 6-13; droplet effects are most significant at large values of θ^{-1} which correspond to high air velocities.

Geometry variations are shown in Fig. 6-17 and 6-18 for propane and Jet A, respectively. Again the correlation coefficient

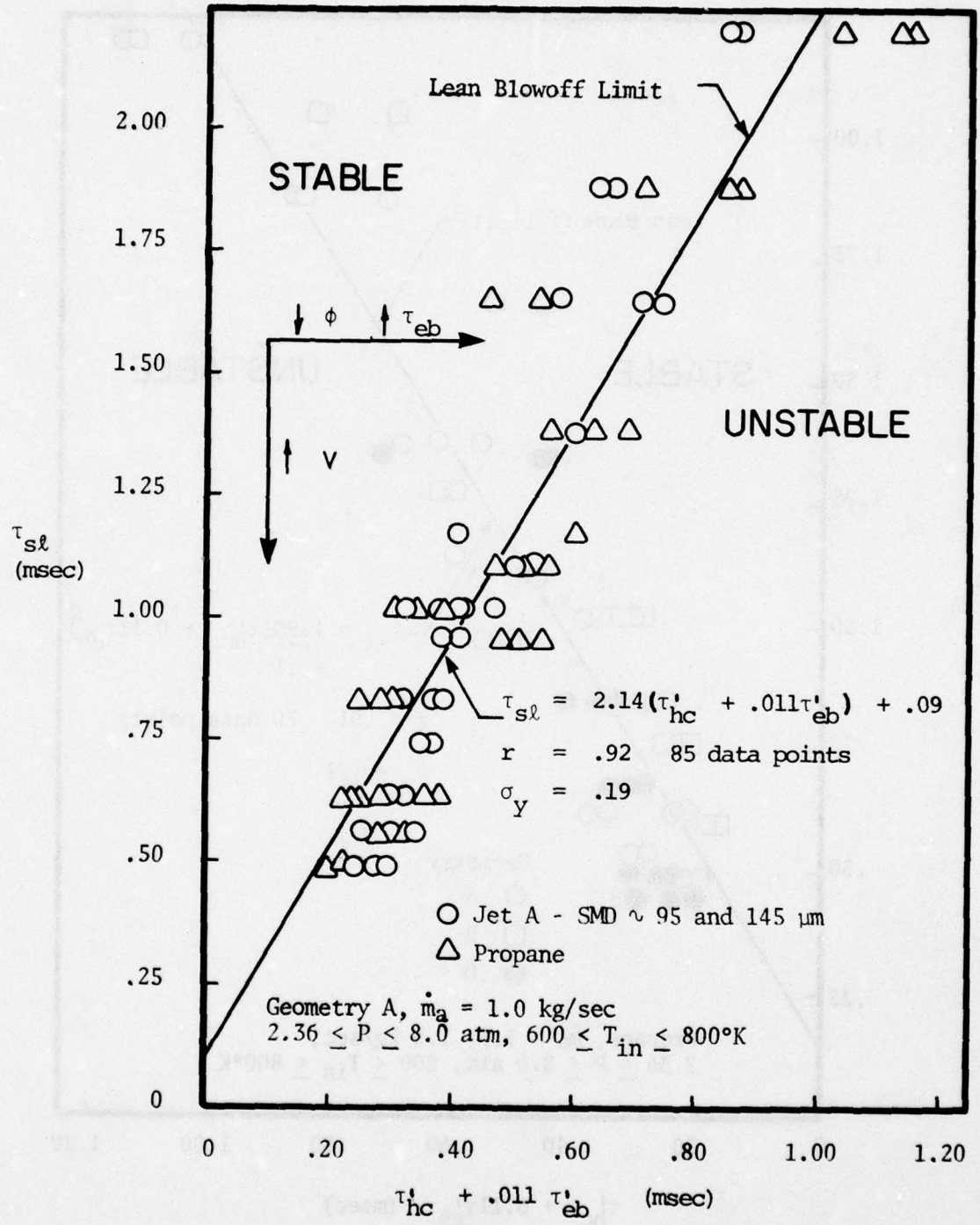

Figure 6-16. Characteristic time correlation for blowoff (Jet A and Propane, Geometry A).

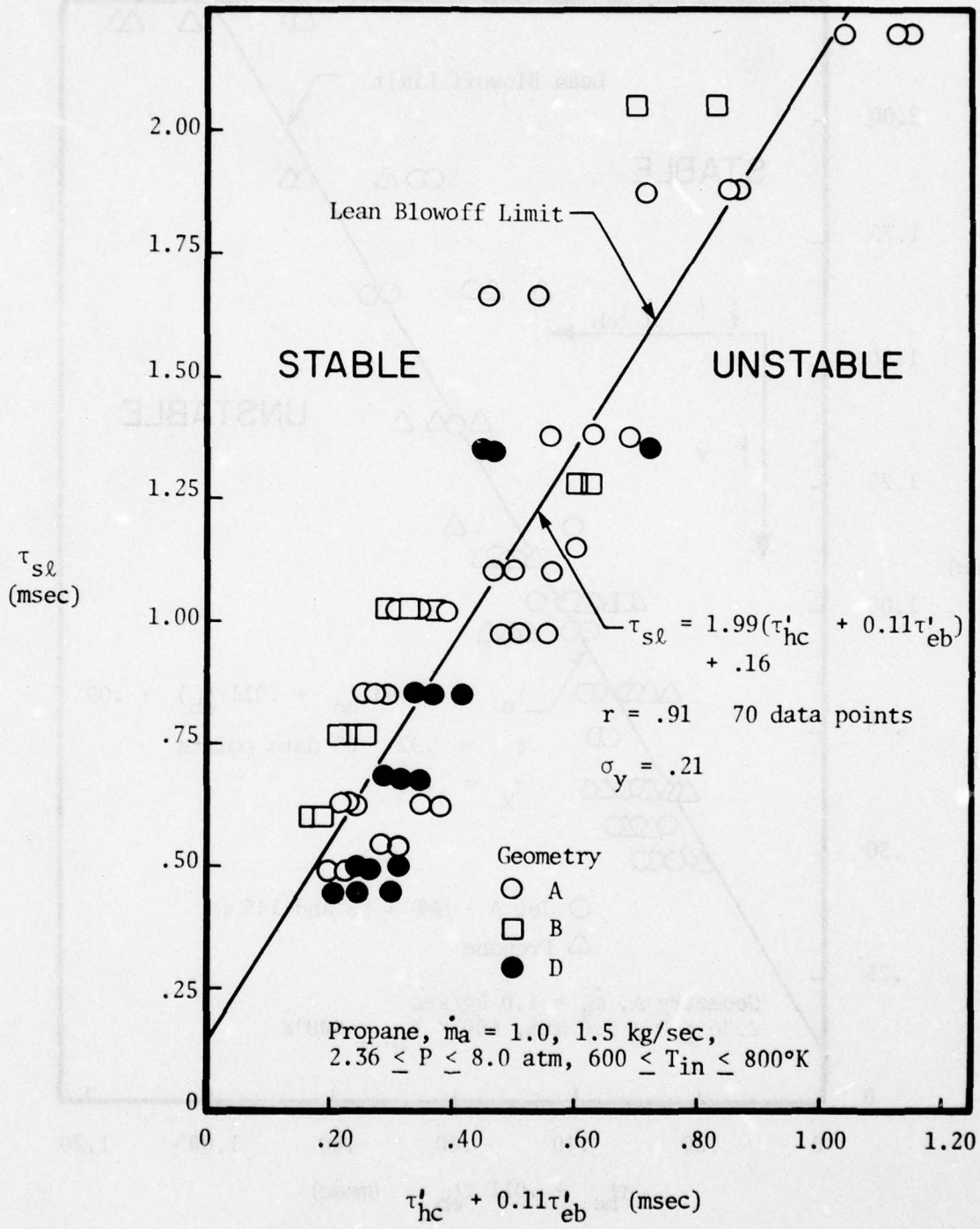

Figure 6-17. Characteristic time correlation for blowoff (Propane, all geometry variations).

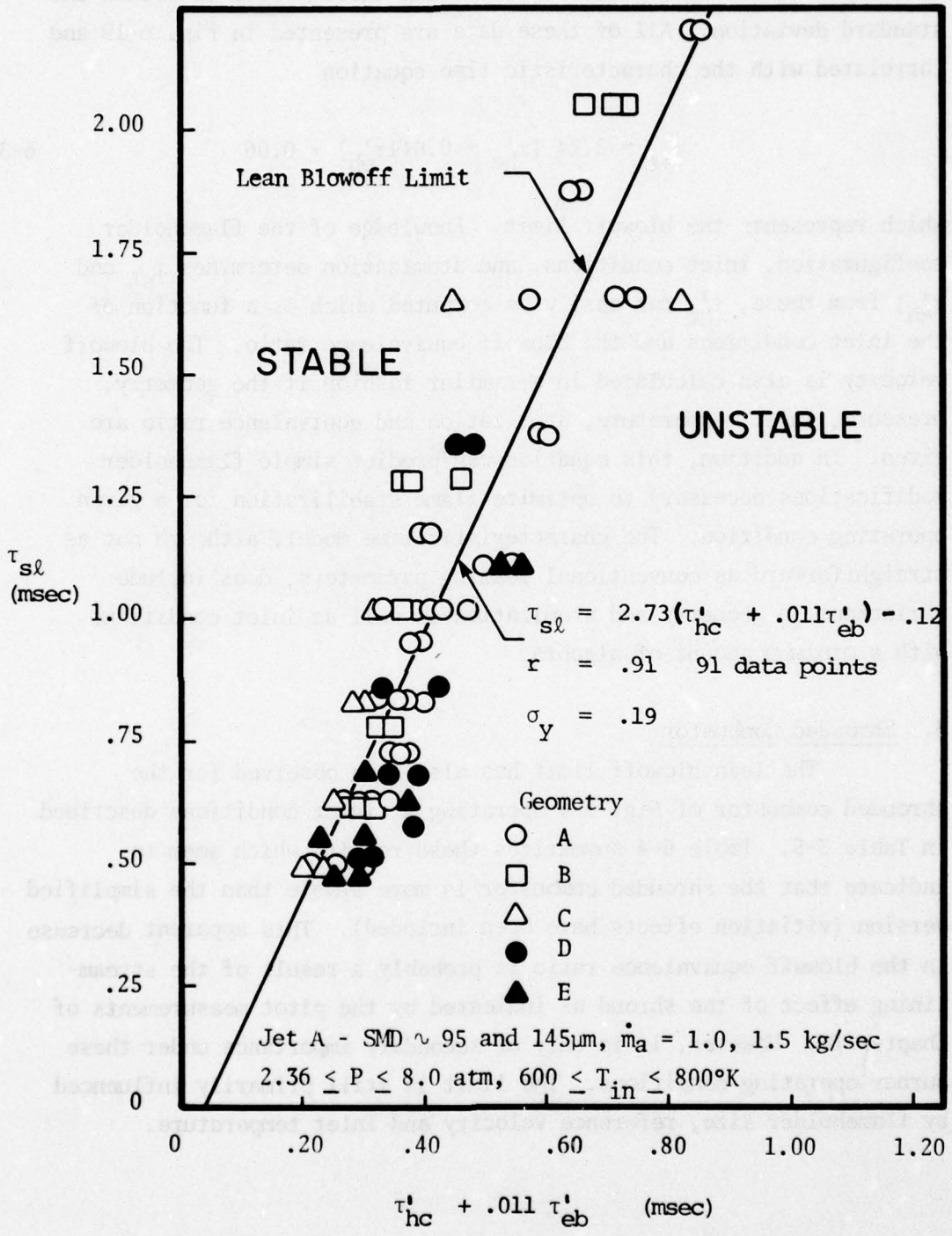

Figure 6-18. Characteristic time correlation for blowoff (Jet A, all geometry variations).

CL-916

is acceptable with the y-intercept passing through zero to within one standard deviation. All of these data are presented in Fig. 6-19 and correlated with the characteristic time equation

$$\tau_{s\ell} = 2.24\ (\tau'_{hc} + 0.011\tau'_{eb}) + 0.06 \qquad 6\text{-}39$$

which represents the blowoff limit. Knowledge of the flameholder configuration, inlet conditions, and atomization determines $\tau_{s\ell}$ and τ'_{eb}; from these, τ'_{hc} can easily be computed which is a function of the inlet conditions and the blowoff equivalence ratio. The blowoff velocity is also calculated in a similar fashion if the geometry, pressure, inlet temperature, atomization and equivalence ratio are given. In addition, this equation can predict simple flameholder modifications necessary to optimize flame stabilization for a given operating condition. The characteristic time model, although not as straightforward as conventional loading parameters, does include variations in geometry and atomization as well as inlet conditions with a minimum amount of algebra.

3. Shrouded Combustor

The lean blowoff limit has also been observed for the shrouded combustor of Fig. 3-4 operating at inlet conditions described in Table 3-5. Table 6-4 summarizes these results which seem to indicate that the shrouded combustor is more stable than the simplified version (vitiation effects have been included). This apparent decrease in the blowoff equivalence ratio is probably a result of the streamlining effect of the shroud as indicated by the pitot measurements of Chapter IV. However, it is only of secondary importance under these burner operating conditions. The limit is still primarily influenced by flameholder size, reference velocity and inlet temperature.

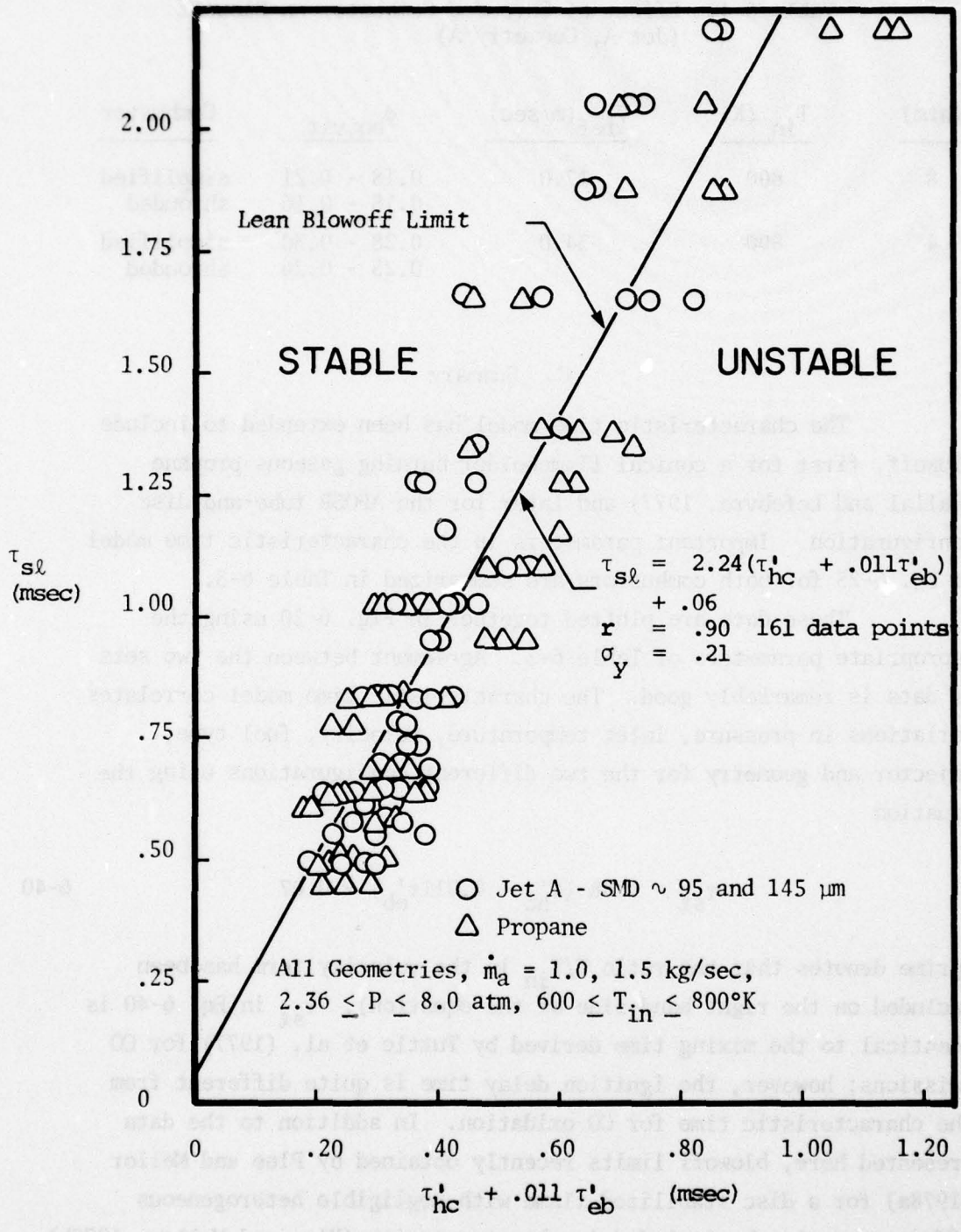

Figure 6-19. Characteristic time correlation for blowoff (all data).

Table 6-4. Effect of Shrouded Combustor on Blowoff (Jet A, Geometry A)

P(atm)	T_{in} (K)	V_{ref}(m/sec)	$\phi_{bo,vit}$	Combustor
8	800	17.0	0.18 - 0.21	simplified
			0.15 - 0.16	shrouded
4	800	34.0	0.28 - 0.30	simplified
			0.25 - 0.26	shrouded

C. Summary

The characteristic time model has been extended to include blowoff, first for a conical flameholder burning gaseous propane (Ballal and Lefebvre, 1977) and later for the AFOSR tube-and-disc configuration. Important parameters in the characteristic time model of Eq. 6-25 for both combustors are summarized in Table 6-3.

These data are plotted together in Fig. 6-20 using the appropriate parameters of Table 6-3. Agreement between the two sets of data is remarkably good. The characteristic time model correlates variations in pressure, inlet temperature, velocity, fuel type, injector and geometry for the two different configurations using the equation

$$\tau_{s\ell} = 1.88\ (\tau'_{hc} + 0.011\tau'_{eb}) + 0.07 \qquad 6\text{-}40$$

(prime denotes that the ratio T/T_{in} in the velocity term has been included on the right hand side of the equation). $\tau_{s\ell}$ in Eq. 6-40 is identical to the mixing time derived by Tuttle et al. (1977) for CO emissions; however, the ignition delay time is quite different from the characteristic time for CO oxidation. In addition to the data presented here, blowoff limits recently obtained by Plee and Mellor (1978a) for a disc stabilized flame with negligible heterogeneous effects can also be included in the correlation (Plee and Mellor, 1978b).

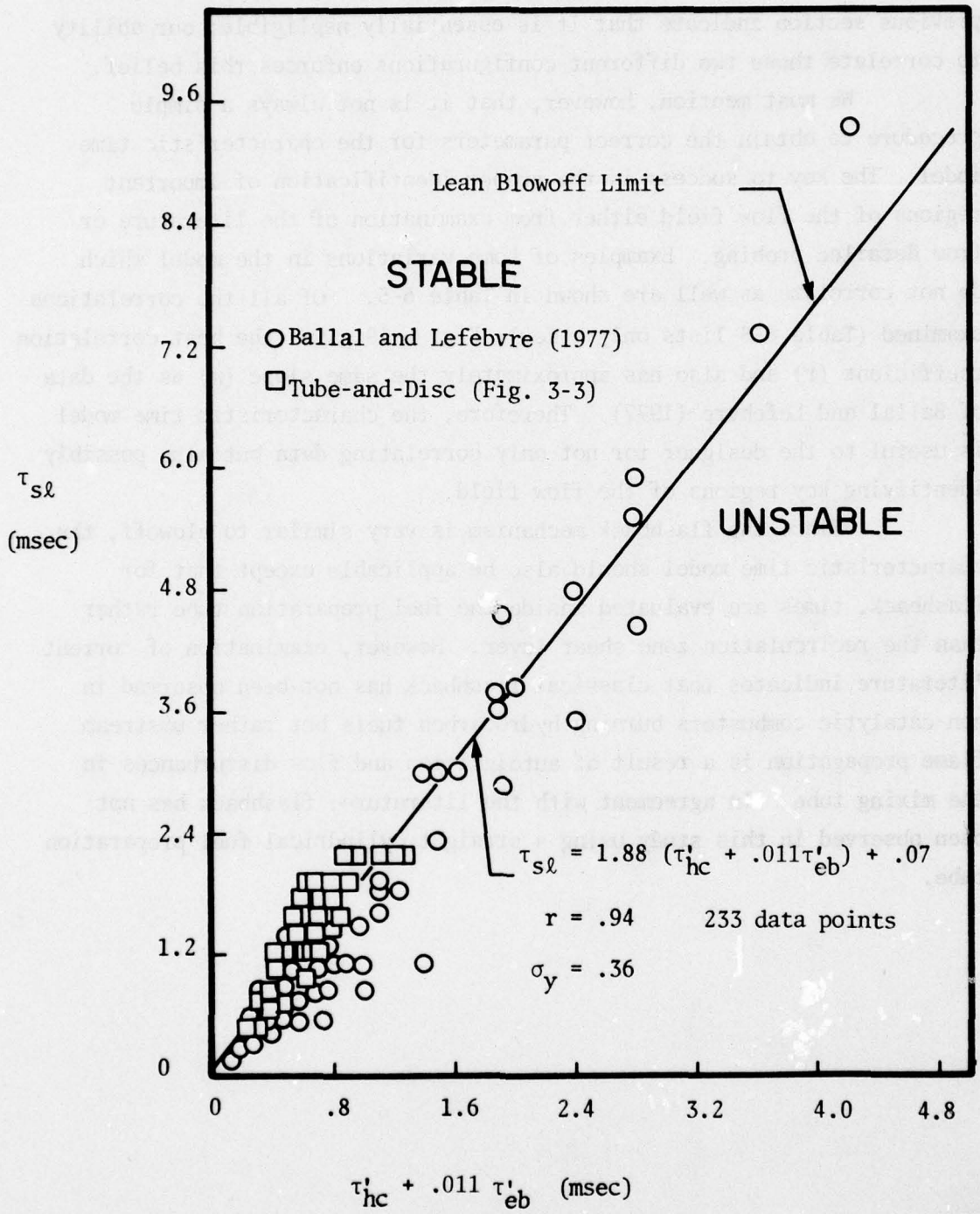

Figure 6-20. Characteristic time model for lean blowoff data obtained from bluff body stabilized flames.

Flameholder shape is not included in the model since results in the previous section indicate that it is essentially negligible; our ability to correlate these two different configurations enforces this belief.

We must mention, however, that it is not always a simple procedure to obtain the correct parameters for the characteristic time model. The key to success is the proper identification of important regions of the flow field either from examination of the literature or from detailed probing. Examples of some variations in the model which do not correlate as well are shown in Table 6-5. Of all the correlations examined (Table 6-5 lists only a few), Fig. 6-19 gives the best correlation coefficient (r) and also has approximately the same slope (m) as the data of Ballal and Lefebvre (1977). Therefore, the characteristic time model is useful to the designer for not only correlating data but also possibly identifying key regions of the flow field.

Since the flashback mechanism is very similar to blowoff, the characteristic time model should also be applicable except that for flashback, times are evaluated inside the fuel preparation tube rather than the recirculation zone shear layer. However, examination of current literature indicates that classical flashback has not been observed in non-catalytic combustors burning hydrocarbon fuels but rather upstream flame propagation is a result of autoignition and flow disturbances in the mixing tube. In agreement with the literature, flashback has not been observed in this study using a straight cylindrical fuel preparation tube.

Table 6-5. Comparison of Various Parameters in the Model (tube-and-disc geometry, E = 21,000 cal/mole)

Case	V	L	ϕ	T	r	m	B
Fig. 6-19	V_a	D - d	ϕ_t	$(T\phi_t + T_{in})/2$	.90	2.24	.065
1	V_{ref}	D - d	ϕ_t	$(T\phi_t + T_{in})/2$	.87	6.11	.096
2	V_a	D	ϕ_t	$(T\phi_t + T_{in})/2$	.87	3.53	.083
3	V_a	D - d	ϕ_{ov}	$(T\phi_{ov} + T_{in})/2$	.60	6.81×10^{-3}	.70
4	V_a	D - d	ϕ_t	T_{ϕ_t}	<.50	-----	-----

VII. FUTURE EFFORTS

One primary objective of the program continuation is the relocation of the Purdue combustion tunnel to an adjacent building in order to take advantage of an indirect fired air heater and computerized data acquisition system. These major improvements should greatly increase the quantity as well as the reliability and accuracy of our experiments. Assuming that the new laboratory is operational in the near future, detailed experiments to better characterize the combustion flow field and flame stabilization process are proposed. Lean blowoff limits have already been successfully correlated using the characteristic time model; however, the classical flashback limit still remains unknown for our prevaporizing/premixing combustors. This is due to the fact that the minimum θ^{-1} (velocity) attainable in the current facility is limited by flame stabilization in the pre-heat combustor. The indirect fired air heater in the new laboratory not only eliminates vitiation effects but also allows much lower reference velocities needed for determination of the classical flashback limit.

In addition, results of the combustion efficiency section clearly indicate the need for a better understanding of the combustion flow field. To date, the characteristic time model for combustion efficiency cannot include variations in pressure, inlet temperature, equivalence ratio, air velocity, fuel type and geometry simultaneously for the tube-and-disc flameholder. Thus in order to better identify key regions of incomplete combustion, flames of high and low combustion efficiency will be probed for selected geometries and inlet conditions. Both time averaged species concentration (NO_x, CO, HC, O_2, CO_2) and temperature can be obtained using a single point probe which is positioned both axially and radially in the combustor. This probing technique has already proven successful in determining regions of NO_x and CO emissions in disc stabilized flames (Tuttle et al., 1975) and in turbojet combustors (Mellor, 1976). Identification of

appropriate regions of combustion inefficiency greatly assists in the choice of length scales, velocities and temperatures relevant to the characteristic time model.

To further characterize the flow field, we are also planning the design and construction of a laser Doppler velocimeter (LDV). The LDV is an optical device which makes use of the frequency shift in monochromatic light scattered by a moving object to provide a non-intrusive means of measuring local flow velocities. Because the frequency shift is small relative to the frequency of the incident light, it is necessary to split the beam and use one part as a reference. This has given use to two basic LDV designs: the reference beam system, in which only one of the beams is scattered while the other is focused directly onto the photomultiplier tube; and the differential LDV, in which both beams are focused to a point in the flow and scattered light from both beams is collected and processed. Because the output of the reference beam LDV is dependent on the angle at which the scattered light is collected and the device itself is difficult to align, we will make use of the differential design. To insure the presence of adequate numbers of scattering centers within the flow, it will probably be necessary to introduce artificial seeding. In so doing, however, care will be taken to insure that the particles introduced will be small enough to follow the fluid accurately.

Once the device is built we plan to make detailed maps of the combustor flow field in both hot and cold nonreacting flows and in various flames. Though the number of axial points at which we make measurements in the test section is limited by the need for optical access to the flow to the five window positions, the radial resolution of the device should allow us two-component velocity data at twenty or more points at each such axial position. By using our microcomputer operated data acquisition system to collect and reduce the data, we will be able to take enough measurements at each point in a short enough period of time to insure a statistically valid result.

These detailed velocity magnitude and direction measurements coupled with the species concentration and temperature profiles mentioned earlier should aid in the selection of scaling parameters for the characteristic time model. Furthermore, these detailed measurements will not only help refine our model but will also provide a data base for comparison with the modular modeling techniques proposed by Edelman (1977).

LIST OF REFERENCES

Altenkirch, R. A. and Mellor, A. M., (1973). "Emissions and performance of gas turbine liners. I: Stability," Rep. No. PURDU-CL-73-05, School of Mech. Eng., Purdue Univ.

Altenkirch, R. A. and Mellor, A. M., (1974). "Emissions and performance of gas turbine liners. II: Internal species concentrations," Rep. No. PURDU-CL-74-03, School of Mech. Eng., Purdue Univ.

Altenkirch, R. A. and Mellor, A. M., (1975). "Emissions and performance of continuous flow combustors," 1181-1189, Fifteenth Symposium (International) on Combustion, The Combustion Institute, Pittsburgh.

Anderson, D., (1975). "Effects of equivalence ratio and dwell time on exhaust emissions from an experimental premixing prevaporizing burner," ASME Paper No. 75-GT-69.

Anderson, D. N., (1976). "Emissions of oxides of nitrogen from an experimental premixed-hydrogen burner," NASA TM X-3393.

Anderson, D. N., Tacina, R. R. and Mroz, T. S., (1975). "Performance of a catalytic reactor at simulated gas turbine combustor operating conditions," NASA TM X-71747.

Azelborn, N. A., Wade, W. R., Secord, J. R. and McLean, A. F., (1973). "Low emissions combustion for the regenerative gas turbine: Part 2 - experimental techniques, results, and assessment," ASME Paper No. 73-GT-12.

Bahr, D. W., (1975). "Attainment of ultra-low NO_x emissions levels in aircraft turbine engines," Proceedings of the Fourth Conference on the Climatic Impact Assessment Program, DOT-TSC-OST-75-38, p. 109-117.

Ballal, D. R. and Lefebvre, A. H., (1977). "Weak extinction limits of turbulent flowing mixtures," Unpublished paper.

Blazowski, W. S. and Bresowar, G. E., (1974). "Preliminary study of the catalytic combustor concept as applied to aircraft gas turbines," AFAPL-TR-74-32.

Blazowski, W. S. and Henderson, R. E., (1974). "Aircraft exhaust pollution and its effect on the U.S. Air Force," AFAPL-TR-74-64.

Blazowski, W. S. and Henderson, R. E., (1977). "A review of turbopropulsion combustion," AFAPL-TR-77-41.

Blazowski, W. S. and Walsh, D. E., (1975). "Catalytic combustion: an important consideration for future applications," Comb. Sci. Tech. 10, 233-244.

Boyer, M. H. and Friebertshauser, P. E., (1957). "An investigation of the behavior and reaction mechanisms of nitric acid-hydrocarbon flames," Comb. Flame 1, 264-280.

Clayton, R. M., (1976). "Reduction of gaseous pollutant emissions from gas turbine combustors using hydrogen-enriched jet fuel - A Progress Report," NASA TM 33-790.

Cooke, D. G. and Williams, A., (1975). "Shock tube studies of methane and ethane oxidation," Comb. Flame 24, 245-256.

Craig, R. R., (1976). Wright Patterson Air Force Base. Personal Communication.

De Zubay, E. A., (1950). "Characteristics of disk-controlled flame," Aero. Digest, July, 54.

Dodds, W. J., Colket, M. B. and Mellor, A. M., (1976). "Radiation and smoke from gas turbine flames. Part 1. Carbon particulate measurements within a model turbine combustor," USATACOM Tech. Rep. No. 12163, Part 1.

Dodds, W. J., Renie, J. P. and Mellor, A. M., (1975). "Gas turbine engine stability and performance as determined by fuel and injector type," USATACOM Tech. Rep. No. 12065.

Dugger, G. L., (1950). "Effect of initial mixture temperature on flame speeds and blow-off limits of propane-air flames," NACA TN-2170.

Edelman, R. B., (1976). SAI, Woodland Hills, Ca. Personal Communication to A. M. Mellor, Purdue University.

Edelman, R. B., (1977). SAI, Woodland Hills, Ca. Personal Communication to A. M. Mellor, Purdue University.

Engleman, V. S., Bartok, W., Longwell, J. P. and Edelman, R. B., (1973). "Experimental and theoretical studies of NO_x formation in a jet-stirred combustor," 755-765, Fourteenth Symposium (International) on Combustion, The Combustion Institute, Pittsburgh.

Environmental Protection Agency, (1973). "Control of air pollution from aircraft and aircraft engines," U.S. Federal Register 38, (136) Part II, July 17.

Fear, J. S., (1976). "The NASA pollution-reduction technology program for small jet aircraft engines - A Status Report," NASA TM X-73419.

Fine, B., (1958). "The flashback of laminar and turbulent burner flames at reduced pressure," Comb. Flame 2, 253-266.

Fontijn, A., Sabadell, A. J. and Ronco, R. J., (1970). "Homogeneous chemiluminescent measurement of nitric oxide with ozone. Implications for continuous selective monitoring of gaseous air pollutants," Anal. Chem. 42, 575-579.

Gleason, C. C., Rogers, D. W. and Bahr, D. W., (1976). "Experimental clean combustor program: Phase II," NASA CR-134971.

Godsave, G. A. E., (1953). "Studies of the combustion of drops in a fuel spray - the burning of single drops of fuel," 818-830, Fourth Symposium (International) on Combustion, Williams and Wilkins, Baltimore.

Gordon, S. and McBride, B. J., (1971). "Computer program for calculation of complex chemical equilibrium compositions, rocket performance, incident and reflected shocks, and Chapman-Jouquet detonations," NASA SP-273.

Gosman, A. D., Pun, W. M., Runchal, A. K., Spalding, D. B. and Wolfstein, M., (1969). Heat and Mass Transfer in Recirculating Flows, Academic Press, New York.

Grobman, J. S., (1972). "Effect of operating variables on pollutant emissions from aircraft turbine engine combustors," Emissions from Continuous Combustion Systems, 279-303, Plenum Press, New York.

Grumer, J., (1958). "Flashback and blowoff limits of unpiloted turbulent flames," Jet Prop. 28, 756-759.

Grumer, J., Harris, M. E. and Rowe, V. R., (1956). "Fundamental flashback, blowoff, and yellow-tip limits of fuel gas-air mixtures," Bur. Mines. RI-5225.

Grumer, J., Harris, M. E. and Schultz, H., (1953). "Flame stabilization on burners with short ports or non-circular ports," 695-701, Fourth Symposium (International) on Combustion, Williams and Wilkins, Baltimore.

Hammond, D. C., (1977). "Evaluating characteristic time emission prediction for three vehicular gas turbine combustors," AIAA Journal of Energy 1, 250-256.

Hammond, D. C., Jr. and Mellor, A. M., (1970). "A preliminary investigation of gas turbine combustor modeling," Comb. Sci. Tech. 2, 67-80.

Hottel, H. C., Williams, G. C. and Bonnell, A. H., (1958). "Application of well-stirred reactor theory to the prediction of combustor performance," Comb. Flame 2, 13-31.

Hunter, S. C., Johnson, K. M., Mongia, H. C. and Wood, M. P., (1974). "Advanced, small, high-temperature-rise combustor program. Volume I: analytical model derivation and combustor-element rig tests (phases I and II)," USAAMRDL Tech. Rep. 74-3A.

Khitrin, L. N., Moin, P. B., Smirnov, D. B. and Shevchuk, V. U., (1965). "Peculiarities of laminar and turbulent flame flashbacks," 1285-1291, Tenth Symposium (International) on Combustion, The Combustion Institute, Pittsburgh.

Layne, J., (1975). Purdue University. Personal Communication to S. L. Plee, Purdue University.

Lefebvre, A. H., (1966). "Theoretical aspects of gas turbine combustion performance," CoA Note Aero. No. 163, The College of Aeronautics, Dept. of Prop., Cranfield Inst. of Tech.

Lewis, B. and von Elbe, G., (1961). Combustion, Flames, and Explosions of Gases, Second Edition, Academic Press, New York.

Lipfert, F. W., (1972). "Correlation of gas turbine emissions data," ASME Paper No. 72-GT-60.

Longwell, J. P., (1953). "Flame stabilization by bluff bodies and turbulent flames in ducts," 90-97, Fourth Symposium (International) on Combustion, Williams and Wilkins, Baltimore.

Longwell, J. P., Chenevey, J. E., Clark, W. W. and Frost, E. E., (1949). "Flame stabilization by baffles in a high velocity gas stream," 40-44, Third Symposium on Combustion and Flame and Explosion Phenomena, Williams and Wilkins, Baltimore.

Longwell, J. P., Frost, E. E. and Weiss, M. A., (1953). "Flame stability in bluff body recirculation zones," Ind. Eng. Chem. 45, 1629-1633.

Longwell, J. P. and Weiss, M. A., (1955). "High temperature reaction rates in hydrocarbon combustion," Ing. Eng. Chem. 47, 1634.

Marek, C. J. and Papathakos, L. C., (1976). "Exhaust emissions from a premixing, prevaporizing flame tube using liquid Jet A fuel," NASA TM X-3383.

Marek, C. J., Papathakos, L. C. and Verbulecz, P. W., (1977). "Preliminary studies of autoignition and flashback in a premixing-prevaporizing flame tube using Jet A fuel at lean equivalence ratios," NASA TM X-3526.

Mellor, A. M., (1972). "Current kinetic modeling techniques for continuous flow combustors," Emissions from Continuous Combustion Systems, 23-53, Plenum Press, New York.

Mellor, A. M., (1976). "Gas turbine engine pollution," Pollution Formation and Destruction in Flames, Vol. I of Progress in Energy and Combustion Science, Chigier, N. A. Editor, Pergamon, Oxford, 111-133.

Mellor, A. M., (1977a). "Characteristic time emissions correlations and sample optimization: GT-309 gas turbine combustor," AIAA Journal of Energy 1, 244-249.

Mellor, A. M., (1977b). "Characteristic time emissions correlations: the T-63 helicopter gas turbine combustor," AIAA Journal of Energy 1, 257-262.

Mellor, A. M., Anderson, R. D., Altenkirch, R. A. and Tuttle, J. H., (1972). "Emissions from and within an Allison J-33 combustor," Comb. Sci. Tech. 6, 169-176.

Mellor, A. M. and Washam, R. M., (1978). "Correlation technique for ambient effects on oxides of nitrogen," submitted to the AIAA Journal of Aircraft.

Moses, C. A., (1975). "Studies of fuel volatility effects on turbine combustor performance," presented at Joint Spring Meeting of Western and Central States Section of the Combustion Institute.

Mosier, S. A. and Roberts, R., (1974). "Low-power turbopropulsion combustor exhaust emissions. Vol II: Demonstration and total emission analysis and prediction," AFAPL-TR-73-36, Vol. II.

Nelson, A. W., (1976). Pratt and Whitney Aircraft. Personal Communication to R. Munt, Environmental Protection Agency, 12 October 1976.

Niedzwiecki, R. W., (1975). "The experimental clean combustor program - description and status to November 1975," NASA TM X-71849.

Odgers, J., (1975). "Current theories of combustion within gas turbine chambers," 1321-1338, Fifteenth Symposium (International) on Combustion, The Combustion Institute, Pittsburgh.

Plee, S. L. and Mellor, A. M., (1977). "Review of flashback reported in prevaporizing/premixing combustors," accepted for publication in Comb. Flame.

Plee, S. L. and Mellor, A. M., (1978a). "Flame stabilization in simplified prevaporizing, partially vaporizing and conventional gas turbine combustors," submitted for presentation at AIAA/SAE 14th Joint Propulsion Conference, Las Vegas, Nevada.

Plee, S. L. and Mellor, A. M., (1978b). "Characteristic time correlation for lean blowoff of bluff body stabilized flames," Unpublished paper.

Putnam, A. A. and Jensen, R. A., (1949). "Application of dimensionless numbers to flashback and other combustion phenomena," 89-98, Third Symposium on Combustion and Flame and Explosion Phenomena, Williams and Wilkins, Baltimore.

Ranz, W. E. and Marshall, W. R., Jr., (1952). "Evaporation from drops," Chem. Eng. Prog. 48, 141-146 (Part I); 173-180 (Part II).

Roberts, P. B., Shekleton, J. R., White, D. R. and Butze, H. F., (1976). "Advanced low NO_x combustors for supersonic high-altitude aircraft gas turbines," ASME Paper No. 76-GT-12.

Roberts, R., Fiorentino, A. J. and Greene, W., (1976). "Pollution technology program, can-annular combustor engines," NASA CR-135027.

Roberts, R., Peduzzi, A. and Vitti, G. E., (1975). "Experimental clean combustor program: Phase 1," NASA CR-134736.

Roffe, G., (1976). "Effect of inlet temperature and pressure on emissions from a premixing gas turbine primary zone combustor," NASA CR-2740.

Roffe, G. and Ferri, A., (1975). "Prevaporization and premixing to obtain low oxides of nitrogen in gas turbine combustors," NASA CR-2495.

Roffe, G. and Ferri, A., (1976). "Effect of premixing quality on oxides of nitrogen in gas turbine combustors," NASA CR-2657.

Sawyer, R. F., Cernansky, N. P. and Oppenheim, A. K., (1973). "Factors controlling pollutant emissions from gas turbine engines," Atmospheric Pollution by Aircraft Engines, AGARD, CP No. 125.

Shisler, R. A., Tuttle, J. H. and Mellor, A. M., (1974). "Emissions from and within a film-cooled combustor," Report No. PURDU-CL-74-01, School of Mech. Eng., Purdue Univ.

Spadaccini, L. J., (1976). "Autoignition characteristics of hydrocarbon fuels at elevated temperatures and pressures," ASME Paper No. 76-GT-3.

Spadaccini, L. J. and Szetela, E. J., (1975). "Approaches to the prevaporized-premixed combustor concept for gas turbines," ASME Paper No. 75-GT-85.

Spalding, D. B., (1955). Some Fundamentals of Combustion, Butterworths, London.

Spalding, D. B., (1971). "Mixing and chemical reaction in steady confined turbulent flames," 649-657, Thirteenth Symposium (International) on Combustion, The Combustion Institute, Pittsburgh.

Spalding, D. B. and Tall, B. S., (1954). "Flame stabilization in high velocity gas streams and the effect of heat losses at low pressures," The Aero. Quarterly, V, 195-215.

Stull, F. D., Craig, R. R. and Hojnacki, J. T., (1974). "Dump combustor parametric investigations," Fluid Mechanics of Combustion, ASME, New York, 135-154.

Tacina, R., (1976). "Experimental evaluation of two premixing-prevaporizing fuel injection concepts for a gas turbine catalytic combustor," NASA TM X-73422.

Troth, D. L., Verdouw, A. J. and Verkamp, F. J., (1973). "Investigation of aircraft gas turbine combustor having low mass emissions," USAAMRDL Tech. Rep. 73-6.

Troth, D. L., Verdouw, A. J., Williams, J. R. and Dodd, R. G., (1974). "Investigation of aircraft gas turbine combustor having low mass emissions," ASME Paper No. 74-GT-36.

Turunen, W. A. and Collman, J. S., (1965). "The General Motors research GT-309 gas turbine engine," SAE Paper 650714.

Tuttle, J. H., Altenkirch, R. A. and Mellor, A. M., (1973). "Emissions from and within an Allison J-33 combustor. II. The effect of inlet air temperature," Comb. Sci. Tech. 7, 125-134.

Tuttle, J. H., Colket, M. B., Bilger, R. W. and Mellor, A. M., (1977). "Characteristic times for combustion and pollutant formation in spray combustion," 209-219, Sixteenth Symposium (International) on Combustion, The Combustion Institute, Pittsburgh.

Tuttle, J. H., Colket, M. B. and Mellor, A. M., (1976). "Characteristic time correlation of emissions from conventional aircraft type flames," Rep. No. PURDU-CL-76-05, School of Mech. Eng., Purdue Univ.

Tuttle, J. H., Shisler, R. A., Bilger, R. W. and Mellor, A. M., (1975). "Emissions from aircraft fuel nozzle flames," Report No. PURDU-CL-75-04, School of Mech. Eng., Purdue Univ.

Tuttle, J. H., Shisler, R. A. and Mellor, A. M., (1974). "Nitrogen dioxide formation in gas turbine engines: measurements and measurement methods," Comb. Sci. Tech. 9, 261-271.

Vaught, J. M., Johnsen, S. E. J., Parks, W. M. and Johnson, R. L., (1971). "Collection and assessment of aircraft emissions base-line data -- turbo-prop engines (Allison T56-A-15)," Report EDR-7200, Detroit Diesel Allison Div., General Motors Corp.

Verkamp, F. J., Verdouw, A. J. and Tomlinson, J. G., (1974). "Impact of emission regulations on future gas turbine engine combustors," J. Aircraft 11, 340-344.

Wade, W. R. and Cornelius, W., (1972). "Emissions characteristics of continuous combustion systems of vehicular powerplants-gas turbine, steam, Stirling," Emissions from Continuous Combustion Systems, 375-450, Plenum Press, New York.

Wampler, F. B., Clark, D. W. and Gaines, F. A., (1976). "Catalytic combustion of C_3H_8 on Pt coated monolith," Comb. Sci. Tech. 14, 25-31.

Williams, G. C., Hottel, H. C. and Scurlock, A. C., (1949). "Flame stabilization and propagation in high velocity gas streams," 21-40, Third Symposium on Combustion and Flame and Explosion Phenomena, Williams and Wilkins, Baltimore.

Williams, G. C. and Shipman, C. W., (1953). "Some properties of rod-stabilized flames of homogeneous gas mixtures," 733-742, Fourth Symposium (International) on Combustion, Williams and Wilkins, Baltimore.

Wohl, K., (1953). "Quenching, flashback, and blowoff - theory and experiment," 68-89, Fourth Symposium (International) on Combustion, Williams and Wilkins, Baltimore.

Wohl, K., Kapp, N. M. and Gazley, C., (1949). "The stability of open flames," 3-21, Third Symposium on Combustion and Flame and Explosion Phenomena, Williams and Wilkins, Baltimore.

Zukoski, E. E. and Marble, F. E., (1956). "Experiments concerning the mechanism of flame blowoff from bluff bodies," Proc. Gas Dynamics Symposium on Aerothermochemistry, Northwestern Univ.

Appendix A

Data Listing

All of the combustion efficiency and lean blowoff data obtained for the simplified prevaporizing/premixing combustor of Fig. 3-3 are listed in this section. The computer print out includes nozzle size, fuel type, (starting with Jet A), geometry, pressure, inlet temperature, air flow rate and overall equivalence ratio. (Note that the equivalence ratio listed here is an apparent ϕ and does not include vitiation effects). In addition to inlet conditions, the theta parameter of Lefebvre (1966) has been computed for each data point as well as the initial fuel spray SMD and the droplet evaporation time. Parameters in τ_{eb} are evaluated in the same manner as did Tuttle et al. (1976).

Both the blowoff and combustion efficiency experiments were performed at the same time since it was convenient to first obtain stable combustor operation, measure the emissions and then slowly decrease the fuel flow rate to the lean limit. The comment column indicates whether the data point is for blowoff or combustion efficiency. If a blowoff point has been obtained, all emissions and combustion efficiency values are printed as zeros. However, for the combustion efficiency data, a NO_xEI value of zero or * indicates sampling problems usually associated with the interaction of unburned hydrocarbons with NO_x in the gas sampling system (Tuttle et al., 1974).

RUN NUMBER: 8 NOZZLE: 16-90 FUEL: JETA

DISC = 12.70 CM, TUBE DIA = 4.44 CM, TUBE LENGTH = 14.40 CM

COMBUSTOR HOUSING DIAMETER = 14.06 CM.

P	TIN	MDA	PHI	THETA	SMD	TEB	NOXEI	HCEI	COEI	ETA	COMMENT
ATM	K	KG/SEC			UM	MSEC	G/KG	G/KG	G/KG	PCT	
3.00	800.	1.0	.256	.390	98.	4.57	0	0	0	0	BLOWOFF
5.00	800.	1.0	.213	.952	106.	4.60	0	0	0	0	BLOWOFF
8.00	800.	1.0	.156	2.168	119.	4.96	0	0	0	0	BLOWOFF
2.36	800.	1.0	.345	.256	86.	3.86	0	0	0	0	BLOWOFF

RUN NUMBER: 9 NOZZLE: 16-90 FUEL: JETA

DISC = 12.70 CM, TUBE DIA = 4.44 CM, TUBE LENGTH = 14.40 CM

COMBUSTOR HOUSING DIAMETER = 14.06 CM.

P	TIN	MDA	PHI	THETA	SMD	TEB	NOXEI	HCEI	COEI	ETA	COMMENT
ATM	K	KG/SEC			UM	MSEC	G/KG	G/KG	G/KG	PCT	
3.00	800.	1.0	.262	.390	100.	4.73	0	0	0	0	BLOWOFF
3.00	800.	1.0	.293	.390	91.	4.07	*	380.3	409.8	46.8	COMB. EFF.
5.00	800.	1.0	.293	.952	91.	3.60	*	109.9	193.2	82.9	COMB. EFF.
5.00	800.	1.0	.211	.952	108.	4.76	0	0	0	0	BLOWOFF
5.00	800.	1.0	.235	.952	101.	4.31	*	84.0	174.8	86.3	COMB. EFF.
8.00	800.	1.0	.235	2.168	99.	3.74	2.68	18.2	62.3	96.5	COMB. EFF.
8.00	800.	1.0	.293	2.168	90.	3.20	2.52	10.6	79.9	96.9	COMB. EFF.
8.00	800.	1.0	.195	2.168	111.	4.48	1.75	4.6	44.8	98.4	COMB. EFF.

RUN NUMBER: 10 NOZZLE: 16-90 FUEL: JETA

DISC = 12.70 CM, TUBE DIA = 4.44 CM, TUBE LENGTH = 14.40 CM

COMBUSTOR HOUSING DIAMETER = 14.06 CM.

P	TIN	MDA	PHI	THETA	SMD	TEB	NOXEI	HCEI	COEI	ETA	COMMENT
ATM	K	KG/SEC			UM	MSEC	G/KG	G/KG	G/KG	PCT	
8.00	800.	1.0	.372	2.168	83.	2.79	0	0	0	0	BLOWOFF
8.00	800.	1.0	.293	2.168	92.	3.30	0	0	0	0	BLOWOFF
8.00	800.	1.0	.235	2.168	100.	3.80	0	0	0	0	BLOWOFF
8.00	800.	1.0	.195	2.168	111.	4.48	0	0	0	0	BLOWOFF
8.00	800.	1.0	.154	2.168	123.	5.25	0	0	0	0	BLOWOFF
5.00	800.	1.0	.184	.952	115.	5.29	0	0	0	0	BLOWOFF
3.00	800.	1.0	.248	.390	99.	4.64	0	0	0	0	BLOWOFF
2.36	800.	1.0	.334	.256	101.	5.02	0	0	0	0	BLOWOFF

RUN NUMBER: 11 NOZZLE: 16-90 FUEL: JETA

DISC = 12.70 CM, TUBE DIA = 4.44 CM, TUBE LENGTH = 14.40 CM

COMBUSTOR HOUSING DIAMETER = 14.06 CM.

P	TIN	MDA	PHI	THETA	SMD	TEB	NOXEI	HCEI	COEI	ETA	COMMENT
ATM	K	KG/SEC			UM	MSEC	G/KG	G/KG	G/KG	PCT	
3.00	800.	1.0	.293	.390	91.	4.07	*	295.8	376.2	57.3	COMB. EFF.
5.00	800.	1.0	.293	.952	91.	3.64	*	102.8	223.6	83.0	COMB. EFF.
5.00	800.	1.0	.235	.952	102.	4.38	*	50.7	147.4	90.7	COMB. EFF.
8.00	800.	1.0	.235	2.168	101.	3.85	1.82	8.7	50.1	97.8	COMB. EFF.
8.00	800.	1.0	.293	2.168	92.	3.30	2.38	8.0	58.4	97.7	COMB. EFF.
8.00	800.	1.0	.195	2.168	112.	4.52	2.19	8.8	47.2	97.9	COMB. EFF.
8.00	800.	1.0	.169	2.168	121.	5.10	0	0	0	0	BLOWOFF

RUN NUMBER: 13 NOZZLE: 30-90 FUEL: JETA

DISC = 12.70 CM, TUBE DIA = 4.44 CM, TUBE LENGTH = 14.40 CM

COMBUSTOR HOUSING DIAMETER = 14.06 CM.

P	TIN	MDA	PHI	THETA	SMD	TEB	NOXEI	HCEI	COEI	ETA	COMMENT
ATM	K	KG/SEC			UM	MSEC	G/KG	G/KG	G/KG	PCT	
2.36	800.	1.0	.372	.256	131.	7.80	0	0	0	0	BLOWOFF
3.00	800.	1.0	.390	.390	130.	7.24	*	478.7	354.7	36.8	COMB. EFF.
3.00	800.	1.0	.326	.390	139.	8.14	0	0	0	0	BLOWOFF
3.00	800.	1.0	.320	.390	140.	8.25	0	0	0	0	BLOWOFF
5.00	800.	1.0	.293	.952	143.	7.52	*	146.5	359.7	74.8	COMB. EFF.
5.00	800.	1.0	.390	.952	131.	6.53	*	244.7	506.8	60.1	COMB. EFF.
8.00	800.	1.0	.390	2.168	129.	5.70	*	63.8	271.7	86.3	COMB. EFF.
8.00	800.	1.0	.293	2.168	143.	6.70	2.48	33.8	100.4	93.8	COMB. EFF.
5.00	800.	1.0	.213	.952	159.	8.87	0	0	0	0	BLOWOFF
5.00	800.	1.0	.227	.952	161.	9.07	0	0	0	0	BLOWOFF

RUN NUMBER: 14 NOZZLE: 30-90 FUEL: JETA

DISC = 12.70 CM, TUBE DIA = 4.44 CM, TUBE LENGTH = 14.40 CM

COMBUSTOR HOUSING DIAMETER = 14.06 CM.

P	TIN	MDA	PHI	THETA	SMD	TEB	NOXEI	HCEI	COEI	ETA	COMMENT
ATM	K	KG/SEC			UM	MSEC	G/KG	G/KG	G/KG	PCT	
8.00	800.	1.0	.293	2.168	146.	6.94	1.73	10.6	75.0	97.0	COMB. EFF.
8.00	800.	1.0	.235	2.168	152.	7.36	2.22	7.9	62.3	97.6	COMB. EFF.
5.00	800.	1.0	.293	.952	143.	7.52	0	132.4	326.8	77.2	COMB. EFF.
5.00	800.	1.0	.235	.952	157.	8.69	0	0	0	0	BLOWOFF
4.00	800.	1.0	.293	.844	144.	8.00	*	236.6	504.4	61.1	COMB. EFF.
2.36	800.	1.0	.390	.256	128.	7.50	0	0	0	0	BLOWOFF

RUN NUMBER: 15 NOZZLE: 30-90 FUEL: JETA

DISC = 12.70 CM, TUBE DIA = 4.44 CM, TUBE LENGTH = 14.40 CM

COMBUSTOR HOUSING DIAMETER = 14.06 CM.

P	TIN	MDA	PHI	THETA	SMD	TEB	NOXEI	HCEI	COEI	ETA	COMMENT
ATM	K	KG/SEC			UM	MSEC	G/KG	G/KG	G/KG	PCT	
8.00	800.	1.0	.293	2.168	141.	6.56	2.70	5.4	68.2	97.8	COMB. EFF.
8.00	800.	1.0	.235	2.168	151.	7.30	2.68	6.1	58.6	97.9	COMB. EFF.
5.00	800.	1.0	.293	.952	143.	7.47	.18	119.7	418.2	76.5	COMB. EFF.
4.00	800.	1.0	.293	.644	141.	7.73	*	239.4	522.1	60.4	COMB. EFF.
4.00	800.	1.0	.235	.644	155.	9.00	0	0	0	0	BLOWOFF
3.50	800.	1.0	.293	.511	143.	8.14	*	338.0	603.6	47.2	COMB. EFF.
3.50	800.	1.0	.277	.511	145.	8.40	0	0	0	0	BLOWOFF
3.50	800.	1.0	.282	.511	148.	8.66	0	0	0	0	BLOWOFF
4.00	800.	1.0	.272	.644	148.	8.42	0	0	0	0	BLOWOFF

RUN NUMBER: 16 NOZZLE: 30-90 FUEL: JETA

DISC = 12.70 CM, TUBE DIA = 4.44 CM, TUBE LENGTH = 14.40 CM

COMBUSTOR HOUSING DIAMETER = 14.06 CM.

P	TIN	MDA	PHI	THETA	SMD	TEB	NOXEI	HCEI	COEI	ETA	COMMENT
ATM	K	KG/SEC			UM	MSEC	G/KG	G/KG	G/KG	PCT	
3.00	800.	1.0	.298	.390	142.	8.44	0	0	0	0	BLOWOFF
2.36	800.	1.0	.385	.256	221.	18.35	0	0	0	0	BLOWOFF
3.50	800.	1.0	.261	.511	149.	8.79	0	0	0	0	BLOWOFF
4.00	800.	1.0	.246	.644	152.	8.72	0	0	0	0	BLOWOFF
5.00	800.	1.0	.211	.952	158.	8.85	0	0	0	0	BLOWOFF

RUN NUMBER: 28 NOZZLE: 16-90 FUEL: JETA

DISC = 12.70 CM, TUBE DIA = 4.44 CM, TUBE LENGTH = 14.40 CM

COMBUSTOR HOUSING DIAMETER = 14.06 CM.

P	TIN	MDA	PHI	THETA	SMD	TEB	NOXEI	HCEI	COEI	ETA	COMMENT
ATM	K	KG/SEC			UM	MSEC	G/KG	G/KG	G/KG	PCT	
8.00	800.	1.0	.293	2.168	94.	3.40	2.66	5.6	68.2	97.8	COMB. EFF.
8.00	700.	1.0	.293	1.553	93.	3.35	2.66	6.3	53.3	98.0	COMB. EFF.
8.00	600.	1.0	.293	1.113	92.	3.33	1.76	35.2	70.4	94.3	COMB. EFF.
5.00	700.	1.0	.293	.682	93.	3.75	.18	101.4	173.0	84.3	COMB. EFF.
5.00	600.	1.0	.293	.489	93.	3.71	*	169.0	359.7	72.2	COMB. EFF.
4.00	800.	1.0	.293	.644	94.	4.03	*	259.2	513.2	58.3	COMB. EFF.
4.00	700.	1.0	.293	.462	94.	4.03	*	231.0	435.2	63.4	COMB. EFF.
4.00	600.	1.0	.293	.331	93.	3.94	*	281.7	401.3	58.3	COMB. EFF.

RUN NUMBER: 29 NOZZLE: 16-90 FUEL: JETA

DISC = 12.70 CM, TUBE DIA = 4.44 CM, TUBE LENGTH = 14.40 CM

COMBUSTOR HOUSING DIAMETER = 14.06 CM.

P	TIN	MDA	PHI	THETA	SMD	TEB	NOXEI	HCEI	COEI	ETA	COMMENT
ATM	K	KG/SEC			UM	MSEC	G/KG	G/KG	G/KG	PCT	
8.00	700.	1.0	.293	1.553	93.	3.34	2.57	16.3	55.0	96.8	COMB. EFF.
8.00	600.	1.0	.293	1.113	94.	3.40	1.39	35.2	72.6	94.3	COMB. EFF.
5.00	700.	1.0	.293	.682	94.	3.79	.18	112.7	161.5	83.3	COMB. EFF.
5.00	600.	1.0	.293	.489	94.	3.79	*	191.5	367.9	69.4	COMB. EFF.
4.00	800.	1.0	.293	.644	95.	4.07	*	267.6	504.4	57.5	COMB. EFF.
4.00	700.	1.0	.293	.462	94.	4.01	*	295.8	452.3	55.5	COMB. EFF.
4.00	600.	1.0	.293	.331	94.	4.01	*	394.4	418.2	45.0	COMB. EFF.
4.00	600.	1.0	.256	.331	103.	4.67	0	0	0	0	BLOWOFF
3.99	700.	1.0	.253	.460	104.	4.72	0	0	0	0	BLOWOFF
4.00	800.	1.0	.248	.644	107.	4.92	0	0	0	0	BLOWOFF
4.00	800.	1.0	.259	.644	105.	4.83	0	0	0	0	BLOWOFF
4.00	700.	1.0	.262	.462	104.	4.70	0	0	0	0	BLOWOFF
4.00	600.	1.0	.268	.331	101.	4.53	0	0	0	0	BLOWOFF

RUN NUMBER: 30 NOZZLE: 16-90 FUEL: JETA

DISC = 12.70 CM, TUBE DIA = 4.44 CM, TUBE LENGTH = 14.40 CM

COMBUSTOR HOUSING DIAMETER = 14.06 CM.

P	TIN	MDA	PHI	THETA	SMD	TEB	NOXEI	HCEI	COEI	ETA	COMMENT
ATM	K	KG/SEC			UM	MSEC	G/KG	G/KG	G/KG	PCT	
8.00	700.	1.0	.187	1.553	117.	4.85	0	0	0	0	BLOWOFF
8.00	600.	1.0	.201	1.113	113.	4.62	0	0	0	0	BLOWOFF
5.00	700.	1.0	.227	.682	105.	4.59	0	0	0	0	BLOWOFF
5.00	600.	1.0	.227	.489	106.	4.62	0	0	0	0	BLOWOFF
8.00	700.	1.0	.189	1.553	115.	4.75	0	0	0	0	BLOWOFF
8.00	600.	1.0	.201	1.113	113.	4.62	0	0	0	0	BLOWOFF
5.00	700.	1.0	.226	.682	106.	4.61	0	0	0	0	BLOWOFF
5.00	600.	1.0	.227	.489	106.	4.62	0	0	0	0	BLOWOFF

RUN NUMBER: 31 NOZZLE: 16-90 FUEL: JETA

DISC = 12.70 CM, TUBE DIA = 4.44 CM, TUBE LENGTH = 14.40 CM

COMBUSTOR HOUSING DIAMETER = 14.06 CM.

P	TIN	MDA	PHI	THETA	SMD	TEB	NOXEI	HCEI	COEI	ETA	COMMENT
ATM	K	KG/SEC			UM	MSEC	G/KG	G/KG	G/KG	PCT	
8.00	800.	1.0	.390	2.168	130.	5.75	1.23	45.7	140.1	91.5	COMB. EFF.
5.00	800.	1.0	.390	.952	129.	6.33	*	166.0	462.9	70.2	COMB. EFF.
4.00	800.	1.0	.390	.644	129.	6.68	*	319.2	446.3	53.0	COMB. EFF.
4.00	800.	1.0	.390	.644	129.	6.68	*	297.9	477.1	54.7	COMB. EFF.
5.00	800.	1.0	.390	.952	130.	6.47	*	208.5	448.9	65.6	COMB. EFF.
8.00	800.	1.0	.390	2.168	130.	5.75	.27	51.1	204.3	89.4	COMB. EFF.

RUN NUMBER: 34 NOZZLE: 16-90 FUEL: JETA

DISC = 12.70 CM, TUBE DIA = 4.44 CM, TUBE LENGTH = 14.45 CM

COMBUSTOR HOUSING DIAMETER = 14.06 CM.

P	TIN	MDA	PHI	THETA	SMD	TEB	NOXEI	HCEI	COEI	ETA	COMMENT
ATM	K	KG/SEC			UM	MSEC	G/KG	G/KG	G/KG	PCT	
8.00	800.	1.0	.293	2.168	95.	3.47	1.78	11.8	77.4	96.8	COMB. EFF.
5.00	800.	1.0	.293	.952	91.	3.64	*	169.0	486.9	69.3	COMB. EFF.
5.00	800.	1.0	.363	.952	81.	2.96	*	216.6	587.0	61.5	COMB. EFF.
5.00	800.	1.0	.235	.952	101.	4.31	*	59.5	297.0	86.2	COMB. EFF.
4.00	800.	1.0	.293	.644	96.	4.17	0	197.2	522.1	65.2	COMB. EFF.

RUN NUMBER: 35 NOZZLE: 16-90 FUEL: JETA

DISC = 12.70 CM, TUBE DIA = 4.44 CM, TUBE LENGTH = 8.10 CM

COMBUSTOR HOUSING DIAMETER = 14.06 CM.

P	TIN	MDA	PHI	THETA	SMD	TEB	NOXEI	HCEI	COEI	ETA	COMMENT
ATM	K	KG/SEC			UM	MSEC	G/KG	G/KG	G/KG	PCT	
8.00	800.	1.0	.293	2.168	98.	3.63	2.77	10.1	90.9	96.7	COMB. EFF.
5.00	800.	1.0	.293	.952	96.	3.92	*	169.0	513.2	68.6	COMB. EFF.
5.00	800.	1.0	.363	.952	81.	2.98	*	228.0	699.1	57.5	COMB. EFF.
4.00	800.	1.0	.293	.644	93.	3.94	*	253.5	670.9	55.3	COMB. EFF.

RUN NUMBER: 36 NOZZLE: 16-90 FUEL: JETA

DISC = 12.70 CM, TUBE DIA = 4.44 CM, TUBE LENGTH = 14.45 CM

COMBUSTOR HOUSING DIAMETER = 14.06 CM.

P	TIN	MDA	PHI	THETA	SMD	TEB	NOXEI	HCEI	COEI	ETA	COMMENT
ATM	K	KG/SEC			UM	MSEC	G/KG	G/KG	G/KG	PCT	
8.00	800.	1.0	.293	2.168	92.	3.33	1.68	12.7	90.9	96.4	COMB. EFF.
5.00	800.	1.0	.293	.952	91.	3.60	*	146.5	486.9	71.8	COMB. EFF.
5.00	800.	1.0	.235	.952	101.	4.31	*	125.9	207.6	80.7	COMB. EFF.
5.00	800.	1.0	.363	.952	80.	2.94	*	205.2	587.0	62.8	COMB. EFF.
5.00	800.	1.0	.216	.952	108.	4.79	0	0	0	0	BLOWOFF
4.00	800.	1.0	.293	.644	93.	3.94	*	239.4	660.2	57.1	COMB. EFF.
4.00	800.	1.0	.235	.644	100.	4.47	0	0	0	0	BLOWOFF
3.50	800.	1.0	.293	.511	92.	3.98	*	267.6	660.2	53.9	COMB. EFF.
3.00	800.	1.0	.290	.390	94.	4.23	0	0	0	0	BLOWOFF
2.36	800.	1.0	.325	.256	87.	3.91	0	0	0	0	BLOWOFF

RUN NUMBER: 37 NOZZLE: 16-90 FUEL: JETA

DISC = 12.70 CM, TUBE DIA = 4.44 CM, TUBE LENGTH = 8.10 CM

COMBUSTOR HOUSING DIAMETER = 14.06 CM.

P	TIN	MDA	PHI	THETA	SMD	TEB	NOXEI	HCEI	COEI	ETA	COMMENT
ATM	K	KG/SEC			UM	MSEC	G/KG	G/KG	G/KG	PCT	
8.00	800.	1.0	.293	2.168	90.	3.20	1.53	19.7	114.7	95.1	COMB. EFF.
8.00	800.	1.0	.184	2.168	115.	4.71	0	0	0	0	BLOWOFF
5.00	800.	1.0	.293	.952	90.	3.57	*	154.9	539.9	69.6	COMB. EFF.
5.00	800.	1.0	.235	.952	99.	4.13	*	122.4	457.0	75.3	COMB. EFF.
5.00	800.	1.0	.363	.952	77.	2.73	*	239.4	676.4	56.8	COMB. EFF.
5.00	800.	1.0	.216	.952	106.	4.62	0	0	0	0	BLOWOFF
4.00	800.	1.0	.293	.644	91.	3.79	0	245.1	603.6	57.8	COMB. EFF.
4.00	800.	1.0	.251	.644	95.	4.10	0	0	0	0	BLOWOFF
3.50	800.	1.0	.293	.511	89.	3.77	0	338.0	612.9	46.9	COMB. EFF.
3.00	800.	1.0	.293	.390	88.	3.84	0	0	0	0	BLOWOFF
2.36	800.	1.0	.376	.256	79.	3.36	0	0	0	0	BLOWOFF

RUN NUMBER: 38 NOZZLE: 16-90 FUEL: JETA

DISC = 12.70 CM, TUBE DIA = 4.44 CM, TUBE LENGTH = 8.10 CM

COMBUSTOR HOUSING DIAMETER = 14.06 CM.

P	TIN	MDA	PHI	THETA	SMD	TEB	NOXEI	HCEI	COEI	ETA	COMMENT
ATM	K	KG/SEC			UM	MSEC	G/KG	G/KG	G/KG	PCT	
8.00	800.	1.0	.293	2.168	89.	3.14	1.15	63.4	110.9	90.1	COMB. EFF.
8.00	800.	1.0	.149	2.168	129.	5.65	0	0	0	0	BLOWOFF
5.00	800.	1.0	.293	.952	89.	3.47	*	163.4	539.9	68.7	COMB. EFF.
5.00	800.	1.0	.235	.952	99.	4.13	0	125.9	457.0	74.9	COMB. EFF.
5.00	800.	1.0	.363	.952	77.	2.73	0	239.4	653.9	57.3	COMB. EFF.
5.00	800.	1.0	.218	.952	106.	4.64	0	0	0	0	BLOWOFF
4.00	800.	1.0	.293	.644	89.	3.65	0	267.6	576.0	55.9	COMB. EFF.
4.00	800.	1.0	.230	.644	101.	4.50	0	0	0	0	BLOWOFF
3.50	800.	1.0	.293	.511	89.	3.74	0	276.1	504.4	56.6	COMB. EFF.
3.00	800.	1.0	.277	.390	92.	4.12	0	0	0	0	BLOWOFF
2.36	800.	1.0	.315	.256	86.	3.87	0	0	0	0	BLOWOFF

RUN NUMBER: 39 NOZZLE: 16-90 FUEL: JETA

DISC = 10.80 CM, TUBE DIA = 4.44 CM, TUBE LENGTH = 14.45 CM

COMBUSTOR HOUSING DIAMETER = 14.06 CM.

P	TIN	MDA	PHI	THETA	SMD	TEB	NOXEI	HCEI	COEI	ETA	COMMENT
ATM	K	KG/SEC			UM	MSEC	G/KG	G/KG	G/KG	PCT	
8.00	800.	1.0	.293	2.168	90.	3.17	1.98	11.3	62.1	97.3	COMB. EFF.
8.00	800.	1.0	.097	2.168	147.	6.99	0	0	0	0	BLOWOFF
5.00	800.	1.0	.293	.952	90.	3.54	.40	57.7	278.5	86.9	COMB. EFF.
5.00	800.	1.0	.235	.952	99.	4.13	.74	26.2	99.2	94.7	COMB. EFF.
5.00	800.	1.0	.363	.952	77.	2.73	*	200.7	444.3	66.6	COMB. EFF.
5.00	800.	1.0	.133	.952	131.	6.56	0	0	0	0	BLOWOFF
4.00	800.	1.0	.141	.644	128.	6.61	0	0	0	0	BLOWOFF
3.00	800.	1.0	.156	.390	121.	6.48	0	0	0	0	BLOWOFF
2.36	800.	1.0	.181	.256	112.	6.03	0	0	0	0	BLOWOFF

RUN NUMBER: 40 NOZZLE: 16-90 FUEL: JETA

DISC = 10.80 CM, TUBE DIA = 4.44 CM, TUBE LENGTH = 14.45 CM

COMBUSTOR HOUSING DIAMETER = 14.06 CM.

P	TIN	MDA	PHI	THETA	SMD	TEB	NOXEI	HCEI	COEI	ETA	COMMENT
ATM	K	KG/SEC			UM	MSEC	G/KG	G/KG	G/KG	PCT	
5.00	800.	1.0	.293	2.168	89.	3.14	1.45	22.5	75.0	95.7	COMB. EFF.
5.00	800.	1.0	.235	.952	100.	4.18	1.20	22.7	102.5	95.0	COMB. EFF.
5.00	800.	1.0	.293	.952	90.	3.54	.39	70.4	270.5	85.6	COMB. EFF.
5.00	800.	1.0	.363	.952	77.	2.76	*	182.4	437.1	68.9	COMB. EFF.
4.00	800.	1.0	.293	.644	89.	3.68	*	140.8	302.5	76.8	COMB. EFF.
3.50	800.	1.0	.293	.511	90.	3.87	*	132.4	318.7	77.4	COMB. EFF.

RUN NUMBER: 41 NOZZLE: 16-90 FUEL: JETA

DISC = 10.80 CM, TUBE DIA = 4.44 CM, TUBE LENGTH = 14.45 CM

COMBUSTOR HOUSING DIAMETER = 14.06 CM.

P	TIN	MDA	PHI	THETA	SMD	TEB	NOXEI	HCEI	COEI	ETA	COMMENT
ATM	K	KG/SEC			UM	MSEC	G/KG	G/KG	G/KG	PCT	
8.00	800.	1.0	.293	2.168	89.	3.11	1.62	8.5	56.7	97.7	COMB. EFF.
5.00	800.	1.0	.235	.952	100.	4.24	1.38	15.7	68.3	96.6	COMB. EFF.
5.00	800.	1.0	.293	.952	89.	3.47	.51	59.2	131.4	90.1	COMB. EFF.
5.00	800.	1.0	.363	.952	77.	2.73	*	159.6	304.6	74.6	COMB. EFF.
4.00	800.	1.0	.293	.644	89.	3.68	*	91.5	254.7	83.6	COMB. EFF.
3.50	800.	1.0	.293	.511	89.	3.77	*	109.9	310.6	80.2	COMB. EFF.

RUN NUMBER: 42 NOZZLE: 16-90 FUEL: JETA

DISC = 11.73 CM, TUBE DIA = 3.51 CM, TUBE LENGTH = 14.45 CM

COMBUSTOR HOUSING DIAMETER = 14.06 CM.

P	TIN	MDA	PHI	THETA	SMD	TEB	NOXEI	HCEI	COEI	ETA	COMMENT
ATM	K	KG/SEC			UM	MSEC	G/KG	G/KG	G/KG	PCT	
8.00	800.	1.0	.293	2.168	90.	3.17	.29	67.6	167.2	88.3	COMB. EFF.
5.00	800.	1.0	.235	.952	100.	4.18	.96	45.5	93.1	92.6	COMB. EFF.
5.00	800.	1.0	.293	.952	90.	3.57	*	70.4	88.0	89.9	COMB. EFF.
5.00	800.	1.0	.363	.952	77.	2.73	*	114.0	86.9	84.9	COMB. EFF.
4.00	800.	1.0	.293	.644	89.	3.68	*	112.7	118.7	84.3	COMB. EFF.
3.50	800.	1.0	.293	.511	89.	3.76	*	87.3	90.9	87.9	COMB. EFF.

RUN NUMBER: 43 NOZZLE: 16-90 FUEL: JETA

DISC = 12.70 CM, TUBE DIA = 3.51 CM, TUBE LENGTH = 14.45 CM

COMBUSTOR HOUSING DIAMETER = 14.06 CM.

P	TIN	MDA	PHI	THETA	SMD	TEB	NOXEI	HCEI	COEI	ETA	COMMENT
ATM	K	KG/SEC			UM	MSEC	G/KG	G/KG	G/KG	PCT	
8.00	800.	1.0	.293	2.168	86.	2.98	1.66	8.7	30.4	98.3	COMB. EFF.
5.00	800.	1.0	.235	.952	97.	4.01	1.29	11.4	41.6	97.7	COMB. EFF.
5.00	800.	1.0	.293	.952	87.	3.35	1.14	35.2	72.6	94.3	COMB. EFF.
5.00	800.	1.0	.363	.952	76.	2.72	.34	66.1	102.8	90.0	COMB. EFF.
4.00	800.	1.0	.293	.644	87.	3.52	.31	80.3	136.0	87.6	COMB. EFF.
3.50	800.	1.0	.293	.511	86.	3.54	.31	84.5	127.0	87.3	COMB. EFF.

RUN NUMBER: 44 NOZZLE: 16-90 FUEL: JETA

DISC = 12.70 CM, TUBE DIA = 3.51 CM, TUBE LENGTH = 14.45 CM

COMBUSTOR HOUSING DIAMETER = 14.06 CM.

P	TIN	MDA	PHI	THETA	SMD	TEB	NOXEI	HCEI	COEI	ETA	COMMENT
ATM	K	KG/SEC			UM	MSEC	G/KG	G/KG	G/KG	PCT	
8.00	800.	1.0	.293	2.168	86.	2.98	1.96	28.2	110.9	94.2	COMB. EFF.
5.00	800.	1.0	.235	.952	95.	3.86	1.92	26.2	93.1	94.8	COMB. EFF.
5.00	800.	1.0	.293	.952	89.	3.50	.52	64.8	145.6	89.2	COMB. EFF.
5.00	800.	1.0	.363	.952	76.	2.72	*	127.7	193.6	80.8	COMB. EFF.
4.00	800.	1.0	.293	.644	88.	3.61	0	91.5	150.7	86.0	COMB. EFF.
3.50	800.	1.0	.293	.511	86.	3.54	0	81.7	114.7	88.0	COMB. EFF.

RUN NUMBER: 45 NOZZLE: 16-90 FUEL: JETA

DISC = 12.70 CM, TUBE DIA = 3.51 CM, TUBE LENGTH = 14.45 CM

COMBUSTOR HOUSING DIAMETER = 14.06 CM.

P	TIN	MDA	PHI	THETA	SMD	TEB	NOXEI	HCEI	COEI	ETA	COMMENT
ATM	K	KG/SEC			UM	MSEC	G/KG	G/KG	G/KG	PCT	
8.00	800.	1.0	.293	2.168	86.	2.96	1.56	24.8	88.0	95.1	COMB. EFF.
5.00	800.	1.0	.235	.952	96.	3.95	1.57	21.0	50.2	96.4	COMB. EFF.
5.00	800.	1.0	.293	.952	87.	3.38	.78	56.3	97.1	91.3	COMB. EFF.
5.00	800.	1.0	.363	.952	77.	2.73	*	93.5	135.3	86.1	COMB. EFF.

RUN NUMBER: 46 NOZZLE: 16-90 FUEL: JETA

DISC = 11.73 CM, TUBE DIA = 3.51 CM, TUBE LENGTH = 14.45 CM

COMBUSTOR HOUSING DIAMETER = 14.06 CM.

P	TIN	MDA	PHI	THETA	SMD	TEB	NOXEI	HCEI	COEI	ETA	COMMENT
ATM	K	KG/SEC			UM	MSEC	G/KG	G/KG	G/KG	PCT	
8.00	800.	1.0	.293	2.168	87.	3.01	*	54.9	150.7	90.2	COMB. EFF.
5.00	800.	1.0	.235	.952	97.	4.01	*	38.5	72.6	93.9	COMB. EFF.
5.00	800.	1.0	.293	.952	87.	3.38	*	81.7	114.7	88.0	COMB. EFF.
5.00	800.	1.0	.363	.952	77.	2.76	*	114.0	96.1	84.7	COMB. EFF.
4.00	800.	1.0	.293	.644	87.	3.52	*	62.0	64.1	91.4	COMB. EFF.
3.50	800.	1.0	.293	.511	88.	3.67	*	70.4	77.4	90.1	COMB. EFF.

RUN NUMBER: 47 NOZZLE: 16-90 FUEL: JETA

DISC = 11.73 CM, TUBE DIA = 3.51 CM, TUBE LENGTH = 14.45 CM

COMBUSTOR HOUSING DIAMETER = 14.06 CM.

P	TIN	MDA	PHI	THETA	SMD	TEB	NOXEI	HCEI	COEI	ETA	COMMENT
ATM	K	KG/SEC			UM	MSEC	G/KG	G/KG	G/KG	PCT	
8.00	800.	1.0	.293	2.168	88.	3.06	.49	35.2	75.0	94.2	COMB. EFF.
5.00	800.	1.0	.235	.952	97.	4.01	1.11	43.7	82.1	93.1	COMB. EFF.
5.00	800.	1.0	.293	.952	88.	3.44	*	87.3	107.3	87.5	COMB. EFF.
5.00	800.	1.0	.363	.952	78.	2.82	*	63.8	45.9	91.6	COMB. EFF.
4.00	800.	1.0	.293	.644	87.	3.55	*	77.5	94.0	88.9	COMB. EFF.
3.50	800.	1.0	.293	.511	87.	3.64	*	71.8	79.9	89.9	COMB. EFF.

RUN NUMBER: 48 NOZZLE: 16-90 FUEL: JETA

DISC = 11.73 CM, TUBE DIA = 3.51 CM, TUBE LENGTH = 4.45 CM

COMBUSTOR HOUSING DIAMETER = 14.06 CM.

P	TIN	MDA	PHI	THETA	SMD	TEB	NOXEI	HCEI	COEI	ETA	COMMENT
ATM	K	KG/SEC			UM	MSEC	G/KG	G/KG	G/KG	PCT	
3.38	800.	1.5	.108	.320	124.	6.50	0	0	0	0	BLOWOFF

RUN NUMBER: 49 NOZZLE: 16-90 FUEL: JETA

DISC = 11.73 CM, TUBE DIA = 3.51 CM, TUBE LENGTH = 4.45 CM

COMBUSTOR HOUSING DIAMETER = 14.06 CM.

P	TIN	MDA	PHI	THETA	SMD	TEB	NOXEI	HCEI	COEI	ETA	COMMENT
ATM	K	KG/SEC			UM	MSEC	G/KG	G/KG	G/KG	PCT	
3.00	800.	1.5	.141	.260	108.	5.35	0	0	0	0	BLOWOFF
7.99	800.	1.5	.097	1.443	129.	5.70	0	0	0	0	BLOWOFF
5.00	800.	1.5	.115	.635	119.	5.61	0	0	0	0	BLOWOFF
4.00	800.	1.5	.116	.430	122.	6.10	0	0	0	0	BLOWOFF
3.00	800.	1.5	.130	.260	112.	5.65	0	0	0	0	BLOWOFF
8.00	800.	1.5	.094	1.445	136.	6.18	0	0	0	0	BLOWOFF
5.00	800.	1.5	.100	.635	123.	5.90	0	0	0	0	BLOWOFF
4.00	800.	1.5	.106	.430	125.	6.35	0	0	0	0	BLOWOFF

RUN NUMBER: 50 NOZZLE: 16-90 FUEL: JETA

DISC = 12.70 CM, TUBE DIA = 3.51 CM, TUBE LENGTH = 4.45 CM

COMBUSTOR HOUSING DIAMETER = 14.06 CM.

P	TIN	MDA	PHI	THETA	SMD	TEB	NOXEI	HCEI	COEI	ETA	COMMENT
ATM	K	KG/SEC			UM	MSEC	G/KG	G/KG	G/KG	PCT	
5.00	800.	1.5	.151	.635	104.	4.46	0	0	0	0	BLOWOFF
8.00	800.	1.5	.121	1.445	117.	4.85	0	0	0	0	BLOWOFF
4.00	800.	1.5	.211	.430	87.	3.52	0	0	0	0	BLOWOFF
3.00	800.	1.0	.153	.390	124.	6.75	0	0	0	0	BLOWOFF
2.36	800.	1.0	.236	.256	98.	4.82	0	0	0	0	BLOWOFF

RUN NUMBER: 51 NOZZLE: 16-90 FUEL: JETA

DISC = 12.70 CM, TUBE DIA = 3.51 CM, TUBE LENGTH = 4.45 CM

COMBUSTOR HOUSING DIAMETER = 14.06 CM.

P	TIN	MDA	PHI	THETA	SMD	TEB	NOXEI	HCEI	COEI	ETA	COMMENT
ATM	K	KG/SEC			UM	MSEC	G/KG	G/KG	G/KG	PCT	
8.00	800.	1.5	.120	1.445	116.	4.79	0	0	0	0	BLOWOFF
2.36	800.	1.0	.205	.256	109.	5.71	0	0	0	0	BLOWOFF
4.00	800.	1.5	.163	.430	100.	4.39	0	0	0	0	BLOWOFF

RUN NUMBER: 52 NOZZLE: 16-90 FUEL: JETA

DISC = 10.80 CM, TUBE DIA = 4.44 CM, TUBE LENGTH = 14.45 CM

COMBUSTOR HOUSING DIAMETER = 14.06 CM.

P	TIN	MDA	PHI	THETA	SMD	TEB	NOXEI	HCEI	COEI	ETA	COMMENT
ATM	K	KG/SEC			UM	MSEC	G/KG	G/KG	G/KG	PCT	
8.00	800.	1.0	.293	2.168	87.	3.01	1.28	16.3	75.0	96.4	COMB. EFF.
5.00	800.	1.0	.235	.952	96.	3.96	1.22	22.7	77.2	95.6	COMB. EFF.
5.00	800.	1.0	.293	.952	87.	3.38	.30	70.4	167.2	88.0	COMB. EFF.
4.00	800.	1.0	.293	.644	87.	3.52	*	98.6	173.0	84.7	COMB. EFF.
3.50	800.	1.0	.293	.511	88.	3.67	*	126.8	185.4	81.1	COMB. EFF.

RUN NUMBER: 53 NOZZLE: 16-90 FUEL: JETA

DISC = 10.80 CM, TUBE DIA = 4.44 CM, TUBE LENGTH = 14.45 CM

COMBUSTOR HOUSING DIAMETER = 14.06 CM.

P	TIN	MDA	PHI	THETA	SMD	TEB	NOXEI	HCEI	COEI	ETA	COMMENT
ATM	K	KG/SEC			UM	MSEC	G/KG	G/KG	G/KG	PCT	
5.00	800.	1.0	.235	.952	97.	4.01	.51	29.7	90.2	94.5	COMB. EFF.
5.00	800.	1.0	.293	.952	88.	3.41	0	62.0	161.5	89.1	COMB. EFF.
5.00	800.	1.0	.363	.952	77.	2.78	*	141.4	318.1	76.4	COMB. EFF.
8.00	800.	1.0	.293	2.168	88.	3.06	*	33.8	68.2	94.5	COMB. EFF.
4.00	800.	1.0	.293	.644	87.	3.54	*	112.7	192.0	82.6	COMB. EFF.
3.50	800.	1.0	.293	.511	88.	3.70	*	115.5	179.1	82.6	COMB. EFF.

AD-A053 635 PURDUE UNIV LAFAYETTE IND COMBUSTION LAB F/G 20/2
FLAME EFFICIENCY, STABILIZATION AND PERFORMANCE IN PREVAPORIZIN--ETC(U)
DEC 77 S L PLEE, D A SCHMIDT, A M MELLOR AFOSR-76-2936
UNCLASSIFIED PURDU-CL-77-07 AFOSR-TR-78-0736 NL

3 OF 3
ADA
053635

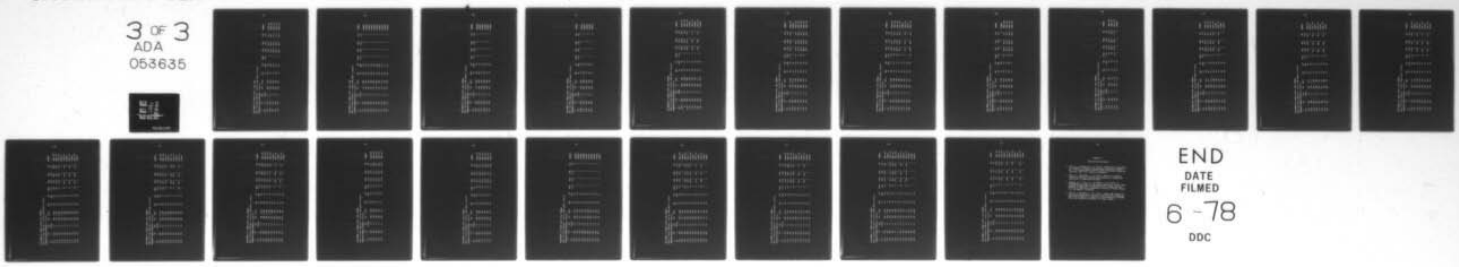

END
DATE
FILMED
6-78
DDC

RUN NUMBER: 54 NOZZLE: 16-90 FUEL: JETA

DISC = 12.70 CM, TUBE DIA = 4.44 CM, TUBE LENGTH = 14.45 CM

COMBUSTOR HOUSING DIAMETER = 14.06 CM.

P	TIN	MDA	PHI	THETA	SMD	TEB	NOXEI	HCEI	COEI	ETA	COMMENT
ATM	K	KG/SEC			UM	MSEC	G/KG	G/KG	G/KG	PCT	
5.00	800.	1.0	.293	.952	87.	3.35	0	98.6	310.6	81.4	COMB. EFF.
4.00	800.	1.0	.293	.644	87.	3.52	0	191.5	367.9	69.4	COMB. EFF.
5.00	800.	1.0	.363	.952	77.	2.78	0	159.6	422.6	71.8	COMB. EFF.
5.00	800.	1.0	.293	.952	88.	3.41	0	197.2	302.5	70.3	COMB. EFF.
3.50	800.	1.0	.293	.511	87.	3.61	0	267.6	384.6	60.3	COMB. EFF.

RUN NUMBER: 79 NOZZLE: 16-90 FUEL: JETA

DISC = 10.80 CM, TUBE DIA = 4.44 CM, TUBE LENGTH = 14.45 CM

COMBUSTOR HOUSING DIAMETER = 14.06 CM.

P	TIN	MDA	PHI	THETA	SMD	TEB	NOXEI	HCEI	COEI	ETA	COMMENT
ATM	K	KG/SEC			UM	MSEC	G/KG	G/KG	G/KG	PCT	
8.00	800.	1.0	.111	2.168	155.	7.64	0	0	0	0	BLOWOFF
5.00	800.	1.0	.135	.952	145.	7.64	0	0	0	0	BLOWOFF
4.00	800.	1.0	.138	.644	140.	7.70	0	0	0	0	BLOWOFF
3.00	800.	1.0	.157	.390	133.	7.50	0	0	0	0	BLOWOFF
2.36	800.	1.0	.178	.256	125.	7.20	0	0	0	0	BLOWOFF
8.00	800.	1.0	.102	2.168	161.	8.06	0	0	0	0	BLOWOFF
5.00	800.	1.0	.122	.952	153.	8.36	0	0	0	0	BLOWOFF
4.00	800.	1.0	.143	.644	141.	7.78	0	0	0	0	BLOWOFF
3.00	800.	1.0	.164	.390	130.	7.31	0	0	0	0	BLOWOFF
2.36	800.	1.0	.191	.256	120.	6.74	0	0	0	0	BLOWOFF

RUN NUMBER: 55 NOZZLE: 35-90 FUEL: PROPANE

DISC = 12.70 CM, TUBE DIA = 4.44 CM, TUBE LENGTH = 14.45 CM

COMBUSTOR HOUSING DIAMETER = 14.06 CM.

P	TIN	MDA	PHI	THETA	SMD	TEB	NOXEI	HCEI	COEI	ETA	COMMENT
ATM	K	KG/SEC			UM	MSEC	G/KG	G/KG	G/KG	PCT	
8.00	800.	1.0	.174	2.168	58.	.76	0	0	0	0	BLOWOFF
5.00	800.	1.0	.192	.952	52.	.72	0	0	0	0	BLOWOFF
4.00	800.	1.0	.205	.644	53.	.80	0	0	0	0	BLOWOFF
3.00	800.	1.0	.249	.390	52.	.83	0	0	0	0	BLOWOFF
2.36	800.	1.0	.249	.256	50.	.82	0	0	0	0	BLOWOFF
3.00	800.	1.0	.231	.390	51.	.80	0	0	0	0	BLOWOFF

RUN NUMBER: 56 NOZZLE: 35-90 FUEL: PROPANE

DISC = 12.70 CM, TUBE DIA = 4.44 CM, TUBE LENGTH = 14.45 CM

COMBUSTOR HOUSING DIAMETER = 14.06 CM.

P	TIN	MDA	PHI	THETA	SMD	TEB	NOXEI	HCEI	COEI	ETA	COMMENT
ATM	K	KG/SEC			UM	MSEC	G/KG	G/KG	G/KG	PCT	
2.36	800.	1.0	.276	.256	53.	.92	0	0	0	0	BLOWOFF
5.00	800.	1.0	.200	.952	56.	.82	0	0	0	0	BLOWOFF
4.00	800.	1.0	.218	.644	54.	.83	0	0	0	0	BLOWOFF
3.00	800.	1.0	.254	.390	53.	.86	0	0	0	0	BLOWOFF
2.36	800.	1.0	.263	.256	51.	.87	0	0	0	0	BLOWOFF

RUN NUMBER: 57 NOZZLE: 35-90 FUEL: PROPANE

DISC = 12.70 CM, TUBE DIA = 4.44 CM, TUBE LENGTH = 14.45 CM

COMBUSTOR HOUSING DIAMETER = 14.06 CM.

P	TIN	MDA	PHI	THETA	SMD	TEB	NOXEI	HCEI	COEI	ETA	COMMENT
ATM	K	KG/SEC			UM	MSEC	G/KG	G/KG	G/KG	PCT	
5.00	800.	1.0	.294	.952	55.	.80	0	359.8	382.8	52.8	COMB. EFF.
5.00	800.	1.0	.236	.952	55.	.81	0	186.1	275.2	73.9	COMB. EFF.
5.00	800.	1.0	.365	.952	51.	.71	0	605.8	426.4	25.4	COMB. EFF.
5.00	800.	1.0	.192	.952	54.	.77	0	0	0	0	BLOWOFF
4.00	800.	1.0	.294	.644	53.	.81	0	464.8	343.5	42.4	COMB. EFF.
4.00	800.	1.0	.205	.644	52.	.78	0	0	0	0	BLOWOFF
3.50	800.	1.0	.294	.511	52.	.81	0	539.7	339.2	34.4	COMB. EFF.
3.00	800.	1.0	.222	.390	51.	.80	0	0	0	0	BLOWOFF

RUN NUMBER: 62 NOZZLE: 35-90 FUEL: PROPANE

DISC = 12.70 CM, TUBE DIA = 4.44 CM, TUBE LENGTH = 14.45 CM

COMBUSTOR HOUSING DIAMETER = 14.06 CM.

P	TIN	MDA	PHI	THETA	SMD	TEB	NOXEI	HCEI	COEI	ETA	COMMENT
ATM	K	KG/SEC			UM	MSEC	G/KG	G/KG	G/KG	PCT	
8.00	800.	1.0	.294	2.168	64.	.88	1.62	101.9	254.5	83.4	COMB. EFF.
8.00	800.	1.0	.165	2.168	61.	.84	0	0	0	0	BLOWOFF
5.00	800.	1.0	.236	.952	55.	.80	1.00	174.9	347.0	73.5	COMB. EFF.
5.00	800.	1.0	.294	.952	57.	.85	.71	314.8	463.3	55.9	COMB. EFF.
5.00	800.	1.0	.365	.952	56.	.84	.49	484.7	456.8	37.8	COMB. EFF.
4.00	800.	1.0	.294	.644	56.	.87	.40	389.8	427.2	48.6	COMB. EFF.
3.50	800.	1.0	.294	.511	54.	.85	*	479.7	463.3	38.2	COMB. EFF.

RUN NUMBER: 63 NOZZLE: 35-90 FUEL: PROPANE

DISC = 12.70 CM, TUBE DIA = 4.44 CM, TUBE LENGTH = 14.45 CM

COMBUSTOR HOUSING DIAMETER = 14.06 CM.

P	TIN	MDA	PHI	THETA	SMD	TEB	NOXEI	HCEI	COEI	ETA	COMMENT
ATM	K	KG/SEC			UM	MSEC	G/KG	G/KG	G/KG	PCT	
8.00	800.	1.0	.294	2.168	58.	.76	1.32	149.9	271.1	77.9	COMB. EFF.
5.00	800.	1.0	.236	.952	54.	.78	.96	186.1	213.4	75.3	COMB. EFF.
5.00	800.	1.0	.294	.952	54.	.79	.88	269.9	339.2	63.5	COMB. EFF.
5.00	800.	1.0	.365	.952	51.	.71	.53	581.6	426.4	28.0	COMB. EFF.
5.00	800.	1.0	.183	.952	54.	.78	0	0	0	0	BLOWOFF
4.00	800.	1.0	.294	.644	52.	.79	.77	374.8	347.9	52.0	COMB. EFF.
4.00	800.	1.0	.209	.644	51.	.76	0	0	0	0	BLOWOFF
3.50	800.	1.0	.294	.511	52.	.80	.66	389.8	322.0	50.9	COMB. EFF.

RUN NUMBER: 64 NOZZLE: 35-90 FUEL: PROPANE

DISC = 12.70 CM, TUBE DIA = 4.44 CM, TUBE LENGTH = 14.45 CM

COMBUSTOR HOUSING DIAMETER = 14.06 CM.

P	TIN	MDA	PHI	THETA	SMD	TEB	NOXEI	HCEI	COEI	ETA	COMMENT
ATM	K	KG/SEC			UM	MSEC	G/KG	G/KG	G/KG	PCT	
2.36	800.	1.0	.267	.256	52.	.88	0	0	0	0	BLOWOFF
8.00	800.	1.0	.294	2.168	58.	.76	1.09	185.9	391.6	71.4	COMB. EFF.
5.00	800.	1.0	.236	.952	54.	.78	.54	167.5	173.6	78.1	COMB. EFF.
5.00	800.	1.0	.294	.952	55.	.80	.76	260.9	382.8	63.5	COMB. EFF.
5.00	800.	1.0	.365	.952	51.	.71	.61	545.3	503.4	30.2	COMB. EFF.

RUN NUMBER: 65 NOZZLE: 35-90 FUEL: PROPANE

DISC = 12.70 CM, TUBE DIA = 4.44 CM, TUBE LENGTH = 14.45 CM

COMBUSTOR HOUSING DIAMETER = 14.06 CM.

P	TIN	MDA	PHI	THETA	SMD	TEB	NOXEI	HCEI	COEI	ETA	COMMENT
ATM	K	KG/SEC			UM	MSEC	G/KG	G/KG	G/KG	PCT	
4.00	800.	1.0	.365	.644	51.	.76	.35	605.8	434.0	25.2	COMB. EFF.
3.50	800.	1.0	.365	.511	51.	.78	.35	618.0	374.4	25.2	COMB. EFF.
8.00	600.	1.0	.294	1.113	60.	.81	1.19	167.9	246.2	76.5	COMB. EFF.
8.00	600.	1.0	.183	1.113	64.	.90	0	0	0	0	BLOWOFF

RUN NUMBER: 66 NOZZLE: 35-90 FUEL: PROPANE

DISC = 12.70 CM, TUBE DIA = 4.44 CM, TUBE LENGTH = 14.45 CM

COMBUSTOR HOUSING DIAMETER = 14.06 CM.

P	TIN	MDA	PHI	THETA	SMD	TEB	NOXEI	HCEI	COEI	ETA	COMMENT
ATM	K	KG/SEC			UM	MSEC	G/KG	G/KG	G/KG	PCT	
4.00	800.	1.0	.365	.644	52.	.77	.26	605.8	464.5	24.5	COMB. EFF.
3.50	800.	1.0	.365	.511	52.	.79	.18	727.0	411.4	12.7	COMB. EFF.
8.00	600.	1.0	.294	1.113	61.	.82	1.11	239.9	356.6	66.3	COMB. EFF.
5.00	600.	1.0	.294	.489	58.	.86	.72	359.8	347.9	53.6	COMB. EFF.
5.00	600.	1.0	.214	.489	56.	.83	0	0	0	0	BLOWOFF
4.00	600.	1.0	.294	.331	54.	.83	.33	629.7	356.6	24.3	COMB. EFF.
4.00	600.	1.0	.236	.331	54.	.84	0	0	0	0	BLOWOFF
2.36	600.	1.0	.312	.131	53.	.93	0	0	0	0	BLOWOFF

RUN NUMBER: 67 NOZZLE: 35-90 FUEL: PROPANE

DISC = 12.70 CM, TUBE DIA = 4.44 CM, TUBE LENGTH = 14.45 CM

COMBUSTOR HOUSING DIAMETER = 14.06 CM.

P	TIN	MDA	PHI	THETA	SMD	TEB	NOXEI	HCEI	COEI	ETA	COMMENT
ATM	K	KG/SEC			UM	MSEC	G/KG	G/KG	G/KG	PCT	
8.00	600.	1.0	.294	1.113	60.	.81	1.16	119.9	155.0	83.7	COMB. EFF.
8.00	600.	1.0	.187	1.113	61.	.82	0	0	0	0	BLOWOFF
5.00	600.	1.0	.294	.489	53.	.75	.68	479.7	427.2	38.9	COMB. EFF.
5.00	600.	1.0	.222	.489	54.	.78	0	0	0	0	BLOWOFF
4.00	600.	1.0	.294	.331	53.	.80	.47	554.7	356.6	32.4	COMB. EFF.
4.00	600.	1.0	.231	.331	53.	.81	0	0	0	0	BLOWOFF
3.50	600.	1.0	.294	.262	53.	.84	.49	539.7	322.0	34.8	COMB. EFF.
2.36	600.	1.0	.289	.131	51.	.88	0	0	0	0	BLOWOFF

RUN NUMBER: 68 NOZZLE: 35-90 FUEL: PROPANE

DISC = 12.70 CM, TUBE DIA = 4.44 CM, TUBE LENGTH = 14.45 CM

COMBUSTOR HOUSING DIAMETER = 14.06 CM.

P	TIN	MDA	PHI	THETA	SMD	TEB	NOXEI	HCEI	COEI	ETA	COMMENT
ATM	K	KG/SEC			UM	MSEC	G/KG	G/KG	G/KG	PCT	
8.00	600.	1.0	.294	1.113	63.	.86	1.39	95.9	130.7	86.8	COMB. EFF.
8.00	600.	1.0	.183	1.113	62.	.86	0	0	0	0	BLOWOFF
5.00	600.	1.0	.294	.489	56.	.83	.79	344.8	313.4	56.0	COMB. EFF.
5.00	600.	1.0	.209	.489	55.	.80	0	0	0	0	BLOWOFF
4.00	600.	1.0	.294	.331	54.	.84	.45	524.7	418.3	34.3	COMB. EFF.
4.00	600.	1.0	.222	.331	53.	.79	0	0	0	0	BLOWOFF
3.50	600.	1.0	.294	.262	53.	.84	.37	539.7	322.0	34.8	COMB. EFF.
2.36	600.	1.0	.298	.131	50.	.85	0	0	0	0	BLOWOFF

RUN NUMBER: 69 NOZZLE: 35-90 FUEL: PROPANE

DISC = 12.70 CM, TUBE DIA = 4.44 CM, TUBE LENGTH = 14.45 CM

COMBUSTOR HOUSING DIAMETER = 14.06 CM.

P	TIN	MDA	PHI	THETA	SMD	TEB	NOXEI	HCEI	COEI	ETA	COMMENT
ATM	K	KG/SEC			UM	MSEC	G/KG	G/KG	G/KG	PCT	
8.00	800.	1.0	.236	2.168	63.	.87	1.45	37.2	109.0	93.6	COMB. EFF.
8.00	800.	1.0	.196	2.168	61.	.84	1.43	22.3	84.4	95.7	COMB. EFF.
8.00	700.	1.0	.294	1.553	62.	.84	.91	113.9	166.1	84.1	COMB. EFF.
8.00	700.	1.0	.169	1.553	59.	.78	0	0	0	0	BLOWOFF
5.00	700.	1.0	.294	.682	55.	.80	.69	314.8	339.2	58.6	COMB. EFF.
5.00	700.	1.0	.187	.682	53.	.75	0	0	0	0	BLOWOFF
4.00	700.	1.0	.294	.462	53.	.80	.64	449.8	347.9	43.9	COMB. EFF.
4.00	700.	1.0	.200	.462	51.	.75	0	0	0	0	BLOWOFF
3.50	700.	1.0	.294	.366	52.	.81	.53	464.8	287.9	43.6	COMB. EFF.
2.36	700.	1.0	.267	.183	50.	.84	0	0	0	0	BLOWOFF

RUN NUMBER: 70 NOZZLE: 35-90 FUEL: PROPANE

DISC = 12.70 CM, TUBE DIA = 4.44 CM, TUBE LENGTH = 14.45 CM

COMBUSTOR HOUSING DIAMETER = 14.06 CM.

P	TIN	MDA	PHI	THETA	SMD	TEB	NOXEI	HCEI	COEI	ETA	COMMENT
ATM	K	KG/SEC			UM	MSEC	G/KG	G/KG	G/KG	PCT	
8.00	800.	1.0	.236	2.168	60.	.80	1.89	26.1	93.0	95.2	COMB. EFF.
8.00	800.	1.0	.196	2.168	58.	.77	1.92	107.1	49.3	87.4	COMB. EFF.
8.00	700.	1.0	.294	1.553	60.	.81	1.32	69.0	118.1	90.0	COMB. EFF.
8.00	700.	1.0	.168	1.553	56.	.73	0	0	0	0	BLOWOFF
5.00	700.	1.0	.294	.682	52.	.73	.99	434.8	427.2	43.8	COMB. EFF.
4.00	700.	1.0	.294	.462	50.	.74	.74	524.7	454.2	33.5	COMB. EFF.
4.00	700.	1.0	.192	.462	49.	.71	0	0	0	0	BLOWOFF
3.50	700.	1.0	.294	.366	49.	.74	2.85	524.7	427.2	34.1	COMB. EFF.
2.36	700.	1.0	.240	.183	48.	.79	0	0	0	0	BLOWOFF

RUN NUMBER: 71 NOZZLE: 35-90 FUEL: PROPANE

DISC = 12.70 CM, TUBE DIA = 4.44 CM, TUBE LENGTH = 14.45 CM

COMBUSTOR HOUSING DIAMETER = 14.06 CM.

P	TIN	MDA	PHI	THETA	SMD	TEB	NOXEI	HCEI	COEI	ETA	COMMENT
ATM	K	KG/SEC			UM	MSEC	G/KG	G/KG	G/KG	PCT	
8.00	800.	1.0	.196	2.168	60.	.81	1.73	21.0	68.2	96.2	COMB. EFF.
8.00	800.	1.0	.236	2.168	59.	.78	1.58	35.4	109.0	93.8	COMB. EFF.
8.00	800.	1.0	.196	2.168	58.	.77	1.90	20.5	77.1	96.1	COMB. EFF.
8.00	700.	1.0	.294	1.553	61.	.84	1.36	116.9	171.9	83.6	COMB. EFF.
8.00	700.	1.0	.178	1.553	58.	.77	0	0	0	0	BLOWOFF
4.00	700.	1.0	.294	.462	51.	.75	.73	539.7	454.2	31.9	COMB. EFF.
4.00	700.	1.0	.196	.462	50.	.72	0	0	0	0	BLOWOFF
3.50	700.	1.0	.294	.366	51.	.79	.55	464.8	374.0	41.7	COMB. EFF.
2.36	700.	1.0	.245	.183	49.	.80	0	0	0	0	BLOWOFF

RUN NUMBER: 72 NOZZLE: 35-90 FUEL: PROAPNE

DISC = 11.73 CM, TUBE DIA = 3.51 CM, TUBE LENGTH = 14.45 CM

COMBUSTOR HOUSING DIAMETER = 14.06 CM.

P	TIN	MDA	PHI	THETA	SMD	TEB	NOXEI	HCEI	COEI	ETA	COMMENT
ATM	K	KG/SEC			UM	MSEC	G/KG	G/KG	G/KG	PCT	
8.00	800.	1.0	.294	2.168	58.	.76	1.27	69.0	55.0	91.4	COMB. EFF.
5.00	800.	1.0	.236	.952	52.	.73	1.43	81.9	70.4	89.6	COMB. EFF.
5.00	800.	1.0	.365	.952	50.	.69	.84	218.1	66.6	75.0	COMB. EFF.
4.00	800.	1.0	.294	.644	51.	.76	.81	113.9	60.3	86.4	COMB. EFF.
3.50	800.	1.0	.294	.511	51.	.78	.62	131.9	68.2	84.3	COMB. EFF.

RUN NUMBER: 73 NOZZLE: 35-90 FUEL: PROPANE

DISC = 11.73 CM, TUBE DIA = 3.51 CM, TUBE LENGTH = 14.45 CM

COMBUSTOR HOUSING DIAMETER = 14.06 CM.

P	TIN	MDA	PHI	THETA	SMD	TEB	NOXEI	HCEI	COEI	ETA	COMMENT
ATM	K	KG/SEC			UM	MSEC	G/KG	G/KG	G/KG	PCT	
8.00	800.	1.0	.294	2.168	63.	.86	.98	94.4	50.2	88.7	COMB. EFF.
5.00	800.	1.0	.236	.952	56.	.82	1.22	68.9	56.8	91.3	COMB. EFF.
5.00	800.	1.0	.294	.952	56.	.83	.98	106.4	62.2	87.2	COMB. EFF.
5.00	800.	1.0	.365	.952	55.	.81	.85	140.6	56.9	83.6	COMB. EFF.
4.00	800.	1.0	.294	.644	54.	.82	.73	134.9	70.4	83.9	COMB. EFF.
3.50	800.	1.0	.294	.511	52.	.79	.71	146.9	56.7	82.9	COMB. EFF.

RUN NUMBER: 74 NOZZLE: 35-90 FUEL: PROAPNE

DISC = 11.73 CM, TUBE DIA = 3.51 CM, TUBE LENGTH = 14.45 CM

COMBUSTOR HOUSING DIAMETER = 14.06 CM.

P	TIN	MDA	PHI	THETA	SMD	TEB	NOXEI	HCEI	COEI	ETA	COMMENT
ATM	K	KG/SEC			UM	MSEC	G/KG	G/KG	G/KG	PCT	
8.00	800.	1.5	.089	1.445	60.	.81	0	0	0	0	BLOWOFF
5.00	800.	1.5	.098	.635	53.	.76	0	0	0	0	BLOWOFF
4.00	800.	1.5	.104	.430	51.	.74	0	0	0	0	BLOWOFF
3.00	800.	1.5	.116	.260	50.	.80	0	0	0	0	BLOWOFF
2.70	800.	1.5	.130	.216	50.	.81	0	0	0	0	BLOWOFF
8.00	800.	1.5	.089	1.445	59.	.78	0	0	0	0	BLOWOFF
5.00	800.	1.5	.098	.635	52.	.72	0	0	0	0	BLOWOFF
4.00	800.	1.5	.101	.430	50.	.73	0	0	0	0	BLOWOFF
3.00	800.	1.5	.108	.260	50.	.78	0	0	0	0	BLOWOFF
2.70	800.	1.5	.116	.216	50.	.81	0	0	0	0	BLOWOFF

RUN NUMBER: 75 NOZZLE: 35-90 FUEL: PROPANE

DISC = 11.73 CM, TUBE DIA = 3.51 CM, TUBE LENGTH = 14.45 CM

COMBUSTOR HOUSING DIAMETER = 14.06 CM.

P	TIN	MDA	PHI	THETA	SMD	TEB	NOXEI	HCEI	COEI	ETA	COMMENT
ATM	K	KG/SEC			UM	MSEC	G/KG	G/KG	G/KG	PCT	
8.00	800.	1.0	.294	2.168	61.	.82	.98	87.0	53.4	89.5	COMB. EFF.
8.00	800.	1.5	.077	1.445	54.	.67	0	0	0	0	BLOWOFF
5.00	800.	1.0	.236	.952	54.	.78	1.09	68.9	53.4	91.4	COMB. EFF.
5.00	800.	1.0	.294	.952	55.	.80	.78	95.9	51.8	88.5	COMB. EFF.
5.00	800.	1.0	.365	.952	51.	.72	.63	230.2	64.5	73.8	COMB. EFF.
5.00	800.	1.5	.092	.635	51.	.71	0	0	0	0	BLOWOFF
4.00	800.	1.0	.294	.644	54.	.82	.74	107.9	56.7	87.1	COMB. EFF.
4.00	800.	1.5	.098	.430	50.	.72	0	0	0	0	BLOWOFF
3.50	800.	1.0	.294	.511	52.	.81	.68	125.9	60.3	85.1	COMB. EFF.
3.00	800.	1.5	.101	.260	49.	.75	0	0	0	0	BLOWOFF
2.70	800.	1.5	.104	.216	49.	.77	0	0	0	0	BLOWOFF

RUN NUMBER: 76 NOZZLE: 35-90 FUEL: PROPANE

DISC = 10.80 CM, TUBE DIA = 4.44 CM, TUBE LENGTH = 14.45 CM

COMBUSTOR HOUSING DIAMETER = 14.06 CM.

P	TIN	MDA	PHI	THETA	SMD	TEB	NOXEI	HCEI	COEI	ETA	COMMENT
ATM	K	KG/SEC			UM	MSEC	G/KG	G/KG	G/KG	PCT	
8.00	800.	1.0	.294	2.168	63.	.88	1.01	116.9	139.9	84.3	COMB. EFF.
5.00	800.	1.0	.236	.952	57.	.84	1.00	81.9	102.2	88.9	COMB. EFF.
5.00	800.	1.0	.294	.952	57.	.86	.77	158.9	114.2	80.4	COMB. EFF.
5.00	800.	1.0	.365	.952	52.	.74	.62	302.9	148.9	64.1	COMB. EFF.
5.00	800.	1.0	.099	.952	50.	.69	0	0	0	0	BLOWOFF
4.00	800.	1.0	.294	.644	55.	.86	.40	215.9	155.0	73.3	COMB. EFF.
4.00	800.	1.0	.121	.644	50.	.72	0	0	0	0	BLOWOFF
3.50	800.	1.0	.294	.511	54.	.85	.61	260.9	160.4	68.4	COMB. EFF.
3.00	800.	1.0	.132	.390	48.	.74	0	0	0	0	BLOWOFF
2.36	800.	1.0	.183	.256	50.	.84	0	0	0	0	BLOWOFF

RUN NUMBER: 77 NOZZLE: 35-90 FUEL: PROPANE

DISC = 10.80 CM, TUBE DIA = 4.44 CM, TUBE LENGTH = 14.45 CM

COMBUSTOR HOUSING DIAMETER = 14.06 CM.

P	TIN	MDA	PHI	THETA	SMD	TEB	NOXEI	HCEI	COEI	ETA	COMMENT
ATM	K	KG/SEC			UM	MSEC	G/KG	G/KG	G/KG	PCT	
8.00	800.	1.0	.294	2.168	61.	.82	.80	110.9	135.2	85.1	COMB. EFF.
8.00	800.	1.0	.089	2.168	54.	.68	0	0	0	0	BLOWOFF
5.00	800.	1.0	.236	.952	55.	.79	.82	83.7	93.0	88.9	COMB. EFF.
5.00	800.	1.0	.294	.952	55.	.80	.76	140.9	122.1	82.1	COMB. EFF.
5.00	800.	1.0	.365	.952	51.	.71	.53	315.0	148.9	62.8	COMB. EFF.
5.00	800.	1.0	.097	.952	48.	.65	0	0	0	0	BLOWOFF
4.00	800.	1.0	.294	.644	54.	.82	.46	254.9	160.4	69.0	COMB. EFF.
4.00	800.	1.0	.124	.644	49.	.70	0	0	0	0	BLOWOFF
3.50	800.	1.0	.294	.511	53.	.82	.50	275.9	177.9	66.4	COMB. EFF.
3.00	800.	1.0	.156	.390	49.	.75	0	0	0	0	BLOWOFF
2.36	800.	1.0	.183	.256	49.	.81	0	0	0	0	BLOWOFF
8.00	800.	1.0	.094	2.168	54.	.68	0	0	0	0	BLOWOFF

RUN NUMBER: 78 NOZZLE: 35-90 FUEL: PROPANE

DISC = 10.80 CM, TUBE DIA = 4.44 CM, TUBE LENGTH = 14.45 CM

COMBUSTOR HOUSING DIAMETER = 14.06 CM.

P	TIN	MDA	PHI	THETA	SMD	TEB	NOXEI	HCEI	COEI	ETA	COMMENT
ATM	K	KG/SEC			UM	MSEC	G/KG	G/KG	G/KG	PCT	
5.00	800.	1.0	.236	.952	58.	.87	.54	76.3	90.1	89.8	COMB. EFF.
5.00	800.	1.0	.294	.952	59.	.89	.67	155.9	110.5	80.8	COMB. EFF.
5.00	800.	1.0	.365	.952	53.	.76	.42	315.0	148.9	62.8	COMB. EFF.
5.00	800.	1.0	097	.952	50.	.69	0	0	0	0	BLOWOFF
4.00	800.	1.0	.294	.644	54.	.83	.42	284.8	160.4	65.8	COMB. EFF.
4.00	800.	1.0	.115	.644	49.	.71	0	0	0	0	BLOWOFF
3.50	800.	1.0	.294	.511	55.	.88	.31	260.9	139.9	68.8	COMB. EFF.
3.00	800.	1.0	.147	.390	49.	.77	0	0	0	0	BLOWOFF
2.36	800.	1.0	.187	.256	50.	.85	0	0	0	0	BLOWOFF
8.00	800.	1.0	.294	2.168	62.	.84	.83	95.9	114.2	87.2	COMB. EFF.
8.00	800.	1.0	.093	2.168	57.	.73	0	0	0	0	BLOWOFF

Appendix B

Publications and Reports

1. Plee, S. L. and Mellor, A. M. (1977a), "Preliminary investigation of flashback in prevaporizing/premixing combustors," Preprint No. 77-22, Spring Meeting, Western States Section/The Combustion Institute, April 1977, Seattle, Washington.

2. Plee, S. L. and Mellor, A. M. (1977b), "Review of flashback reported in prevaporizing/premixing combustors," accepted for publication in Combustion and Flame.

3. Schmidt, D. A., Plee, S. L. and Mellor, A. M. (1978), "A phenomenological model for gas turbine emissions," invited paper prepared for Department of Energy/Division of Power Systems Workshop on Modeling of Combustion in Practical Systems, January 4-6, Los Angeles, California.

4. Plee, S. L. and Mellor, A. M. (1978), "Flame stabilization in simplified prevaporizing, partially vaporizing and conventional gas turbine combustors," submitted for presentation at AIAA/SAE 14th Joint Propulsion Conference, Las Vegas, Nevada.